

Technische Universität München

Department of Mathematics

Geometric Analysis of the Discrete Fast-Slow Fold Singularity

Master's Thesis

by

Sara-Viola Kuntz

Supervisor:	Prof. Dr. Christian Kühn
Advisor:	Dr. Samuel Jelbart
Submission Date:	27$^{\text{th}}$ of January, 2022

I assure the single handed composition of this master's thesis only supported by declared resources.

Garching, 27^{th} of January, 2022

Acknowledgment

First and foremost, I would like to thank my thesis supervisor Prof. Dr. Christian Kühn for his guidance through this project. Thank you for proposing the subject, formulating concrete mathematical questions and having time for helpful and interesting discussions. Furthermore, I am pleased you gave me the opportunity to work as a student assistant at the SFB 'Discretization in Geometry and Dynamics'.

Secondly, I would like to thank my advisor Dr. Samuel Jelbart for all our meetings and exchanges. Thanks for the detailed discussions, your valuable feedback and the reference literature you provided me. You have taught me to formulate mathematical results in a beautiful way and helped me to keep the big picture in mind.

Finally, I would like to thank my family and all my friends for supporting me. Thanks to my parents Beate and Martin Kuntz and my brother Patrick Kuntz for always encouraging my love to mathematics and being there for me. Thanks to my boyfriend Lukas Bührend for your emotional support and interesting discussions about mathematics and physics. Finally, I would like to thank my friends from university for our shared time during the studies and your interest in my topic.

Abstract

In this master's thesis, the normal form of a fast-slow map that exhibits a slow passage through a discrete fold bifurcation is considered. Due to this behavior, a three timescale ODE system exhibiting in the partial singular limit a fold bifurcation of limit cycles is studied. We show exponential contraction of trajectories towards an invariant slow manifold and then track the extension of the invariant manifold through a neighborhood of the fold limit cycle. This is proven using a method of geometric desingularization known as the the blowup method, adapted to non-hyperbolic limit cycles. Our analysis is build upon the work by Krupa and Szmolyan for the normal form of the continuous fast-slow fold [17]. We adapt the techniques used and extend the results obtained by Krupa and Szmolyan. By defining a Poincaré return map, we transfer the results of the continuous system locally to the normal form of the discrete fast-slow fold singularity, though globally the embedding is not well-defined. Several extensions to resolve this issue are proposed.

Zusammenfassung

In dieser Masterarbeit wird die Normalform einer schnell-langsamen Abbildung, welche eine langsame Passage durch eine diskrete Falten-Bifurkation beschreibt, untersucht. Aufgrund dieses Verhaltens wird ein drei Zeitskalen System aus gewöhnlichen Differentialgleichungen betrachtet, welches im partiellen singulären Grenzwert eine Falten-Bifurkation von Grenzzyklen aufweist. Es wird eine exponentielle Kontraktion von Lösungskurven hin zu einer langsamen, invarianten Mannigfaltigkeit gezeigt und dann die Fortführung der invarianten Mannigfaltigkeit in der Nähe des singulären Grenzzyklus analysiert. Der zugehörige Beweis basiert auf einer Methode der geometrischen Desingularisierung, welche auch Blowup Methode genannt wird. Im Rahmen dieser Masterarbeit wird die Blowup Methode an nicht-hyperbolische Grenzzyklen angepasst. Die Analyse basiert auf der Arbeit von Krupa und Szmolyan für die Normalform der kontinuierlichen schnell-langsamen Falten-Singularität [17]. Die dadurch erhaltenen Ergebnisse erweitern jene von Krupa und Szmolyan. Durch das Definieren einer Poincaré Abbildung werden die Ergebnisse lokal auf die Normalform der diskreten schnell-langsamen Falten-Singularität übertragen, global ist die Einbettung jedoch nicht wohldefiniert. Zusätzlich werden verschiedene Erweiterungen vorgeschlagen, die das Ziel haben, eine global definierte Einbettung zu erhalten.

Contents

1. Introduction **1**

2. Background of Multiple Time Scale Dynamics **5**
2.1. Fast-Slow Systems . . . 5
2.1.1. Fast-Slow Ordinary Differential Equations . . . 5
2.1.2. Fast-Slow Maps . . . 7
2.2. Fast-Slow Fold Singularity . . . 8
2.2.1. Continuous Fast-Slow Fold Singularity . . . 8
2.2.2. Discrete Fast-Slow Fold Singularity . . . 12
2.3. Geometric Singular Perturbation Theory . . . 16
2.4. Blowup Method . . . 18
2.5. Existing Results for the Continuous Fast-Slow Fold . . . 22

3. Problem Formulation and Main Results **24**
3.1. Embedding as a Poincaré Return Map . . . 24
3.2. Assumptions and Setting . . . 28
3.3. Blowup of the Fast-Slow LC Fold . . . 31
3.4. Main Results . . . 34
3.4.1. Theorem for the Fast-Slow LC Fold . . . 34
3.4.2. Local Theorem for the Discrete Fast-Slow Fold . . . 35
3.4.3. Break Down of the Fold Embedding . . . 38

4. Analysis of the Fast-Slow LC Fold **39**
4.1. Dynamics in the Entry Chart . . . 39
4.2. Dynamics in the Rescaling Chart . . . 48
4.3. Dynamics in the Exit Chart . . . 55
4.4. Proof of Main Theorem 1 . . . 65

5. Analysis of the Discrete Fast-Slow Fold **69**
5.1. Dynamics in the Entry Chart . . . 69
5.2. Dynamics in the Rescaling Chart . . . 78
5.3. Proof of Main Theorem 2 . . . 86
5.4. Dynamics in the Exit Chart . . . 89
5.5. Proof of Main Theorem 3 . . . 94

6. Outlook, Extensions and Limitations **96**
6.1. Outlook . . . 96
6.2. Different Rotation Velocities . . . 97
6.3. The Dual Limit $\varepsilon, s \to 0$ . . . 97
6.4. Extension to the Fast-Slow Flip Singularity . . . 97
6.5. Alternate Approaches for Fast-Slow Maps . . . 98

Appendix A. Background of Ordinary Differential Equations **99**
A.1. Elementary Theorems of Differential Calculus 99
A.2. Conjugacy and Equivalence 100
A.3. Coordinate Transformations and Time Rescaling 101
A.4. Hartman-Grobman and Belitski Theorem 103
A.5. Invariant Manifold Theory 103

Appendix B. Discussion about the Rotation Velocity **105**
B.1. Fast Rotation Velocity 105
B.2. Relationship between δ and ε 106
B.3. Non-Constant Rotation Velocity 106

Appendix C. The Dual Limit $\varepsilon, s \to 0$ **108**
C.1. Validity of the Local Results 108
C.2. Extension to the Exit Chart 112

Appendix D. Geometric Analysis of the Fast-Slow Flip Singularity **113**
D.1. Flip Bifurcation 113
D.2. Embedding as a Poincaré Return Map 115

Appendix E. Blowup of Discrete Fast-Slow Singularities **119**
E.1. Blowup of Maps in Spherical Coordinates 119
E.2. Results for the Discrete Fast-Slow Fold 122
E.3. Results for the Fast-Slow Flip 123

Bibliography **125**

Chapter 1

Introduction

In various areas of application, such as biology, chemistry and electrical engineering, processes on multiple time scales occur [18]. Often it is possible to distinguish one fast and one slow time scale. These systems arise when a slow process disturbs the overarching fast process.

Two fundamentally different types of processes exist: Processes on a continuous time scale, which may be modelled by ordinary or partial differential equations, and processes on a discrete time scale, which may be modelled by maps.

For instance, concentrations in chemical processes are usually measured on a continuous time scale and modelled by ordinary differential equations. The derivatives in the ODE system determine the rate at which the concentration of a substance increases or decreases. The general form of a *fast-slow ordinary differential equation* is given by

$$\begin{aligned} \frac{\mathrm{d}x}{\mathrm{d}t} &= x' = \ f(x, y, \varepsilon), \\ \frac{\mathrm{d}y}{\mathrm{d}t} &= y' = \varepsilon g(x, y, \varepsilon), \end{aligned} \tag{1.1}$$

with fast variables $x \in \mathbb{R}^n$, slow variables $y \in \mathbb{R}^m$, a small time scale parameter $\varepsilon \in \mathbb{R}_{>0}$, a function $f : \mathbb{R}^n \times \mathbb{R}^m \times \mathbb{R} \to \mathbb{R}^m$ and a function $g : \mathbb{R}^n \times \mathbb{R}^m \times \mathbb{R} \to \mathbb{R}^n$ [18]. In the context of chemical reactions, the singularly perturbed ordinary differential equation (1.1) could be interpreted as follows: the concentration of a substrate is modelled by the fast variable x. Under presence of an enzyme, the substrate forms a complex, represented by the slow variable y. The time scale separation is induced by defining ε as the small ratio from enzyme to substance.

However, biological processes are frequently measured on a discrete time scale if, for example, the population size at week n is modelled. In many cases, the population size at week $n+1$ can be determined as a function of the population size at week n. Iterating the map describing this change leads to a *discrete dynamical system*. The general form of a *fast-slow map* is given by

$$\begin{aligned} x &\mapsto x + \ f(x, y, \varepsilon), \\ y &\mapsto y + \varepsilon g(x, y, \varepsilon), \end{aligned} \tag{1.2}$$

with fast variables $x \in \mathbb{R}^n$, slow variables $y \in \mathbb{R}^m$, a small time scale parameter $\varepsilon \in \mathbb{R}_{>0}$, a function $f : \mathbb{R}^n \times \mathbb{R}^m \times \mathbb{R} \to \mathbb{R}^m$ and a function $g : \mathbb{R}^n \times \mathbb{R}^m \times \mathbb{R} \to \mathbb{R}^n$ [18]. In a demographic context, the singularly perturbed map (1.2) could be interpreted as follows: the dynamics of the population size is modelled by the fast variable x. This dynamics is influenced by the number of people y having a new rare and fatal disease, which spreads on a slow time scale.

An important question in both continuous and discrete dynamical systems is how the qualitative dynamics changes under variation of system parameters. A fundamental change of the phase portrait under parameter variation is called a *bifurcation* [19]. One of the simplest possible bifurcations in the discrete time setting is observed in the one-dimensional map

$$x \mapsto \ x + x^2 - y, \tag{1.3}$$

where $x \in \mathbb{R}$ is a variable and $y \in \mathbb{R}$ is a parameter. This map is called the *discrete fold bifurcation* [19]. Dependent on the parameter y, different dynamical behavior is observed. For

$y < 0$, no fixed points exists, for $y = 0$, the only fixed point is $x = 0$, and for $y > 0$, two fixed points $x = \pm\sqrt{y}$ arise. For $y = 0$, the fixed point $x = 0$ is non-hyperbolic, which means that we cannot determine its stability properties by the linearization of the map in x. In the case of two fixed points, for $y > 0$, both fixed points are hyperbolic and by the linearization we deduce, that the fixed point $x = -\sqrt{y}$ is stable and the fixed point $x = \sqrt{y}$ is unstable.

In many applications, it is more accurate to consider the 'dynamic' case, in which a parameter varies slowly in time. In this master's thesis, we aim to analyze the dynamic version of the one-dimensional discrete fold bifurcation, occurring in the two-dimensional fast-slow map

$$\begin{aligned} x &\mapsto x + x^2 - y, \\ y &\mapsto y - \varepsilon, \end{aligned} \tag{1.4}$$

with a fast variable $x \in \mathbb{R}$, a slow variable $y \in \mathbb{R}$, and a small parameter $\varepsilon \in \mathbb{R}_{>0}$. We call system (1.4) the normal form of the *discrete fast-slow fold singularity* and the point $(x, y) = (0, 0)$ the *singular fold point*. The parameter drift vanishes in the *singular limit* $\varepsilon = 0$, such that the variable y is constant and can therefore be seen as a parameter for the dynamics in x. The map (1.4) then reduces to the one-dimensional discrete fold bifurcation with normal form (1.3).

To study the behavior of fast-slow systems, many techniques like asymptotic, numerical and geometric methods as well as the theory of dynamical systems are applied. In the singular limit $\varepsilon = 0$, the fixed points of the normal form of the discrete fast-slow fold singularity (1.4) are given by

$$S_0 = \left\{(x, y) \in \mathbb{R}^2 : y = x^2\right\},$$

which is called the *critical manifold*, abbreviated by S_0 [18]. For $\varepsilon > 0$, parts of the critical manifold S_0 perturb to nearby invariant manifolds S_ε [13, 15]. Issues occur for the singular fold point $(x, y) = (0, 0)$, hence other methods are required.

For continuous time problems, it has been useful to apply a method of geometric desingularization, called the blowup method, to analyze the dynamics in a neighborhood of singular points [6, 7]. The method was first applied on fast-slow ordinary differential equations by Dumortier and Roussarie [8]. By inserting a higher dimensional object, such as a sphere, in place of the singularity, it is possible to gain information about the dynamics near a non-hyperbolic equilibrium. Krupa and Szmolyan used the blowup method to analyze the fold, transcritical and pitchfork singularity in fast-slow ordinary differential equations [16, 17]. Nipp and Stoffer extended the blowup method for continuous fast-slow singularities to Runge-Kutta discretizations. They proved with an abstract theory the existence of slow manifolds around the discrete fast-slow fold singularity [22]. Arcidiacono, Engel and Kühn used the blowup method and direct estimates to prove the extension of Fenichel's slow manifold near discretized transcritical and pitchfork singularities [1, 9]. For all three discretized blowups to work, it is necessary to find the right rescaling of the step size parameter.

For fast-slow maps which are not obtained by discretizing a fast-slow ordinary differential equation, no step size exists as an additional parameter. Without the freedom to rescale the step size parameter, the blowup method is not directly applicable to fast-slow maps. In this master's thesis, we aim to overcome this issue by locally embedding the normal form of the discrete fast-slow fold singularity (1.4) in a higher dimensional system of ordinary differential equations, given by

$$\begin{aligned} x' &= x^2 - y, \\ \theta' &= \tilde{\varepsilon}, \\ y' &= -\varepsilon, \end{aligned} \tag{1.5}$$

with $x, y \in \mathbb{R}$ and two small parameters $\varepsilon > 0$ and $\tilde{\varepsilon} > 0$. System (1.5) can be considered as a normal form for the *continuous fast-slow fold singularity* with an additional rotational coordinate θ with constant rotation velocity $\tilde{\varepsilon}$. As the rotational coordinate θ decouples from x and y, this system undergoes a *fold bifurcation of limit cycles* in the (partial) singular limit $\varepsilon = 0$, $\tilde{\varepsilon} > 0$.

This limit is valid in the case that $0 < \varepsilon \ll \tilde{\varepsilon} \ll 1$, for which system (1.5) is an ODE system on three time scales. Thus, we consider system (1.5) as a normal form for the *fast-slow fold of limit cycles*, abbreviated by *fast-slow LC fold*. To see the relationship between the ODE (1.5) and the map (1.4), we observe that the functions f and g coincide for both systems. By introducing a hyperplane, which is transversal to the flow of the continuous system, we can define a Poincaré return map. This Poincaré map tracks the intersections of the flow with the hyperplane. The resulting Poincaré return map is topologically equivalent to the normal form of the discrete fast-slow fold singularity (1.4). Our goal is to analyze the normal form of the fast-slow LC fold (1.5) around its non-hyperbolic limit cycle to gain insight into the dynamics of the normal form of the discrete fast-slow fold singularity (1.4) in a neighborhood of the fold point $(x, y) = (0, 0)$.

The structure of this master's thesis is as follows: in Chapter 2, background of multiple time scale dynamics is introduced. This includes in Section 2.1 the general theory of fast-slow ordinary differential equations and fast-slow maps. In Section 2.2, the normal forms of the continuous and the discrete fast-slow fold singularities are derived. Section 2.3 continues with geometric singular perturbation theory in continuous-time systems including Fenichel's Theorems on the existence of slow manifolds. The polar blowup method and its improvement for quasi-homogeneous vector fields are introduced in Section 2.4. The second chapter ends in Section 2.5 with the results of Krupa and Szmolyan obtained for a normal form of the continuous fast-slow fold singularity in their work 'Geometric Analysis of the Singularly Perturbed Planar Fold' [17].

Chapter 3 introduces the topic of this master's thesis and states the main results obtained. In Section 3.1, the embedding of the normal form of the discrete fast-slow fold singularity (1.4) as a Poincaré return map of the normal form of the fast-slow LC fold (1.5) is defined. Afterwards, Fenichel theory is applied to system (1.5) and the setting for the main theorems is specified in Section 3.2. In Section 3.3, the blowup method is applied to the normal form of the fast-slow LC fold. Thereby three charts are defined, in which system (1.5) is analyzed in Chapter 4. A relationship between the time scales $\tilde{\varepsilon}$ and ε is determined being able to desingularize the non-hyperbolic limit cycle. Finally, the main results obtained in this master's thesis are stated in Section 3.4. The results obtained for the normal form of the fast-slow LC fold extend the results obtained by Krupa and Szmolyan in [17]. For the normal form of the discrete fast-slow fold singularity (1.4), we obtain via the Poincaré return map a local theorem characterizing the dynamics in an ε-dependent neighborhood of the fold point and a second theorem showing that the embedding is not globally well-defined.

In Chapter 4, the normal form of the fast-slow LC fold (1.5) is analyzed in three charts, the entry, rescaling and exit chart. Additionally to the results obtained by Krupa and Szmolyan, we gain insight into the transition time and the evolution of the rotational coordinate θ. The chapter ends with the proof of the main theorem for the normal form of the LC fold singularity.

Chapter 5 builds upon the findings of Chapter 4 and determines in each chart the Poincaré return map. After the analysis in the entry and rescaling chart, a local theorem for the normal form of the discrete fast-slow fold singularity (1.4) is proven. In the exit chart, we observe the loss of well-definedness of the embedding. Afterwards, we prove in a second theorem for the normal form of the discrete fast-slow fold singularity, that it is not possible to define a globally well-defined embedding with a constant rotation velocity.

Extensions and limitations are considered in Chapter 6. A general overview of what we have achieved and what are remaining open questions is given in Section 6.1. The following Sections 6.2-6.5 propose ideas how to overcome the limitations of the setting of this master's thesis. Several details of the mentioned extensions are specified in the Appendix.

Appendix A covers background of ordinary differential equations needed for the analysis. In Appendix B, the choice of the rotation velocity $\tilde{\varepsilon}$ in system (1.5) is discussed. Another choice of a second parameter defining the local embedding is proposed in Appendix C. Both extensions in Appendix B and in Appendix C have the goal to find a globally well-defined embedding for the discrete fast-slow fold singularity.

The initial motivation of this master's thesis was to study a normal form of the fast-slow flip singularity, which is based on a discrete one-dimensional bifurcation without continuous analogue. The flip bifurcation is introduced in Appendix D and an embedding is proposed, such that a similar analysis to the one carried out in this master's thesis should be possible. Finally, Appendix E presents the first ideas of applying the blowup method directly to fast-slow maps without using an embedding. The findings for the discrete fast-slow fold and the fast-slow flip singularity are shown.

Chapter 2

Background of Multiple Time Scale Dynamics

In this chapter, background on the theory of multiple time scale analysis is introduced. Section 2.1 presents the general form of fast-slow systems in continuous and in discrete time. Afterwards, the normal forms of the continuous and the discrete fast-slow fold singularity are derived in Section 2.2. In Section 2.3, geometric singular perturbation theory and Fenichel's Theorems are explained, both characterizing the flow of continuous fast-slow systems for small $\varepsilon > 0$ in regions without singularities. To analyze the flow of a system of ordinary differential equations in a neighborhood of a singularity, we introduce the blowup method in Section 2.4. Section 2.5 finally presents the results Krupa and Szmolyan have derived with the blowup method for a normal form of the continuous fast-slow fold singularity [17].

2.1. Fast-Slow Systems

Often continuous or discrete processes on multiple time scales occur in applications. The simplest, but already non-trivial case is given by systems on two time scales, a fast and a slow one. We first introduce in Section 2.1.1 fast-slow ordinary differential equations following [18] and continue in Section 2.1.2 with fast-slow maps.

2.1.1. Fast-Slow Ordinary Differential Equations

Continuous processes are often modeled by ordinary differential equations. In the case of two time scales, they frequently arise in the standard form

$$\begin{aligned} \frac{\mathrm{d}x}{\mathrm{d}t} &= x' = \ f(x, y, \varepsilon), \\ \frac{\mathrm{d}y}{\mathrm{d}t} &= y' = \varepsilon g(x, y, \varepsilon), \end{aligned} \tag{2.1}$$

where $f : \mathbb{R}^m \times \mathbb{R}^n \times \mathbb{R} \to \mathbb{R}^m$ and $g : \mathbb{R}^m \times \mathbb{R}^n \times \mathbb{R} \to \mathbb{R}^n$ are C^k functions with $k \geq 1$ and ε is a time scale parameter with $0 < \varepsilon \ll 1$. This notation indicates, since the parameter ε is small and positive, that the dynamics in x and y takes place on different time scales. The ODE in x describes the fast dynamics, the ODE in y the slow dynamics. The time scale t is called the *fast time scale*. We can rewrite system (2.1) by introducing the *slow time scale* $\tau = \varepsilon t$:

$$\begin{aligned} \varepsilon \frac{\mathrm{d}x}{\mathrm{d}\tau} &= \varepsilon \dot{x} = f(x, y, \varepsilon), \\ \frac{\mathrm{d}y}{\mathrm{d}\tau} &= \ \dot{y} = g(x, y, \varepsilon). \end{aligned} \tag{2.2}$$

In the *singular limit* $\varepsilon = 0$ in system (2.1), we obtain the *fast subsystem*

$$\begin{aligned} x' &= f(x, y, 0), \\ y' &= 0, \end{aligned}$$

which is also called the *layer problem*. The *slow subsystem* is obtained in the singular limit $\varepsilon = 0$ in system (2.2)

$$\begin{aligned} 0 &= f(x, y, 0), \\ \dot{y} &= g(x, y, 0), \end{aligned}$$

which results in a differential-algebraic equation, also called the *reduced problem*. The slow subsystem is a dynamical system on the *critical manifold*

$$S_0 := \{(x, y) \in \mathbb{R}^m \times \mathbb{R}^n : f(x, y, 0) = 0\},$$

which consists of the equilibria of the layer problem. The flow on the critical manifold S_0 is called the *slow flow*. To analyze the fast-slow system (2.1), a first idea is to study the reduced and the layer problem separately. Close to the critical manifold S_0, the dynamics should be governed by the slow motion. Away from S_0, the slow dynamics should be negligible, such that it is sufficient to consider the layer problem. Dependent on the stability properties of the critical manifold S_0, results of geometric singular perturbation theory for the dynamics of the fast-slow system exist, which are discussed in Section 2.3. These results apply near the critical manifold S_0 as long as one stays away from singularities, corresponding to bifurcations in the layer problem. Additional methods are needed to understand the dynamics near singular points.

In the following, we illustrate in an example the notations introduced. We call the following system the normal form of the *continuous fast-slow fold singularity*, which plays a fundamental role in this thesis.

Example 2.1. *We consider the fast-slow ODE system*

$$\begin{aligned} x' &= x^2 - y, \\ y' &= -\varepsilon, \end{aligned}$$

with $x, y \in \mathbb{R}$ and $0 < \varepsilon \ll 1$. The singular limit dynamics is visualized in Figure 2.1. The critical manifold is given by

$$S_0 := \{(x, y) \in \mathbb{R}^2 : y = x^2\}.$$

On the critical manifold, the slow flow of the reduced problem is directed to the origin, as $y' < 0$. In the layer problem, the fast flow is directed in positive x-direction for points below the parabola, as then $x' > 0$, and in negative x-direction for points above the parabola, as then $x' < 0$. In the full system, no equilibrium point exists.

The considered fast-slow ODE is obtained from the system analyzed by Krupa and Szmolyan in [17] by truncating the higher order terms.

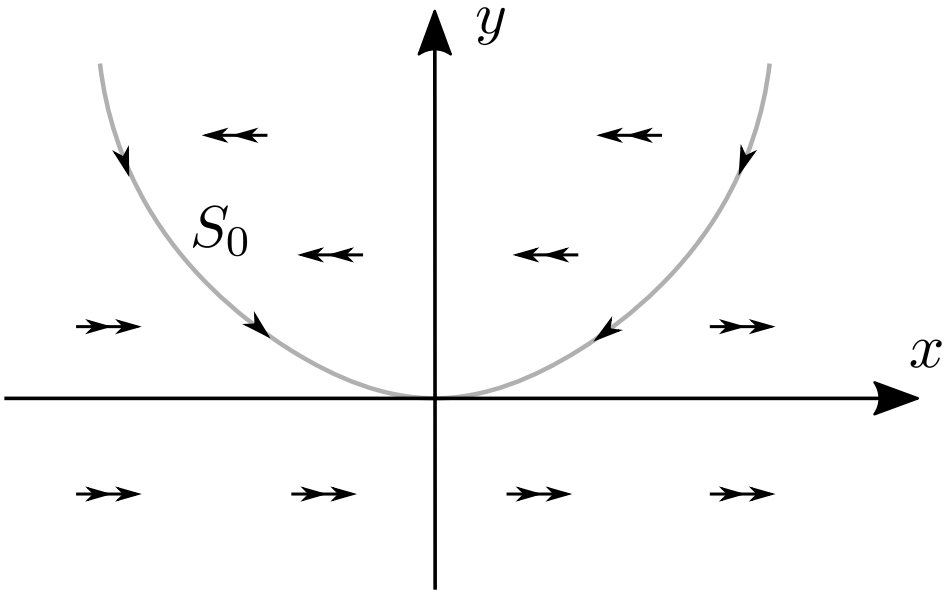


Figure 2.1.: In gray, the critical manifold S_0 of the normal form of the continuous fast-slow fold singularity is shown. The slow flow on S_0 is indicated by single arrows and the fast flow of the layer problem is indicated by double arrows.

2.1.2. Fast-Slow Maps

Discrete processes are often modelled using maps. In the case of two time scales, they frequently arise in the standard form

$$\begin{aligned} x &\mapsto x + \ f(x, y, \varepsilon), \\ y &\mapsto y + \varepsilon g(x, y, \varepsilon), \end{aligned} \tag{2.3}$$

where $f : \mathbb{R}^m \times \mathbb{R}^n \times \mathbb{R} \to \mathbb{R}^m$ and $g : \mathbb{R}^m \times \mathbb{R}^n \times \mathbb{R} \to \mathbb{R}^n$ are C^k functions with $k \geq 1$ and ε is a time scale parameter with $0 < \varepsilon \ll 1$. The map in x describes the 'fast' dynamics and the map in y describes the 'slow' dynamics. As the time scale is discrete, it is not possible to define a slow time scale as in the continuous case.

In the *singular limit* $\varepsilon = 0$ in system (2.3), the map

$$\begin{aligned} x &\mapsto x + f(x, y, \varepsilon), \\ y &\mapsto y, \end{aligned}$$

is obtained, in which y is a fixed point and hence becomes a parameter for the map in x. We introduce the *critical manifold*

$$S_0 \coloneqq \{(x, y) \in \mathbb{R}^m \times \mathbb{R}^n : f(x, y, 0) = 0\},$$

which consists of the fixed points of the fast-slow map in the singular limit $\varepsilon = 0$. Near the critical manifold, the dynamics is given by the slow dynamics in y. Away from the critical manifold S_0, the dynamics can be approximated by the map in x, as the slow dynamics should be negligible.

To end this section, we consider as an example the following two-dimensional fast-slow map, which we call the normal form of the *discrete fast-slow fold singularity*. This is the fundamental system we study in this master's thesis.

Example 2.2. *As an example, we consider the fast-slow map*

$$\begin{aligned} x &\mapsto x + x^2 - y, \\ y &\mapsto y - \varepsilon, \end{aligned}$$

with $x, y \in \mathbb{R}$ and $0 < \varepsilon \ll 1$. The singular limit dynamics is visualized in Figure 2.2 for different initial conditions. The critical manifold is given by

$$S_0 \coloneqq \{(x, y) \in \mathbb{R}^2 : y = x^2\}.$$

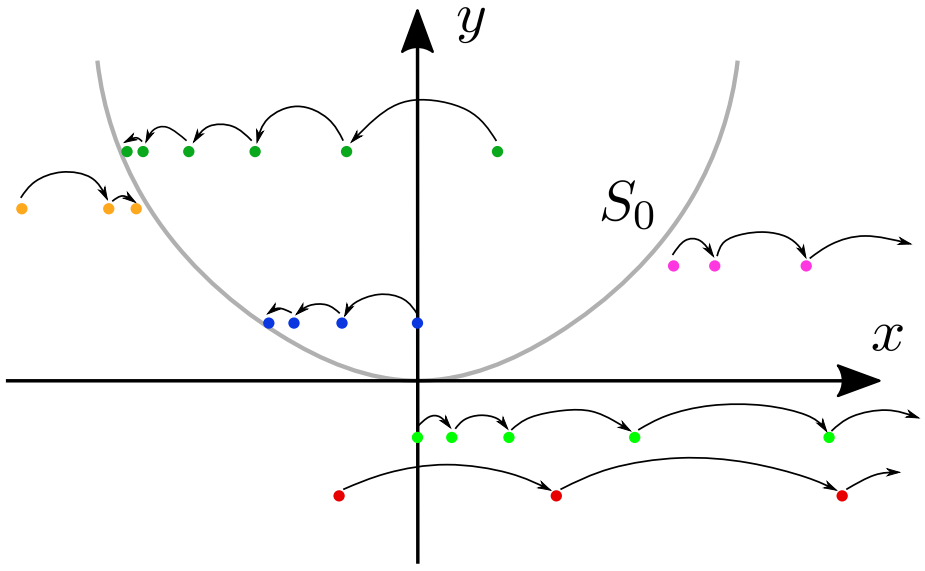


Figure 2.2.: In gray, the critical manifold S_0 of the normal form of the discrete fast-slow fold singularity is shown. For different initial conditions, the iterates in the singular limit are visualized.

In the singular limit $\varepsilon = 0$, all points on the critical manifold are fixed points. For $\varepsilon > 0$, near the critical manifold, the x-coordinate stays fixed and the y-coordinate decreases by ε. Away from the critical manifold, the fast flow in x dominates the slow dynamics in y. In the full system, no fixed points exist.

2.2. Fast-Slow Fold Singularity

In this section, we derive the normal forms of the continuous and the discrete fast-slow fold singularities, which are the fundamental systems analyzed in this thesis. These two systems were already used as examples in Sections 2.1.1 and 2.1.2. The singularities are defined by certain conditions on the vector fields of the fast-slow systems. Through Taylor expansions, the concrete forms of the functions f and g can be approximated.

2.2.1. Continuous Fast-Slow Fold Singularity

We consider the singular perturbed ODE

$$\begin{aligned} x' &= f(x, y, \varepsilon), \\ y' &= \varepsilon g(x, y, \varepsilon), \end{aligned} \tag{2.4}$$

with $(x, y) \in \mathbb{R}^2$, a time scale parameter $0 < \varepsilon \ll 1$ and two functions $f : \mathbb{R}^3 \to \mathbb{R}$ and $g : \mathbb{R}^3 \to \mathbb{R}$, which are at least C^2. We require, that in the singular limit $\varepsilon = 0$, system (2.4) has a non-hyperbolic equilibrium point at $(0, 0) \in \mathbb{R}^2$, characterized by the conditions

$$f(0, 0, 0) = 0, \qquad \frac{\partial f}{\partial x}(0, 0, 0) = 0. \tag{2.5}$$

As it is possible to shift coordinates in the phase space, we can without loss of generality assume, that the equilibrium is located at the origin $(0, 0) \in \mathbb{R}^2$. Furthermore, we suppose that in system (2.4) the following non-degeneracy conditions hold [17]:

$$\frac{\partial^2 f}{\partial x^2}(0, 0, 0) \neq 0, \qquad \frac{\partial f}{\partial y}(0, 0, 0) \neq 0, \qquad g(0, 0, 0) \neq 0. \tag{2.6}$$

The first condition guarantees, that the term x^2 does not vanish in the Taylor expansion of the function f. The second condition ensures, that the eigenvalue $\lambda(y)$ of the ODE in x transverses the origin with non-zero speed. The last condition is a requirement on the reduced flow of system (2.4), such that a slow passage trough the non-hyperbolic equilibrium point $(0, 0)$ of the fast subsystem is described for all $\varepsilon > 0$. Without loss of generality, we assume that

$$\frac{\partial^2 f}{\partial x^2}(0, 0, 0) > 0, \qquad \frac{\partial f}{\partial y}(0, 0, 0) < 0. \tag{2.7}$$

In the following proposition, we derive the normal form of the continuous fast-slow fold singularity, specified by the conditions (2.5), (2.6) and (2.7). Afterwards, we explain why the assumptions in (2.7) are no restrictions.

Proposition 2.3. *Suppose, that the two-dimensional system* (2.4) *with* $(x, y) \in \mathbb{R}^2$, *the parameter* $0 < \varepsilon \ll 1$ *and the functions* $f : \mathbb{R}^3 \to \mathbb{R}$, $g : \mathbb{R}^3 \to \mathbb{R}$ *with* $f, g \in C^2$, *fulfills the conditions* (2.5), (2.6) *and* (2.7). *Then system* (2.4) *is locally near* $(x, y, \varepsilon) = (0, 0, 0)$ *topologically equivalent to either of the ODE systems*

$$\begin{aligned} x' &= x^2 - y + \mathcal{O}\left(x^3, \varepsilon\right), \\ y' &= \pm\varepsilon + \mathcal{O}\left(\varepsilon x, \varepsilon y, \varepsilon^2\right). \end{aligned}$$

Proof. The idea of the proof is based on [19], showing the derivation of the normal form of the one-dimensional continuous fold bifurcation. In system (2.4), we consider additionally the parameter ε and the slow dynamics in the variable y.

The Taylor expansion of the function g near the origin is

$$g(x, y, \varepsilon) = g(0, 0, 0) + \mathcal{O}(x, y, \varepsilon).$$

By condition (2.6) it holds $g(0, 0, 0) \neq 0$. Hence, the ODE in y is given by

$$y' = \varepsilon g(x, y, \varepsilon) = \varepsilon g(0, 0, 0) + \mathcal{O}(\varepsilon x, \varepsilon y, \varepsilon^2).$$

For the ODE in x we use, that $y' \in \mathcal{O}(\varepsilon)$. The Taylor expansion of the function f near the origin is

$$f(x, y, \varepsilon) = f_0(y, \varepsilon) + f_1(y, \varepsilon)x + f_2(y, \varepsilon)x^2 + \mathcal{O}(x^3),$$

with $f_0(0, 0) = f(0, 0, 0) = 0$ and $f_1(0, 0) = \partial_x f(0, 0, 0) = 0$ by condition (2.6). We now perform a coordinate change by introducing the variable ξ:

$$\xi = x + \delta(y, \varepsilon) = x + \delta,$$

where the function $\delta(y, \varepsilon)$ with $\delta(0, 0) = 0$ will be specified below. The coordinate shift leads with the conditions on the dynamics in x to

$$\begin{aligned}
\xi' &= x' + \delta'(y, \varepsilon) \\
&= f(\xi - \delta, y, \varepsilon) + \delta'(y, \varepsilon) \\
&= f_0(y, \varepsilon) + f_1(y, \varepsilon)(\xi - \delta) + f_2(y, \varepsilon)(\xi - \delta)^2 + \mathcal{O}\left((\xi - \delta)^3\right) + \delta'(y, \varepsilon) \\
&= [f_0(y, \varepsilon) - f_1(y, \varepsilon)\delta + f_2(y, \varepsilon)\delta^2 + \mathcal{O}(\delta^3)] \\
&\quad + [f_1(y, \varepsilon) - 2f_2(y, \varepsilon)\delta + \mathcal{O}(\delta^2)]\xi + [f_2(y, \varepsilon) + \mathcal{O}(\delta)]\xi^2 + \mathcal{O}\left(\xi^3\right) + \delta'(y, \varepsilon).
\end{aligned}$$

We can eliminate the linear term in ξ with the Implicit Function Theorem A.2. Let

$$F(y, \varepsilon, \delta) \coloneqq [f_1(y, \varepsilon) - 2f_2(y, \varepsilon)\delta + \delta^2\psi(y, \varepsilon, \delta)] \stackrel{!}{=} 0$$

with some smooth function ψ. By condition (2.6) it follows

$$\partial_\delta F(0, 0, 0) = -2f_2(0, 0) = -2\partial_{xx} f(0, 0, 0) \neq 0.$$

Furthermore, we have $F(0, 0, 0) = 0$, such that the Implicit Function Theorem A.2 implies, that a unique smooth function $\delta = \delta(y, \varepsilon)$ exists locally near $(0, 0, 0)$ with $\delta(0, 0) = 0$ and $F(y, \varepsilon, \delta(y, \varepsilon)) \equiv 0$. To find an expression for the function $\delta(y, \varepsilon)$, we Taylor-expand the functions $f_1(y, \varepsilon)$ and $f_2(y, \varepsilon)$ and use condition (2.5):

$$\begin{aligned}
f_1(y, \varepsilon) &= f_1(0, 0) + \partial_y f_1(0, 0)y + \partial_\varepsilon f_1(0, 0)\varepsilon + \mathcal{O}(y^2, \varepsilon^2, \varepsilon y) \\
&= \partial_y f_1(0, 0)y + \mathcal{O}(y^2, \varepsilon), \\
f_2(y, \varepsilon) &= f_2(0, 0) + \partial_y f_2(0, 0)y + \partial_\varepsilon f_2(0, 0)\varepsilon + \mathcal{O}(y^2, \varepsilon^2, \varepsilon y) \\
&= f_2(0, 0) + \partial_y f_2(0, 0)y + \mathcal{O}(y^2, \varepsilon).
\end{aligned}$$

Plugging these expressions into the equation $F(y, \varepsilon, \delta) = 0$ leads to

$$\delta(y, \varepsilon) = \frac{\partial_y f_1(0, 0)}{2f_2(0, 0)}y + \mathcal{O}(y^2, \varepsilon).$$

Using that $y' \in \mathcal{O}(\varepsilon)$, it follows

$$\delta'(y, \varepsilon) = \frac{\partial_y f_1(0, 0)}{2f_2(0, 0)}y' + \mathcal{O}(yy', \varepsilon') \in \mathcal{O}(\varepsilon).$$

With

$$\begin{aligned} f_0(y,\varepsilon) &= f_0(0,0) + \partial_y f_0(0,0)y + \partial_\varepsilon f_0(0,0)\varepsilon + \mathcal{O}(y^2,\varepsilon^2,\varepsilon y) \\ &= \partial_y f_0(0,0)y + \mathcal{O}(y^2,\varepsilon), \end{aligned}$$

the remaining ODE is given by

$$\xi' = [\partial_y f_0(0,0)y + \mathcal{O}(y^2,\varepsilon)] + [f_2(0,0) + \mathcal{O}(y,\varepsilon)]\xi^2 + \mathcal{O}(\xi^3,\varepsilon).$$

We introduce now as a new variable the leading order term of the ODE above:

$$\mu(y,\varepsilon) \coloneqq \partial_y f_0(0,0)y + y^2\phi_1(y,\varepsilon) + \varepsilon\phi_2(y,\varepsilon),$$

where ϕ_1 and ϕ_2 are smooth functions. As $\partial_y f_0(0,0) = \partial_y f(0,0,0) < 0$, μ has locally the opposite sign to y. It holds

$$\mu(0,\varepsilon) \in \mathcal{O}(\varepsilon), \qquad \partial_y\mu(0,\varepsilon) = \partial_y f_0(0,0) + \varepsilon\partial_y\phi_2(0,\varepsilon) = \partial_y f(0,0,0) + \varepsilon\partial_y\phi_2(0,\varepsilon) < 0$$

for ε sufficiently small, as $\partial_y f(0,0,0) < 0$ by condition (2.14) and $\phi_2(0,\varepsilon)$ is a smooth function. Hence, by the Inverse Function Theorem A.3, locally near $(0,0,0)$ a smooth inverse function $y(\mu,\varepsilon)$ of $\mu(y,\varepsilon)$ with $y(0,\varepsilon) \in \mathcal{O}(\varepsilon)$ exists. For the derivative μ' it holds

$$\mu'(y,\varepsilon) = \partial_y f_0(0,0)y' + yy'\phi_1(y,\varepsilon) + y^2\phi_1'(y,\varepsilon)y' + \varepsilon\phi_2'(y,\varepsilon)y' = \partial_y f_0(0,0)y' + \mathcal{O}(\varepsilon y,\varepsilon^2).$$

The ODE in ξ becomes with the variable μ

$$\xi' = \mu(y,\varepsilon) + b(y,\varepsilon)\xi^2 + \mathcal{O}(\xi^3,\varepsilon),$$

where $b(y,\varepsilon) = f_2(0,0) + \mathcal{O}(y,\varepsilon) \in \mathcal{O}(1)$ is a smooth function with

$$b(0,\varepsilon) = f_2(0,0) + \mathcal{O}(\varepsilon) = \partial_{xx} f(0,0,0) + \mathcal{O}(\varepsilon) > 0$$

by condition (2.7) and ε sufficiently small. Let $\eta = b(y,\varepsilon)\xi$. Then

$$\eta'(y,\varepsilon) = b(y,\varepsilon)\xi' + b'(y,\varepsilon)\xi = b(y,\varepsilon)\xi' + \mathcal{O}(y'\xi) = b(y,\varepsilon)\xi' + \mathcal{O}(\varepsilon).$$

Furthermore let $\beta = b(y,\varepsilon)\mu(y,\varepsilon)$, such that β has the opposite sign to y. With these relationships the ODE in ξ transforms into

$$\begin{aligned} & \xi' = \mu(y,\varepsilon) + b(y,\varepsilon)\xi^2 + \mathcal{O}(\xi^3,\varepsilon) \\ \Leftrightarrow \quad & b(y,\varepsilon)\xi' = b(y,\varepsilon)\mu(y) + b(y,\varepsilon)^2\xi^2 + \mathcal{O}((b\xi)^3, b\varepsilon) \\ \Leftrightarrow \quad & \eta' = \beta + \eta^2 + \mathcal{O}(\eta^3,\varepsilon). \end{aligned}$$

For the ODE in y respectively β it follows

$$\begin{aligned} \beta' &= b(y,\varepsilon)\mu'(y,\varepsilon) + b'(y,\varepsilon)\mu(y,\varepsilon) \\ &= (f_2(0,0) + \mathcal{O}(y,\varepsilon))(\partial_y f_0(0,0)y' + \mathcal{O}(\varepsilon y,\varepsilon^2)) + \mathcal{O}(y')(\partial_y f_0(0,0)y + \mathcal{O}(y^2,\varepsilon)) \\ &= f_2(0,0)\partial_y f_0(0,0)(\varepsilon g(0,0,0) + \mathcal{O}(\varepsilon x,\varepsilon y,\varepsilon^2)) + \mathcal{O}(\varepsilon x,\varepsilon y,\varepsilon^2) \\ &= \varepsilon f_2(0,0)\partial_y f_0(0,0)g(0,0,0) + \mathcal{O}(\varepsilon\eta,\varepsilon\beta,\varepsilon^2). \end{aligned}$$

With the change of variables $\nu = \varepsilon f_2(0,0)\partial_y f_0(0,0)g(0,0,0)$, we obtain

$$\beta' = \beta + \nu + \mathcal{O}(\nu\eta,\nu\beta,\nu^2).$$

As $\varepsilon \in \mathcal{O}(\nu)$, this implies for the map in η, that

$$\eta' = \beta + \eta^2 + \mathcal{O}(\eta^3,\nu).$$

The result follows by renaming the variables. □

Through the conditions in (2.7), we determined the sign of the terms y and x^2 in the fast dynamics. This is no restriction, as through the coordinate changes $x \mapsto -x$ and $y \mapsto -y$, each variant of the normal forms

$$x' = \pm x^2 \pm y + \mathcal{O}(x^3, \varepsilon)$$

of the fast dynamics can be obtained. The direction of the reduced flow is determined locally near the origin by the sign of $g(0,0,0)$. The sign in front of the term ε is the same as in the ODE for y in Proposition 2.3. In this thesis, we restrict ourselves to the case $g(0,0,0) < 0$, such that the reduced flow on the critical manifold is directed towards the origin, as visualized in Figure 2.1. The case $g(0,0,0) > 0$ can be treated in a similar way.

To save computational effort, we use throughout this thesis the normal form of the *continuous fast-slow fold singularity* without the higher order terms, which is given by

$$\begin{aligned} x' &= x^2 - y \\ y' &= -\varepsilon. \end{aligned} \tag{2.8}$$

System (2.8) is a fast-slow version of the one-dimensional *continuous fold bifurcation* with normal form

$$x' = x^2 - y = f(x, y), \tag{2.9}$$

where $x \in \mathbb{R}$ is a variable and $y \in \mathbb{R}$ is a parameter. Dependent on the value of the parameter y, a different dynamical behavior is observed. The linearization around an equilibrium x^* is given by $\partial_x f(x^*, y^*) = 2x^*$. For $y^* = 0$, system (2.9) has the non-hyperbolic equilibrium $x^* = 0$. For $y^* < 0$, no equilibria exist and for $y^* > 0$, there are two equilibria: the stable equilibrium $x^* = -\sqrt{y}$ with linearization $\partial_x f(x^*, y^*) < 0$ and the unstable equilibrium $x^* = \sqrt{y}$ with linearization $\partial_x f(x^*, y^*) > 0$. The fundamental change of the phase portrait under parameter variation is called a *bifurcation* and the non-hyperbolic fixed point $(x^*, y^*) = (0,0)$ is called the *fold point* [19]. A visualization of the continuous fold bifurcation is shown in Figure 2.3.

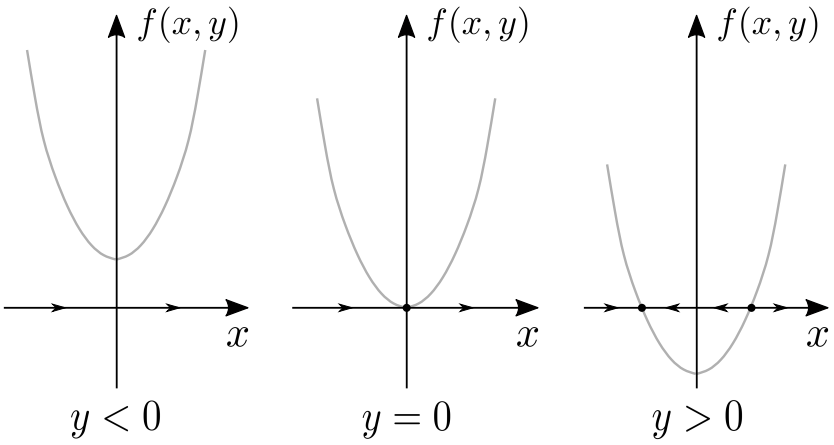


Figure 2.3.: One-dimensional continuous fold bifurcation.

In the fast-slow system (2.8), y is not constant, but decreases in an ε-dependent way. The following lemma shows for the normal form of the continuous fold bifurcation (2.9), in which y is a parameter, that the qualitative behavior near the origin is not influenced by higher order terms.

Lemma 2.4 [19]**.** *Near the origin, the system*

$$x' = x^2 - y + \mathcal{O}(x^3)$$

is locally topologically equivalent to the system

$$x' = x^2 - y.$$

Hence, system (2.8) can also be derived from the normal form in Lemma 2.4 by allowing for a simple evolution in y.

2.2.2. Discrete Fast-Slow Fold Singularity

Similar to the continuous case, we now derive the normal form of the *discrete fast-slow fold singularity*. To that end, we consider the singularly perturbed map

$$\begin{aligned} x &\mapsto x + \ f(x, y, \varepsilon), \\ y &\mapsto y + \varepsilon g(x, y, \varepsilon), \end{aligned} \tag{2.10}$$

with $(x, y) \in \mathbb{R}^2$, a 'time scale' parameter $0 < \varepsilon \ll 1$ and two functions $f : \mathbb{R}^3 \to \mathbb{R}$ and $g : \mathbb{R}^3 \to \mathbb{R}$, which are at least C^2. In the singular limit $\varepsilon = 0$, we assume that system (2.10) has a non-hyperbolic fixed point at $(0, 0) \in \mathbb{R}^2$, which is defined by the conditions

$$f(0, 0, 0) = 0, \qquad \frac{\partial f}{\partial x}(0, 0, 0) = 0. \tag{2.11}$$

Again, it is no restriction to assume that the fixed point is located at the origin $(0, 0) \in \mathbb{R}^2$, as it is possible to shift coordinates in the phase space. Furthermore, we suppose that in system (2.10) the following non-degeneracy conditions hold for the map in x [19]:

$$\frac{\partial^2 f}{\partial x^2}(0, 0, 0) \neq 0, \qquad \frac{\partial f}{\partial y}(0, 0, 0) \neq 0. \tag{2.12}$$

For the map in y we assume the non-degeneracy condition

$$g(0, 0, 0) \neq 0. \tag{2.13}$$

The interpretation of the non-degeneracy conditions is the same as in the continuous case: the first condition guarantees, that the term x^2 does not vanish in the Taylor expansion of the function f. The second condition ensures, that the multiplier $\lambda(y)$ of the map in x transverses the unit circle with non-zero speed. The last condition guarantees, that a slow passage through the non-hyperbolic fixed point $(0, 0)$ is described for all $\varepsilon > 0$. Without loss of generality, we assume that

$$\frac{\partial^2 f}{\partial x^2}(0, 0, 0) > 0, \qquad \frac{\partial f}{\partial y}(0, 0, 0) < 0. \tag{2.14}$$

In the following proposition, the normal form of the discrete fast-slow fold singularity is derived, which is specified by the conditions (2.11) - (2.14).

Proposition 2.5. *Suppose, that the two-dimensional map* (2.10) *with* $(x, y) \in \mathbb{R}^2$*, the parameter* $0 < \varepsilon \ll 1$ *and the functions* $f : \mathbb{R}^3 \to \mathbb{R}$*,* $g : \mathbb{R}^3 \to \mathbb{R}$ *with* $f, g \in C^2$*, fulfills the conditions* (2.11) - (2.14)*. Then system* (2.10) *is locally near* $(x, y, \varepsilon) = (0, 0, 0)$ *topologically equivalent to either of the maps*

$$\begin{aligned} x &\mapsto x + x^2 - y + \mathcal{O}\left(x^3, \varepsilon\right), \\ y &\mapsto y \pm \varepsilon + \mathcal{O}\left(\varepsilon x, \varepsilon y, \varepsilon^2\right). \end{aligned}$$

Proof. The idea of the proof is based on [19], where the normal form of the one-dimensional discrete fold bifurcation is derived. In the map (2.10), we consider additionally the parameter ε and the slow dynamics in the variable y. Throughout the proof we mark next iterates under the map (2.10) by a tilde. i.e. we write $(x, y) \mapsto (\tilde{x}, \tilde{y})$.

The Taylor expansion of the function g near the origin is

$$g(x, y, \varepsilon) = g(0, 0, 0) + \mathcal{O}(x, y, \varepsilon).$$

By condition (2.13) it holds $g(0, 0, 0) \neq 0$. Hence, the map in y is given by

$$\tilde{y} = y + \varepsilon g(x, y, \varepsilon) = y + \varepsilon g(0, 0, 0) + \mathcal{O}(\varepsilon x, \varepsilon y, \varepsilon^2).$$

For the map in x we use that $\tilde{y} = y + \mathcal{O}(\varepsilon)$. The Taylor expansion of the function f near the origin is

$$f(x, y, \varepsilon) = f_0(y, \varepsilon) + f_1(y, \varepsilon)x + f_2(y, \varepsilon)x^2 + \mathcal{O}(x^3),$$

with $f_0(0,0) = f(0,0,0) = 0$ and $f_1(0,0) = \partial_x f(0,0,0) = 0$ by condition (2.12).

We now perform a coordinate change by introducing the variable ξ:

$$\xi = x + \delta(y, \varepsilon)$$

where the function $\delta(y, \varepsilon)$ with $\delta(0,0) = 0$ will be specified below. In the following, we abbreviate by $\delta \coloneqq \delta(y, \varepsilon)$ the value of the function δ at the current iterate (y, ε). The coordinate shift yields

$$\begin{aligned}
\tilde{\xi} &= \tilde{x} + \delta(\tilde{y}, \varepsilon) \\
&= x + f(x, y, \varepsilon) + \delta(\tilde{y}, \varepsilon) \\
&= \xi - \delta + f(\xi - \delta, y, \varepsilon) + \delta(\tilde{y}, \varepsilon) \\
&= f_0(y, \varepsilon) + f_1(y, \varepsilon)(\xi - \delta) + f_2(y, \varepsilon)(\xi - \delta)^2 + \mathcal{O}\left((\xi - \delta)^3\right) + \xi - \delta + \delta(\tilde{y}, \varepsilon) \\
&= [f_0(y, \varepsilon) - f_1(y, \varepsilon)\delta + f_2(y, \varepsilon)\delta^2 + \mathcal{O}(\delta^3)] \\
&\quad + \xi + [f_1(y, \varepsilon) - 2f_2(y, \varepsilon)\delta + \mathcal{O}(\delta^2)]\xi + [f_2(y, \varepsilon) + \mathcal{O}(\delta)]\xi^2 + \mathcal{O}\left(\xi^3\right) - \delta + \delta(\tilde{y}, \varepsilon).
\end{aligned}$$

We can eliminate the linear term in ξ in the parentheses with the Implicit Function Theorem A.2. Let

$$F(y, \varepsilon, \delta) \coloneqq [f_1(y, \varepsilon) - 2f_2(y, \varepsilon)\delta + \delta^2\psi(y, \varepsilon, \delta)] \stackrel{!}{=} 0$$

with some smooth function ψ. By condition (2.12) it follows

$$\partial_\delta F(0,0,0) = -2f_2(0,0) = -2\partial_{xx} f(0,0,0) \neq 0.$$

Furthermore, we have $F(0,0,0) = 0$, such that the Implicit Function Theorem A.2 implies, that locally near $(0,0,0)$ a unique smooth function $\delta(y, \varepsilon)$ exists, such that $\delta(0,0) = 0$ and $F(y, \varepsilon, \delta(y, \varepsilon)) \equiv 0$. To find an expression for the function $\delta(y, \varepsilon)$, we Taylor-expand the functions $f_1(y, \varepsilon)$ and $f_2(y, \varepsilon)$ and use condition (2.11):

$$\begin{aligned}
f_1(y, \varepsilon) &= f_1(0,0) + \partial_y f_1(0,0)y + \partial_\varepsilon f_1(0,0)\varepsilon + \mathcal{O}(y^2, \varepsilon^2, \varepsilon y) \\
&= \partial_y f_1(0,0)y + \mathcal{O}(y^2, \varepsilon), \\
f_2(y, \varepsilon) &= f_2(0,0) + \partial_y f_2(0,0)y + \partial_\varepsilon f_2(0,0)\varepsilon + \mathcal{O}(y^2, \varepsilon^2, \varepsilon y) \\
&= f_2(0,0) + \partial_y f_2(0,0)y + \mathcal{O}(y^2, \varepsilon).
\end{aligned}$$

Plugging these expressions into the equation $F(y, \varepsilon, \delta) = 0$ leads to

$$\delta(y, \varepsilon) = \frac{\partial_y f_1(0,0)}{2f_2(0,0)}y + \mathcal{O}(y^2, \varepsilon) \in \mathcal{O}(y, \varepsilon).$$

As y is evolving slowly in time, it holds

$$\delta(\tilde{y}, \varepsilon) = \frac{\partial_y f_1(0,0)}{2f_2(0,0)}(y + \mathcal{O}(\varepsilon)) + \mathcal{O}((y + \mathcal{O}(\varepsilon))^2, \varepsilon) = \delta(y, \varepsilon) + \mathcal{O}(\varepsilon).$$

With

$$\begin{aligned}
f_0(y, \varepsilon) &= f_0(0,0) + \partial_y f_0(0,0)y + \partial_\varepsilon f_0(0,0)\varepsilon + \mathcal{O}(y^2, \varepsilon^2, \varepsilon y) \\
&= \partial_y f_0(0,0)y + \mathcal{O}(y^2, \varepsilon),
\end{aligned}$$

the map written in terms of ξ is given by

$$\tilde{\xi} = [\partial_y f_0(0,0)y + \mathcal{O}(y^2, \varepsilon)] + \xi + [f_2(0,0) + \mathcal{O}(y, \varepsilon)]\xi^2 + \mathcal{O}(\xi^3, \varepsilon).$$

We introduce now as a new variable the leading order term of the map above:

$$\mu(y,\varepsilon) \coloneqq \partial_y f_0(0,0)y + y^2\phi_1(y,\varepsilon) + \varepsilon\phi_2(y,\varepsilon),$$

where ϕ_1 and ϕ_2 are smooth functions. It holds $\partial_y f_0(0,0) = \partial_y f(0,0,0) < 0$, hence μ has locally the opposite sign to y. It holds

$$\mu(0,\varepsilon) \in \mathcal{O}(\varepsilon), \qquad \partial_y\mu(0,\varepsilon) = \partial_y f_0(0,0) + \varepsilon\partial_y\phi_2(0,\varepsilon) = \partial_y f(0,0,0) + \varepsilon\partial_y\phi_2(0,\varepsilon) < 0$$

for ε sufficiently small, as $\partial_y f(0,0,0) < 0$ by condition (2.14) and $\phi_2(0,\varepsilon)$ is a smooth function. Hence, by the Inverse Function Theorem A.3, locally near $(0,0,0)$ a smooth inverse function $y(\mu,\varepsilon)$ of $\mu(y,\varepsilon)$ with $y(0,\varepsilon) \in \mathcal{O}(\varepsilon)$ exists. As y is evolving slowly in time, also μ evolves slowly in time such that it holds

$$\begin{aligned}\tilde{\mu} &\coloneqq \mu(\tilde{y},\varepsilon)\\ &= \partial_y f_0(0,0)(y + \varepsilon g(0,0,0) + \mathcal{O}(\varepsilon x, \varepsilon y, \varepsilon^2)) + (y + \mathcal{O}(\varepsilon))^2\phi_1(y + \mathcal{O}(\varepsilon),\varepsilon) + \varepsilon\phi_2(y + \mathcal{O}(\varepsilon),\varepsilon)\\ &= \mu(y,\varepsilon) + \varepsilon\partial_y f_0(0,0)\varepsilon g(0,0,0) + \mathcal{O}(\varepsilon x, \varepsilon y, \varepsilon^2).\end{aligned}$$

The map in ξ becomes

$$\tilde{\xi} = \mu(y,\varepsilon) + \xi + b(y,\varepsilon)\xi^2 + \mathcal{O}(\xi^3,\varepsilon),$$

where $b(y,\varepsilon) = f_2(0,0) + \mathcal{O}(y,\varepsilon) \in \mathcal{O}(1)$ is a smooth function with

$$b(0,\varepsilon) = f_2(0,0) + \mathcal{O}(\varepsilon) = \partial_{xx} f(0,0,0) + \mathcal{O}(\varepsilon) > 0$$

by condition (2.14) and ε sufficiently small. As y is evolving slowly in time, also $b(y,\varepsilon)$ evolves slowly in time with

$$\tilde{b} \coloneqq b(\tilde{y},\varepsilon) = f_2(0,0) + \mathcal{O}(y + \mathcal{O}(\varepsilon),\varepsilon) = b(y,\varepsilon) + \mathcal{O}(\varepsilon).$$

Let $\eta = b(y,\varepsilon)\xi$. Then

$$\tilde{\eta} = \tilde{b}\tilde{\xi} = (b(y,\varepsilon) + \mathcal{O}(\varepsilon))\tilde{\xi} = b(y,\varepsilon)\tilde{\xi} + \mathcal{O}(\varepsilon).$$

Define additionally $\beta = b(y,\varepsilon)\mu$, such that β has the opposite sign to y. With these relationships the map above transforms into

$$\begin{aligned} & \tilde{\xi} = \mu(y,\varepsilon) + \xi + b(y,\varepsilon)\xi^2 + \mathcal{O}(\xi^3,\varepsilon)\\ \Leftrightarrow \quad & b(y,\varepsilon)\tilde{\xi} = b(y,\varepsilon)\mu(y) + b(y,\varepsilon)\xi + b(y,\varepsilon)^2\xi^2 + \mathcal{O}((b\xi)^3, b\varepsilon)\\ \Leftrightarrow \quad & \tilde{\eta} = \beta + \eta + \eta^2 + \mathcal{O}(\eta^3,\varepsilon).\end{aligned}$$

For the map in y respectively β it holds

$$\begin{aligned}\tilde{\beta} &= \tilde{b}\tilde{\mu}\\ &= (b(y,\varepsilon) + \mathcal{O}(\varepsilon))(\mu(y,\varepsilon) + \varepsilon\partial_y f_0(0,0)\varepsilon g(0,0,0) + \mathcal{O}(\varepsilon x, \varepsilon y, \varepsilon^2))\\ &= \beta + \varepsilon\partial_y f_0(0,0)g(0,0,0)b(y,\varepsilon) + \mathcal{O}(\varepsilon x, \varepsilon y, \varepsilon^2)\\ &= \beta + \varepsilon\partial_y f_0(0,0)g(0,0,0)f_2(0,0) + \mathcal{O}(\varepsilon\xi, \varepsilon\beta, \varepsilon^2).\end{aligned}$$

With the change of variables $\nu = \varepsilon\partial_y f_0(0,0)g(0,0,0)f_2(0,0)$, we obtain

$$\tilde{\beta} = \beta + \nu + \mathcal{O}(\nu\xi, \nu\beta, \nu^2).$$

As $\varepsilon \in \mathcal{O}(\nu)$, this implies for the map in η, that

$$\tilde{\eta} = \beta + \eta + \eta^2 + \mathcal{O}(\eta^3, \nu).$$

The result follows by renaming the variables. □

The conditions (2.14) specified the sign of the terms y and x^2 in the map for the fast dynamics. Through the coordinate changes $x \mapsto -x$ and $y \mapsto -y$, each variant of the normal forms

$$x \mapsto x \pm x^2 \pm y + \mathcal{O}(x^3, \varepsilon)$$

of the fast dynamics can be obtained. Locally near the origin, the direction of the map in y is determined by the sign of $g(0,0,0)$, which is the same sign as in front of the term ε in the map for y in Proposition 2.5. Analogously to the continuous case, we restrict ourselves to the case $g(0,0,0) < 0$, the case $g(0,0,0) > 0$ can be treated in a similar way.

To save computational effort, we use throughout this thesis the normal form of the *discrete fast-slow fold singularity* without the higher order terms, which is given by

$$\begin{aligned} x &\mapsto x + x^2 - y, \\ y &\mapsto y - \varepsilon. \end{aligned} \tag{2.15}$$

System (2.15) is a fast-slow version of the one-dimensional *discrete fold bifurcation*, occurring in the map

$$x \mapsto x + x^2 - y = h(x, y) \tag{2.16}$$

where $x \in \mathbb{R}$ is a variable and $y \in \mathbb{R}$ is a parameter. Dependent on the value of the parameter y, system (2.16) shows different dynamical behavior. The linearization around a fixed point x^* is given by $\partial_x h(x^*, y^*) = 1 + 2x^*$. For $y^* = 0$, system (2.16) has the non-hyperbolic fixed point $x^* = 0$. For $y^* < 0$, no fixed point exist and for $y^* > 0$, two fixed points arise: locally near the origin, the fixed point $x^* = -\sqrt{y}$ is stable with linearization $|\partial_x h(x^*, y^*)| < 1$ and the fixed point $x^* = \sqrt{y}$ is unstable with linearization $|\partial_x h(x^*, y^*)| > 1$. A visualization of the discrete fold bifurcation is shown in Figure 2.4. The iterates in a neighborhood of the fold point $(x^*, y^*) = (0, 0)$ are depicted by cobwebbing [19].

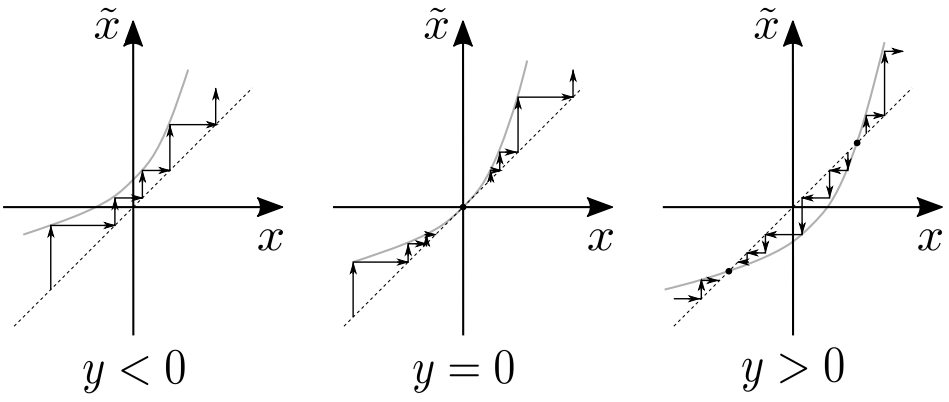


Figure 2.4.: One-dimensional discrete fold bifurcation visualized by cobwebbing.

In the normal form of the discrete fast-slow fold singularity (2.15), y is not fixed, but decreases in an ε-dependent way. For the normal form of the one-dimensional discrete fold bifurcation (2.16), the qualitative behavior of the map (2.16) near the origin is not influenced by higher order terms, as shown in the following lemma:

Lemma 2.6 [19]**.** *Near the origin the map*

$$x \mapsto x + x^2 - y + \mathcal{O}(x^3)$$

is locally topologically equivalent to the map

$$x \mapsto x + x^2 - y.$$

Hence, the fast-slow map (2.15) can also be derived from the normal form in Lemma 2.6 by adding a slow parameter drift in y.

2.3. Geometric Singular Perturbation Theory

In this section, we introduce geometric singular perturbation theory and Fenichel's Theorems for continuous fast-slow systems. We use the notation for fast-slow ordinary differential equations introduced in Section 2.1.1. In the singular limit $\varepsilon = 0$, the dynamics is subdivided into the layer problem and the reduced problem. The slow flow of the reduced problem is restricted to the critical manifold S_0. Fenichel theory characterizes, how and under which conditions the critical manifold S_0 persists as a nearby slow manifold S_ε for $\varepsilon > 0$.

To state Fenichel's Theorems, we define normal hyperbolicity for the critical manifold S_0.

Definition 2.7 [18]. *A subset $S \subset S_0$ of the critical manifold is called normally hyperbolic, if all eigenvalues of the Jacobian matrix $\mathrm{D}_x f(x, y, 0) \in \mathbb{R}^{m\times m}$ of the fast variables have non-zero real part for all $(x, y) \in S$.*

An equilibrium point is defined to be hyperbolic, if its Jacobian matrix has no eigenvalue with zero real part. Consequently, a subset $S \subset S_0$ is normally hyperbolic if and only if for every point $(x^*, y^*) \in S$, it holds that x^* is a hyperbolic equilibrium point of the corresponding layer problem $x' = f(x, y^*, 0)$, where y^* is considered as a parameter. Dependent on the direction of the fast flow, the hyperbolic parts of the critical manifold can be attracting, repelling or saddle type.

Definition 2.8 [18]. *A normally hyperbolic subset $S \subset S_0$ of the critical manifold is called attracting (repelling), if all eigenvalues of the Jacobian matrix $\mathrm{D}_x f(x, y, 0) \in \mathbb{R}^{m\times m}$ of the fast variables have negative (positive) real part for all $(x, y) \in S$. The subset $S \subset S_0$ is called to be of saddle type, if it is normally hyperbolic, but neither attracting nor repelling.*

Fenichel theory now describes, how the normally hyperbolic parts of the critical manifold S_0 perturb to slow manifolds S_ε for small $\varepsilon > 0$. The restriction to the slow manifold is a small, smooth perturbation of the slow subsystem.

Theorem 2.9 (Fenichel's Theorems) [18]. *Let $S \subset S_0$ be a compact normally hyperbolic submanifold (possibly with boundary) of the critical manifold S_0 of a fast-slow ODE system*

$$\begin{aligned} x' &= f(x, y, \varepsilon), \\ y' &= \varepsilon g(x, y, \varepsilon), \end{aligned}$$

with $x \in \mathbb{R}^m$, $y \in \mathbb{R}^n$, $\varepsilon \in \mathbb{R}$ and $f, g \in C^r$, $r \geq 1$. Then it holds for $\varepsilon > 0$ sufficiently small:

(a) There exists a locally invariant manifold S_ε, called the slow manifold, which is diffeomorphic to the critical manifold S_0. Local invariance means, that trajectories can enter or leave the slow manifold S_ε only through its boundaries.

(b) The slow manifold S_ε has Hausdorff distance $\mathcal{O}(\varepsilon)$ from the critical manifold S_0, i.e.

$$d_H(S_\varepsilon, S_0) := \max\left\{ \sup_{v\in S_\varepsilon} \inf_{w\in S_0} \|v - w\|, \sup_{w\in S_0} \inf_{v\in S_\varepsilon} \|v - w\| \right\} \qquad \text{as } \varepsilon \to 0.$$

(c) The flow on the slow manifold S_ε converges to the slow flow on S_0 as $\varepsilon \to 0$.

(d) The slow manifold S_ε is, like the critical manifold S_0, C^r-smooth.

(e) The slow manifold S_ε is normally hyperbolic and has with respect to the fast variables the same stability properties as the critical manifold S_0.

(f) The slow manifold S_ε is usually not unique. Locally, all manifolds satisfying the conditions (a)-(e) lie in a Hausdorff distance $\mathcal{O}\left(e^{-K/\varepsilon}\right)$ from each other for some constant $K > 0$.

The conclusions (a)-(f) made for the critical manifold S_0 also hold locally for its stable and unstable manifolds, which are defined as

$$\mathcal{W}^s_{loc}(S_0) := \bigcup_{p\in S_0} \mathcal{W}^s_{loc}(p), \qquad \mathcal{W}^u_{loc}(S_0) := \bigcup_{p\in S_0} \mathcal{W}^u_{loc}(p),$$

where all points $p \in S_0$ are by definition equilibria of the layer problem. For $\varepsilon > 0$ sufficiently small, also the manifolds $\mathcal{W}^s_{loc}(S_0)$ and $\mathcal{W}^u_{loc}(S_0)$ persist as local stable and unstable manifolds $\mathcal{W}^s_{loc}(S_\varepsilon)$ and $\mathcal{W}^u_{loc}(S_\varepsilon)$ respectively. The conclusions (a)-(f) hold by replacing S_ε and S_0 by $\mathcal{W}^s_{loc}(S_\varepsilon)$ and $\mathcal{W}^s_{loc}(S_0)$ or $\mathcal{W}^u_{loc}(S_\varepsilon)$ and $\mathcal{W}^u_{loc}(S_0)$.

In the following example, we illustrate the definition of normal hyperbolicity and Fenichel's Theorems for the normal form of the continuous fast-slow fold singularity.

Example 2.10. *In the case of the normal form of the continuous fast-slow fold singularity*

$$\begin{aligned} x' &= x^2 - y, \\ y' &= -\varepsilon, \end{aligned}$$

the Jacobian matrix $D_x f(x, y, 0) \in \mathbb{R}$ of the fast variables is given by

$$D_x f(x, y, 0) = 2x.$$

Hence, the critical manifold

$$S_0 = \{(x, y) \in \mathbb{R}^2 : y = x^2\}$$

subdivides into the singular point $S_0^c := \{(x, y) \in S_0 : x = 0\}$, the attracting branch $S_0^a := \{(x, y) \in S_0 : x < 0\}$ and the repelling branch $S_0^r := \{(x, y) \in S_0 : x > 0\}$, which are visualized in Figure 2.5.

By Fenichel's Theorems, for $\varepsilon > 0$ sufficiently small, compact submanifolds of the attracting branch S_0^a and the repelling branch S_0^r perturb to nearby slow manifolds S_ε^a and S_ε^r. The two slow manifolds as well as a solution of the layer problem are shown in Figure 2.5. It has to be analyzed how the attracting slow manifold extends into a neighborhood of the fold point.

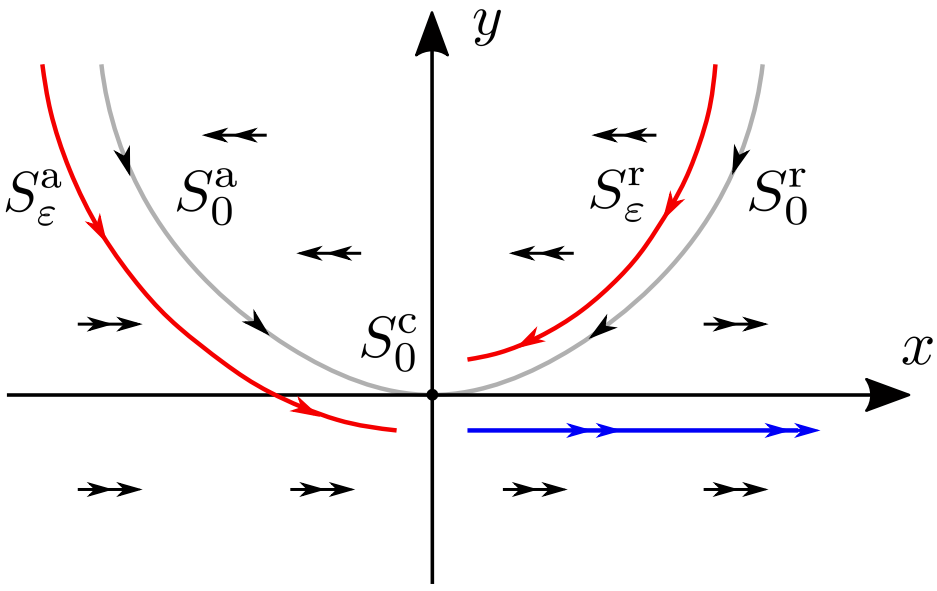


Figure 2.5.: The critical manifold S_0 of the normal form of the continuous fast-slow fold singularity subdivides in the singular point S_0^c, an attracting branch S_0^{a} and a repelling branch S_0^{r}. The two normally hyperbolic branches perturb for $\varepsilon > 0$ to the slow manifolds $S_\varepsilon^{\mathrm{a}}$ and $S_\varepsilon^{\mathrm{r}}$, which are shown in red. Furthermore, a solution of the layer problem is visualized in blue.

The geometric theory near the normally hyperbolic parts of a critical manifold S_0 of a fast-slow ODE system is quite complete. Issues occur at the singular points, where normal hyperbolicity breaks down. To analyze, how the slow manifold behaves close to a singular point, other techniques like the blowup method are used, which is introduced for continuous fast-slow systems in the following Section 2.4.

Remark 2.11. *To the best of our knowledge, no direct analogue of geometric singular perturbation theory for maps existed during the creation of this master's thesis. In the discrete setting, also an abstract invariant manifold theory is provided for the 'normally hyperbolic' parts of the critical manifold by Hirsch, Pugh and Shub [13] or Pötzsche [23]. In Nipp and Stoffer [21, 22] a more applicable theory is presented based on the identification of suitable coordinates. For a geometric analysis of maps, the distinction of two non-equivalent limiting problems like the layer and the reduced problem is not directly transferable from the continuous case, as we cannot identify a 'slow time scale'. During the writing of this master's thesis, Jelbart and Kühn [15] proposed a discrete geometric singular perturbation theory in which limiting problems associated to both 'fast' and 'slow' iteration under the map can be coupled to the invariant manifold theory in the works by Nipp and Stoffer cited above.*

2.4. Blowup Method

In the context of the Van der Pol equation, Dumortier and Roussarie showed first, that the blowup method may be useful to study singularities in continuous fast-slow systems by inserting a suitable manifold at the singularity, for example a sphere [8].

In the following, we introduce the polar blowup method and its improvement for quasi-homogeneous vector fields, which allows for more efficient computations. We start with general ODE systems and show in an example, how to apply the blowup method to fast-slow systems.

For $x \in \mathbb{R}^n$, we consider the ODE system

$$x' = F(x), \tag{2.17}$$

where $F : \mathbb{R}^n \to \mathbb{R}^n$ is a smooth vector field with $F(0) = 0$, such that system (2.17) has an equilibrium at the origin. The idea of the polar blowup is to insert a sphere at the equilibrium point, such that this point is blown-up to a sphere. The unit $(n\text{-}1)$-sphere in $\mathbb{R}^n$ is defined as

$$S^{n-1} := \{x \in \mathbb{R}^n : \|x\|_2 = 1\},$$

where $\|x\|_2 = \left(\sum_{i=1}^n x_i^2\right)^{\frac{1}{2}}$ denotes the Euclidean norm of $x \in \mathbb{R}^n$. For two-dimensional ODE systems, the polar blowup can be defined in the following way:

Definition 2.12 [18]**.** *Let $I \subset \mathbb{R}$ be a (possibly infinite) interval with $0 \in I$ and $\theta \in [0, 2\pi)$ be a parametrization of the unit circle $S^1 \subset \mathbb{R}^2$. Consider the polar coordinate transformation*

$$\varphi : S^1 \times I \to \mathbb{R}^2, \quad \varphi(\theta, \rho) = (\rho \cos\theta, \rho \sin\theta).$$

Then the polar blowup $\hat{F}$ of a C^∞ vector field $F : \mathbb{R}^2 \to \mathbb{R}^2$ with $F(0) = 0$ is for $\rho \neq 0$ defined by

$$\hat{F}(\theta, \rho) := (D\varphi^{-1}_{(\theta,\rho)} \circ F \circ \varphi)(\theta, \rho) \tag{2.18}$$

and for $\rho = 0$ by continuous extension of (2.18)*.*

The polar blowup $\hat{F}$ is a vector field on $S^1 \times I$. A common choice, for which it is easy to visualize the planar blowup, is $I = [0, \infty)$. Then θ describes the angle and $\rho \in I$ is the radial component of the usual polar coordinates. The diffeomorphic structure of the polar coordinate transformation φ is clear for $(\theta, \rho) \in S^1 \times (0, \infty)$. By Proposition A.6, the vector field F and its polar blowup $\hat{F}$ are locally conjugate for $(\theta, \rho) \in S^1 \times (0, \infty)$ and they are related by formula (2.18). For $\rho = 0$, the polar coordinate transformation φ is not one-to-one, such that the origin is blown-up to a circle by its inverse φ^{-1}.

Example 2.13. *In Figure 2.6, the polar blowup is visualized for the planar vector field*

$$x_1' = -x_1^3,$$
$$x_2' = x_2^3,$$

which has a non-hyperbolic equilibrium at the origin $(0,0)$*. Applying the polar coordinate transformation of Definition 2.12 leads to the polar blowup*

$$\hat{F}(\theta,\varphi) = \rho^2 \begin{pmatrix} \sin\theta\cos\theta \\ \rho\sin^3\theta - \rho\cos^3\theta \end{pmatrix}.$$

By Theorem A.8, dividing the vector field $\hat{F}$ *by the common factor* ρ^2 *does not change the orbits and therefore also not the qualitative structure of the corresponding ODE system outside of the circle* $S^1 \times \{\rho = 0\}$*. On* $S^1 \times \{\rho = 0\}$*, there are four equilibria, which are all hyperbolic saddles for the vector field* $\frac{1}{\rho^2}\hat{F}$*. Thus, we have desingularized the vector field* F*, by blowing it up to a circle with four hyperbolic equilibria on it.*

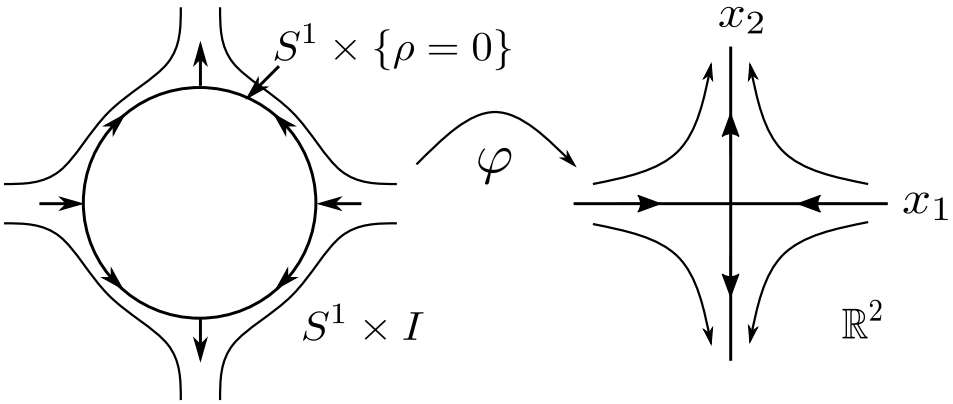


Figure 2.6.: Visualization of the two-dimensional polar blowup in Example 2.13. A non-hyperbolic equilibrium is desingularized by blowing it up to a circle with four hyperbolic equilibria on it.

In more than two dimensions, it becomes complicated using explicit trigonometric functions to parameterize the unit sphere S^{n-1} in $\mathbb{R}^n$. Hence, we generalize the polar blowup in $\mathbb{R}^n$ in the following way:

Definition 2.14 [18]**.** *Let* $I \subset \mathbb{R}$ *be a (possibly infinite) interval with* $0 \in I$*. Consider the generalized polar coordinate transformation*

$$\varphi : S^{n-1} \times I \to \mathbb{R}^n, \quad \varphi(\bar{z}_1, \ldots, \bar{z}_n, \rho) = (\rho\bar{z}_1, \ldots, \rho\bar{z}_n),$$

where $\bar{z} = (\bar{z}_1, \ldots, \bar{z}_n) \in S^{n-1}$*. Then the polar blowup* $\hat{F}$ *of a* C^∞ *vector field* $F : \mathbb{R}^n \to \mathbb{R}^n$ *with* $F(0) = 0$ *is for* $\rho \neq 0$ *defined by*

$$\hat{F}(\bar{z}_1, \ldots, \bar{z}_n, \rho) = (D\varphi^{-1}_{(\bar{z}_1,\ldots,\bar{z}_n,\rho)} \circ F \circ \varphi)(\bar{z}_1, \ldots, \bar{z}_n, \rho) \tag{2.19}$$

and for $\rho = 0$ *by continuous extension of* (2.19)*.*

The following theorem guarantees, that it is possible in Definition 2.14, and thus also in the special case of the planar polar blowup in Definition 2.12, to extend the blown-up vector field continuously in the limit $\rho = 0$.

Theorem 2.15 [24]**.** *Let* $F : \mathbb{R}^n \to \mathbb{R}^n$ *be a* C^∞ *vector field with* $F(0) = 0$*. Then the generalized polar blowup* $\hat{F}$ *in Definition 2.14 is a* C^∞ *vector field on* $S^{n-1} \times I$*.*

Our goal is to use the blowup method to desingularize vector fields. Often singularities of polynomial vector fields are more degenerate, such that after the blowup transformation a common factor ρ^k, $k \geq 1$ occurs in each component of the polar blowup $\hat{F}$ like in Example 2.13. Dividing a vector field by a factor ρ^k corresponds by Theorem A.8 to a positive transformation of time along the solution curves of the associated ODE. The qualitative structure of the original and the transformed system is the same, as they are orbitally equivalent. Dividing the blown-up vector field by a factor ρ until the vector field is not identically to zero on the sphere can result in a desingularization of the vector field. We characterize this phenomenon by introducing jets:

Definition 2.16 [18]. *The k-jet of a function $f : \mathbb{R} \to \mathbb{R}$ at a point $p \in \mathbb{R}$ is defined as the truncated Taylor polynomial*

$$j_k(f)(x) = f(p) + f'(p)x + \cdots + \frac{1}{k!}\left[\frac{\mathrm{d}^k f}{\mathrm{d}x^k}(p)\right] x^k.$$

Definition 2.17 [18]. *Let $F : \mathbb{R}^n \to \mathbb{R}^n$ be a C^∞ vector field with $F(0) = 0$ and denote by $F_i : \mathbb{R} \to \mathbb{R}$ the i-th component of F interpreted as a function of z_i, which denotes the i-th component of $z \in \mathbb{R}^n$. If it holds $j_l(F_i) = 0$ for $l \in \{0, 1, \ldots, k\}$ and $i \in \{1, \ldots, n\}$ at the equilibrium $p = 0$ and $j_{k+1}(F_i) \neq 0$ for some $i \in \{1, \ldots, n\}$ at $p = 0$, then we define the rescaled polar blowup by $\bar{F} := \frac{1}{\rho^k}\hat{F}$, where $\hat{F}$ denotes the polar blowup of F.*

For each division of a vector field by ρ, we lose one degree of differentiability, but as we consider only smooth vector fields, they stay smooth.

Sometimes it is necessary to apply several blowups to achieve a desingularization of a non-hyperbolic equilibrium. In the following, we introduce an improved method for quasi-homogeneous vector fields, where the particular structure of the vector field is used.

Definition 2.18 [18]. *A function $f : \mathbb{R}^n \to \mathbb{R}$ is called quasi-homogeneous of degree k and type $(a_1, \ldots, a_n) \in \mathbb{N}^n_{\geq 0}$, if for every $\rho \in \mathbb{R}$ it holds*

$$f(\rho^{a_1} z_1, \ldots, \rho^{a_n} z_n) = \rho^k f(z_1, \ldots, z_n).$$

A vector field $F : \mathbb{R}^n \to \mathbb{R}^m$ is called quasi-homogeneous of degree $k + 1$ and type $(a_1, \ldots, a_n)$ if its i-th component $F_i : \mathbb{R}^n \to \mathbb{R}$ is quasi-homogeneous of degree $k + a_j$ and type $(a_1, \ldots, a_n)$.

Then we can use this structure and improve the generalized polar blowup by weighting the coefficients of the coordinate transformation:

Definition 2.19 [18]. *Let $I \subset \mathbb{R}$ be a (possibly infinite) interval with $0 \in I$. Consider for $(a_1, \ldots, a_n) \in \mathbb{N}^n_{>0}$ the quasi-homogeneous coordinate transformation*

$$\varphi : S^{n-1} \times I \to \mathbb{R}^n, \quad \varphi(\bar{z}_1, \ldots, \bar{z}_n, \rho) = (\rho^{a_1}\bar{z}_1, \ldots, \rho^{a_n}\bar{z}_n),$$

where $\bar{z} = (\bar{z}_1, \ldots, \bar{z}_n) \in S^{n-1}$. Then the quasi-homogeneous blowup $\hat{F}$ of a C^∞ vector field $F : \mathbb{R}^n \to \mathbb{R}^n$ with $F(0) = 0$ is for $\rho \neq 0$ defined by

$$\hat{F}(\bar{z}_1, \ldots, \bar{z}_n, \rho) = (D\varphi^{-1}_{(\bar{z}_1, \ldots, \bar{z}_n, \rho)} \circ F \circ \varphi)(\bar{z}_1, \ldots, \bar{z}_n, \rho) \tag{2.20}$$

and for $\rho = 0$ by continuous extension of (2.20).

Denote by $F_i : \mathbb{R} \to \mathbb{R}$ the i-th component of F interpreted as a function of z_i, which is the i-th component of $z \in \mathbb{R}^n$. If it holds $j_l(F_i) = 0$ for $l \in \{0, 1, \ldots, k\}$ and $i \in \{1, \ldots, n\}$ at the equilibrium $p = 0$ and $j_{k+1}(F_i) \neq 0$ for some $i \in \{1, \ldots, n\}$ at $p = 0$, then we define the rescaled quasi-homogeneous blowup by $\bar{F} := \frac{1}{\rho^k}\hat{F}$.

In principle, it is possible to use spherical coordinates to calculate the quasi-homogeneous blowup, however this would lead to rather lengthy computations. This can be avoided by introducing different charts for the manifold $S^{n-1} \times I$ to simplify the analysis. The local analysis is then easier, but we have to work in multiple charts. In the following example of the normal form of the continuous fast-slow singularity, we sketch how to define the blowup in different charts.

Example 2.20. *To blow up the normal form of the continuous fast-slow fold singularity, we use the extended system*

$$\begin{aligned} x' &= x^2 - y, \\ y' &= -\varepsilon, \\ \varepsilon' &= 0, \end{aligned}$$

and observe, that this system is quasi-homogeneous of degree 2 and type $(1, 2, 3)$. *Hence, we define for a constant* $P > 0$ *the two manifolds*

$$B = S^2 \times \mathbb{R}, \qquad B_0 = S^2 \times [0, P]$$

and the blowup transformation

$$\varphi : B_0 \to \mathbb{R}^3 : (\bar{x}, \bar{y}, \bar{\varepsilon}, \rho) \mapsto (x, y, \varepsilon) = (\rho\bar{x}, \rho^2\bar{y}, \rho^3\bar{\varepsilon})$$

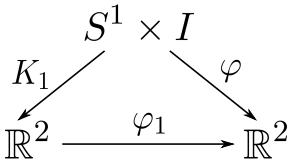
with $(\bar{x}, \bar{y}, \bar{\varepsilon}) \in S^2$ *[17]. We aim to introduce the chart* K_1 *by eliminating the variable* $\bar{y}$. *For the set* $B_{\bar{y}}^+ := \{(\bar{x}, \bar{y}, \bar{\varepsilon}, \rho) \in B : \bar{y} > 0\}$, *we consider the coordinate chart*

$$K_1 : B_{\bar{y}}^+ \to \mathbb{R}^3, \qquad K_1(\bar{x}, \bar{y}, \bar{\varepsilon}, \rho) = \left(\frac{\bar{x}}{\bar{y}^{b_1}}, \frac{\bar{\varepsilon}}{\bar{y}^{b_2}}, \frac{\rho}{\bar{y}^{b_3}} \right) = (x_1, \varepsilon_1, \rho_1)$$

with some coefficients $b_1, b_2, b_3 \in \mathbb{R}$ *[18]. Our goal is, that the polar blowup in the local coordinates of chart* K_1 *has the form*

$$\varphi_1(x_1, \varepsilon_1, \rho_1) = (x, y, \varepsilon) = (\rho_1 x_1, \rho_1^2, \rho_1^3 \varepsilon_1)$$

to reflect the structure of the quasi-homogeneous blowup in the hyperplane $\{\bar{y} = 1\}$. *The coefficients* $b_1, b_2, b_3 \in \mathbb{R}$ *should be chosen in the way, that the following diagram commutes:*



This condition is satisfied if $b_1 = \frac{1}{2}$, $b_2 = \frac{3}{2}$ *and* $b_3 = -\frac{1}{2}$. *In the same way, we can determine the coordinate chart* K_2 *by eliminating the variable* $\bar{\varepsilon}$ *and the coordinate chart* K_3 *by eliminating the variable* $\bar{x}$. *The dynamics locally near the fold point, which is blown-up to the sphere* S^2 *can then be analyzed in different charts and combined afterwards. In Figure 2.7, the manifold* B_0 *and the three charts are visualized.*

In Chapter 3, we define the system analyzed in this thesis and introduce the coordinate charts as well as the local polar blowups with more details.

Remark 2.21. *In principle, it is possible to apply the introduced blowup transformation to maps. The problem is, that no non-trivial flow is obtained on the sphere, as the desingularization step via time rescaling is not possible in the same way as in the continuous case. In Appendix E, an alternative way of rescaling the blown-up map is introduced, which leads in the case of the normal form of the discrete fast-slow fold singularity* (2.15) *to a non-trivial map on the sphere. The problem is, that all fixed points obtained on the sphere* S^2 *are still non-hyperbolic.*

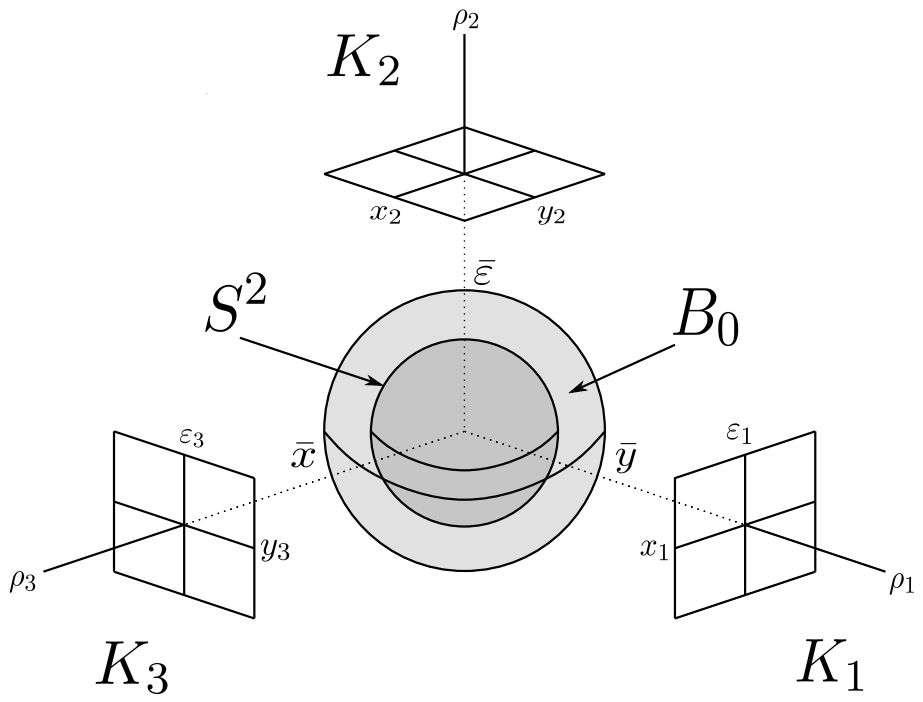


Figure 2.7.: The manifold B_0 and the charts K_1, K_2 and K_3 for the submanifolds of B.

2.5. Existing Results for the Continuous Fast-Slow Fold

The asymptotic behavior of the dynamics near continuous fast-slow fold singularities has already been investigated in the context of relaxation oscillations with the method of matched asymptotic expansions [11, 20].

A geometric approach to analyze the dynamics near the continuous fast-slow fold is given in the paper 'Geometric Analysis of the Singularly Perturbed Planar Fold' by Krupa and Szmolyan [17]. It is based on the blowup method, which was first applied to fast-slow systems by Dumortier and Roussarie [8]. In the following, we briefly describe their results for the slow manifolds of planar, singularly perturbed ODE systems including fold points. The fundamental system of their analysis is given by

$$\begin{aligned} x' &= f(x,y,\varepsilon) = x^2 - y + \mathcal{O}(\varepsilon, xy, y^2, x^3), \\ y' &= \varepsilon g(x,y,\varepsilon) = \varepsilon(-1 + \mathcal{O}(x,y,\varepsilon)) \end{aligned} \tag{2.21}$$

which is a normal form of the continuous fast-slow fold singularity including higher order terms. To be able to apply the blowup method, the system is extended by the equation $\varepsilon' = 0$. As in Example 2.10, there exist by Fenichel's Theorems for $\varepsilon > 0$ sufficiently small a slow attracting manifold S^a_ε for the attracting branch S^a_0 of the critical manifold S_0. To analyze the behavior of the slow manifold in a neighborhood of the fold point, the entry section

$$\Delta^{\text{in}} = \{(x,y) \in \mathbb{R}^2 : \; x \in I^{\text{in}}, \; y = R^2\}$$

and the exit section

$$\Delta^{\text{out}} = \{(x,y) \in \mathbb{R}^2 : \; x = R\}$$

are defined for a small positive constant $R > 0$ and a suitable interval $I^{\text{in}} \subset \mathbb{R}$. The entry and exit section, which are transverse to the attracting slow manifold and its extension into a neighborhood of the fold point, are visualized in Figure 2.8. The transition map from Δ^{in} to Δ^{out} is denoted by $\pi : \Delta^{\text{in}} \to \Delta^{\text{out}}$. For the quasi-homogeneous blowup, the coordinate transformations introduced in Example 2.20 are used to obtain a non-trivial flow on the sphere.

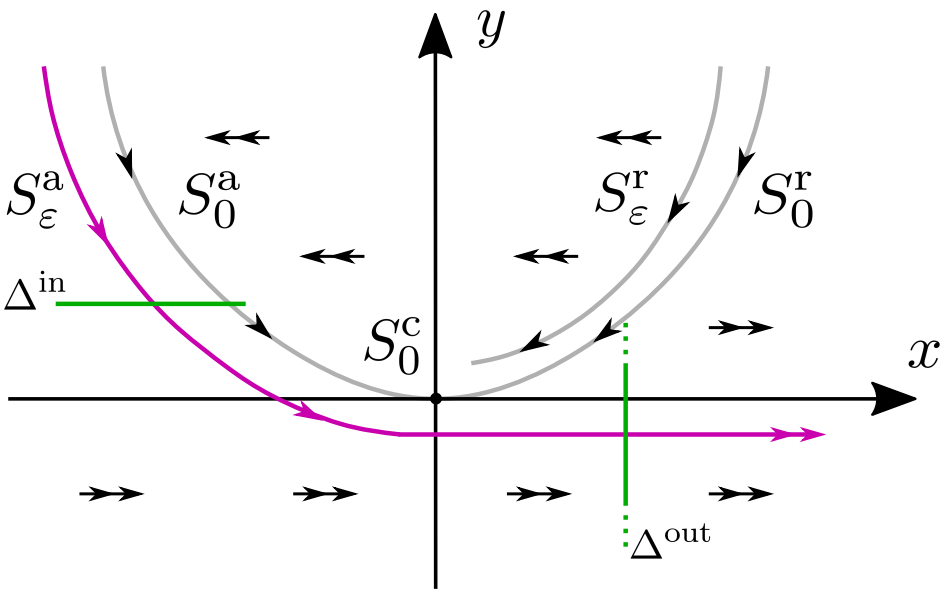


Figure 2.8.: Entry section Δ^{in} and exit section Δ^{out} for the transition map $\pi : \Delta^{\mathrm{in}} \to \Delta^{\mathrm{out}}$ of system (2.21).

The following theorem has been proven as Theorems 2.1 and 2.2 in the work by Krupa and Szmolyan.

Theorem 2.22 [17]. *Under the assumptions made in this section, a constant $\varepsilon_0 > 0$ exists, such that the following holds in system (2.21) for all $\varepsilon \in (0, \varepsilon_0]$:*

(a) The attracting slow manifold S_ε^a passes through the exit section Δ^{out} at a point $(R, h_y(\varepsilon))$, where $h_y(\varepsilon) \in \mathcal{O}\left(\varepsilon^{2/3}\right)$.

(b) The function $h_y(\varepsilon)$ has the asymptotic expansion

$$h_y(\varepsilon) = c_1\varepsilon^{\frac{2}{3}} + c_2\varepsilon \ln \varepsilon + c_3\varepsilon + \mathcal{O}\left(\varepsilon^{\frac{4}{3}} \ln \varepsilon\right) \qquad \text{as } \varepsilon \to 0,$$

where the constants c_i, $i = 1, 2, 3$ are computable functionals of the functions f and g of system (2.21).

(c) The entry section Δ^{in} is mapped under the transition map π to an interval around $S_\varepsilon^a \cap \Delta^{out}$ of size $\mathcal{O}\left(e^{-C/\varepsilon}\right)$, where C is a positive constant.

This theorem characterizes, how the attracting Fenichel slow manifold $S_\varepsilon^{\mathrm{a}}$ extends through a neighborhood of the fold point. The asymptotic expansion of the transition map from a point on the slow manifold $S_\varepsilon^{\mathrm{a}}$ to the exit section Δ^{out} is provided. The exit section has a fixed distance R in x-direction from the fold point, the distance in y-direction depends on ε and is determined by the function $h_y(\varepsilon)$. Furthermore, initial points in Δ^{in} close to $S_\varepsilon^{\mathrm{a}}$ are exponentially contracted towards the slow manifold.

For the discrete analogue, the behavior of the map close to the fold point is not completely understood yet. The following Chapter 3 formulates the problem for the discrete fast-slow fold singularity and embeds its normal form into a higher dimensional ODE system to gain insight into the dynamics near the fold point.

Chapter 3

Problem Formulation and Main Results

In this chapter, we embed the normal form of the discrete fast-slow fold singularity (2.15) into a higher dimensional system of ordinary differential equations, which we use for the geometric analysis. In Section 3.1, we define the embedding as a Poincaré return map of a normal form of the fast-slow fold of limit cycles. Afterwards, we apply in Section 3.2 results of geometric singular perturbation theory, introduced in Section 2.3. In Section 3.3, the quasi-homogeneous blowup transformation of Section 2.4 is applied to the normal form of the fast-slow LC fold and three charts for the analysis are defined. Additionally, a particular rotation velocity of the ODE system is determined, which allows us to desingularize the non-hyperbolic fold limit cycle. In Section 3.4, we state the main results obtained in this master's thesis. The Main Theorem 1 is derived for the fast-slow LC fold, which extends the results obtained by Krupa and Szmolyan for the continuous fast-slow fold singularity in [17] by the asymptotic description of the transition time and the rotational coordinate. Then we continue with Main Theorem 2, which characterizes the dynamics of the Poincaré return map of the normal form of the fast-slow LC fold in the first two charts. It is followed by Main Corollary 2, which transfers the result obtained to the discrete fast-slow fold singularity (2.15). Main Theorem 3 shows, how the embedding defined in Section 3.1 loses its well-definedness in the exit chart.

3.1. Embedding as a Poincaré Return Map

From now on, the following normal form of the discrete fast-slow fold singularity

$$\begin{aligned} r &\mapsto r + r^2 - y, \\ y &\mapsto y - \tilde{\varepsilon}, \end{aligned} \tag{3.1}$$

with $0 < \tilde{\varepsilon} \ll 1$ is considered. We aim to embed this map in a three-dimensional ODE system, which undergoes in the singular limit $\tilde{\varepsilon} = 0$ a fold bifurcation of limit cycles. The goal is to re-obtain the normal form of the discrete fast-slow fold singularity (3.1) as a Poincaré return map of a continuous ODE system. The variable x is replaced by the variable r to indicate, that the fast dynamics is observed in the radial component of the higher dimensional ODE.

The idea of a Poincaré return map $\mathcal{P}$ in $\mathbb{R}^n$ is to define an $(n\text{-}1)$-dimensional Poincaré section P, which is hit transversally by the flow of the system, see Figure 3.1. Suppose that a limit cycle μ, which is an isolated periodic orbit, intersects the Poincaré section P at a point x^*. By Theorem A.1, the solutions of an ODE system with a smooth vector field depend smoothly on the initial conditions. Hence, an orbit starting at $x \in P$ sufficiently close to x^* will return to some point $\mathcal{P}(x) \in P$, where it also intersects P transversally. The map

$$\mathcal{P} : P \to P, \quad x \mapsto \mathcal{P}(x)$$

induced by the flow of the ODE is called Poincaré return map associated with the limit cycle μ and is well-defined in a neighborhood of x^* [19]. By construction, periodic orbits of the ODE system correspond to fixed points of the Poincaré return map and the stability properties of the periodic orbits are the same as for the corresponding fixed point. The following theorem is well known in dynamical systems and guarantees, that not only the stability properties are transferred, but also the multipliers of the Jacobian matrix of the Poincaré return map associated

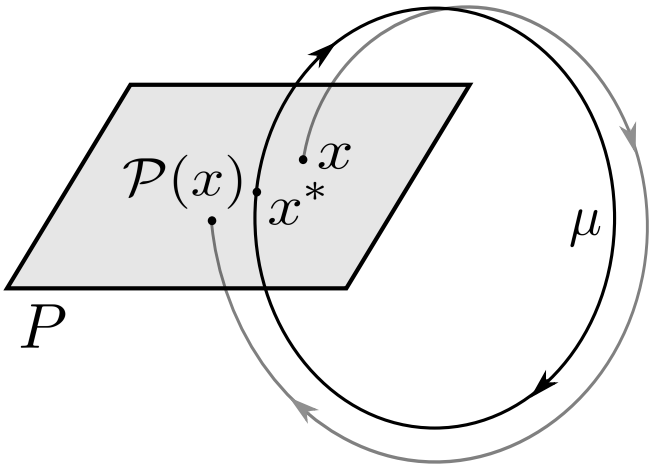


Figure 3.1.: Poincaré section P, Poincaré return map $\mathcal{P}$ and limit cycle μ through x^*.

with a limit cycle are invariant. This allows the usage of the term 'the' instead of 'a' Poincaré return map.

Theorem 3.1 [19]. *The multipliers of the Jacobian matrix of the Poincaré return map $\mathcal{P}$ at x^* associated with the limit cycle μ are independent of the choice of the point $x^* \in \mu$, the Poincaré section P as well as the local coordinates on it.*

A possibility to model limit cycles in $\mathbb{R}^3$, is to introduce an additional rotational coordinate θ and parameterize the space $\mathbb{R}^3$ by

$$(r, \theta, y) \in \mathcal{D} := \mathbb{R}_{\geq -v} \times \mathbb{R}/(s\mathbb{Z}) \times \mathbb{R} \cong \mathbb{R}^3,$$

with fixed parameters $s, v \in \mathbb{R}_{>0}$. The coordinates $z = v + r$ and θ can be interpreted as the usual polar coordinates parameterizing the space $\mathbb{R}^2$. A point $x \in \mathbb{R}^3$ in Euclidean coordinates is given by

$$x = (x_1, x_2, x_3) = \left((v + r) \cdot \cos\left(\frac{2\pi}{s}\theta\right), (v + r) \cdot \sin\left(\frac{2\pi}{s}\theta\right), y \right).$$

If r is constant and θ is variable in $[0, s)$, a limit cycle with radius $z = v + r$ occurs in the first two coordinates. We define the parameter shift $z = r + v$ in the radial component, as we aim to have the fold point located at $r = 0$ to simplify the calculations. Hence, r can be interpreted as the signed distance from the cycle with radius v, see Figure 3.2.

In our new coordinates, we consider the ODE system

$$\begin{aligned} r' &= r^2 - y, \\ \theta' &= \varepsilon, \\ y' &= -\delta, \end{aligned} \tag{3.2}$$

with $0 < \delta \ll \varepsilon \ll 1$, which is a system on three time scales: the fast time scale $\mathcal{O}(1)$ for the dynamics in r, the slow time scale $\mathcal{O}(\varepsilon)$ for the rotation velocity and the super slow time scale $\mathcal{O}(\delta)$ for the parameter drift. This system is the normal form of the continuous fast-slow fold singularity (2.8) with an additional rotational coordinate θ with rotation velocity ε. System (3.2) is also called the normal form of the *fast-slow LC fold*. In the following we show, that system (3.2) is locally an embedding of the normal form of the discrete fast-slow fold (3.1).

In the (partial) singular limit $\delta = 0$, $\varepsilon \neq 0$, system (3.2) undergoes a fold bifurcation of limit cycles: in Section 2.2.1 we showed, that a fold bifurcation occurs in the r-coordinate of system (3.2), when interpreting y as a parameter. Due to the non-vanishing rotation in θ, a *fold*

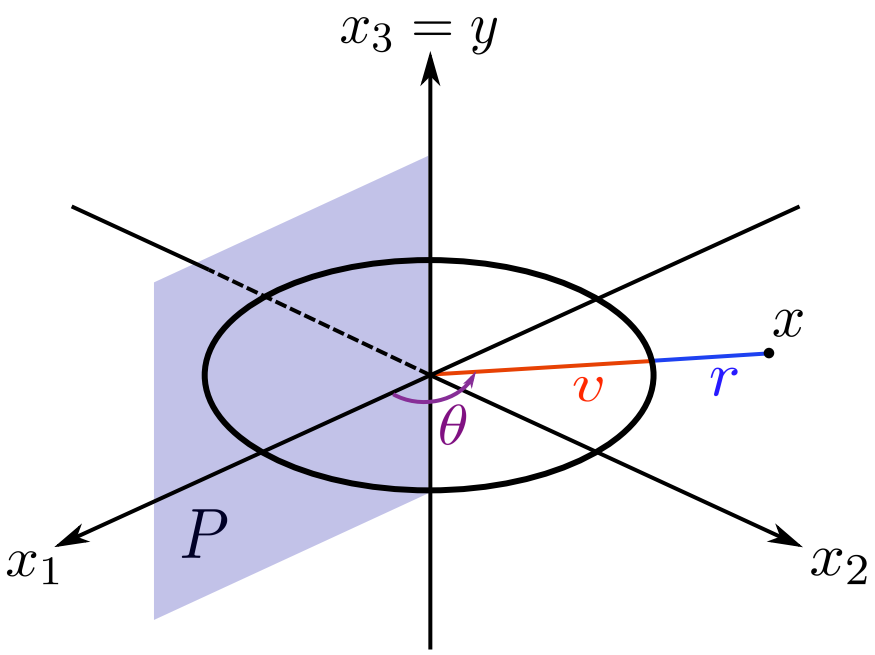


Figure 3.2.: New parametrization of $\mathbb{R}^3$ in the coordinates r, y and θ and Poincaré section P.

bifurcation of limit cycles occurs. The stability properties are the same as in Section 2.2.1: for $y = 0$, a non-hyperbolic limit cycle with radial component $r = 0$ exists and for small $y > 0$, the limit cycle with $r = -\sqrt{y}$ is stable and the limit cycle with $r = \sqrt{y}$ is unstable. For $\delta > 0$, a slow parameter drift is added, such that we say that system (3.2) undergoes a fold bifurcation of limit cycles with a slow parameter drift.

To re-obtain the normal form of the discrete fast-slow fold singularity (3.1) from the normal form of the fast-slow LC fold (3.2), we define the Poincaré section

$$P = \{(r, \theta, y) \in \mathcal{D} : \ \theta = 0\} = \{(x_1, x_2, x_3) \in \mathbb{R}^3 : \ x_1 \geq 0, \ x_2 = 0\},$$

which is a smooth, two-dimensional surface intersecting transversally any limit cycle induced by a constant r- and y-coordinate. The iterates $\mathcal{P}^n$, $n \in \mathbb{N}$ can now be described only by the coordinates (r, y) on the two-dimensional Poincaré section P. In the singular limit $\delta = 0$, no fixed point of the Poincaré return map $\mathcal{P}$ exists for $y < 0$, we have for $y = 0$ one non-hyperbolic fixed point at $r = 0$ and for small $y > 0$ one stable and one unstable fixed point at the positions of the limit cycles $r = \pm\sqrt{y}$. Thus, by varying y, a discrete fold bifurcation occurs in the layer problem. The local embedding of the discrete fold bifurcation as a fold bifurcation of limit cycles is shown in Figure 3.3.

As the rotation velocity $\theta' = \varepsilon$ is constant in system (3.2), the n-th return time to the Poincaré section P is

$$T_{\mathcal{P}}(n) = \frac{ns}{\varepsilon},$$

independently of the initial condition x^* for $\varepsilon > 0$. As also the slow parameter drift $y' = -\delta$ in y is constant in system (3.2), the parameter drift in the y-component of the Poincaré return map $\mathcal{P}$ is

$$-\delta \cdot T_{\mathcal{P}}(1) = -\frac{\delta s}{\varepsilon} = -\tilde{\varepsilon}.$$

The parameter drift $-\tilde{\varepsilon}$ is constant and due to the assumption $0 < \delta \ll \varepsilon \ll 1$ also slow. Therefore we have locally embedded, up to a rescaling of the variables, the map (3.1) in system (3.2). The aim is to apply the blowup method for continuous time problems to the ODE system (3.2) and then gain insight into the discrete fast-slow fold singularity (3.1) by considering the Poincaré return map defined in this section.

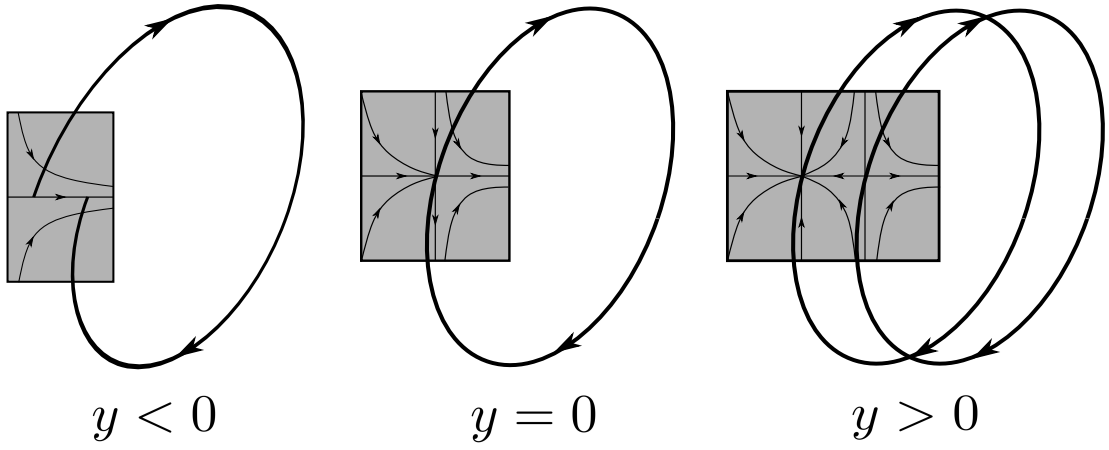


Figure 3.3.: Discrete fold bifurcation embedded as a fold bifurcation of limit cycles.

The following lemma shows, that the embedding with a constant rotation velocity only allows us to observe finitely many iterates of the Poincaré return map, such that it is only well-defined locally near the fold point.

Lemma 3.2. *For a constant rotation velocity $\theta' = \varepsilon$, only finitely many iterates of the Poincaré map $\mathcal{P}$ are observed for the normal form of the fast-slow LC fold* (3.2).

Proof. Suppose, that we start with an initial condition on the Poincaré section P with $r^* > 0$ and $y^* < 0$. Then the dynamics in the r-coordinate is given by

$$r' = r^2 - y > r^2.$$

The ODE $r' = r^2$ with initial condition $r(0) = r^* > 0$ has the solution

$$r(t) = \frac{1}{\frac{1}{r^*} - t},$$

which exists for $t \in \left[0, \frac{1}{r^*}\right)$ and blows up for $t \to \frac{1}{r^*}$. Hence, for an initial point on the Poincaré section P with $r^* > 0$ and $y^* < 0$, the solution blows up in finite time. As the rotation velocity $\theta' = \varepsilon$ is constant, its solution with initial condition $\theta(0) = 0$ is given by

$$\theta(t) = \varepsilon t \mod s,$$

such that the angular position θ as a variable in $\mathbb{R}$ is directly proportional to the time t. Consequently, only finitely many returns to the Poincaré section P are observed, as the solution blows up in finite time.

If it does not hold $r^* > 0$ and $y^* < 0$, then in each of the following cases, after finitely many iterates a point with $r^* > 0$ and $y^* < 0$ is obtained by the Poincaré return map or the well-definedness is lost after finitely many iterates.

Suppose $y^* \geq 0$. As the decrease $y' = -\delta > 0$ is constant and non-vanishing, it holds

$$y(t) = y^* - \delta t = y^* - \delta \frac{ns}{\varepsilon},$$

as the n-th return time to the Poincaré section P is $\mathcal{T}_{\mathcal{P}}(n) = \frac{ns}{\varepsilon}$. Hence, a number of iterates $n < \infty$ exists, such that $y^* < 0$ or the well-definedness of the embedding is lost before due to a blowup of the r-coordinate.

Suppose $r^* \leq 0$. With the explicit solution for $y(t)$, we can estimate

$$r' = r^2 - y \geq -y^* + \delta t \qquad \Rightarrow \qquad r(t) \geq r^* - y^* t + \frac{1}{2}\delta t^2.$$

Thus, $r(t) \to \infty$ for $t \to \infty$. As $T_{\mathcal{P}}(n) = \frac{ns}{\varepsilon}$, a number of iterates $n < \infty$ exists, such that the r-coordinate is positive or the well-definedness of the embedding is lost before due to a blowup of the r-coordinate.

Altogether we have shown, that it is not possible to embed infinitely many iterates of the Poincaré map with a constant rotation velocity in system (3.2). □

Remark 3.3. *As the r- and the y-component of the normal form of the fast-slow LC fold* (3.2) *do not depend on the variable θ, the rotational coordinate decouples. Thus, the observed iterates of the Poincaré return map $\mathcal{P}$ lie on the invariant solution curves defined by the normal form of the continuous fast-slow fold singularity* (2.8).

Remark 3.4. *The choice of the rotation velocity is directly related to the well-definedness of the embedding. The assumption $0 < \delta \ll \varepsilon$ is necessary to observe in the (partial) singular limit $\delta = 0$, $\varepsilon \neq 0$ a fold bifurcation of limit cycles, which has a slow parameter drift in the full system. The relationship between δ and ε, for which it is possible to desingularize the non-hyperbolic limit cycle is determined by the blowup transformation in Section 3.3. A further discussion about the rotation velocity can be found in Appendix B. This includes also an argument, why the condition $\varepsilon \ll 1$ is necessary to achieve a desingularization with the blowup method.*

3.2. Assumptions and Setting

The layer problem of the normal form of the fast-slow LC fold 3.2 is given by

$$\begin{aligned} r' &= r^2 - y = f(r, y), \\ \theta' &= 0, \\ y' &= 0, \end{aligned} \tag{3.3}$$

as in the singular limit $\varepsilon = 0$, it also holds $\delta = 0$. The two-dimensional critical manifold

$$S_0 = \{(r, \theta, y) \in \mathcal{D} : \ f(r, y) = 0\} = \{(r, \theta, y) \in \mathcal{D} : \ y = r^2\},$$

consists of the equilibria of the layer problem. S_0 is visualized in Figure 3.4 and locally near $r = 0$ shaped like a Bundt cake upside down (this is a cake characterized by the form of a pastry called 'Gugelhupf' in German). We can rescale system (3.2) on the slow time scale $\tau = \varepsilon t$ and obtain

$$\begin{aligned} \varepsilon \dot{r} &= r^2 - y, \\ \dot{\theta} &= 1, \\ \dot{y} &= -\frac{\delta}{\varepsilon}, \end{aligned}$$

which becomes in the singular limit $\delta = 0$, $\varepsilon = 0$ the reduced problem

$$\begin{aligned} 0 &= r^2 - y, \\ \dot{\theta} &= 1, \\ \dot{y} &= 0, \end{aligned}$$

as $\delta \ll \varepsilon$. Hence, on the slow time scale we observe rotation on the critical manifold S_0. It is not possible to rescale system (3.2) on the super slow time scale δt, as the dynamics in θ has for $\varepsilon > 0$ no equilibrium, such that a rescaling would result in an infinite rotation velocity.

To apply the results of geometric singular perturbation theory introduced in Section 2.3 to system (3.2), we define r to be a fast variable and θ and y to be slow variables. The Jacobian matrix with respect to the fast variable r is given by

$$\partial_r f(r, y) = 2r.$$

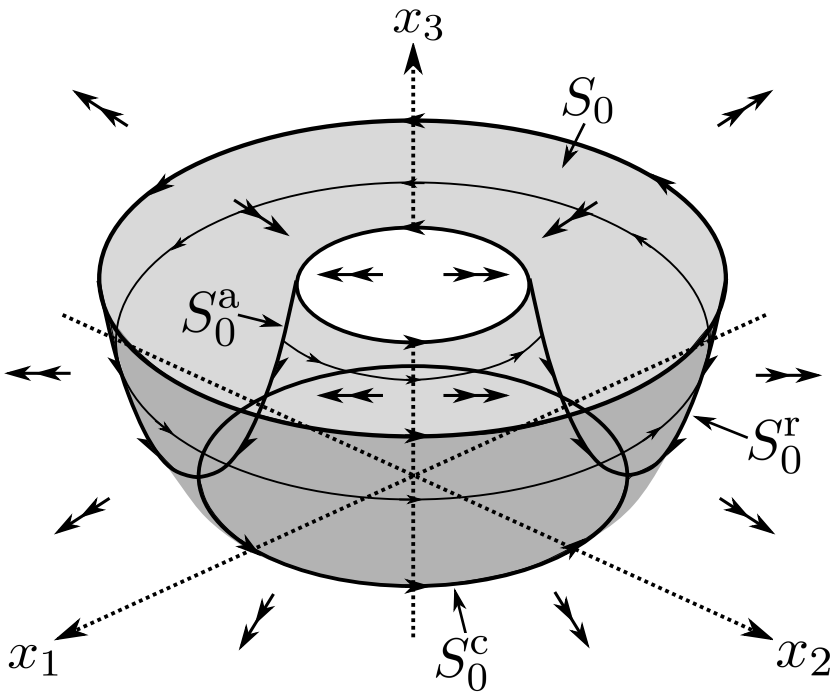


Figure 3.4.: Critical manifold S_0 of the layer problem, which subdivides in the non-hyperbolic circle S_0^{c}, the attracting manifold S_0^{a} and the repelling manifold S_0^{c}. The super slow dynamics is visualized by half arrows, the slow dynamics by single arrows and the fast dynamics by double arrows.

Thus, by Definition 2.7, normal hyperbolicity is lost at the non-hyperbolic circle of equilibria

$$S_0^{\mathrm{c}} = \{(r,\theta,y) \in S_0 :\ \partial_r f(r,y) = 0\} = \{(r,\theta,y) \in \mathcal{D} :\ r = 0,\ y = 0\}.$$

We introduce the normally hyperbolic attracting subset S_0^{a} of the critical manifold S_0 as

$$S_0^{\mathrm{a}} = \{(r,\theta,y) \in S_0 :\ \partial_r f(r,y) < 0\} = \{(r,\theta,y) \in \mathcal{D} :\ r < 0,\ y = r^2\},$$

and the normally hyperbolic repelling subset S_0^{r} of the critical manifold S_0 as

$$S_0^{\mathrm{r}} = \{(r,\theta,y) \in S_0 :\ \partial_r f(r,y) > 0\} = \{(r,\theta,y) \in \mathcal{D} :\ r > 0,\ y = r^2\}.$$

For $0 < \delta \ll \varepsilon \ll 1$, Fenichel's Theorems 2.9 imply, that compact submanifolds of the normally hyperbolic critical manifolds S_0^{a} and S_0^{r} persist as $\mathcal{O}(\varepsilon)$-close slow manifolds $S_\varepsilon^{\mathrm{a}}$ and $S_\varepsilon^{\mathrm{r}}$. Outside of a neighborhood of the circle S_0^{c}, the locally invariant manifolds $S_\varepsilon^{\mathrm{a}}$ and $S_\varepsilon^{\mathrm{r}}$ are smooth perturbations of the branches S_0^{a} and S_0^{r}. The critical manifold S_0 and the Fenichel slow manifolds are shown in Figure 3.5 in the coordinates r and y.

Our goal is to describe the attracting slow manifold $S_\varepsilon^{\mathrm{a}}$ and its behavior close to the non-hyperbolic circle S_0^{c} of the normal form of the fast-slow LC fold (3.2). To that end, we introduce for small positive constants E, R and β the entry section

$$\Delta^{\mathrm{in}} := \left\{(r,\theta,y) \in \mathcal{D} :\ r \in I^{\mathrm{in}},\ y = R^2\right\}$$

with the interval

$$I^{\mathrm{in}} = \left\{r \in \mathbb{R}_{\geq -v} :\ \left|-1 + \frac{r}{R}\right| \leq \beta\right\}.$$

The entry section Δ^{in} is due to the rotational coordinate θ topologically equivalent to an annulus. Furthermore, we define the exit section

$$\Delta^{\mathrm{out}} := \{(r,\theta,y) \in \mathcal{D} :\ r = R\},$$

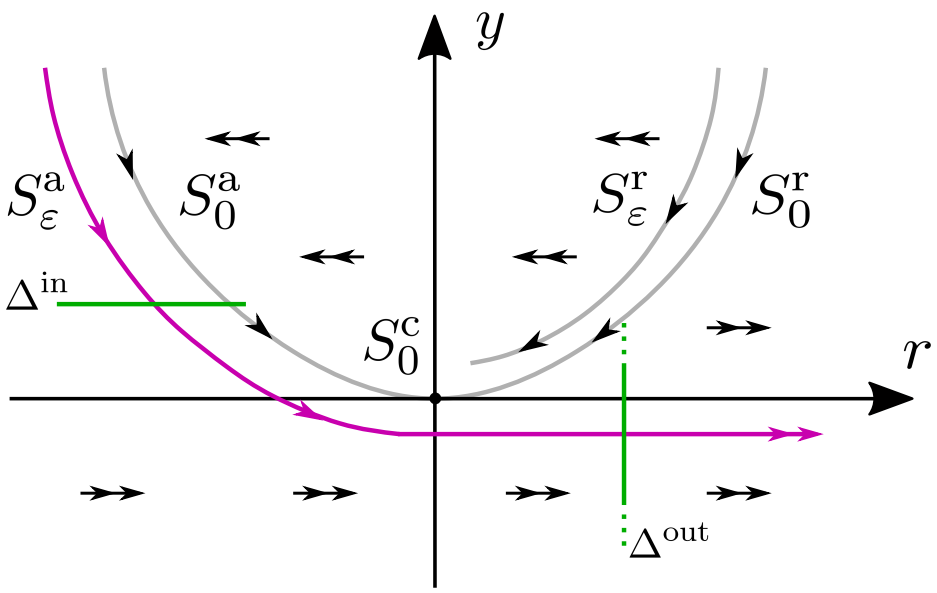


Figure 3.5.: Setting in the coordinates r and y: the critical manifold S_0 subdivides in the non-hyperbolic circle S^{c}_0, the attracting manifold S^{a}_0 and the repelling manifold S^{c}_0. The two normally hyperbolic manifolds perturb to slow manifolds $S^{\mathrm{a}}_\varepsilon$ and $S^{\mathrm{r}}_\varepsilon$ for $\varepsilon > 0$. Furthermore, the entry annulus Δ^{in} and exit cylinder Δ^{out} are shown.

which is due to the rotational coordinate topologically equivalent to a cylinder. The entry and the exit sections are visualized in the r-y plane in Figure 3.5. The transition map for the flow of all trajectories close to the attracting slow manifold $S^{\mathrm{a}}_\varepsilon$ near the singular circle S^{c}_0 is a map $\pi : \Delta^{\mathrm{in}} \to \Delta^{\mathrm{out}}$. The well-definedness of the map π is part of Main Theorem 1 for the fast-slow LC fold.

To work only with one time scale parameter, we assume that we can describe the slow and the super slow dynamics in terms of one parameter ε. To apply in the following section the blowup method, we study from now on the extended system

$$\begin{aligned} r' &= r^2 - y, \\ \theta' &= \varepsilon, \\ y' &= -\varepsilon^\alpha, \\ \varepsilon' &= 0, \end{aligned} \tag{3.4}$$

with $\alpha \in \mathbb{R}_{>1}$ and

$$(r, \theta, y, \varepsilon) \in \mathcal{D}_0 := \mathbb{R}_{\geq -v} \times \mathbb{R}/(s\mathbb{Z}) \times \mathbb{R} \times \mathbb{R}_{\geq 0} \cong \mathbb{R}^3 \times \mathbb{R}_{\geq 0}.$$

We assume $\alpha > 1$ to model, that the rotation velocity is asymptotically larger than the slow parameter drift, which is consistent with the assumption $0 < \delta = \varepsilon^\alpha \ll \varepsilon \ll 1$. The extended critical manifold $S_0 \times \{\varepsilon = 0\}$ is a manifold of equilibria in system (3.4), whose linearization is given by

$$J(r, \theta, y, \varepsilon) = \begin{pmatrix} 2r & 0 & -1 & 0 \\ 0 & 0 & 0 & 1 \\ 0 & 0 & 0 & -\alpha\varepsilon^{\alpha-1} \\ 0 & 0 & 0 & 0 \end{pmatrix}.$$

As $\alpha \in \mathbb{N}_{>1}$, all entries of the Jacobian matrix are finite. Evaluated at the extended manifolds $S^{\mathrm{a}}_0 \times \{\varepsilon = 0\}$ and $S^{\mathrm{r}}_0 \times \{\varepsilon = 0\}$, we obtain in both cases a triple zero eigenvalue and one non-trivial eigenvalue $\lambda_1 = 2r$, attracting for $S^{\mathrm{a}}_0 \times \{\varepsilon = 0\}$ and repelling for $S^{\mathrm{r}}_0 \times \{\varepsilon = 0\}$. This

allows us to prove with the Center Manifold Theorem A.11 the existence of a three-dimensional attracting center manifold M^{a} and a tree-dimensional repelling center manifold M^{r} in system (3.4). The slow manifolds of the normal form of the fast-slow LC fold (3.2) are obtained as sections $\varepsilon = const.$ of the manifolds M^{a} and M^{r}.

Remark 3.5. *Note that in general, center-manifolds are not unique. As the Fenichel slow manifolds are unique up to order $\mathcal{O}\left(e^{-K/\varepsilon}\right)$ for some constant $K > 0$, also their extensions M^a and M^r are unique up to order $\mathcal{O}\left(e^{-K/\varepsilon}\right)$ for some constant $K > 0$. When stating the main theorems in Section 3.4, we explain, why the non-uniqueness of center-manifolds does not affect our results.*

As the extended non-hyperbolic circle $S_0^{\mathrm{c}} \times \{\varepsilon = 0\}$ has a quadruple zero eigenvalue, the construction of the slow manifolds fails and the behavior of the slow manifold is not controlled by the slow subsystem anymore. We resolve this problem by applying the blowup method.

To study the attracting slow manifold M^{a} in the extended system, we introduce for small constants E, R, β the entry set

$$\Delta_\varepsilon^{\mathrm{in}} := \left\{(r, \theta, y, \varepsilon) \in \mathcal{D}_0 : \; r \in I^{\mathrm{in}}, \; y = R^2, \; \varepsilon \leq ER\right\}$$

with the interval

$$I^{\mathrm{in}} = \left\{r \in \mathbb{R}_{\geq -v} : \; \left|-1 + \frac{r}{R}\right| \leq \beta\right\}$$

and the exit set

$$\Delta_\varepsilon^{\mathrm{out}} := \{(r, \theta, y, \varepsilon) \in \mathcal{D}_0 : \; r = R, \; \varepsilon \leq ER\}.$$

In the extended system, the transition map is defined as $\pi_\varepsilon : \Delta_\varepsilon^{\mathrm{in}} \to \Delta_\varepsilon^{\mathrm{out}}$ and coincides in the first three components with the transition map $\pi : \Delta^{\mathrm{in}} \to \Delta^{\mathrm{out}}$.

3.3. Blowup of the Fast-Slow LC Fold

To desingularize the non-hyperbolic circle S_0^{c}, we aim to use the quasi-homogeneous blowup transformation introduced in Section 2.4. We apply the blowup transformation only to the coordinates r, y and ε, to maintain the rotation property of the extended system (3.4). This is important, as we aim to determine the Poincaré return map of system (3.4) to study for the normal form of the discrete fast-slow fold singularity (3.1). To that end, we need to describe θ-values that are in $\mathcal{O}(1)$ with respect to the variable ε. Including θ in the blowup would restrict us to some ε-dependent neighborhood of $\theta = 0$, such that no returns are observed during the analysis. Geometrically, we apply a three-dimensional quasi-homogeneous blowup at each point of the non-hyperbolic circle S_0^{c}. Thus, the blowup surface we consider is topologically equivalent to $S^1 \times S^2$.

In order to apply the quasi-homogeneous blowup transformation of Definition 2.19, we need the right hand side of system (3.4) to be a quasi-homogeneous vector field. Furthermore, the coefficient for the θ-coordinate has to be zero, as we apply the blowup only to the coordinates r, y and ε. It turns out, that this is only the case for a certain value of the coefficient α, which is determined in the following Proposition.

Proposition 3.6. *To be able to apply the quasi-homogeneous blowup transformation of Definition 2.19 to system* (3.4)*, we need $\alpha = 3$, leading to the ODE system*

$$\begin{aligned} r' &= r^2 - y, \\ \theta' &= \varepsilon, \\ y' &= -\varepsilon^3, \\ \varepsilon' &= 0, \end{aligned} \tag{3.5}$$

which is quasi-homogeneous of degree 2 with coefficients $a_1 = 1$, $a_2 = 0$, $a_3 = 2$ and $a_4 = 1$.

Proof. To apply the quasi-homogeneous blowup transformation for each point on the singular circle S_0^c, we need system (3.4) to be a quasi-homogeneous vector field of type (a_1, a_2, a_3, a_4) with $a_2 = 0$ and degree $k + 1$. Inserting Definition 2.18 of quasi-homogeneity into system (3.4) leads to

$$\begin{aligned} \rho^{2a_1} r^2 - \rho^{a_3} y &\stackrel{!}{=} \rho^{a_1+k}(r^2 - y), \\ \rho^{a_4}\varepsilon &\stackrel{!}{=} \rho^{a_2+k}\varepsilon, \\ -\rho^{a_4\alpha}\varepsilon^\alpha &\stackrel{!}{=} -\rho^{a_3+k}\varepsilon^\alpha, \\ 0 &\stackrel{!}{=} \rho^{a_4+k}\cdot 0. \end{aligned}$$

This yields the following system of algebraic equations:

$$2a_1 = a_1 + k, \quad a_3 = a_1 + k, \quad a_4 = k, \quad a_4\alpha = a_3 + k.$$

We have some choices as the last constraint does not give any algebraic relation. Using these equations we obtain the following value for α:

$$\alpha = \frac{a_3 + k}{a_4} = \frac{a_1 + 2k}{k} = \frac{3k}{k} = 3.$$

To keep the system as easy as possible, we choose $k = 1$ and obtain system (3.5) with the coefficients

$$a_1 = 1, \quad a_2 = 0, \quad a_3 = 2, \quad a_4 = 1. \qquad \square$$

Remark 3.7. *By choosing $\alpha > 3$, the rotation velocity is too fast compared to the slow variables, such that the desingularization step by rescaling of the blown-up vector field introduced in Section 2.4 is not possible. For $\alpha < 3$, the rotation velocity is too slow, such that a desingularization step is possible, but no returns of the Poincaré return map are observed. In Appendix B, a further discussion about the rotation velocity is given.*

For the quasi-homogeneous blowup transformation of Definition 2.19, we choose the interval $I = [0, P]$ with $P > 0$ and introduce the two manifolds

$$B = S^2 \times \mathbb{R} \times \mathbb{R}/(s\mathbb{Z}) \quad \text{and} \quad B_0 = S^2 \times [0, P] \times \mathbb{R}/(s\mathbb{Z}).$$

The coefficients of Proposition 3.6 imply, that the quasi-homogeneous blowup transformation for system (3.5) is given by

$$\varphi : B_0 \to \mathcal{D}_0, \quad (\bar{r}, \bar{y}, \bar{\varepsilon}, \rho, \theta) \mapsto (r, \theta, y, \varepsilon) = (\rho\bar{r}, \theta, \rho^2\bar{y}, \rho\bar{\varepsilon}), \tag{3.6}$$

with $(\bar{r}, \bar{y}, \bar{\varepsilon}) \in S^2$ and $\mathcal{D}_0 = \mathbb{R}_{\geq -v} \times \mathbb{R}/(s\mathbb{Z}) \times \mathbb{R} \times \mathbb{R}_{\geq 0}$.

Let X denote the vector field on $\mathcal{D}_0$ induced by system (3.5). The blowup induces a vector field $\bar{X}$ on B_0 with $\varphi_*(\bar{X}) = X$, where φ_* is the push-forward map corresponding to φ [17]. Our goal is to describe the attracting Fenichel slow manifold S_ε^a near the non-hyperbolic circle S_0^c. Since $\varphi(B_0)$ is a full neighborhood of S_0^c, it suffices to study the vector field $\bar{X}$ on the manifold B_0 instead of on the manifold B. To simplify the calculations, the analysis is done in different charts, as introduced in Section 2.4. In the entry chart K_1, the attracting slow manifold is studied as it approaches the singular circle S_0^c. The rescaling chart K_2 analyzes how the flow moves along $S^1 \times S^2$ and the exit chart K_3 covers the departure from the singular circle S_0^c. For the main theorems stated in Section 3.4, the results of the three charts are joined.

The parts of the manifold B, which are relevant for the analysis of the blown-up vector field are given by

$$B_{\bar{y}}^+ := B \cap \{\bar{y} > 0\}, \qquad B_{\bar{\varepsilon}}^+ := B \cap \{\bar{\varepsilon} > 0\}, \qquad B_{\bar{r}}^+ := B \cap \{\bar{r} > 0\}.$$

The three charts for these submanifolds of B are defined as

$$\mathcal{K}_1 : B_{\bar{y}}^+ \to \mathbb{R}\times\mathbb{R}/(s\mathbb{Z})\times\mathbb{R}\times\mathbb{R}, \quad (\bar{r},\bar{y},\bar{\varepsilon},\rho,\theta)\mapsto(r_1,\theta_1,\rho_1,\varepsilon_1) = (\bar{r}\bar{y}^{-\frac{1}{2}},\theta,\rho\bar{y}^{\frac{1}{2}},\bar{\varepsilon}\bar{y}^{-\frac{1}{2}}), \quad (3.7)$$

$$\mathcal{K}_2 : B_{\bar{\varepsilon}}^+ \to \mathbb{R}\times\mathbb{R}/(s\mathbb{Z})\times\mathbb{R}\times\mathbb{R}, \quad (\bar{r},\bar{y},\bar{\varepsilon},\rho,\theta)\mapsto(r_2,\theta_2,y_2,\rho_2) = (\bar{r}\bar{\varepsilon}^{-1},\theta,\bar{y}\bar{\varepsilon}^{-2},\rho\bar{\varepsilon}), \quad (3.8)$$

$$\mathcal{K}_3 : B_{\bar{r}}^+ \to \mathbb{R}\times\mathbb{R}/(s\mathbb{Z})\times\mathbb{R}\times\mathbb{R}, \quad (\bar{r},\bar{y},\bar{\varepsilon},\rho,\theta)\mapsto(\rho_3,\theta_3,y_3,\varepsilon_3) = (\rho\bar{r},\theta,\bar{y}\bar{r}^{-2},\bar{\varepsilon}\bar{r}^{-1}). \quad (3.9)$$

The following lemma states, how the blowup transformation is calculated in the different chart coordinates.

Lemma 3.8. *The polar blowups induced by the blowup transformation* (3.6) *in the charts* $\mathcal{K}_1$, $\mathcal{K}_2$ *and* $\mathcal{K}_3$ *are given by*

$$\begin{aligned}
&\text{for } \mathcal{K}_1 : && (r,\theta,y,\varepsilon) = (\rho_1 r_1,\theta_1,\rho_1^2,\rho_1\varepsilon_1),\\
&\text{for } \mathcal{K}_2 : && (r,\theta,y,\varepsilon) = (\rho_2 r_2,\theta_2,\rho_2^2 y_2,\rho_2),\\
&\text{for } \mathcal{K}_3 : && (r,\theta,y,\varepsilon) = (\rho_3,\theta_3,\rho_3^2 y_3,\rho_3\varepsilon_3).
\end{aligned}$$

Proof. For $\mathcal{K}_1$, the blowup transformation (3.6) and the chart coordinates (3.7) yield:

$$\begin{aligned}
r &= \rho\bar{r} = \rho\bar{y}^{\frac{1}{2}}\bar{r}\bar{y}^{-\frac{1}{2}} = \rho_1 r_1,\\
\theta &= \theta = \theta_1,\\
y &= \rho^2\bar{y} = (\rho\bar{y}^{\frac{1}{2}})^2 = \rho_1^2,\\
\varepsilon &= \rho\bar{\varepsilon} = \rho\bar{y}^{\frac{1}{2}}\bar{\varepsilon}\bar{y}^{-\frac{1}{2}} = \rho_1\varepsilon_1.
\end{aligned}$$

For $\mathcal{K}_2$, the blowup transformation (3.6) and the chart coordinates (3.8) yield:

$$\begin{aligned}
r &= \rho\bar{r} = \rho\bar{\varepsilon}\bar{r}\bar{\varepsilon}^{-1} = \rho_2 r_2,\\
\theta &= \theta = \theta_2,\\
y &= \rho^2\bar{y} = (\rho\bar{\varepsilon})^2\bar{y}\bar{\varepsilon}^{-2} = \rho_2^2 y_2,\\
\varepsilon &= \rho\bar{\varepsilon} = \rho_2.
\end{aligned}$$

For $\mathcal{K}_3$, the blowup transformation (3.6) and the chart coordinates (3.9) yield:

$$\begin{aligned}
r &= \rho\bar{r} = \rho_3,\\
\theta &= \theta = \theta_3,\\
y &= \rho^2\bar{y} = (\rho\bar{r})^2\bar{y}\bar{r}^{-2} = \rho_3^2 y_3,\\
\varepsilon &= (\rho\bar{r})(\bar{\varepsilon}\bar{r}^{-1}) = \rho_3\varepsilon_3.
\end{aligned}$$

□

In the analysis, it will be necessary to transfer results from one to another chart. Therefore, the next lemma gives the transition maps between consecutive charts.

Lemma 3.9. *The transition maps* κ_{ij} *from* $\mathcal{K}_i$ *to* $\mathcal{K}_j$ *are given by*

$$\begin{aligned}
&\kappa_{12} : && r_2 = r_1\varepsilon_1^{-1}, && \theta_2 = \theta_1, && y_2 = \varepsilon_1^{-2}, && \rho_2 = \rho_1\varepsilon_1, && \text{for } \varepsilon_1 > 0,\\
&\kappa_{12}^{-1} : && r_1 = r_2 y_2^{-\frac{1}{2}}, && \theta_1 = \theta_2, && \rho_1 = \rho_2 y_2^{\frac{1}{2}}, && \varepsilon_1 = y_2^{-\frac{1}{2}}, && \text{for } y_2 > 0,\\
&\kappa_{23} : && \rho_3 = \rho_2 r_2, && \theta_3 = \theta_2, && y_3 = y_2 r_2^{-2}, && \varepsilon_3 = r_2^{-1}, && \text{for } r_2 > 0,\\
&\kappa_{23}^{-1} : && r_2 = \varepsilon_3^{-1}, && \theta_2 = \theta_3, && y_2 = y_3\varepsilon_3^{-2}, && \rho_2 = \rho_3\varepsilon_3, && \text{for } \varepsilon_3 > 0.
\end{aligned}$$

Proof. For the transition map κ_{12} from $\mathcal{K}_1$ to $\mathcal{K}_2$ we obtain for $\varepsilon_1 > 0$:

$$\begin{aligned}
r_2 &= \bar{r}\bar{\varepsilon}^{-1} = \bar{r}\bar{y}^{-\frac{1}{2}}(\bar{\varepsilon}\bar{y}^{-\frac{1}{2}})^{-1} = r_1\varepsilon_1^{-1},\\
\theta_2 &= \theta = \theta_1,\\
y_2 &= \bar{y}\bar{\varepsilon}^{-2} = (\bar{\varepsilon}\bar{y}^{-\frac{1}{2}})^{-2} = \varepsilon_1^{-2},\\
\rho_2 &= \rho\bar{\varepsilon} = \rho\bar{y}^{\frac{1}{2}}\bar{\varepsilon}\bar{y}^{-\frac{1}{2}} = \rho_1\varepsilon_1.
\end{aligned}$$

For the transition map κ_{12}^{-1} from K_2 to K_1 we obtain for $y_2 > 0$:

$$\begin{aligned}
r_1 &= \bar{r}\bar{y}^{-\frac{1}{2}} = \bar{r}\bar{\varepsilon}^{-1}(\bar{y}\bar{\varepsilon}^{-2})^{-\frac{1}{2}} = r_2 y_2^{-\frac{1}{2}},\\
\theta_1 &= \theta = \theta_2,\\
\rho_1 &= \rho\bar{y}^{\frac{1}{2}} = \rho\bar{\varepsilon}(\bar{y}\bar{\varepsilon}^{-2})^{\frac{1}{2}} = \rho_2 y_2^{\frac{1}{2}},\\
\varepsilon_1 &= \bar{\varepsilon}\bar{y}^{-\frac{1}{2}} = (\bar{y}\bar{\varepsilon}^{-2})^{-\frac{1}{2}} = y_2^{-\frac{1}{2}}.
\end{aligned}$$

For the transition map κ_{23} from K_2 to K_3 we obtain for $r_2 > 0$:

$$\begin{aligned}
\rho_3 &= -\rho\bar{r} = \rho\bar{\varepsilon}\bar{r}\bar{\varepsilon}^{-1} = \rho_2 r_2,\\
\theta_3 &= \theta = \theta_2,\\
y_3 &= \bar{y}\bar{r}^{-2} = \bar{y}\bar{\varepsilon}^{-2}(\bar{r}\bar{\varepsilon}^{-1})^{-2} = y_2 r_2^{-2},\\
\varepsilon_3 &= \bar{\varepsilon}\bar{r}^{-1} = (\bar{r}\bar{\varepsilon}^{-1})^{-1} = r_2^{-1}.
\end{aligned}$$

For the transition map κ_{23}^{-1} from K_3 to K_2 we obtain for $\varepsilon_3 > 0$:

$$\begin{aligned}
r_2 &= \bar{r}\bar{\varepsilon}^{-1} = (\bar{\varepsilon}\bar{r}^{-1})^{-1} = \varepsilon_3^{-1},\\
\theta_2 &= \theta = \theta_3,\\
y_2 &= \bar{y}\bar{\varepsilon}^{-2} = \bar{y}\bar{r}^{-2}(-\bar{\varepsilon}\bar{r}^{-1})^{-2} = y_3\varepsilon_3^{-2},\\
\rho_2 &= \rho\bar{\varepsilon} = (\rho\bar{r})(-\bar{\varepsilon}\bar{r}^{-1}) = \rho_3\varepsilon_3.
\end{aligned}$$

□

3.4. Main Results

In this section, we state the main theorems proven in this master's thesis, for which we assume the setting of Section 3.2. Section 3.4.1 treats the normal form of the fast-slow LC fold (3.2), with the particular rotation velocity determined in Section 3.3. We continue in Section 3.4.2 with a local theorem for the normal form of the discrete fast-slow fold singularity (3.1), which describes the dynamics of the Poincaré return map of the continuous system visible in charts K_1 and K_2. Section 3.4.3 states a second theorem for the normal form of the discrete fast-slow singularity, which characterizes that the embedding of Section 3.1 is not globally well-defined.

3.4.1. Theorem for the Fast-Slow LC Fold

In Proposition 3.6, we determined the rotation velocity, for which it is possible to desingularize the normal form of the fast-slow LC fold with the blowup method. The resulting, non-extended system is given by

$$\begin{aligned}
r' &= r^2 - y,\\
\theta' &= \varepsilon,\\
y' &= -\varepsilon^3.
\end{aligned} \tag{3.10}$$

In Chapter 4, we prove the following theorem for the transition map $\pi : \Delta^{\text{in}} \to \Delta^{\text{out}}$:

Main Theorem 1. *Under the assumptions made in Section 3.2 and R and β sufficiently small, a constant $\varepsilon_0 > 0$ exists, such that for the transition map $\pi : \Delta^{in} \to \Delta^{out}$ the following holds for all $\varepsilon \in (0, \varepsilon_0]$:*

(a) The attracting slow manifold S_ε^a with initial value $\theta(0) = \theta^* \in \mathbb{R}/(s\mathbb{Z})$ in Δ^{in} passes through Δ^{out} at a point $(R, h_\theta(\varepsilon), h_y(\varepsilon))$ after the time $T(\varepsilon)$. It holds

$$\begin{aligned}
h_y(\varepsilon) &= -\Omega_0\varepsilon^2 + \mathcal{O}\left(\varepsilon^3 \ln(\varepsilon)\right),\\
h_\theta(\varepsilon) &\equiv \theta^* + \frac{R^2}{\varepsilon^2} + \Omega_0 - \frac{\varepsilon}{R} + \mathcal{O}\left(\varepsilon^3 \ln(\varepsilon)\right) \mod s,
\end{aligned}$$

$$T(\varepsilon) = \frac{R^2}{\varepsilon^3} + \frac{\Omega_0}{\varepsilon} - \frac{1}{R} + \mathcal{O}\left(\varepsilon^2 \ln(\varepsilon)\right),$$

as $\varepsilon \to 0$.

The constant Ω_0 *is the smallest positive zero of*

$$J_{-\frac{1}{3}}\left(\frac{2z^{\frac{3}{2}}}{3}\right) + J_{\frac{1}{3}}\left(\frac{2z^{\frac{3}{2}}}{3}\right),$$

where $J_{-\frac{1}{3}}$ *and* $J_{\frac{1}{3}}$ *are Bessel functions of the first kind.*

(b) The y-component $\pi_y(r,\varepsilon)$ *of the transition map* π *is a strong contraction with respect to the coordinate* r*, i.e.*

$$\frac{\partial \pi_y(r,\varepsilon)}{\partial r} = \mathcal{O}\left(\exp\left(\frac{2cR^2}{3\varepsilon^3}\right)\right)$$

for some negative constant $c > -2$ *as* $\varepsilon \to 0$*. Hence,* Δ^{in} *is mapped under* π *to an interval around* $S^a_\varepsilon \cap \Delta^{out}$ *of size* $\mathcal{O}\left(\exp\left(\frac{2cR^3}{3\varepsilon^3}\right)\right)$*. Points of the image* $\pi(\Delta^{in})$ *have the same r-coordinate* R *and a y-component exponentially close to* $h_y(\varepsilon)$*, thus the expansion of the function* $h_y(\varepsilon)$ *is valid for the y-coordinate of all points in* $\pi(\Delta^{in})$*.*

Remark 3.10. *In general, slow manifolds are not unique and only determined up to* $\mathcal{O}\left(e^{-\frac{C}{\varepsilon}}\right)$ *with a constant* $C > 0$ *by Fenichel's Theorems 2.9. The slow manifolds are exponentially close in the entry set* Δ^{in} *and become even closer due to the strong contraction property of the map* π*. Hence, the asymptotic expansions of part (b) do not depend on the choice of the slow manifold.*

Main Theorem 1, which will be proven in Section 4.4, resembles Theorem 2.22 of Krupa and Szmolyan stated in Section 2.5. It characterizes, how the attracting Fenichel slow manifold $S^{\mathrm{a}}_\varepsilon$ continues in a neighborhood of the fold limit cycle for the normal form of the fast-slow LC fold (3.10). The leading order term of the asymptotic expansion of the function $h_y(\varepsilon)$ coincides with the finding by Krupa and Szmolyan by changing the velocity of the parameter drift from ε^3 to ε. The exponential contraction property stays the same. Additionally, Main Theorem 1 includes statements about the evolution of the rotational coordinate θ and the transition time T.

3.4.2. Local Theorem for the Discrete Fast-Slow Fold

To state a theorem about the Poincaré return map of system (3.10), we introduce the entry section

$$\Delta^{\mathrm{in}}_{\mathcal{P}} := \Delta^{\mathrm{in}} \cap \{\theta = 0\} = \left\{(r,\theta,y) \in \mathcal{D} :\ r \in I^{\mathrm{in}},\ \theta = 0,\ y = R^2\right\}$$

with the interval

$$I^{\mathrm{in}} = \left\{r \in \mathbb{R}_{\geq -v} :\ \left|-1 + \frac{r}{R}\right| \leq \beta\right\}.$$

In this section, we first state a local theorem covering the dynamics of the Poincaré return map of system (3.10) visible in charts K_1 and K_2. Afterwards, the results obtained for the Poincaré return map are transferred to the normal form of the discrete fast-slow fold singularity (3.1) in a corollary. To state the results, we define the local exit set

$$\Delta^{\mathrm{out}}_{\mathcal{P}} := \left\{(r,\theta,y) \in \mathcal{D} :\ 0 \leq r \leq \varepsilon H,\ \theta = 0,\ \varepsilon^2(-\Omega_0 + s) \leq y \leq \varepsilon^2(-\Omega_0 + 2s)\right\}$$

for the constant $H = h_r(s)$. The function h_r and the constant Ω_0 are specified in the following theorem. We denote the local transition map by $\pi^{\mathrm{loc}} : \Delta^{\mathrm{in}}_{\mathcal{P}} \to \Delta^{\mathrm{out}}_{\mathcal{P}}$. Main Theorem 2 provides conditions for the well-definedness of the embedding of Section 3.1 in the first two charts. Furthermore, it determines the number of iterates to map from $\Delta^{\mathrm{in}}_{\mathcal{P}}$ to $\Delta^{\mathrm{out}}_{\mathcal{P}}$ as well as the asymptotic expansion of the image of the point $x := S^{\mathrm{a}}_\varepsilon \cap \Delta^{\mathrm{in}}_{\mathcal{P}}$ under the map π^{loc}.

Main Theorem 2. *Under the assumptions made in Section 3.2 and s sufficiently small and fixed, a constant $\varepsilon_0 > 0$ exists, such that for the transition map $\pi^{loc} : \Delta_{\mathcal{P}}^{in} \to \Delta_{\mathcal{P}}^{out}$ the following holds for all $\varepsilon \in (0, \varepsilon_0]$:*

(a) Let δ^{loc} be defined as

$$\delta^{loc}(\varepsilon) := \frac{1}{s}\left(\frac{R^2}{\varepsilon^2} + \Omega_0\right) \mod 1.$$

Then the point $x := S_\varepsilon^a \cap \Delta_{\mathcal{P}}^{in}$ on the attracting slow manifold maps under the transition map π^{loc}, which is defined to be the n-th Poincaré return map $\mathcal{P}^n$ with

$$n(\varepsilon) := \left\lfloor \frac{1}{s}\left(\frac{R^2}{\varepsilon^2} + \Omega_0\right) \right\rfloor - 1 = \frac{1}{s}\left(\frac{R^2}{\varepsilon^2} + \Omega_0\right) - 1 - \delta^{loc} \geq 2,$$

to the point

$$\pi^{loc}(x) = \mathcal{P}^n(x) = \left(\varepsilon h_r((1 + \delta^{loc})s), 0, -\Omega_0\varepsilon^2 + (1 + \delta^{loc})s\varepsilon^2\right) \in \Delta_{\mathcal{P}}^{out},$$

as $\varepsilon \to 0$, where

$$h_r(\alpha) = \frac{1}{\alpha + \mathcal{O}(\alpha^3)} \qquad \text{as } \alpha \to 0^+.$$

The constant Ω_0 is the smallest positive zero of

$$J_{-\frac{1}{3}}\left(\frac{2z^{\frac{3}{2}}}{3}\right) + J_{\frac{1}{3}}\left(\frac{2z^{\frac{3}{2}}}{3}\right),$$

where $J_{-\frac{1}{3}}$ and $J_{\frac{1}{3}}$ are Bessel functions of the first kind.

(b) The r-component π_r^{loc} of the transition map π^{loc} is a strong contraction with respect to the coordinate r, i.e.

$$\frac{\partial \pi_r^{loc}(r, \varepsilon)}{\partial r} = \mathcal{O}\left(\exp\left(\frac{2cR^2}{3\varepsilon^3}\right)\right)$$

for some negative constant $c > -2$ as $\varepsilon \to 0$. Points of the image $\pi^{loc}(\Delta_{\mathcal{P}}^{in})$ have the same number of iterates $n(\varepsilon)$ and thus the same y-coordinate. The r-component is exponentially close to the r-coordinate $\pi_r^{loc}(x)$ of the point x on the slow manifold S_ε^a.

(c) The constant s is sufficiently small for this theorem, if it holds $s < \frac{\Omega_0 - \gamma_0}{2}$. The constant $\gamma_0 < \Omega_0$ is defined as $\gamma_0 := -h_y(0) > 0$, where h_y describes the y-component of the special solution of the Riccati equation

$$\begin{aligned} r' &= r^2 - y, \\ y' &= -1, \end{aligned}$$

which is further specified in Proposition 4.14 and [20].

Main Theorem 2 will be proven in Section 5.3. It determines a number of iterates n depending on ε, such that the n-th Poincaré return map maps a point x on the Fenichel slow manifold $S_\varepsilon^{\mathrm{a}}$ into the exit set $\Delta_{\mathcal{P}}^{\mathrm{out}}$. To achieve this, it is necessary to restrict in assertion (c) the constant s, which defines the embedding, to be small enough. The upper bound for the constant s is independent of the other constants ε_0 and R and can be expressed in terms of constants given by the Riccati equation. The iterates of the Poincaré return map lie on the solution curves of the normal form of the fast-slow LC fold (3.10). The exponential contraction property transfers for the Poincaré return map from the y- to the r-coordinate, as we apply to all initial conditions in $\Delta_{\mathcal{P}}^{\mathrm{in}}$ the same number of iterates of the Poincaré return map.

The assertions of Main Theorem 2 can be transferred to the discrete fast-slow fold singularity: as explained in Section 3.1, system (3.10) describes a slow and constant passage trough a fold bifurcation of limit cycles. By considering the Poincaré return map, a slow and constant passage through a discrete fold bifurcation is described. As $\theta' = \varepsilon$, the transition time of the continuous system (3.10) between the hits of the Poincaré section is $T_{\mathcal{P}}(1) = \frac{s}{\varepsilon}$. As $y' = -\varepsilon^3$, the decrease in y during one iteration is $\Delta y = -\varepsilon^2 s$. Hence, the Poincaré return map of system (3.10) is topologically equivalent to the normal form of the discrete fast-slow fold singularity

$$p: \quad \begin{cases} r \mapsto r + r^2 - y, \\ y \mapsto y - \tilde{\varepsilon}, \end{cases} \tag{3.11}$$

after a possible rescaling of the variables r and y. The parameter drift can be expressed as $\tilde{\varepsilon} = \varepsilon^2 s$, where the parameters ε and s belong to the normal form of the fast-slow LC fold (3.10). As the attracting slow manifold $S^{\mathrm{a}}_{\varepsilon}$ of system (3.10) is invariant, also the iterates of the normal form of the discrete fast-slow fold singularity (3.11) stay by construction on $S^{\mathrm{a}}_{\varepsilon}$. Consequently, the following corollary holds for system (3.11):

Main Corollary 2. *Under the assumptions made in Section 3.2 and s sufficiently small and fixed, a constant $\varepsilon_0 > 0$ exists, such that the following holds for all $\tilde{\varepsilon} \in (0, s\varepsilon_0^2]$:*

(a) Let δ^{loc} be defined as

$$\delta^{loc}(\tilde{\varepsilon}) := \frac{R^2}{\tilde{\varepsilon}} + \frac{\Omega_0}{s} \mod 1.$$

Then the point $x := S^a_\varepsilon \cap \Delta^{in}_{\mathcal{P}}$ on the attracting slow manifold of the normal form of the continuous fast-slow LC fold (3.10) restricted to the r- and y-component maps under the n-th iterate p^n of the normal form of the fast-slow map (3.11) with

$$n(\tilde{\varepsilon}) := \left\lfloor \frac{R^2}{\tilde{\varepsilon}} + \frac{\Omega_0}{s} \right\rfloor - 1 = \frac{R^2}{\tilde{\varepsilon}} + \frac{\Omega_0}{s} - 1 - \delta^{loc} \geq 2,$$

to the point

$$p^n(x) = \left(\tilde{\varepsilon}^{\frac{1}{2}} s^{-\frac{1}{2}} h_r((1 + \delta^{loc})s), -\frac{\Omega_0 \tilde{\varepsilon}}{s} + (1 + \delta^{loc})\tilde{\varepsilon} \right),$$

as $\tilde{\varepsilon} \to 0$, where

$$h_r(\alpha) = \frac{1}{\alpha + \mathcal{O}(\alpha^3)} \qquad \text{as } \alpha \to 0^+.$$

The constant Ω_0 is the smallest positive zero of

$$J_{-\frac{1}{3}}\left(\frac{2z^{\frac{3}{2}}}{3}\right) + J_{\frac{1}{3}}\left(\frac{2z^{\frac{3}{2}}}{3}\right),$$

where $J_{-\frac{1}{3}}$ and $J_{\frac{1}{3}}$ are Bessel functions of the first kind.

(b) The r-component p^n_r of the transition map p^n is a strong contraction with respect to the coordinate r, i.e.

$$\frac{\partial p^n_r(r, \tilde{\varepsilon})}{\partial r} = \mathcal{O}\left(\exp\left(\frac{2cR^2 s^{\frac{3}{2}}}{3\tilde{\varepsilon}^{\frac{3}{2}}} \right) \right)$$

for some negative constant $c > -2$ as $\tilde{\varepsilon} \to 0$. Points of the image $p^n(\Delta^{in}_{\mathcal{P}})$ have the same number of iterates $n(\varepsilon)$ and thus the same y-coordinate. The r-component is exponentially close to the r-coordinate $p^n_r(x)$ of the point x on the slow manifold S^a_ε.

(c) *The constant s is sufficiently small for this corollary, if it holds $s < \frac{\Omega_0 - \blacksquare_0}{2}$. The constant $\blacksquare_0 < \Omega_0$ is defined as $\blacksquare_0 := -h_y(0) > 0$, where h_y describes the y-component of the special solution of the Riccati equation*

$$\begin{aligned} r' &= r^2 - y, \\ y' &= -1, \end{aligned}$$

which is further specified in Proposition 4.14 and [20].

Main Corollary 2 shares the same properties as Main Theorem 2 regarding the number of iterates and the exponential contraction. As we have not introduced invariant manifold theory for fast-slow maps, the initial condition x is considered to be located on the Fenichel slow manifold $S^{\mathrm{a}}_\varepsilon$ of the higher dimensional ODE system (3.10). As the slow parameter drift in the map (3.11) depends on the constant s, the result of Main Corollary 2 is obtained for all $\tilde{\varepsilon}$ in the interval $(0, s\varepsilon_0^2]$, which depends on s.

3.4.3. Break Down of the Fold Embedding

As already discussed in Lemma 3.2, not all iterates of the normal form of the discrete fast-slow fold singularity can be tracked by an embedding with a constant rotation velocity. Main Theorem 3 characterizes the loss of well-definedness in the exit chart.

Main Theorem 3. *Under the assumptions made in Section 3.2 and in Main Theorem 2, no constants $\blacksquare_0 > 0$, $s > 0$ and $\varepsilon_0 > 0$ exist, such that the point $x := S^a_\varepsilon \cap \Delta^{in}_{\mathcal{P}}$ can for each $\varepsilon \in (0, \varepsilon_0]$ be mapped under Poincaré return maps into the half-space*

$$\{(r, \theta, y) \in \mathcal{D} : \; r \geq \blacksquare_0, \; y \in \mathbb{R}\}.$$

Hence, the embedding of the normal form of the discrete fast-slow fold singularity (3.11) *in the normal form of the continuous fast-slow fold singularity* (3.10) *loses its well-definedness, as no returns to the Poincaré section P are observed for $r \geq \blacksquare_0 > 0$.*

Main Theorem 3 will be proven in Section 5.5. This theorem shows, that the embedding defined in Section 3.1 is only well-defined in an ε-dependent neighborhood of the fold point. In Lemma 3.2, we already observed the finite time blowup of the solution curves of the normal form of the fast-slow LC fold (3.10). Main Theorem 3 additionally shows, that it is not possible to choose s or ε_0 small enough to leave the ε-dependent neighborhood of the fold point with finitely many iterates.

Remark 3.11. *In Section 6.3, the idea of the dual limit $\varepsilon, s \to 0$ is introduced. By allowing the constant s to depend on ε, we can adapt the return time to the Poincaré section and hence influence the number of returns. In that way it could be possible to define a transition map in the exit chart.*

Chapter 4

Analysis of the Fast-Slow LC Fold

In this chapter, we analyze the fast-slow fold of limit cycles with normal form (3.10). Several of the results derived will also be useful in Chapter 5, where we consider the discrete fast-slow fold singularity (3.11).

The idea of the analysis is based on the paper 'Geometric Analysis of the Singularly Perturbed Planar Fold' by Krupa and Szmolyan [17]. The main tool is the blowup method and the analysis is done in the three charts defined in Section 3.3. Section 4.1 treats the dynamics in the entry chart, Section 4.2 continues with the rescaling chart and Section 4.3 completes the analysis in the exit chart. The results obtained are combined in Section 4.4 to prove Main Theorem 1 for the normal form of the fast-slow LC fold (3.10).

4.1. Dynamics in the Entry Chart

In chart K_1, we aim to analyze the attracting Fenichel slow manifold $S^{\mathrm{a}}_{\varepsilon}$, when it approaches the non-hyperbolic circle S^{c}_0 of system (3.5), which is system (3.10) extended by the equation $\varepsilon' = 0$. Therefore we transfer system (3.5) in the coordinates of chart K_1 and study it afterwards.

Lemma 4.1. *In the entry chart, the blown-up vector field is given by*

$$\begin{aligned} r_1' &= \rho_1(1 - r_1^2) + \frac{1}{2}\rho_1\varepsilon_1^3 r_1, \\ \theta_1' &= \rho_1\varepsilon_1, \\ \rho_1' &= -\frac{1}{2}\rho_1^2\varepsilon_1^3, \\ \varepsilon_1' &= \frac{1}{2}\rho_1\varepsilon_1^4. \end{aligned} \tag{4.1}$$

Proof. From Lemma 3.8 we know, that the blowup in the entry chart is given by

$$(r, \theta, y, \varepsilon) = (\rho_1 r_1, \theta_1, \rho_1^2, \rho_1\varepsilon_1).$$

Inserting this formula into system (3.5), we obtain

$$\begin{aligned} y' = -\varepsilon^3 \quad &\Rightarrow \quad (\rho_1^2)' = -\rho_1^3\varepsilon_1^3 \quad &&\Rightarrow \quad \rho_1' = -\frac{1}{2}\rho_1^2\varepsilon_1^3, \\ r' = r^2 - y \quad &\Rightarrow \quad (\rho_1 r_1)' = \rho_1^2(r_1^2 - 1) \quad &&\Rightarrow \quad r_1' = \rho_1(r_1^2 - 1) + \frac{1}{2}\rho_1\varepsilon_1^3 r_1, \\ \theta' = \varepsilon \quad &\Rightarrow \quad \theta_1' = \rho_1\varepsilon_1 \quad &&\Rightarrow \quad \theta_1' = \rho_1\varepsilon_1, \\ \varepsilon' = 0 \quad &\Rightarrow \quad (\rho_1\epsilon_1)' = 0 \quad &&\Rightarrow \quad \varepsilon_1' = \frac{1}{2}\rho_1\varepsilon_1^4. \end{aligned}$$

□

As the polynomial vector field of system (4.1) has in each component the common factor ρ_1, we can desingularize the above vector field by dividing the right hand side of system (4.1) by ρ_1, as explained in Section 2.4. By Theorem A.8, the desingularization step corresponds to a positive transformation of time and does not change the orbits of the solution curves. We denote the new time scale by t_1 and have the relationship

$$\rho_1\,\mathrm{d}t = \mathrm{d}t_1.$$

Thus, the desingularized flow in chart K_1 is given by

$$\begin{aligned} r_1' &= r_1^2 - 1 + \frac{1}{2}\varepsilon_1^3 r_1, \\ \theta_1' &= \varepsilon_1, \\ \rho_1' &= -\frac{1}{2}\rho_1\varepsilon_1^3, \\ \varepsilon_1' &= \frac{1}{2}\varepsilon_1^4. \end{aligned} \tag{4.2}$$

We restrict the analysis in chart K_1 to the rectangular box

$$\mathcal{D}_1 := \{(r_1, \theta_1, \rho_1, \varepsilon_1) \in \mathbb{R} \times \mathbb{R}/(s\mathbb{Z}) \times \mathbb{R} \times \mathbb{R} : \ 0 \le \rho_1 \le R, \ 0 \le \varepsilon_1 \le E\},$$

where R is the same constant, which defined the entry set Δ^{in} in Section 3.2 and E is some small, positive constant. $\mathcal{D}_1$ as well as all further upcoming geometrical objects of the entry chart are visualized in Figure 4.1.

Our goal is to prove Main Theorem 1 for all $\varepsilon \in (0, \varepsilon_0]$ with some constant $\varepsilon_0 > 0$. By Lemma 3.8 it holds $\varepsilon = \rho_1\varepsilon_1$, hence we can express ε_0 by the constants defining $\mathcal{D}_1$ and obtain $\varepsilon_0 = ER$. In chart K_1, we define the entry set

$$\Sigma_1^{\text{in}} := \{(r_1, \theta_1, \rho_1, \varepsilon_1) \in \mathcal{D}_1 : \ \rho_1 = R\},$$

which is a three-dimensional face of $\mathcal{D}_1$.

Lemma 4.2. *The entry set Δ_ε^{in} defined in Section 3.2 is expressed in the coordinates of chart K_1 a subset of Σ_1^{in}.*

Proof. By Lemma 3.8 it holds $y = \rho_1^2$, such that the restriction $y = R^2$ in the entry set

$$\Delta_\varepsilon^{\text{in}} := \left\{(r, \theta, y, \varepsilon) \in \mathcal{D}_0 : \ r \in I^{\text{in}}, \ y = R^2, \ \varepsilon \le ER\right\}$$

with some interval $I^{\text{in}} \subset \mathbb{R}$ transfers in chart K_1 to the condition $\rho_1 = R$. This observation and Lemma 3.9 imply, that the condition $0 \le \varepsilon \le ER$ is equivalent to the condition $0 \le \varepsilon_1 \le E$. Thus, the entry set $\Delta_\varepsilon^{\text{in}}$ transferred to chart K_1 is a subset of Σ_1^{in} with an additional restriction for the r- or respectively r_1-coordinate. □

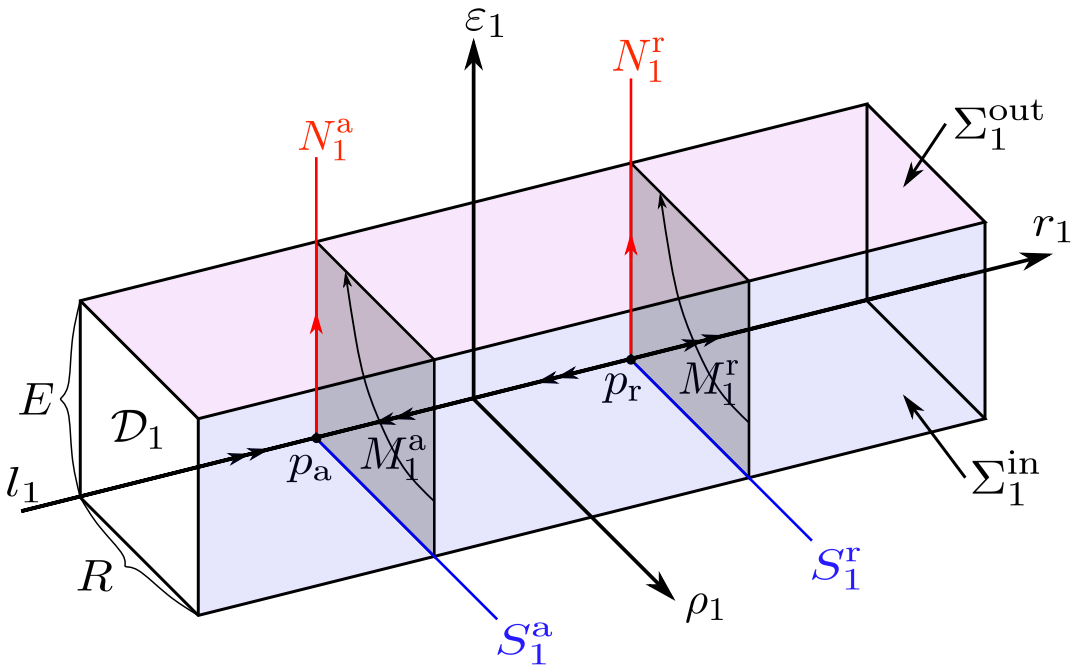


Figure 4.1.: Geometry of the dynamics in chart K_1 in the coordinates r_1, ρ_1 and ε_1.

We define in chart K_1 the exit set

$$\Sigma_1^{\text{out}} := \{(r_1, \theta_1, \rho_1, \varepsilon_1) \in \mathcal{D}_1 : \varepsilon_1 = E\},$$

which is also a three-dimensional face of $\mathcal{D}_1$. Our goal is to describe the flow of system (4.2) as a map from Σ_1^{in} to Σ_1^{out}. For the coordinates θ_1, ρ_1 and ε_1, the explicit solutions of system (4.2) are stated in the next Lemma.

Lemma 4.3. *Starting from initial conditions $\varepsilon_1(0) = \varepsilon_1^*$, $\theta_1(0) = \theta_1^*$ and $\rho_1(0) = \rho_1^*$, the solution of system (4.2) in the coordinates ε_1, θ_1 and ρ_1 is for $t_1 \in \left[0, \frac{2}{3(\varepsilon_1^*)^3}\right)$ given by*

$$\begin{aligned}
\varepsilon_1(t_1) &= \left(\frac{1}{(\varepsilon_1^*)^3} - \frac{3}{2}t_1\right)^{-\frac{1}{3}}, \\
\theta_1(t_1) &\equiv \theta_1^* + \frac{1}{(\varepsilon_1^*)^2} - \left(\frac{1}{(\varepsilon_1^*)^3} - \frac{3}{2}t_1\right)^{\frac{2}{3}} \equiv \theta_1^* + \frac{1}{(\varepsilon_1^*)^2} - \frac{1}{\varepsilon_1(t_1)^2} \mod s, \\
\rho_1(t_1) &= \rho_1^*\varepsilon_1^*\left(\frac{1}{(\varepsilon_1^*)^3} - \frac{3}{2}t_1\right)^{\frac{1}{3}} = \frac{\rho_1^*\varepsilon_1^*}{\varepsilon_1(t_1)}.
\end{aligned}$$

Hence, the solution curves in θ_1 and ρ_1 are given as smooth functions of ε_1 defined by

$$h_{\theta_1}(\varepsilon_1) := \theta_0 + \frac{1}{(\varepsilon_1^*)^2} - \frac{1}{\varepsilon_1^2} \mod s \qquad \text{and} \qquad h_{\rho_1}(\varepsilon_1) := \frac{\rho_1^*\varepsilon_1^*}{\varepsilon_1}.$$

Proof. The ODE for ε_1 can be solved by separation of variables. Inserting the solution for ε_1 into the ODEs for θ_1 and ρ_1, the solutions are obtained by direct integration and separation of variables. We observe, that the solution for ε_1 is well-defined for $t_1 \in \left[0, \frac{2}{3(\varepsilon_1^*)^3}\right)$ and the solutions for θ_1 and ρ_1 are well-defined for $t_1 \in \left[0, \frac{2}{3(\varepsilon_1^*)^3}\right]$. To write the solutions for θ_1 and ρ_1 dependent on the solution for ε_1, we restrict t_1 to the time interval $t_1 \in \left[0, \frac{2}{3(\varepsilon_1^*)^3}\right)$ for all three solutions. □

In system (4.2), the hyperplane $\{\rho_1 = 0\}$ and the hyperplane $\{\varepsilon_1 = 0\}$ are invariant subspaces. In the hyperplane $\{\varepsilon_1 = 0\}$, it holds $\theta_1' = 0$, such that the solution for the θ_1-coordinate is given by $\theta_1(t_1) = \theta_1^*$ for all $t_1 \geq 0$, where $\theta_1^* \in \mathbb{R}/(s\mathbb{Z})$ is the initial condition. The two hyperplanes $\{\rho_1 = 0\}$ and $\{\varepsilon_1 = 0\}$ intersect in the plane

$$l_1 := \{(r_1, \theta_1, \rho_1, \varepsilon_1) \in \mathcal{D}_1 : \rho_1 = 0,\ \varepsilon_1 = 0\},$$

which corresponds in $\{\varepsilon = 0\}$ to the part of the blown-up singular circle S_0^{c} of system (3.2) visible in chart K_1. The plane l_1 is invariant, with dynamics governed by

$$\begin{aligned}
r_1' &= r_1^2 - 1, \\
\theta_1' &= 0,
\end{aligned}$$

and contains the two circles of equilibria

$$p_{\text{a}} := \{(r_1, \theta_1, \rho_1, \varepsilon_1) \in \mathcal{D}_1 : r_1 = -1,\ \rho_1 = 0,\ \varepsilon_1 = 0\}$$

and

$$p_{\text{r}} := \{(r_1, \theta_1, \rho_1, \varepsilon_1) \in \mathcal{D}_1 : r_1 = 1,\ \rho_1 = 0,\ \varepsilon_1 = 0\}.$$

Linearising system (4.2) around the circles of equilibria p_{a} and p_{r} leads to

$$J(r_1, \theta_1, \rho_1, \varepsilon_1) = \begin{pmatrix} 2r_1 + \frac{1}{2}\varepsilon_1^3 & 0 & 0 & \frac{3}{2}\varepsilon_1^2 r_1 \\ 0 & 0 & 0 & 1 \\ 0 & 0 & -\frac{1}{2}\varepsilon_1^3 & -\frac{3}{2}\rho_1\varepsilon_1^2 \\ 0 & 0 & 0 & 2\varepsilon^3 \end{pmatrix},$$

$$\Rightarrow \qquad J(p_a) = \begin{pmatrix} -2 & 0 & 0 & 0 \\ 0 & 0 & 0 & 1 \\ 0 & 0 & 0 & 0 \\ 0 & 0 & 0 & 0 \end{pmatrix}, \qquad J(p_r) = \begin{pmatrix} 2 & 0 & 0 & 0 \\ 0 & 0 & 0 & 1 \\ 0 & 0 & 0 & 0 \\ 0 & 0 & 0 & 0 \end{pmatrix}.$$

Thus, all equilibria on p_a have the eigenvalue -2 and all eigenvalues on p_r have the eigenvalue 2 with eigenvector $(1,0,0,0)$. All fixed points additionally have a triple zero eigenvalue with eigenvectors $(0,1,0,0)$ and $(0,0,1,0)$ and generalized eigenvector $(0,0,0,1)$. Hence, p_a is attracting and p_r is repelling on the plane l_1. Through the blowup transformation we have gained partial hyperbolicity of the circles p_a and p_r in the r_1-coordinate. Figure 4.2 shows the plane l_1 with the attracting and the repelling circle on it.

In the invariant hyperplane $\{\varepsilon_1 = 0\}$, the dynamics is governed by

$$\begin{aligned} r_1' &= r_1^2 - 1, \\ \theta_1' &= 0, \\ \rho_1' &= 0. \end{aligned} \tag{4.3}$$

As θ_1 and ρ_1 are constant in system (4.3), the cylinder

$$S_1^a = \{(r_1, \theta_1, \rho_1, \varepsilon_1) \in \mathcal{D}_1 : r_1 = -1,\ \varepsilon_1 = 0\}$$

consists of equilibria and emanates from the circle p_a. It is normally hyperbolic and attracting, as along S_1^a, the linearization of system (4.3) has the eigenvalue -2 corresponding to the eigenvector $(1,0,0)$, and a double zero-eigenvalue with eigenvectors $(0,1,0)$ and $(0,0,1)$. Likewise, the cylinder of equilibria

$$S_1^r = \{(r_1, \theta_1, \rho_1, \varepsilon_1) \in \mathcal{D}_1 : r_1 = 1,\ \varepsilon_1 = 0\}$$

emanates from the circle p_r and is repelling normally hyperbolic due to the eigenvalue 2 corresponding to the eigenvector $(1,0,0)$, and the double zero-eigenvalue with eigenvectors $(0,1,0)$ and $(0,0,1)$. The two normally hyperbolic cylinders S_1^a and S_1^r are visualized in Figure 4.2 and correspond by Lemma 3.8 to the branches S_0^a and S_0^r of the critical manifold S_0, i.e. the two

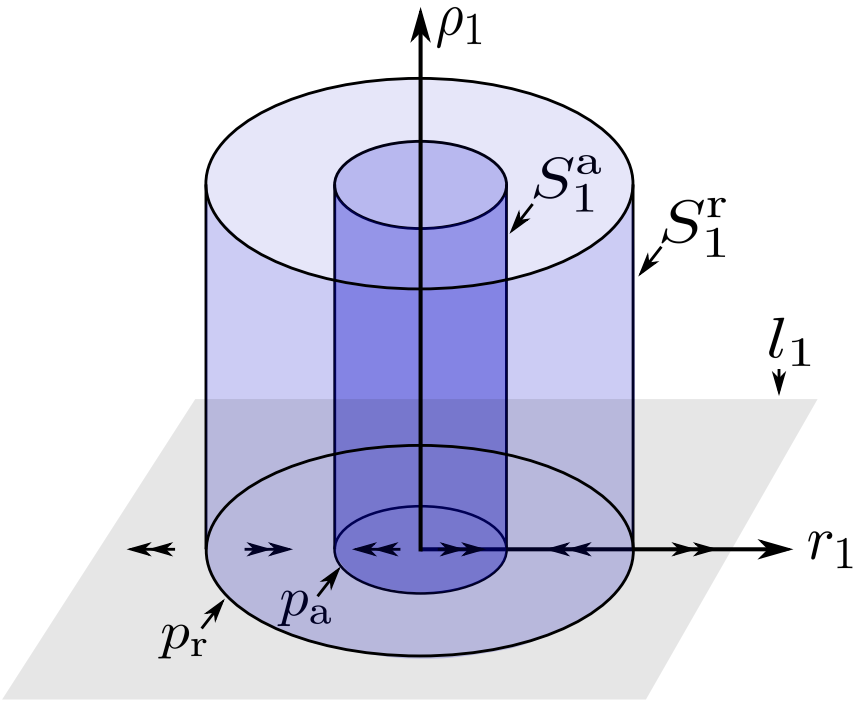


Figure 4.2.: Geometry of the dynamics in chart K_1 in the coordinates r_1, ρ_1 and θ_1 in the hyperplane $\{\varepsilon_1 = 0\}$.

attracting, respectively repelling manifolds coincide where their domains of definition overlap. Thus, the blowup in chart K_1 has extended the normally hyperbolic branches S_1^{a} and S_1^{r} to the blowup surface $S^1 \times S^2$ at the circles p_{a} and p_{r}.

In the invariant hyperplane $\{\rho_1 = 0\}$, the dynamics is governed by

$$\begin{aligned} r_1' &= r_1^2 - 1 + \frac{1}{2}\varepsilon_1^3 r_1, \\ \theta_1' &= \varepsilon_1, \\ \varepsilon_1' &= \frac{1}{2}\varepsilon_1^4. \end{aligned} \tag{4.4}$$

Again, p_{a} and p_{r} form two circles of equilibria. As the linearization of system (4.4) at p_{a} has the eigenvalue -2 with eigenvector $(1,0,0)$ and a double zero eigenvalue with generalized eigenvectors $(0,1,0)$ and $(0,0,1)$, an attracting two-dimensional center manifold M_1^{a} at p_{a} exists by the Center Manifold Theorem A.11. Analogously, a repelling two-dimensional center manifold M_1^{r} at p_{r} exists.

Based on the observations made, we have the following result for the dynamics in chart K_1:

Proposition 4.4. *For $E, R > 0$ sufficiently small, system (4.2) has the following properties:*

(a) There exists a three-dimensional center-stable manifold M_1^a at p_a that contains N_1^a and S_1^a. In $\mathcal{D}_1$, the manifold M_1^a is given as a smooth graph $r_1 = h_{r_1}(\varepsilon_1)$, where

$$h_{r_1}(\varepsilon_1) = -1 - \frac{1}{4}\varepsilon_1^3 + \frac{5}{32}\varepsilon_1^6 + \mathcal{O}(\varepsilon_1^9) \qquad \text{as } \varepsilon_1 \to 0^+.$$

The branch of the attracting center manifold M_1^a in $\{\varepsilon_1 > 0\}$ is unique.

(b) There exists a three-dimensional center-repelling manifold M_1^r at p_r that contains N_1^r and S_1^r. In $\mathcal{D}_1$, the manifold M_1^r is given as a smooth graph $r_1 = \tilde{h}_{r_1}(\varepsilon_1)$, where

$$\tilde{h}_{r_1}(\varepsilon_1) = 1 - \frac{1}{4}\varepsilon_1^3 - \frac{5}{32}\varepsilon_1^6 + \mathcal{O}(\varepsilon_1^9) \qquad \text{as } \varepsilon_1 \to 0^+.$$

The branch of the repelling center manifold M_1^r in $\{\varepsilon_1 > 0\}$ is not unique.

Proof. The existence of the center manifolds M_1^{a} and M_1^{r} follows from the Center Manifold Theorem A.11. M_1^{a} and M_1^{r} contain the two-dimensional manifolds N_1^{a} and S_1^{a} or respectively N_1^{r} and S_1^{r}, since these are obtained by restricting the flow to the invariant hyperplanes $\{\varepsilon_1 = 0\}$ or $\{\rho_1 = 0\}$. As the right hand side of system (4.2) is smooth, also the graph functions describing the center manifolds are smooth.

To calculate the r_1-component of the center manifolds M_1^{a} and M_1^{r}, we recognize, that the dynamics in the r_1-component

$$r_1' = r_1^2 - 1 + \frac{1}{2}\varepsilon_1^3 r_1$$

only depends on ε_1 and r_1. Thus, we insert the power series

$$r_1 = h_{r_1}(\varepsilon_1) = \sum_{n=0}^{\infty} a_n \varepsilon_1^n$$

in the ODE for r_1 in system (4.2) and determine the coefficients $(a_n)_{n\in\mathbb{N}_0}$. Using the equation $\varepsilon_1' = \frac{1}{2}\varepsilon_1^4$, we obtain for the left hand side

$$r_1' = \frac{d}{dt} h_{r_1}(\varepsilon_1) = \frac{d}{d\varepsilon_1} h_{r_1}(\varepsilon_1)\, \varepsilon_1' = \sum_{n=1}^{\infty} a_n n \varepsilon_1^{n-1} \varepsilon_1' = \frac{1}{2}\sum_{n=0}^{\infty} a_{n+1}(n+1)\varepsilon^{n+4}.$$

This has to be equal to the right hand side

$$r_1^2 - 1 + \frac{1}{2}\varepsilon_1^3 r_1 = \left(\sum_{n=0}^{\infty} a_n \varepsilon_1^n\right)^2 - 1 + \frac{1}{2}\varepsilon_1^3 \sum_{n=0}^{\infty} a_n \varepsilon_1^n$$
$$= \sum_{n=0}^{\infty} \left(\sum_{k=0}^{n} a_k a_{n-k}\right) \varepsilon_1^n - 1 + \frac{1}{2}\sum_{n=0}^{\infty} a_n \varepsilon_1^{n+3}.$$

For the different orders in ε_1 up to $\mathcal{O}(\varepsilon_1^8)$ we obtain

$$\begin{aligned}
\mathcal{O}(1): &\quad 0 = a_0^2 - 1 && \Rightarrow \quad a_0 = \pm 1,\\
\mathcal{O}(\varepsilon_1): &\quad 0 = 2a_0 a_1 && \Rightarrow \quad a_1 = 0,\\
\mathcal{O}(\varepsilon_1^2): &\quad 0 = 2a_0 a_2 + a_1^2 && \Rightarrow \quad a_2 = 0,\\
\mathcal{O}(\varepsilon_1^3): &\quad 0 = 2a_0 a_3 + 2a_1 a_2 + \frac{1}{2}a_0 && \Rightarrow \quad a_3 = -\frac{1}{4},\\
\mathcal{O}(\varepsilon_1^4): &\quad \frac{1}{2}a_1 = 2a_0 a_4 + 2a_1 a_3 + a_2^2 + \frac{1}{2}a_1 && \Rightarrow \quad a_4 = 0,\\
\mathcal{O}(\varepsilon_1^5): &\quad a_2 = 2a_0 a_5 + 2a_1 a_4 + 2a_2 a_3 + \frac{1}{2}a_2 && \Rightarrow \quad a_5 = 0,\\
\mathcal{O}(\varepsilon_1^6): &\quad \frac{3}{2}a_3 = 2a_0 a_6 + 2a_1 a_5 + 2a_2 a_4 + a_3^2 + \frac{1}{2}a_3 && \Rightarrow \quad a_6 = -a_0\frac{5}{32},\\
\mathcal{O}(\varepsilon_1^7): &\quad 2a_4 = 2a_0 a_7 + 2a_1 a_6 + 2a_2 a_5 + 2a_3 a_4 + \frac{1}{2}a_4 && \Rightarrow \quad a_7 = 0,\\
\mathcal{O}(\varepsilon_1^8): &\quad \frac{5}{2}a_5 = 2a_0 a_8 + 2a_1 a_7 + 2a_2 a_6 + 2a_3 a_5 + a_4^2 + \frac{1}{2}a_5 && \Rightarrow \quad a_8 = 0.
\end{aligned}$$

Since the manifold $\mathcal{M}_1^{\mathrm{a}}$ contains the circle of equilibria p_{a} in the hyperplane $\{\varepsilon_1 = 0\}$, it follows $a_0 = -1$ and we obtain the function h_{r_1}. The manifold $\mathcal{M}_1^{\mathrm{r}}$ contains the circle of equilibria p_{r} in the hyperplane $\{\varepsilon_1 = 0\}$, such that $a_0 = 1$ and we obtain the function $\tilde{h}_{r_1}$.

In the invariant hyperplane $\{\rho_1 = 0\}$, each equilibrium of the circle p_{a} is a saddle and therefore has a unique emanating trajectory in the half-plane $\{\rho_1 = 0,\ \varepsilon_1 > 0\}$. As the graph representation of $\mathcal{M}_1^{\mathrm{a}}$ only depends on ε_1, the three-dimensional center manifold $\mathcal{M}_1^{\mathrm{a}}$ is also unique.

On the other hand, each equilibrium of the circle p_{r} is a node in the invariant hyperplane $\{\rho_1 = 0\}$. Thus, not only one trajectory emanating from each equilibrium on p_{r} exists, such that the branch of $\mathcal{M}_1^{\mathrm{r}}$ in $\{\varepsilon_1 > 0\}$ is not unique. By Remark 3.5, the center manifold $\mathcal{M}_1^{\mathrm{r}}$ is unique up to order $\mathcal{O}\left(e^{-C/\varepsilon_1}\right)$, but as $e^{-C/\varepsilon_1} \in \mathcal{O}\left(\varepsilon_1^n\right)$ for all $n \geq 0$, all center manifolds $\mathcal{M}_1^{\mathrm{r}}$ have the same graph representation up to order $\mathcal{O}(\varepsilon_1^9)$ in $\tilde{h}_{r_1}$. □

As the center manifold $\mathcal{M}_1^{\mathrm{a}}$ is attracting, local stable manifold $\mathcal{W}_{\mathrm{loc}}^{\mathrm{s}}(\mathcal{M}_1^{\mathrm{a}})$ at $\mathcal{M}_1^{\mathrm{a}}$ exists. Analogously, a local unstable manifold $\mathcal{W}_{\mathrm{loc}}^{\mathrm{u}}(\mathcal{M}_1^{\mathrm{r}})$ at $\mathcal{M}_1^{\mathrm{r}}$ exists, as the center manifold $\mathcal{M}_1^{\mathrm{r}}$ is repelling. By Theorem A.12, there exist foliations $\mathcal{F}^{\mathrm{s}}$ and $\mathcal{F}^{\mathrm{u}}$ for the invariant center manifolds $\mathcal{M}_1^{\mathrm{a}}$ and $\mathcal{M}_1^{\mathrm{r}}$. These consist of fast fibers $\mathcal{F}^{\mathrm{s}}(p)$ or $\mathcal{F}^{\mathrm{u}}(p)$, which are for each point p on the center manifold tangent to the normal bundle at p. Fibers are characterized by the fact, that initial points approach each other at an exponential rate in forward time for the attracting center manifold and in backward time for the repelling center manifold. In that way, $\mathcal{W}_{\mathrm{loc}}^{\mathrm{s}}(\mathcal{M}_1^{\mathrm{a}})$ and $\mathcal{W}_{\mathrm{loc}}^{\mathrm{u}}(\mathcal{M}_1^{\mathrm{r}})$ are foliated by the fibers into submanifolds:

$$\mathcal{F}^{\mathrm{s}} := \bigcup_{p \in \mathcal{M}_1^{\mathrm{a}}} \mathcal{F}^{\mathrm{s}}(p) = \mathcal{W}_{\mathrm{loc}}^{\mathrm{s}}(\mathcal{M}_1^{\mathrm{a}}), \qquad \mathcal{F}^{\mathrm{u}} := \bigcup_{p \in \mathcal{M}_1^{\mathrm{r}}} \mathcal{F}^{\mathrm{u}}(p) = \mathcal{W}_{\mathrm{loc}}^{\mathrm{u}}(\mathcal{M}_1^{\mathrm{r}}).$$

The fibers are one-dimensional, as the invariant manifolds $\mathcal{M}_1^{\mathrm{a}}$ and $\mathcal{M}_1^{\mathrm{r}}$ are three-dimensional objects in $\mathbb{R} \times \mathbb{R}/(s\mathbb{Z}) \times \mathbb{R} \times \mathbb{R}$. The set of stable fibers is positively invariant, i.e.

$$\phi_t(\mathcal{F}^{\mathrm{s}}(p)) \subset \mathcal{F}^{\mathrm{s}}(\phi_t(p)) \qquad \text{for } t \geq 0$$

and $p \in \mathcal{M}_i^{\mathrm{a}}$, where ϕ_t is the flow map, whereas the set of unstable fibers is negatively invariant, in the sense that

$$\phi_{-t}(\mathcal{F}^{\mathrm{s}}(p)) \subset \mathcal{F}^{\mathrm{s}}(\phi_{-t}(p)) \qquad \text{for } t \geq 0$$

and $p \in \mathcal{M}_i^{\mathrm{r}}$. Note that the fibers themselves are not necessarily invariant manifolds. The following proposition characterizes the exponential contraction rates for the fibers of the foliations $\mathcal{F}^{\mathrm{s}}$ and $\mathcal{F}^{\mathrm{u}}$:

Proposition 4.5. *For $E, R > 0$ sufficiently small, system (4.2) has the following properties:*

(a) There exists a stable invariant foliation $\mathcal{F}^s$ with base $\mathcal{M}_i^a$ and one-dimensional fibers. For every $c > -2$, a choice of $E > 0$ exists, such that the contraction along $\mathcal{F}^s$ is stronger than e^{ct_i}.

(b) There exists a unstable invariant foliation $\mathcal{F}^u$ with base $\mathcal{M}_i^r$ and one-dimensional fibers. For every $c < 2$, a choice of $E > 0$ exists, such that the expansion along $\mathcal{F}^u$ is stronger than e^{ct_i}.

Proof. The existence of the stable and unstable invariant foliations $\mathcal{F}^s$ and $\mathcal{F}^u$ follows from Theorem A.12. The leaves of the foliations are one-dimensional fibers, as the base manifolds $\mathcal{M}_i^{\mathrm{a}}$ and $\mathcal{M}_i^{\mathrm{r}}$ are three-dimensional objects in $\mathbb{R} \times \mathbb{R}/(s\mathbb{Z}) \times \mathbb{R} \times \mathbb{R}$. The linearization of system (4.2) implies, that the exponential contraction (expansion) along the stable (unstable) fibers with base point p on $\mathcal{M}_i^{\mathrm{a}}$ ($\mathcal{M}_i^{\mathrm{r}}$) is stronger than $e^{\lambda_{r_i} t_i}$, where λ_{r_i} is the eigenvalue corresponding to the r_i-coordinate. λ_{r_i} is for $E > 0$ sufficiently small the smallest (largest) eigenvalue of system (4.2), which therefore induces the fastest contraction rate in forward (backward) time.

For the stable foliation $\mathcal{F}^{\mathrm{s}}$, we can use the graph representation $h_{r_i}(\varepsilon_i)$ for the r_i-coordinate of the attracting center manifold $\mathcal{M}_i^{\mathrm{a}}$ of Proposition 4.4, such that

$$\lambda_{r_i} = 2h_{r_i}(\varepsilon_i) + \frac{1}{2}\varepsilon_i^3 = -2 + \frac{5}{16}\varepsilon_i^6 + \mathcal{O}\left(\varepsilon_i^9\right) \qquad \text{as } \varepsilon_i \to 0^+.$$

Thus, for each $c > -2$, the constant $E > 0$ can be chosen small enough, such that contraction along the stable fibers is stronger than e^{ct_i}.

For the unstable foliation $\mathcal{F}^{\mathrm{u}}$, we can use the graph representation $\tilde{h}_{r_i}(\varepsilon_i)$ for the r_i-coordinate of the repelling center manifold $\mathcal{M}_i^{\mathrm{r}}$ of Proposition 4.4, such that

$$\lambda_{r_i} = 2\tilde{h}_{r_i}(\varepsilon_i) + \frac{1}{2}\varepsilon_i^3 = 2 - \frac{5}{16}\varepsilon_i^6 + \mathcal{O}\left(\varepsilon_i^9\right) \qquad \text{as } \varepsilon_i \to 0^+.$$

Consequently, for each $c < 2$, the constant $E > 0$ can be chosen small enough, such that the expansion along the unstable fibers is stronger than e^{ct_i}. □

Now we introduce for the constant β, which defines the interval I^{in} of the entry set $\Delta_\varepsilon^{\mathrm{in}}$ in the original coordinates, the rectangular subset R_i of the entry set Σ_i^{in} as

$$R_i := \{(r_i, \theta_i, \rho_i, \varepsilon_i) \in \Sigma_i^{\mathrm{in}} : |-1 + r_i| \leq \beta\}.$$

We choose the constants E, R and β in such a way, that $\Sigma_i^{\mathrm{in}} \cap \mathcal{M}_i^{\mathrm{a}} \subset R_i$. These objects are visualized in Figure 4.3.

Lemma 4.6. *The rectangle R_i in chart K_i corresponds to the entry set Δ_ε^{in} in the original coordinates.*

Proof. By Lemma 4.2, $\Delta_\varepsilon^{\mathrm{in}}$ transferred to the coordinates of chart K_i is a subset of the entry set Σ_i^{in} with the additional restriction $r \in I^{\mathrm{in}}$, where

$$I^{\mathrm{in}} = \left\{ r \in \mathbb{R}_{\geq -v} : \left| -1 + \frac{r}{R} \right| \leq \beta \right\}.$$

The coordinate transformation for chart K_1 of Lemma 3.8 implies that

$$\left|-1 + \frac{r}{R}\right| \leq \beta \Leftrightarrow |-1 + r_1| \leq \beta$$

as $r = \rho_1 r_1 = R r_1$ in Σ_1^{in}. Thus, there is a one-to-one correspondence between the rectangle R_1 and the entry set $\Delta_\varepsilon^{\text{in}}$. □

The following lemma shows, that the flow of system (4.2) maps for $\varepsilon_1 > 0$ the entry set Σ_1^{in} to the exit set Σ_1^{out}. We denote the resulting map by Ψ_1.

Lemma 4.7. *The transition map $\Psi_1 : \Sigma_1^{in} \cap \{\varepsilon_1 > 0\} \to \Sigma_1^{out}$ is well-defined.*

Proof. By Lemma 4.3, the solution for the evolution of ε_1 in system (4.2) with initial condition $\varepsilon_1(0) = \varepsilon_1^* > 0$ is given by

$$\varepsilon_1(t_1) = \left(\frac{1}{(\varepsilon_1^*)^3} - \frac{3}{2}t_1\right)^{-\frac{1}{3}}.$$

This solution is well-defined and increasing for $t_1 \in \left[0, \frac{2}{3(\varepsilon_1^*)^3}\right)$, such that $\varepsilon_1(t_1) > 0$ for $\varepsilon_1^* > 0$ and $t_1 \in \left[0, \frac{2}{3(\varepsilon_1^*)^3}\right)$. For $\varepsilon_1 > 0$ and $\rho_1 > 0$ it holds $\rho_1' < 0$ in system (4.2). As the hyperplane $\{\rho_1 = 0\}$ is invariant, the ρ_1-coordinate of all points with initial condition $\{\rho_1 = R\}$ stays in the interval $(0, \rho_1]$ for $t_1 \geq 0$. For $t_1 \to \frac{2}{3(\varepsilon_1^*)^3}$ the solution in ε_1 blows up to $+\infty$. Thus, the flow hits the exit set Σ_1^{out}, such that the image of $\Sigma_1^{\text{in}} \cap \{\varepsilon_1 > 0\}$ under the map Ψ_1 is contained in the exit set Σ_1^{out}. □

Lemma 4.8. *The transition time T_1 from a point $p = (r_1^*, \theta_1^*, R, \varepsilon_1^*) \in \Sigma_1^{in} \cap \{\varepsilon_1^* > 0\}$ to the point $\Psi_1(p) \in \Sigma_1^{out}$ satisfies*

$$T_1(\varepsilon_1^*) = \frac{2}{3}\left(\frac{1}{(\varepsilon_1^*)^3} - \frac{1}{E^3}\right).$$

Proof. After the transition time T_1 it holds

$$\varepsilon_1(T_1) = \left(\frac{1}{(\varepsilon_1^*)^3} - \frac{3}{2}T_1\right)^{-\frac{1}{3}} = E$$

Solving this equation for T_1 leads to the formula for the transition time. □

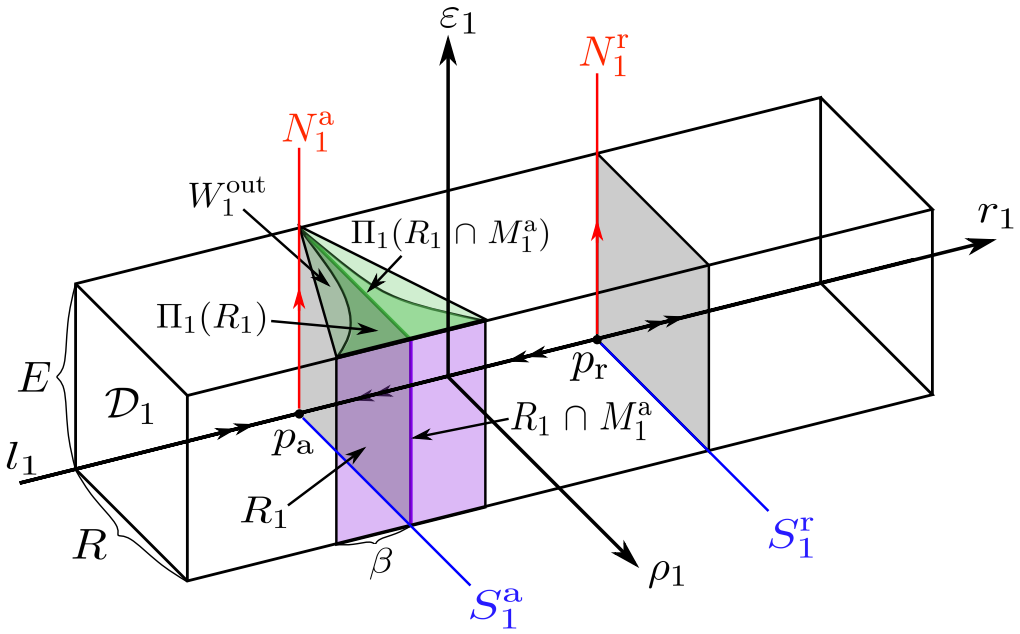


Figure 4.3.: Entry rectangle R_i and its image $\Pi_i(R_i)$ in chart K_i in the coordinates r_i, ρ_i and ε_i. The exponential contraction along the fibers is visualized.

Remark 4.9. *The transition time $T_1(\varepsilon_1^*)$ is finite and smaller than $\frac{2}{3(\varepsilon_1^*)^3}$ for starting points in the entry set $\Sigma_1^{in} \cap \{\varepsilon_1 > 0\}$. Hence, no blowup of the solution in ε_1 is observed in chart K_1.*

Remark 4.10. *Allowing for infinite transition times, the map Ψ_1 has a natural smooth extension to the hyperplane $\{\varepsilon_1 = 0\}$, such that we consider from now on the extended map $\Psi_1 : \Sigma_1^{in} \to \Sigma_1^{out}$.*

In the following proposition, we collect all important properties about the map Ψ_1 describing the dynamics in chart K_1.

Proposition 4.11. *The transition map $\Psi_1 : \Sigma_1^{in} \to \Sigma_1^{out}$ defined by the flow of system (4.2) has the following properties:*

(a) For fixed $c > -2$ and constants E, R and β, the image of a point $p = (r_1^*, \theta_1^*, R, \varepsilon_1^*) \in R_1$ under the map Ψ_1 is the point

$$\Psi_1(r_1^*, \theta_1^*, R, \varepsilon_1^*) = \left(\Psi_{1,r_1}(r_1^*, \varepsilon_1^*), \theta_1^* + \frac{1}{(\varepsilon_1^*)^2} - \frac{1}{E^2} \bmod s, \frac{R}{E}\varepsilon_1^*, E\right),$$

with

$$\Psi_{1,r_1}(r_1^*, \varepsilon_1^*) = h_{r_1}(E) + \mathcal{O}\left(\exp\left(\frac{2c}{3(\varepsilon_1^*)^3}\right)\right),$$

where the function h_{r_1}, describing the r_1-coordinate of points on the center manifold M_1^a, is defined in Proposition 4.4.

(b) Ψ_1 is an exponential contraction in the r_1-coordinate with respect to the initial condition r_1^*, i.e.

$$\frac{\partial \Psi_{1,r_1}}{\partial r_1^*} = \mathcal{O}\left(\exp\left(\frac{2c}{3(\varepsilon_1^*)^3}\right)\right)$$

for some negative constant $c > -2$. Thus, the image $\Psi_1(R_1)$ is a wedge-like region about $\Sigma_1^{out} \cap M_1^a$ in Σ_1^{out}.

(c) $\Psi_1(R_1 \cap M_1^a) \subset \Sigma_1^{out}$ is a smooth surface transverse to the hyperplane $\{\rho_1 = 0\}$ of the form

$$\Sigma_1^{out} \cap M_1^a = \left\{(r_1, \theta_1, \rho_1, \varepsilon_1) \in \Sigma_1^{out} : \ r_1 = h_{r_1}(E)\right\}.$$

Furthermore, the image $\Psi_1(R_1)$ is contained in the set

$$W_1^{out} := \left\{(r_1, \theta_1, \rho_1, \varepsilon_1) \in \Sigma_1^{out} : \ h_{r_1}(E) - \frac{\rho_1}{R}\beta \le r_1 \le h_{r_1}(E) + \frac{\rho_1}{R}\beta\right\}.$$

Proof. By the well-definedness of the map Ψ_1 proven in Lemma 4.7, the ε_1-coordinate of $\Psi_1(p)$ is E. In system (3.5) it holds $\varepsilon' = 0$. As by Lemma 3.8 we have $\varepsilon = \varepsilon_1\rho_1$, it holds

$$\varepsilon_1^* R = \varepsilon_1(0)\rho_1(0) = \varepsilon_1(T_1)\rho_1(T_1) = E\rho_1(T_1).$$

Thus, the ρ_1-coordinate of $\Psi_1(p)$ is $\frac{R}{E}\varepsilon_1^*$. The value of the θ_1-coordinate of $\Psi_1(p)$ follows by plugging in $\varepsilon_1(T_1) = E$ in the formula for the evolution in θ_1 given in Lemma 4.3. By Proposition 4.5 (a) it follows, that for $E > 0$ small enough, there is exponential contraction in the r_1-coordinate. For each $c > -2$, the contraction of the map Ψ_1 along these fibers with base manifold M_1^a is stronger than e^{cT_1}. Therefore, the r_1-coordinate of the image $\Psi_1(p)$ can be represented as the r_1-coordinate of the center manifold M_1^a in Σ_1^{out}, given by $h_{r_1}(E)$, plus some remainder term $R(r_1^*, \varepsilon_1^*) \in \mathcal{O}\left(e^{cT_1}\right)$. Plugging in the transition time $T_1(\varepsilon_1^*)$ yields

$$\Psi_{1,r_1}(r_1^*, \varepsilon_1^*) = h_{r_1}(E) + \mathcal{O}\left(\exp\left(\frac{2c}{3(\varepsilon_1^*)^3}\right)\right).$$

Even though it is possible to bound the distance in r_i-direction by e^{cT_i} times some sufficiently large constant, which only depends on ε_i^*, the higher order terms can depend on r_i^*, such that we write $\boldsymbol{\Psi}_{i,r_i}(r_i^*, \varepsilon_i^*)$. By taking the partial derivative of $\boldsymbol{\Psi}_{i,r_i}(r_i^*, \varepsilon_i^*)$ with respect to r_i^*, the exponential contraction in statement (b) follows immediately.

As the center manifold $\boldsymbol{M}_i^{\mathrm{a}}$ and the flow of system (4.2) are smooth, the image $\boldsymbol{\Psi}_i(\boldsymbol{R}_i \cap \boldsymbol{M}_i^{\mathrm{a}}) \subset \Sigma_i^{\mathrm{out}}$ is a smooth surface. Furthermore, Σ_i^{out} is by definition orthogonal to the hyperplane $\{\rho_i = 0\}$. As the center manifold $\boldsymbol{M}_i^{\mathrm{a}}$ is invariant, $\boldsymbol{\Psi}_i(\boldsymbol{R}_i \cap \boldsymbol{M}_i^{\mathrm{a}})$ has the constant r_i-coordinate $h_{r_i}(E)$, because $\varepsilon_i = E$ in the exit set Σ_i^{out}. Thus, the surface $\boldsymbol{\Psi}_i(\boldsymbol{R}_i \cap \boldsymbol{M}_i^{\mathrm{a}})$ is transverse to the hyperplane $\{\rho_i = 0\}$. In $\boldsymbol{R}_i \cap \boldsymbol{M}_i^{\mathrm{a}}$, the initial condition θ_i^* attains all values in $\mathbb{R}/(s\mathbb{Z})$. Since after the transition time T_i it holds

$$\theta_i(T_i) \equiv \theta_i^* + \frac{1}{(\varepsilon_i^*)^2} - \frac{1}{E^2} \mod s,$$

$\theta_i(T_i)$ attains for each initial condition (r_i^*, ε_i^*) all values in $\mathbb{R}/(s\mathbb{Z})$. Hence, it holds $\theta_i \in \mathbb{R}/(s\mathbb{Z})$ in $\boldsymbol{\Psi}_i(\boldsymbol{R}_i \cap \boldsymbol{M}_i^{\mathrm{a}})$. As $\varepsilon_i^* \in [0, E]$ in $\boldsymbol{R}_i \cap \boldsymbol{M}_i^{\mathrm{a}}$, we finally deduce that $\rho_i = \frac{R}{E}\varepsilon_i^* \in [0, \boldsymbol{R}]$ for $\boldsymbol{\Psi}_i(\boldsymbol{R}_i \cap \boldsymbol{M}_i^{\mathrm{a}})$.

For the last statement, we consider the image of the rectangle $\boldsymbol{R}_i$ under the map $\boldsymbol{\Psi}_i$. As the evolution in the θ_i-, ρ_i- and ε_i-coordinate does not depend on the initial condition r_i^*, the additional expansion in the r_i-coordinate of $\boldsymbol{R}_i$ only influences the r_i-coordinate of the image $\boldsymbol{\Psi}_i(\boldsymbol{R}_i)$. Due to the exponential contraction in the r_i-coordinate, which is stronger than a linear contraction, the image $\boldsymbol{\Psi}_i(\boldsymbol{R}_i)$ is contained in the set

$$\boldsymbol{W}_i^{\mathrm{out}} := \left\{(r_i, \theta_i, \rho_i, \varepsilon_i) \in \Sigma_i^{\mathrm{out}} : \ h_{r_i}(E) - \frac{\rho_i}{\boldsymbol{R}}\beta \le r_i \le h_{r_i}(E) + \frac{\rho_i}{\boldsymbol{R}}\beta\right\}$$

and the result follows. □

4.2. Dynamics in the Rescaling Chart

In chart $\boldsymbol{K}_2$, we study the extension of the attracting Fenichel slow manifold $S_\varepsilon^{\mathrm{a}}$ into the rescaled regime. To that end, we transfer system (3.5) to the coordinates of chart $\boldsymbol{K}_2$.

Lemma 4.12. *In the rescaling chart, the blown-up vector field is given by*

$$\begin{aligned} r_2' &= \rho_2(r_2^2 - y_2), \\ \theta_2' &= \rho_2, \\ y_2' &= -\rho_2, \\ \rho_2' &= 0. \end{aligned} \tag{4.5}$$

Proof. From Lemma 3.8 we know, that the blowup in chart $\boldsymbol{K}_2$ is given by

$$(r, \theta, y, \varepsilon) = (\rho_2 r_2, \theta_2, \rho_2^2 y_2, \rho_2).$$

Inserting this formula into system (3.5), we obtain

$$\begin{array}{lllll} \varepsilon' = 0 & \Rightarrow & \rho_2' = 0 & \Rightarrow & \rho_2' = 0, \\ r' = r^2 - y & \Rightarrow & (\rho_2 r_2)' = \rho_2^2(r_2^2 - y_2) & \Rightarrow & r_2' = \rho_2(r_2^2 - y_2), \\ \theta' = \varepsilon & \Rightarrow & \theta_2' = \rho_2 & \Rightarrow & \theta_2' = \rho_2, \\ y' = -\varepsilon^3 & \Rightarrow & (\rho_2^2 y_2)' = -\rho_2^3 & \Rightarrow & y_2' = -\rho_2. \end{array}$$

□

Now we can desingularize the blown-up vector field (4.5) by dividing the right hand side by the common factor ρ_2, as explained in Section 2.4. As $\rho_2' = 0$, this transformation is a linear

time rescaling by the constant factor ρ_2, which does by Theorem A.8 not change the orbits of the solution curves. We denote the new time scale by t_2 and have the relationship

$$\rho_2 \, \mathrm{d}t = \mathrm{d}t_2.$$

As ρ_2 is constant, it additionally holds $t_2 = \rho_2 t$. The desingularized flow in chart K_2 is then given by

$$\begin{aligned} r_2' &= r_2^2 - y_2, \\ \theta_2' &= 1, \\ y_2' &= -1, \\ \rho_2' &= 0. \end{aligned} \tag{4.6}$$

We want to remark, that as $\varepsilon = \rho_2$, the above transformation is just a rescaling of the coordinates r, θ and y. Therefore K_2 is also called the rescaling chart. System (4.6) can be solved easily for the three coordinates θ_2, y_2 and ρ_2.

Lemma 4.13. *Starting from initial conditions $\theta_2(0) = \theta_2^*$, $y_2(0) = y_2^*$ and $\rho_2(0) = \rho_2^*$, the solution of system (4.6) in the last three coordinates is for $t_2 \in \mathbb{R}_{\geq 0}$ given by*

$$\begin{aligned} \theta_2(t_2) &\equiv \theta_2^* + t_2 \mod s, \\ y_2(t_2) &= y_2^* - t_2, \\ \rho_2(t_2) &= \rho_2^*. \end{aligned}$$

Proof. The solutions are obtained by direct integration and well-defined for $t_2 \in \mathbb{R}_{\geq 0}$. □

As $\rho_2' = 0$ and the θ_2-coordinate decouples in system (4.6), the most interesting dynamics happens in the r_2-y_2 plane. The resulting ODE system is a Riccati equation, whose solution can be written in terms of special functions. The next proposition collects the results of [20], which are needed for our analysis.

Proposition 4.14 [20]**.** *The Riccati equation*

$$\begin{aligned} r_2' &= r_2^2 - y_2, \\ y_2' &= -1, \end{aligned} \tag{4.7}$$

has the following properties:

(a) Every orbit has has a horizontal asymptote $y_2 = y_r$, such that as y_2 approaches y_r from above, it holds $r_2 \to \infty$. The value of y_r depends on the initial conditions.

(b) There is a unique orbit γ_2, which can be described as $(r_2, h_{y_2}(r_2))$ and which approaches asymptotically the left branch of the parabola $r_2^2 - y_2 = 0$ for $r_2 \to -\infty$. The orbit γ_2 has a horizontal asymptote $y_2 = -\Omega_0 < 0$, such that $r_2 \to \infty$ as y_2 approaches $-\Omega_0$ from above. The constant Ω_0 is the smallest positive zero of

$$J_{-\frac{1}{3}}\left(\frac{2z^{\frac{3}{2}}}{3}\right) + J_{\frac{1}{3}}\left(\frac{2z^{\frac{3}{2}}}{3}\right),$$

where $J_{-\frac{1}{3}}$ and $J_{\frac{1}{3}}$ are Bessel functions of the first kind.

(c) The function $h_{y_2}(r_2)$ has the asymptotic expansions

$$\begin{aligned} h_{y_2}(r_2) &= r_2^2 + \frac{1}{2r_2} + \mathcal{O}\left(\frac{1}{r_2^4}\right) && \text{as } r_2 \to -\infty, \\ h_{y_2}(r_2) &= -\Omega_0 + \frac{1}{r_2} + \mathcal{O}\left(\frac{1}{r_2^3}\right) && \text{as } r_2 \to \infty. \end{aligned}$$

(d) *All orbits to the right of γ_2 approach backwards asymptotically the right branch of the parabola $r_2^2 - y_2 = 0$.*

(e) *All orbits to the left of γ_2 have backwards asymptotically a horizontal asymptote $y_2 = y_l$, such that as y_2 approaches y_r from below, it holds $r_2 \to -\infty$. The value of y_l depends on the initial condition. For a fixed orbit it holds $y_l > y_r$.*

Remark 4.15. *Considering again the dynamics including the coordinates ρ_2 and θ_2, the special orbit γ_2 of Proposition 4.14 is defined to be a three-dimensional surface in $\mathbb{R} \times \mathbb{R}/(s\mathbb{Z}) \times \mathbb{R} \times \mathbb{R}$ with $\rho_2 \in \mathbb{R}$ and $\theta_2 \in \mathbb{R}/(s\mathbb{Z})$.*

The dynamics of the Riccati equation is visualized in Figure 4.4. In Proposition 4.14 (c), the asymptotic expansion of the function $h_{y_2}(r_2)$ for $r_2 \to \infty$ is given. In our analysis, we also need the asymptotic expansion of the function $h_{r_2}(y_2)$ as $y_2 \to -\Omega_0$, which is determined in the following Lemma.

Lemma 4.16. *The inverse $h_{r_2}(y_2)$ of the function $h_{y_2}(r_2)$ defined in Proposition 4.14, has the expansion*

$$h_{r_2}(y_2) = \frac{1}{y_2 + \Omega_0 + \mathcal{O}\left((y_2 + \Omega_0)^3\right)} \qquad \text{as } y_2 \to -\Omega_0^+.$$

It determines the r_2-coordinate of a point on the special surface γ_2 dependent on its y_2-coordinate. After the coordinate shift $y_2 \mapsto y_2 + \Omega_0$, the function $\tilde{h}_{r_2}(y_2) := h_{r_2}(y_2 + \Omega_0)$ has the expansion

$$\tilde{h}_{r_2}(y_2) = \frac{1}{y_2 + \mathcal{O}\left(y_2^3\right)} \qquad \text{as } y_2 \to 0^+.$$

Proof. By Proposition 4.14 (c), the function $h_{y_2}(r_2)$ has the expansion

$$h_{y_2}(r_2) = -\Omega_0 + \frac{1}{r_2} + \mathcal{O}\left(\frac{1}{r_2^3}\right) \qquad \text{as } r_2 \to \infty,$$

and $h_{y_2}(r_2) \to -\Omega_0$ for $r_2 \to \infty$. Substituting $u_2 = \frac{1}{r_2}$, we obtain the expansion

$$h_{y_2}(u_2) = -\Omega_0 + u_2 + \mathcal{O}\left(u_2^3\right) \qquad \text{as } u_2 \to 0^+.$$

By the Inverse Function Theorem A.3, the function $h_{y_2}(u_2)$ is invertible in a neighborhood of $u_2 = 0$, as

$$h'_{y_2}(u_2) = 1 + \mathcal{O}\left(u_2^2\right) \qquad \Rightarrow \qquad h'_{y_2}(0) = 1 \neq 0.$$

Hence, also the function $h_{y_2}(r_2)$ is invertible for $r_2 \to \infty$. The function

$$h_{r_2}(y_2) = \frac{1}{y_2 + \Omega_0 + \mathcal{O}\left((y_2 + \Omega_0)^3\right)}$$

is for $y_2 \to -\Omega_0$ the unique inverse of $h_{y_2}(r_2)$ for $r_2 \to \infty$, as

$$\begin{aligned} h_{y_2}(h_{r_2}(y_2)) &= -\Omega_0 + y_2 + \Omega_0 + \mathcal{O}\left((y + \Omega_0)^3\right) + \mathcal{O}\left(\left(y_2 + \Omega_0 + \mathcal{O}\left((y + \Omega_0)^3\right)\right)^3\right) \\ &= y_2 + \mathcal{O}\left((y_2 + \Omega_0)^3\right) + \mathcal{O}\left((y_2 + \Omega_0)^3\right) \end{aligned}$$

becomes the identity function for $y_2 = -\Omega_0$.

Applying the coordinate shift $y_2 \mapsto y_2 + \Omega_0$, the function $\tilde{h}_{r_2}(y_2) := h_{r_2}(y_2 + \Omega_0)$ has the expansion

$$\tilde{h}_{r_2}(y_2) = \frac{1}{y_2 + \mathcal{O}\left(y_2^3\right)} \qquad \text{as } y_2 \to 0^+,$$

and the result follows. □

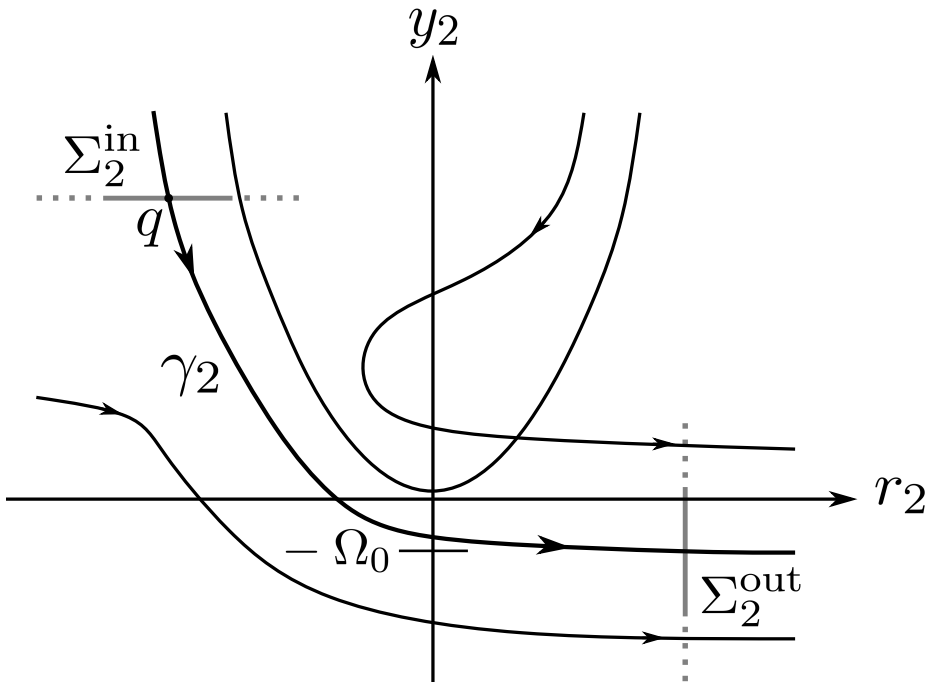


Figure 4.4.: The solutions of the Riccati equation (4.7), the entry set Σ_2^{in} and the exit set Σ_2^{out} of chart K_2 in the r_2-y_2 plane are visualized.

The special surface γ_2 plays an important role in our analysis, as it contains the attracting center manifold M_1^{a} of chart K_1, written in the coordinates of chart K_2.

Proposition 4.17. *The unique branch of the three-dimensional center manifold M_1^a in $\{\varepsilon_1 > 0\}$ in chart K_1 is part of the surface γ_2 in chart K_2. Written in the coordinates of chart K_2, M_1^a corresponds to the part of γ_2, for which $r_2 \in (-\infty, c_2]$ for some constant $c_2 > 0$.*

Proof. By Proposition 4.14 and Remark 4.15, γ_2 has in the coordinates r_2 and y_2 the expansion

$$(r_2, y_2) = \left(r_2, r_2^2 + \frac{1}{2r_2} + \mathcal{O}\left(\frac{1}{r_2^4}\right)\right) \qquad \text{as } r_2 \to -\infty.$$

Additionally it holds $\theta_2 \in \mathbb{R}/(s\mathbb{Z})$ and $\rho_2 \in \mathbb{R}$. By Lemma 3.9, this transfers in the coordinates of chart K_1 to

$$(r_1, \varepsilon_1) = \left(r_2 \left(r_2^2 + \frac{1}{2r_2} + \mathcal{O}\left(\frac{1}{r_2^4}\right)\right)^{-\frac{1}{2}}, \left(r_2^2 + \frac{1}{2r_2} + \mathcal{O}\left(\frac{1}{r_2^4}\right)\right)^{-\frac{1}{2}} \right) \qquad \text{as } r_2 \to -\infty,$$

with $\theta_1 \in \mathbb{R}/(s\mathbb{Z})$ and $\rho_1 \in \mathbb{R}$. Expanding these terms in their Laurent series at $r_2 = -\infty$, we obtain the series expansion

$$(r_1, \varepsilon_1) = \left(-1 + \frac{1}{4r_2^3} + \mathcal{O}\left(r_2^{-6}\right), -\frac{1}{r_2} + \frac{1}{4r_2^4} + \mathcal{O}\left(r_2^{-7}\right)\right) \qquad \text{as } r_2 \to -\infty.$$

We observe, that $\varepsilon_1 \to 0^+ \Leftrightarrow r_2 \to -\infty$ and hence the series expansion of r_1 accords with the graph function

$$h_{r_1}(\varepsilon_1) = -1 - \frac{1}{4}\varepsilon_1^3 + \mathcal{O}(\varepsilon_1^6) \qquad \text{as } \varepsilon_1 \to 0^+$$

describing the r_1-coordinate of the center manifold M_1^{a} defined in Proposition 4.4. Thus, in the limit $r_2 \to -\infty$, $\kappa_{12}^{-1}(\gamma_2)$ converges to the cylinder S_1^{a}, introduced in the analysis of the dynamics in chart K_1. By looking at the partial derivative in the r_2-direction of each component of the expansion above, we observe, that the convergence to the cylinder S_1^{a} is tangent to the center-direction $(0,0,0,1)$ of M_1^a as $r_2 \to -\infty$. This and the fact, that the center manifold M_1^a in $\{\varepsilon_1 > 0\}$ is unique, imply the claim. □

To analyze the flow in chart $\mathcal{K}_2$, we introduce the space

$$\mathcal{D}_2 := \{(r_2, \theta_2, y_2, \rho_2) \in \mathbb{R} \times \mathbb{R}/(s\mathbb{Z}) \times \mathbb{R} \times \mathbb{R} : 0 \le \rho_2 \le E\mathcal{R}\},$$

where E and $\mathcal{R}$ are the same constants used in the entry chart. The flow in chart $\mathcal{K}_1$ is mapped from Σ_1^{in} to Σ_1^{out}. The following lemma transfers Σ_1^{out} to the coordinates of chart $\mathcal{K}_2$.

Lemma 4.18. *The exit set Σ_1^{out} of chart $\mathcal{K}_1$ maps under the coordinate transformation κ_{12} given in Lemma 3.9 to the entry set*

$$\Sigma_2^{in} := \left\{(r_2, \theta_2, y_2, \rho_2) \in \mathcal{D}_2 : \; y_2 = \frac{1}{E^2}\right\}.$$

Furthermore, the image $\kappa_{12}\left(\mathcal{V}_1(\mathcal{R}_1 \cap \mathcal{M}_1^a)\right) \subset \Sigma_2^{in}$ is a smooth surface transverse to the hyperplane $\{\rho_2 = 0\}$ of the form

$$\Sigma_2^{in} \cap \gamma_2 = \left\{(r_2, \theta_2, y_2, \rho_2) \in \Sigma_2^{in} : \; r_2 = h_{r_2}\left(\frac{1}{E^2}\right)\right\}.$$

The exit set $\mathcal{W}_1^{out}$, which is a superset of the image $\mathcal{V}_1(\mathcal{R}_1)$ maps to the entry set

$$\mathcal{W}_2^{in} := \left\{(r_2, \theta_2, y_2, \rho_2) \in \Sigma_2^{in} : \; h_{r_2}\left(\frac{1}{E^2}\right) - \frac{\rho_2}{E^2\mathcal{R}}\beta \le r_2 \le h_{r_2}\left(\frac{1}{E^2}\right) + \frac{\rho_2}{E^2\mathcal{R}}\beta\right\}.$$

Proof. Σ_1^{out} is defined as

$$\begin{aligned}\Sigma_1^{\text{out}} &= \{(r_1, \theta_1, \rho_1, \varepsilon_1) \in \mathcal{D}_1 : \; \varepsilon_1 = E\} \\ &= \{(r_1, \theta_1, \rho_1, \varepsilon_1) \in \mathbb{R} \times \mathbb{R}/(s\mathbb{Z}) \times \mathbb{R} \times \mathbb{R} : \; 0 \le \rho_1 \le \mathcal{R}, \; \varepsilon_1 = E\}.\end{aligned}$$

Therefore we obtain under the coordinate transformation κ_{12} of Lemma 3.9:

$$\begin{aligned} r_2 &= r_1\varepsilon_1^{-1} && \Rightarrow \quad r_2 \in \mathbb{R}, \\ \theta_2 &= \theta_1 && \Rightarrow \quad \theta_2 \in \mathbb{R}/(s\mathbb{Z}), \\ y_2 &= \varepsilon_1^{-2} && \Rightarrow \quad y_2 = E^{-2}, \\ \rho_2 &= \rho_1\varepsilon_1 = \rho_1 E && \Rightarrow \quad 0 \le \rho_2 \le E\mathcal{R}. \end{aligned}$$

The image $\mathcal{V}_1(\mathcal{R}_1 \cap \mathcal{M}_1^{\text{a}})$ has by Proposition 4.11 the additional constraint

$$r_1 = h_{r_1}(E)$$

and the exit set $\mathcal{W}_1^{\text{out}}$ has the additional constraint

$$h_{r_1}(E) - \frac{\rho_1}{\mathcal{R}}\beta \le r_1 \le h_{r_1}(E) + \frac{\rho_1}{\mathcal{R}}\beta.$$

By Proposition 4.17, the unique branch of the center manifold $\mathcal{M}_1^{\text{a}}$ in $\{\varepsilon_1 > 0\}$ corresponds to a part of the surface γ_2 in chart $\mathcal{K}_2$. Consequently, the constraint $r_1 = h_{r_1}(E)$ transfers in chart $\mathcal{K}_2$ to

$$r_2 = h_{r_2}\left(\frac{1}{E^2}\right),$$

where $h_{r_2}(y_2)$ is the r_2-coordinate of a point on the special surface γ_2 dependent on its y_2-coordinate. Its expansion is given by Lemma 4.16. Due to the relationships $\rho_2 = \rho_1 E$ and $r_2 = \frac{r_1}{E}$ in Σ_1^{out}, the additional constraint in the r_1-coordinate of $\mathcal{W}_1^{\text{out}}$ becomes in chart $\mathcal{K}_2$

$$h_{r_2}(y_2) - \frac{\rho_2}{E^2\mathcal{R}}\beta \le r_2 \le h_{r_2}(y_2) + \frac{\rho_2}{E^2\mathcal{R}}\beta. \qquad \square$$

As we restricted our analysis to a neighborhood of the attracting center manifold M_1^a, the important dynamics in chart K_1 takes place for r_1-values close to -1. By Proposition 4.4 and Proposition 4.11, the r_1-coordinate of $T_1(R_1) \subset W_1^{out} \subset \Sigma_1^{out}$ is non-positive for E, R and β small enough. As by Lemma 3.8 it holds $r_1 \leq 0 \Leftrightarrow r_2 \leq 0$ for points on Σ_1^{out}, we consider in chart K_2 only initial points with a non-positive r_2-coordinate. Based on Lemma 4.18, we use the entry set

$$\overline{\Sigma}_2^{in} := \Sigma_2^{in} \cap \{r_2 \leq 0\} = \left\{(r_2, \theta_2, y_2, \rho_2) \in \mathcal{D}_2 : \ r_2 \leq 0, \ y_2 = \frac{1}{E^2}\right\}$$

in chart K_2.

In the y_2-r_2 plane, the dynamics is given by the solution of the Riccati equation (4.7). As the center manifold M_1^a in chart K_1 corresponds by Proposition 4.17 to the surface γ_2 in chart K_2, we are interested in the dynamics of points in a neighborhood of γ_2. Therefore, we define in chart K_2 the transition map T_2 for initial points in $\overline{\Sigma}_2^{in}$, ending in the exit set

$$\Sigma_2^{out} := \left\{(r_2, \theta_2, y_2, \rho_2) \in \mathcal{D}_2 : \ r_2 = \frac{1}{E}\right\},$$

which is orthogonal to the special surface γ_2.

Lemma 4.19. *The transition map $T_2 : \overline{\Sigma}_2^{in} \to \Sigma_2^{out}$ is well-defined.*

Proof. By Proposition 4.14 (a), every orbit converges to a horizontal asymptote $\{y_2 = const.\}$ as $r_2 \to \infty$. As initial points on $\overline{\Sigma}_2^{in}$ have a negative r_2-coordinate, each orbit will transverse the set Σ_2^{out}, which is orthogonal to the r_2-axis. □

The following proposition gives the concrete form of the transition map T_2 for starting points on the special surface γ_2. It approximates also the transition map for points on $\overline{\Sigma}_2^{in}$, which lie in a neighborhood of γ_2. In the overall analysis we are interested in tracking $R_1 \cap M_1^a$. Hence, the following proposition additionally gives a description of the image $\kappa_{12}(T_1(R_1 \cap M_1^a))$ and the set W_2^{in} under the map $T_2 : \overline{\Sigma}_2^{in} \to \Sigma_2^{out}$, which is visualized in Figure 4.5.

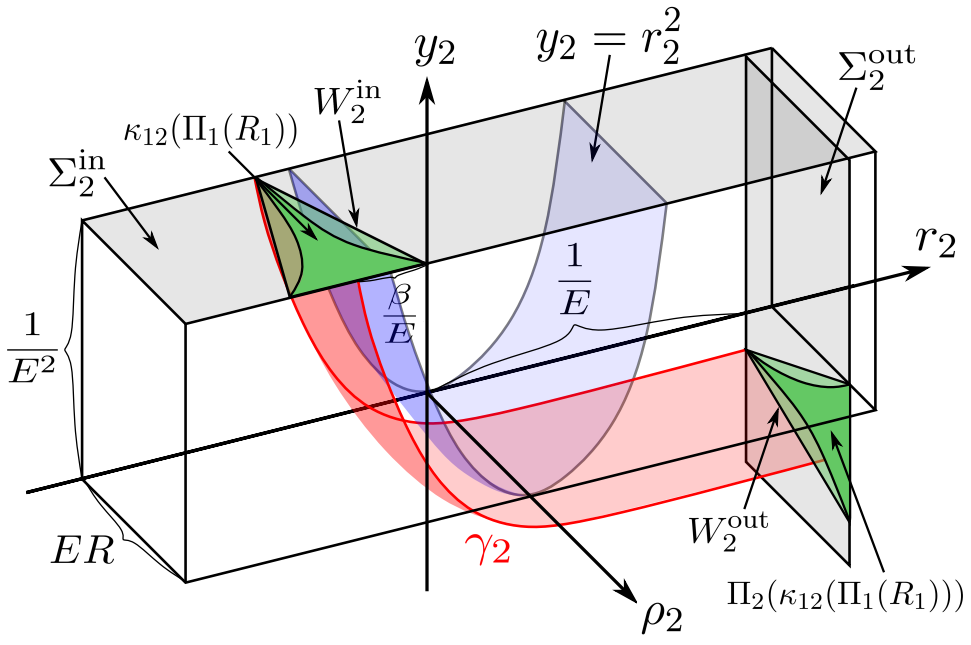


Figure 4.5.: Geometry of the dynamics in chart K_2 in the coordinates r_2, ρ_2 and y_2.

Proposition 4.20. *Let*

$$\varsigma := \left(r_q, \theta_2^*, \frac{1}{E^2}, \rho_2^*\right) \in \overline{\Sigma}_2^{in} \cap \gamma_2$$

with $r_q < 0$ uniquely defined by the property, that $\varsigma \in \overline{\Sigma}_2^{in} \cap \gamma_2$. Then the transition map $\Psi_2 : \overline{\Sigma}_2^{in} \to \Sigma_2^{out}$ has the following properties:

(a) It holds

$$\Psi_2(\varsigma) = \left(\frac{1}{E}, \theta_2^* + \frac{1}{E^2} - h_{y_2}\left(\frac{1}{E}\right) \bmod s, h_{y_2}\left(\frac{1}{E}\right), \rho_2^*\right),$$

where $h_{y_2}\left(\frac{1}{\eta}\right) = -\Omega_0 + \eta + \mathcal{O}(\eta^3)$ as $\eta \to 0^+$.

(b) Each neighborhood of ς is mapped diffeomorphically onto a neighborhood of $\Psi_2(\varsigma)$. This implies, that the transition map $\Psi_2 : \overline{\Sigma}_2^{in} \to \Sigma_2^{out}$ has for a point $\left(r_2^*, \theta_2^*, \frac{1}{E^2}, \rho_2^*\right) \in \overline{\Sigma}_2^{in}$ with $\Delta_{r_2} := r_2^* - r_q$ the form

$$\Psi_2\left(r_2^*, \theta_2^*, \frac{1}{E^2}, \rho_2^*\right) = \left(\frac{1}{E}, \theta_2^* + \frac{1}{E^2} - h_{y_2}\left(\frac{1}{E}\right) + \mathcal{O}(\Delta_{r_2}) \bmod s, h_{y_2}\left(\frac{1}{E}\right) + \mathcal{O}(\Delta_{r_2}), \rho_2^*\right).$$

(c) $\Psi_2(\kappa_{12}(\Psi_1(R_1 \cap M_1^a))) \subset \Sigma_2^{out}$ is a smooth surface transverse to the hyperplane $\{\rho_2 = 0\}$ of the form

$$\Sigma_2^{out} \cap \gamma_2 = \left\{(r_2, \theta_2, y_2, \rho_2) \in \Sigma_2^{out} : \; y_2 = h_{y_2}\left(\frac{1}{E}\right)\right\}.$$

Furthermore, the image $\Psi_2(\kappa_{12}(\Psi_1(R_1))) \subset \Sigma_2^{out}$ is contained in the exit set

$$W_2^{out} := \left\{(r_2, \theta_2, y_2, \rho_2) \in \Sigma_2^{out} : \; h_{y_2}\left(\frac{1}{E}\right) - K\frac{\rho_2}{E^2 R}\beta \le y_2 \le h_{y_2}\left(\frac{1}{E}\right) + K\frac{\rho_2}{E^2 R}\beta\right\}.$$

Proof. As all points in Σ_2^{out} have the r_2-coordinate $\frac{1}{E}$, the first coordinate of $\Psi_2(\varsigma)$ is $\frac{1}{E}$. By Proposition 4.14 (c), the y_2-coordinate of $\Psi_2(\varsigma)$ is $h_{y_2}\left(\frac{1}{E}\right)$, where

$$h_{y_2}\left(\frac{1}{\eta}\right) = -\Omega_0 + \eta + \mathcal{O}(\eta^3) \qquad \text{as } \eta \to 0^+.$$

Using Lemma 4.13, we can determine the transition time $T_2 = T_2(\varsigma)$ of the map Ψ_2 for the point $\varsigma \in \Sigma_2^{\text{in}}$, which has the y_2-coordinate $\frac{1}{E^2}$. It holds

$$h_{y_2}\left(\frac{1}{E}\right) = y_2(T_2) = y_2(0) - T_2 = \frac{1}{E^2} - T_2 \quad \Rightarrow \quad T_2 = \frac{1}{E^2} - h_{y_2}\left(\frac{1}{E}\right).$$

Using again Lemma 4.13, we can determine the θ_2-coordinate after the transition time T_2:

$$\theta_2(T_2) \equiv \theta_2(0) + T_2 \equiv \theta_2^* + \frac{1}{E^2} - h_{y_2}\left(\frac{1}{E}\right) \bmod s.$$

As $\rho_2' = 0$, it holds $\rho_2(T_2) = \rho_2(0) = \rho_2^*$ and the explicit formula for $\Psi_2(\varsigma)$ follows.

By Theorem A.1, the flow map $\Psi_2(\varsigma)$ is a diffeomorphism, such that each neighborhood of ς is mapped diffeomorphically onto a neighborhood of $\Psi_2(\varsigma)$. Taking as an initial point

$$\tilde{\varsigma} := \left(r_2^*, \theta_2^*, \frac{1}{E^2}, \rho_2^*\right) \in \Sigma_2^{\text{in}},$$

the image under the map Ψ_2 has by definition the r_2-coordinate $\frac{1}{E}$ and ρ_2^* stays fixed. As the θ_2- and the ρ_2-coordinate decouple, only the distance $\Delta_{r_2} := r_2^* - r_q$ in the r_2-coordinate influences

the deviation in the y_2-coordinate of $\Psi_2(\tilde{\varrho})$ and $\Psi_2(\varrho)$. As Ψ_2 is a diffeomorphism, it holds for the y_2-coordinate

$$\Psi_{2,y_2}(\tilde{\varrho}) = \Psi_{2,y_2}(\varrho) + \mathcal{O}(\Delta_{r_2}) = h_{y_2}\left(\frac{1}{E}\right) + \mathcal{O}(\Delta_{r_2}).$$

Using Lemma 4.13, the transition time $T_2(\tilde{\varrho})$ is

$$h_{y_2}\left(\frac{1}{E}\right) + \mathcal{O}(\Delta_{r_2}) = \frac{1}{E^2} - T_2(\tilde{\varrho}) \quad \Rightarrow \quad T_2(\tilde{\varrho}) = \frac{1}{E^2} - h_{y_2}\left(\frac{1}{E}\right) + \mathcal{O}(\Delta_{r_2})$$

and the θ_2-coordinate after the transition time $T_2(\tilde{\varrho})$ is

$$\theta_2(T_2(\tilde{\varrho})) \equiv \theta_2^* + \frac{1}{E^2} - h_{y_2}\left(\frac{1}{E}\right) + \mathcal{O}(\Delta_{r_2}) \mod s$$

and the result of statement (b) follows.

For statement (c) we track $R_1 \cap M_1^{\mathrm{a}}$. By Lemma 4.18, we have that $\kappa_{12}(\Psi_1(R_1 \cap M_1^{\mathrm{a}})) \subset \overline{\Sigma}_2^{\mathrm{in}}$ is a smooth surface transverse to the hyperplane $\{\rho_2 = 0\}$ of the form

$$\overline{\Sigma}_2^{\mathrm{in}} \cap \gamma_2 = \left\{(r_2, \theta_2, y_2, \rho_2) \in \mathcal{D}_2 : \; r_2 = h_{r_2}\left(\frac{1}{E^2}\right), \; y_2 = \frac{1}{E^2}\right\}$$

as $h_{r_2}\left(\frac{1}{E^2}\right) \leq 0$. We now apply the transition map Ψ_2 of part (a) and obtain

$$\Psi_2(\kappa_{12}(\Psi_1(R_1 \cap M_1^{\mathrm{a}}))) = \Sigma_2^{\mathrm{out}} \cap \gamma_2 = \left\{(r_2, \theta_2, y_2, \rho_2) \in \mathcal{D}_2 : \; r_2 = \frac{1}{E}, \; y_2 = h_{y_2}\left(\frac{1}{E}\right)\right\}.$$

In $\Psi_2(\kappa_{12}(\Psi_1(R_1 \cap M_1^{\mathrm{a}})))$, θ_2 attains all values in $\mathbb{R}/(s\mathbb{Z})$, as the map Ψ_2 increases each initial position $\theta_2^* \in \mathbb{R}/(s\mathbb{Z})$ by the constant term $\frac{1}{E^2} - h_{y_2}\left(\frac{1}{E}\right)$.

The image $\kappa_{12}(\Psi_1(R_1))$ is by Lemma 4.18 a subset of the entry set

$$W_2^{\mathrm{in}} := \left\{(r_2, \theta_2, y_2, \rho_2) \in \Sigma_2^{\mathrm{in}} : \; h_{r_2}\left(\frac{1}{E^2}\right) - \frac{\rho_2}{E^2 R}\beta \leq r_2 \leq h_{r_2}\left(\frac{1}{E^2}\right) + \frac{\rho_2}{E^2 R}\beta\right\}.$$

We now apply the transition map Ψ_2 of part (b) with $\Delta_{r_2} = \frac{\rho_2}{E^2 R}\beta$ and obtain, that the image $\Psi_2(\kappa_{12}(\Psi_1(R_1)))$ is contained in the exit set

$$W_2^{\mathrm{out}} := \left\{(r_2, \theta_2, y_2, \rho_2) \in \Sigma_2^{\mathrm{out}} : \; h_{y_2}\left(\frac{1}{E}\right) - K\frac{\rho_2}{E^2 R}\beta \leq y_2 \leq h_{y_2}\left(\frac{1}{E}\right) + K\frac{\rho_2}{E^2 R}\beta\right\}$$

for some constant $K > 0$. □

4.3. Dynamics in the Exit Chart

In chart K_3, we analyze the departure of the attracting Fenichel slow manifold $S_\varepsilon^{\mathrm{a}}$ from the non-hyperbolic circle S_0^{c}. The following lemma transfers system (3.5) into the coordinates of the exit chart.

Lemma 4.21. *In chart K_3, the blown-up vector field is given by*

$$\begin{aligned}
\rho_3' &= \rho_3^2(1 - y_3),\\
\theta_3' &= \rho_3\varepsilon_3,\\
y_3' &= -2\rho_3 y_3(1 - y_3) - \rho_3\varepsilon_3^3,\\
\varepsilon_3' &= -\rho_3\varepsilon_3(1 - y_3).
\end{aligned} \tag{4.8}$$

Proof. From Lemma 3.8, we know that the blowup in chart K_3 is given by

$$(r, \theta, y, \varepsilon) = (\rho_3, \theta_3, \rho_3^2 y_3, \rho_3 \varepsilon_3).$$

Inserting this formula into system (3.5), we obtain

$$\begin{array}{lllll} r' = r^2 - y & \Rightarrow & \rho_3' = \rho_3^2(1 - y_3) & \Rightarrow & \rho_3' = \rho_3^2(1 - y_3), \\ \theta' = \varepsilon & \Rightarrow & \theta_3' = \rho_3 \varepsilon_3 & \Rightarrow & \theta_3' = \rho_3 \varepsilon_3, \\ y' = -\varepsilon^3 & \Rightarrow & (\rho_3^2 y_3)' = -\rho_3^3 \varepsilon_3^3 & \Rightarrow & y_3' = -2\rho_3 y_3(1 - y_3) - \rho_3 \varepsilon_3^3, \\ \varepsilon' = 0 & \Rightarrow & (\rho_3 \varepsilon_3)' = 0 & \Rightarrow & \varepsilon_3' = -\rho_3 \varepsilon_3(1 - y_3). \end{array}$$ □

The polynomial vector field of system (4.8) has in each component the common factor ρ_3, thus we can desingularize the above vector field by dividing the right hand side of system (4.8) by ρ_3, as explained Section 2.4. We denote the new time scale by t_3 and have the relationship

$$\rho_3 \, \mathrm{d}t = \mathrm{d}t_3.$$

Hence, the desingularized flow in chart K_3 is given by

$$\begin{aligned} \rho_3' &= \rho_3(1 - y_3), \\ \theta_3' &= \varepsilon_3, \\ y_3' &= -2y_3(1 - y_3) - \varepsilon_3^3, \\ \varepsilon_3' &= -\varepsilon_3(1 - y_3). \end{aligned} \tag{4.9}$$

To analyze this system, we define the rectangular box

$$\mathcal{D}_3 := \{(\rho_3, \theta_3, y_3, \varepsilon_3) \in \mathbb{R} \times \mathbb{R}/(s\mathbb{Z}) \times \mathbb{R} \times \mathbb{R} : \ 0 \le \rho_3 \le R, \ 0 \le \varepsilon_3 \le E\},$$

where E and R are the same positive constants used in charts K_1 and K_2. The hyperplanes $\{\rho_3 = 0\}$ and $\{\varepsilon_3 = 0\}$ are invariant in system (4.9). As θ_3 is constant in the hyperplane $\{\varepsilon_3 = 0\}$, the y_3-axis defined by $\{\rho_3 = 0, \theta_3 = 0, \varepsilon_3 = 0\}$ is also invariant under the flow of system (4.9). The desingularized system (4.9) contains the plane of equilibria

$$\{(\rho_3, \theta_3, y_3, \varepsilon_3) \in \mathcal{D}_3 : \ y_3 = 1, \ \varepsilon_3 = 0\}$$

and the circle of equilibria

$$c := \{(\rho_3, \theta_3, y_3, \varepsilon_3) \in \mathcal{D}_3 : \ \rho_3 = 0, \ y_3 = 0, \ \varepsilon_3 = 0\}.$$

Lemma 4.22. *The circle c of fixed points c in system (4.9) is hyperbolic in the ρ_3-, y_3- and ε_3-direction and non-hyperbolic in the θ_3-direction with the following eigenvalues:*

(a) $\lambda_1 = 1$ with eigenvector $(1, 0, 0, 0)$ corresponding to the flow in the hyperplane $\{\varepsilon_3 = 0\}$.

(b) $\lambda_2 = 0$ with eigenvector $(0, 1, 0, 0)$ corresponding to the circle c of equilibria.

(c) $\lambda_3 = -2$ with eigenvector $(0, 0, 1, 0)$ corresponding to the flow on the y_3-axis.

(d) $\lambda_4 = -1$ with eigenvector $(0, 0, 0, 1)$ corresponding to the flow in the hyperplane $\{\rho_3 = 0\}$.

Proof. The linearization of system (4.9) at the circle of fixed points c is given by

$$J(\rho_3, \theta_3, y_3, \varepsilon_3) = \begin{pmatrix} 1 - y_3 & 0 & -\rho_3 & 0 \\ 0 & 0 & 0 & 1 \\ 0 & 0 & 4y_3 - 2 & -3\varepsilon^2 \\ 0 & 0 & \varepsilon_3 & -1 + y_3 \end{pmatrix} \quad \Rightarrow \quad J(c) = \begin{pmatrix} 1 & 0 & 0 & 0 \\ 0 & 0 & 0 & 1 \\ 0 & 0 & -2 & 0 \\ 0 & 0 & 0 & -1 \end{pmatrix}.$$

$J(c)$ is an upper triangular matrix, consequently it has the eigenvalues $\lambda_1 = 1$, $\lambda_2 = 0$, $\lambda_3 = -2$ and $\lambda_4 = -1$.

The eigenvector to $\lambda_1 = 1$ is $(1,0,0,0)$ and corresponds to the flow in the hyperplane $\{\varepsilon_3 = 0\}$: taking an initial condition on $c + \mu(1,0,0,0)$, $|\mu|$ small in system (4.9) only leads to changes in the ρ_3-coordinate. The flow is therefore part of the invariant hyperplane $\{\varepsilon_3 = 0\}$.

The eigenvector to $\lambda_2 = 0$ is $(0,1,0,0)$ and corresponds to the circle of fixed points c: taking an initial condition on $c + \mu(0,1,0,0)$, $|\mu|$ small in system (4.9) only changes the angle θ_3. The new initial condition is again a fixed point on the circle c.

The eigenvector to $\lambda_3 = -2$ is $(0,0,1,0)$ and corresponds to the flow on the y_3-axis: taking an initial condition on $c + \mu(0,0,1,0)$, $|\mu|$ small in system (4.9) only leads to changes in the y_3-coordinate. Thus, the flow stays on the y_3-axis

The eigenvector to $\lambda_4 = -1$ is $(0,0,0,1)$ and corresponds to the flow in the hyperplane $\{\rho_3 = 0\}$: taking an initial condition on $c + \mu(0,0,0,1)$, $|\mu|$ small in system (4.9) leads to changes in the θ_3-, y_3- and ε_3-coordinate. As the ρ_3-component is not influenced, the flow is part of the invariant hyperplane $\{\rho_3 = 0\}$. □

The following lemma connects the special surface γ_2 of chart K_2 with the circle of fixed points c of system 4.9.

Lemma 4.23. *The part of the special surface γ_2 lying in the hyperplane $\{\rho_2 = 0\}$, converges in the coordinates of chart K_3 in the hyperplane $\{\rho_3 = 0\}$ to the circle c as $r_2 \to \infty$, where it is tangent to the vector $(0,0,0,1)$.*

Proof. By Proposition 4.14 and Remark 4.15, γ_2 has in the hyperplane $\{\rho_2 = 0\}$ the expansion

$$(r_2, \theta_2, \rho_2, \varepsilon_2) = \left(r_2, \theta_2, -\Omega_0 + \frac{1}{r_2} + \mathcal{O}\left(\frac{1}{r_2^3}\right), 0\right) \qquad \text{as } r_2 \to \infty,$$

where $\theta_2 \in \mathbb{R}/(s\mathbb{Z})$. Applying now the coordinate transformation κ_{23} of Lemma 3.9, we obtain for the expansion of γ_2 in the coordinates of chart K_3

$$(\rho_3, \theta_3, y_3, \varepsilon_3) = \left(0, \theta_3, -\frac{\Omega_0}{r_2^2} + \frac{1}{r_2^3} + \mathcal{O}\left(\frac{1}{r_2^5}\right), \frac{1}{r_2}\right) \qquad \text{as } r_2 \to \infty,$$

where $\theta_3 \in \mathbb{R}/(s\mathbb{Z})$. In the limit $r_2 \to \infty$, $\gamma_2 \cap \{\rho_2 = 0\}$ converges to the circle of fixed points c. Taking partial derivatives with respect to r_2 in the expansion above, we deduce that $\gamma_2 \cap \{\rho_2 = 0\}$ is tangent to $(0,0,0,1)$ in the limit $r_2 \to \infty$. □

We aim to analyze the evolution of the center manifold M_1^a, introduced in the analysis in chart K_1, under the flow of the blown-up vector field. In chart K_2, M_1^a corresponds to the special surface γ_2 for $r_2 \in (-\infty, c_2]$ with some constant $c_2 > 0$. By Lemma 4.23, $\gamma_2 \cap \{\rho_2 = 0\}$ converges in chart K_3 to the circle of fixed points c. This implies, that parts of the blown-up center manifold M_1^a come close to the circle of equilibria c. Thus, in the following we will analyze system (4.9) close to the circle c.

For that purpose we use the fact, that the system in ρ_3, y_3 and ε_3 decouples from the θ_3-coordinate in system (4.9). Thus it is sufficient, to first analyze the dynamics in the coordinates ρ_3, y_3 and ε_3. By Lemma 4.22, these three coordinates corresponds to the hyperbolic directions of the linearization at the circle of fixed points c. The Hartman-Grobman Theorem A.9 guarantees the existence of a continuous transformation between the flow and the linearisation of system (4.9). To make statements about the expansion of the flow, we need at least a C^1 coordinate transformation between system (4.9) and its linearisation. For the hyperbolic eigenvalues of the linearization at the circle c it holds $\lambda_4 = \lambda_1 + \lambda_3$. The phenomenon, that one eigenvalue is the sum of two other eigenvalues is called resonance. Due to the resonance in system (4.9), standard results on the existence of local C^1 linearizations such as the Belitskii Theorem A.10 do not apply. Hence, we analyze system (4.9) directly in the following.

First, we transfer the outgoing set Σ_2^{out} as well as the images of $R_i \cap M_i^{\text{a}}$ and R_i under the transitions maps T_1 and T_2 from chart K_2 to chart K_3.

Lemma 4.24. *The exit set Σ_2^{out} of chart K_2 maps under the coordinate transformation κ_{23} given in Lemma 3.9 to the entry set*

$$\Sigma_3^{in} := \{(\rho_3, \theta_3, y_3, \varepsilon_3) \in \mathcal{D}_3 : \varepsilon_3 = E\}.$$

Furthermore, the image $\kappa_{23}(\Sigma_2^{out} \cap \gamma_2) = \kappa_{23}(T_2(\kappa_{12}(T_1(R_1 \cap M_1^a)))) \subset \Sigma_3^{in}$ is a smooth surface transverse to the hyperplane $\{\rho_3 = 0\}$ of the form

$$\kappa_{23}(\Sigma_2^{out} \cap \gamma_2) = \left\{(\rho_3, \theta_3, y_3, \varepsilon_3) \in \Sigma_3^{in} : \; y_3 = E^2 h_{y_2}\left(\frac{1}{E}\right)\right\}.$$

The exit set W_2^{out}, which is a superset of the image $T_2(\kappa_{12}(T_1(R_1)))$, maps in chart K_3 to the entry set

$$W_3^{in} := \left\{(r_2, \theta_2, y_2, \rho_2) \in \Sigma_3^{in} : \; E^2 h_{r_2}\left(\frac{1}{E^2}\right) - K\frac{\rho_3 E\beta}{R} \le y_3 \le E^2 h_{r_2}\left(\frac{1}{E^2}\right) + K\frac{\rho_3 E\beta}{R}\right\}$$

for some constant $K > 0$.

Proof. Σ_2^{out} is defined as

$$\begin{aligned}\Sigma_2^{\text{out}} &= \left\{(r_2, \theta_2, y_2, \rho_2) \in \mathcal{D}_2 : \; r_2 = \frac{1}{E}\right\} \\ &= \{(r_2, \theta_2, y_2, \rho_2) \in \mathbb{R} \times \mathbb{R}/(s\mathbb{Z}) \times \mathbb{R} \times \mathbb{R} : \; r_2 = \frac{1}{E}, \; 0 \le \rho_2 \le RE\}.\end{aligned}$$

With the coordinate transformation κ_{23} given in Lemma 3.9 we obtain:

$$\begin{aligned}\rho_3 &= \rho_2 r_2 && \Rightarrow \quad 0 \le \rho_3 \le R, \\ \theta_3 &= \theta_2 && \Rightarrow \quad \theta_3 \in \mathbb{R}/(s\mathbb{Z}), \\ y_3 &= y_2 r_2^{-2} && \Rightarrow \quad y_2 \in \mathbb{R}, \\ \varepsilon_3 &= r_2^{-1} && \Rightarrow \quad \varepsilon_3 = E.\end{aligned}$$

The image $\Sigma_2^{\text{out}} \cap \gamma_2 = T_2(\kappa_{12}(T_1(R_1 \cap M_1^{\text{a}})))$ has by Proposition 4.20 the additional constraint

$$y_2 = h_{y_2}\left(\frac{1}{E}\right)$$

and the exit set W_2^{out} has the additional constraint

$$h_{y_2}\left(\frac{1}{E}\right) - K\frac{\rho_2}{E^2 R}\beta \le y_2 \le h_{y_2}\left(\frac{1}{E}\right) + K\frac{\rho_2}{E^2 R}\beta$$

for some constant $K > 0$. By Lemma 3.9, the first constraint transfers to

$$y_2 = E^2 h_{y_2}\left(\frac{1}{E}\right)$$

where the function $h_{y_2}(r_2)$ is defined in Proposition 4.14. Due to the relationship $\rho_2 = E\rho_3$, the additional constraint in the y_2-coordinate of W_2^{out} becomes in chart K_3

$$E^2 h_{y_2}\left(\frac{1}{E}\right) - K\frac{E\rho_3}{R}\beta \le y_3 \le E^2 h_{y_2}\left(\frac{1}{E}\right) + K\frac{E\rho_3}{R}\beta$$

for some constant $K > 0$. □

Based on the last Lemma, we use in chart K_3 the entry set

$$\overline{\Sigma}_3^{\text{in}} := \{(\rho_3, \theta_3, y_3, \varepsilon_3) \in \mathcal{D}_3 : \ y_3 \in [-\nu, \nu], \ \varepsilon_3 = E\}$$

with some positive constant $\nu < 1$. For E and β sufficiently small, it holds that $W_3^{\text{in}} \subset \overline{\Sigma}_3^{\text{in}}$, such that it is sufficient to consider only initial conditions in the entry set $\overline{\Sigma}_3^{\text{in}}$ in chart K_3.

Additionally, we define the exit set

$$\Sigma_3^{\text{out}} := \{(\rho_3, \theta_3, y_3, \varepsilon_3) \in \mathcal{D}_3 : \ \rho_3 = R, \ y_3 \in [-\nu, \nu]\}$$

with the same positive constant $\nu < 1$ as in the entry set $\overline{\Sigma}_1^{\text{in}}$. To prove Main Theorem 1, it is important to notice, that the exit set Σ_3^{out} in chart K_3 is part of the exit set $\Delta_\varepsilon^{\text{out}}$ in the original coordinates.

Lemma 4.25. *The exit set Σ_3^{out} of chart K_3 is a subset of the exit set Δ_ε^{out} in the original coordinates.*

Proof. We recall, that the exit set $\Delta_\varepsilon^{\text{out}}$ is defined by

$$\Delta_\varepsilon^{\text{in}} := \{(r, \theta, y, \varepsilon) \in \mathcal{D}_0 : \ r = R, \ \varepsilon \leq ER\}.$$

The coordinate transformation for chart K_3 is given by Lemma 3.8:

$$(r, \theta, y, \varepsilon) = (\rho_3, \theta_3, \rho_3^2 y_3, \rho_3 \varepsilon_3).$$

We deduce that $r = R \Leftrightarrow \rho_3 = R$. From this equality also the equivalence of the inequalities $\varepsilon \leq ER \Leftrightarrow \varepsilon_3 \leq E$ follows. The constraint $y_3 \in [-\nu, \nu]$ transfers to $y \in [-R^2\nu, R^2\nu]$ and $\theta \in \mathbb{R}/(s\mathbb{Z}) \Leftrightarrow \theta_3 \in \mathbb{R}/(s\mathbb{Z})$. Thus, Σ_3^{out} written in the original coordinates is a subset of the exit set $\Delta_\varepsilon^{\text{out}}$. □

The geometry in chart K_3 is shown in the coordinates ρ_3, y_3 and ε_3 in Figure 4.6. Furthermore, the transition map in the exit chart is visualized, which will be determined in the following.

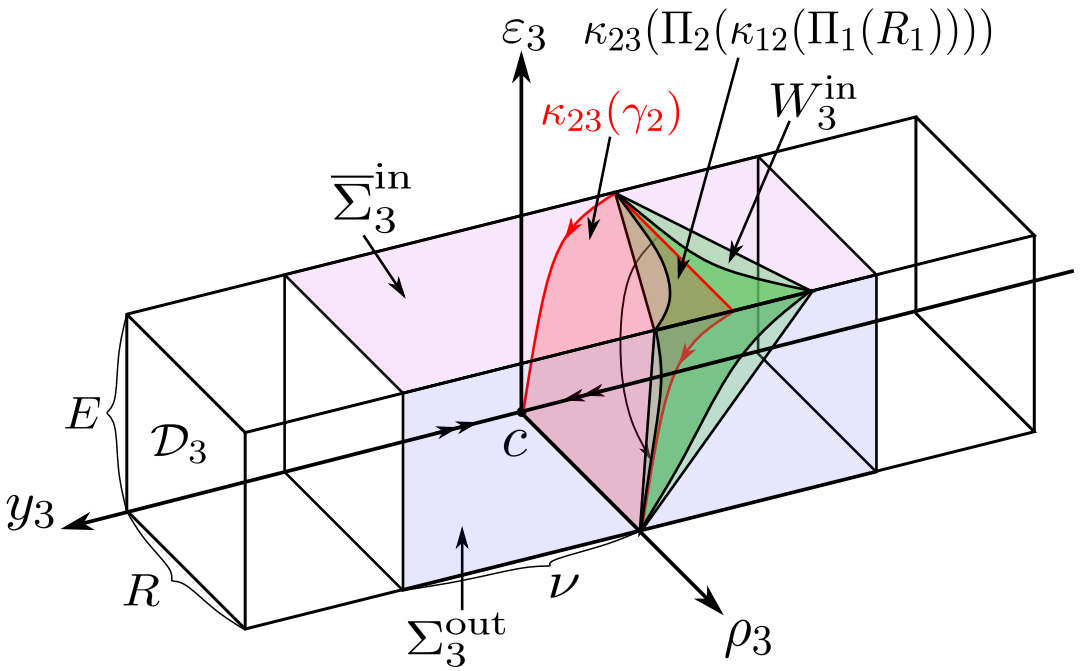


Figure 4.6.: Geometry of the dynamics in chart K_3 near the circle of equilibria c in the coordinates ρ_3, y_3 and ε_3.

We denote by $\mathcal{T}_3$ the transition map from $\overline{\Sigma}_3^{\text{in}}$ to Σ_3^{out}. To obtain a formula for $\mathcal{T}_3$, we simplify the desingularized system (4.9) with a second positive transformation of time by dividing the right hand side through $1 - y_3$. Due to the restriction $y_3 \in [-\nu, \nu]$ in $\overline{\Sigma}_3^{\text{in}}$ with $0 < \nu < 1$ it holds $y_3 \neq 1$ and the positive transformation of time is possible. We denote the new time scale by $\tilde{t}_3$ and have the relationship

$$(1 - y_3)\,\mathrm{d}t_3 = \mathrm{d}\tilde{t}_3.$$

Hence, the system we consider in the following is given by

$$\begin{aligned} \rho_3' &= \rho_3, \\ \theta_3' &= \frac{\varepsilon_3}{1 - y_3}, \\ y_3' &= -2y_3 - \frac{\varepsilon_3^3}{1 - y_3}, \\ \varepsilon_3' &= -\varepsilon_3. \end{aligned} \tag{4.10}$$

The following proposition gives the concrete form of the transition map $\mathcal{T}_3 : \overline{\Sigma}_3^{\text{in}} \cap \{\rho_3 > 0\} \to \Sigma_3^{\text{out}}$ for positive values of the initial condition ρ_3^*.

Proposition 4.26. *The flow of system* (4.10) *has the following properties:*

(a) For $E > 0$ sufficiently small, the transition map $\mathcal{T}_3 : \overline{\Sigma}_3^{in} \cap \{\rho_3 > 0\} \to \Sigma_3^{out}$ is well-defined and has for an initial condition $(\rho_3^*, \theta_3^*, y_3^*, E) \in \overline{\Sigma}_3^{in} \cap \{\rho_3 > 0\}$ the form

$$\mathcal{T}_3(\rho_3^*, \theta_3^*, y_3^*, E) = \left(R, h_{\theta_3}(\rho_3^*), h_{y_3}(\rho_3^*, y_3^*), \frac{\rho_3^*}{R} E\right)$$

with

$$h_{\theta_3}(\rho_3^*) \equiv \theta_3^* + E - E\frac{\rho_3^*}{R} + \mathcal{O}\left((\rho_3^*)^3 \ln\left(\frac{1}{\rho_3^*}\right)\right) \mod s$$

and

$$h_{y_3}(\rho_3^*, y_3^*) = \left(y_3^* - E^3\right)\left(\frac{\rho_3^*}{R}\right)^2 + \mathcal{O}\left((\rho_3^*)^3 \ln\left(\frac{1}{\rho_3^*}\right)\right).$$

(b) The solutions in the ρ_3- and ε_3-coordinate with initial conditions $\rho_3(0) = \rho_3^*$ and $\varepsilon_3(0) = \varepsilon_3^*$ are given by

$$\rho_3(\tilde{t}_3) = \rho_3^* e^{\tilde{t}_3}, \qquad \varepsilon_3(\tilde{t}_3) = \varepsilon_3^* e^{-\tilde{t}_3},$$

for $\tilde{t}_3 \geq 0$.

Proof. We consider an initial condition $(\rho_3^*, \theta_3^*, y_3^*, E) \in \overline{\Sigma}_3^{\text{in}} \cap \{\rho_3 > 0\}$, which gets mapped after the time $\widetilde{T}_3$ to a point $(R, \theta_o, y_o, \varepsilon_o)$ in the hyperplane $\{\rho_3 = R\}$ by the solution $(\rho_3, \theta_3, y_3, \varepsilon_3)(\tilde{t}_3)$ of the system (4.10). We will now work out θ_o, y_o, ε_o and the transition time $\widetilde{T}_3$ as functions of the initial condition $(\rho_3^*, \theta_3^*, y_3^*, E)$ and the value R of the ρ_3-coordinate. Furthermore, we show that $(R, \theta_o, y_o, \varepsilon_o) \in \Sigma_3^{\text{out}}$, such that the transition map is well-defined.

First, we consider the vector field obtained from system (4.10) by neglecting all higher order terms in $\mathcal{O}(\varepsilon_3 y_3)$ in the θ_3- and in the y_3- equation:

$$\begin{aligned} \rho_3' &= \rho_3, \\ \theta_3' &= \varepsilon_3, \\ y_3' &= -2y_3 - \varepsilon_3^3, \\ \varepsilon_3' &= -\varepsilon_3, \end{aligned} \tag{4.11}$$

The solution of system (4.11) with initial condition $(\rho_3^*, \theta_3^*, y_3^*, E)$ is given by

$$\begin{aligned}
\rho_3(\tilde{t}_3) &= \rho_3^* e^{\tilde{t}_3}, \\
\theta_3(\tilde{t}_3) &= \theta_3^* + E - Ee^{-\tilde{t}_3}, \\
y_3(\tilde{t}_3) &= (y_3^* - E^3)e^{-2\tilde{t}_3} + E^3 e^{-3\tilde{t}_3}, \\
\varepsilon_3(\tilde{t}_3) &= Ee^{-\tilde{t}_3},
\end{aligned}$$

where we consider θ_3 as a variable in $\mathbb{R}$ during this proof. The requirement $\rho_3(\widetilde{T}_3) = \rho_3^* e^{\widetilde{T}_3} = R$ leads to the transition time

$$\widetilde{T}_3 = \ln\left(\frac{R}{\rho_3^*}\right),$$

which is finite, as $\rho_3^* > 0$. It follows, that

$$\begin{aligned}
\theta_o &= \theta_3(\widetilde{T}_3) = \theta_3^* + E - E\frac{\rho_3^*}{R} \\
y_o &= y_3(\widetilde{T}_3) = (y_3^* - E^3)\left(\frac{\rho_3^*}{R}\right)^2 + E^3\left(\frac{\rho_3^*}{R}\right)^3 \\
\varepsilon_o &= \varepsilon_3(\widetilde{T}_3) = E\frac{\rho_3^*}{R}.
\end{aligned}$$

Now, we aim to obtain a solution of system (4.10), which solves the θ_3- and y_3-equations including the higher order terms. The equations for ρ_3 and ε_3 are the same as in system (4.11), therefore we already determined their solutions. Plugging them into the θ_3 and y_3 equations of system (4.10) leads to

$$\begin{aligned}
\theta_3' &= \frac{Ee^{-\tilde{t}_3}}{1 - y_3}, \\
y_3' &= -2y_3 - \frac{E^3 e^{-3\tilde{t}_3}}{1 - y_3}.
\end{aligned}$$

As $\varepsilon_o = E\frac{\rho_3^*}{R}$, the condition $0 \leq \varepsilon_o \leq E$ in Σ_3^{out} is fulfilled. By definition, we considered a final point with ρ_3-coordinate R and it holds $\theta_o \in \mathbb{R}/(s\mathbb{Z})$. In Σ_3^{in}, the initial y_3-component is restricted to $y_3^* \in [-\nu, \nu]$. As for E sufficiently small it holds

$$y_3'|_{y_3=-\nu} > 0 \qquad \text{and} \qquad y_3'|_{y_3=\nu} < 0,$$

such that the interval $[-\nu, \nu]$ is invariant under the flow in the y_3-component. Hence, the transition map Ψ_3 is well-defined.

To solve the ODE for y_3, we introduce a new variable z_y depending on $\tilde{t}_3$ by setting

$$y_3(\tilde{t}_3) = (y_3^* - E^3 + z_y(\tilde{t}_3))e^{-2\tilde{t}_3} + E^3 e^{-3\tilde{t}_3}.$$

Differentiating the ansatz for $y_3(\tilde{t}_3)$ and using $\rho_3 = \rho_3^* e^{\tilde{t}_3}$ leads to the following ODE in z_y:

$$z_y' = -\frac{y_3 E^3 e^{-\tilde{t}_3}}{1 - y_3} = -\frac{y_3 E^3 \rho_3^*}{(1 - y_3)\rho_3}$$

with the initial condition $z_y(0) = 0$.

By assumption, we consider a smooth solution $(\rho_3, \theta_3, y_3, \varepsilon_3)(\tilde{t}_3)$, which exists at least until the transition time $\widetilde{T}_3 > 0$. As z_y is continuously differentiable, the right hand side of the ODE for z_y is continuous and therefore bounded for $\tilde{t}_3 \in [0, \widetilde{T}_3]$. Hence, a constant $K_y > 0$ exists, such that

$$|z_y'| = \rho_3^* \left| -\frac{y_3 E^3}{(1 - y_3)\rho_3} \right| \leq \rho_3^* K_y \qquad \text{for } \tilde{t}_3 \in [0, \widetilde{T}_3].$$

It follows, that

$$|z_y(\tilde{t}_3)| \leq \int_0^{\tilde{t}_3} |z_y'| d\bar{t} \leq \rho_3^* K_y \tilde{t}_3 \qquad \text{for } \tilde{t}_3 \in [0, \widetilde{T}_3],$$

such that $z_y(\tilde{t}_3) \in \mathcal{O}(\rho_3^* \tilde{t}_3)$. Using the formula for the transition time $\widetilde{T}_3$ leads to

$$z_y(\widetilde{T}_3) = \mathcal{O}(\rho_3^* \widetilde{T}_3) = \mathcal{O}\left(\rho_3^* \ln\left(\frac{1}{\rho_3^*}\right)\right).$$

Changing the variables back to y_3 results in

$$\begin{aligned} y_3(\widetilde{T}_3) &= (y_3^* - E^3 + z_y(\widetilde{T}_3)) e^{-2\widetilde{T}_3} + E^3 e^{-3\widetilde{T}_3} \\ &= (y_3^* - E^3) \left(\frac{\rho_3^*}{R}\right)^2 + \mathcal{O}\left((\rho_3^*)^3 \ln\left(\frac{1}{\rho_3^*}\right)\right). \end{aligned}$$

Similarly, we can now estimate the evolution in θ_3. To that end, we introduce a new variable z_θ depending on $\tilde{t}_3$ by setting

$$\theta_3(\tilde{t}_3) = \theta_3^* + E - E e^{-\tilde{t}_3} + z_\theta(\tilde{t}_3).$$

Differentiating the ansatz for $\theta_3(\tilde{t}_3)$ and using $\rho_3 = \rho_3^* e^{\tilde{t}_3}$ leads to the following ODE in z_θ:

$$z_\theta' = \frac{y_3 E e^{-\tilde{t}_3}}{1 - y_3} = \frac{y_3 E \rho_3^*}{(1 - y_3)\rho_3}$$

with the initial condition $z_\theta(0) = 0$. As $y_3(\tilde{t}_3) \in \mathcal{O}\left((\rho_3^*)^2\right)$ for $\tilde{t}_3 \in [0, \widetilde{T}_3]$, it follows $z_\theta' \in \mathcal{O}\left((\rho_3^*)^3\right)$, because the remaining factors are continuous and therefore bounded for $\tilde{t}_3 \in [0, \widetilde{T}_3]$. Integrating leads to

$$z_\theta(\tilde{t}_3) \in \mathcal{O}\left((\rho_3^*)^3 \tilde{t}_3\right) \qquad \Rightarrow \qquad z_\theta(\widetilde{T}_3) \in \mathcal{O}\left((\rho_3^*)^3 \ln\left(\frac{1}{\rho_3^*}\right)\right),$$

as $\widetilde{T}_3 = \ln\left(\frac{R}{\rho_3^*}\right)$. Changing the variables back to θ_3 results in

$$\begin{aligned} \theta_3(\widetilde{T}_3) &= \theta_3^* + E - E e^{-\widetilde{T}_3} + z_\theta(\widetilde{T}_3) \\ &= \theta_3^* + E - E\frac{\rho_3^*}{R} + \mathcal{O}\left((\rho_3^*)^3 \ln\left(\frac{1}{\rho_3^*}\right)\right) \end{aligned}$$

and the result follows. □

As the systems (4.8), (4.9) and (4.10) only differ by a positive transformation of time, their orbits are the same. The result of Proposition 4.26 (a) only depends on the initial condition in $\overline{\Sigma}_3^{\text{in}}$ and not on the transition time. Thus, Proposition 4.26 (a) holds as well for the systems (4.8) and (4.9).

Remark 4.27. *Allowing for infinite transition times, the map M_3 has a natural smooth extension to the hyperplane $\{\rho_3 = 0\}$, such that we consider from now on the extended map $M_3 : \overline{\Sigma}_3^{in} \to \Sigma_3^{out}$.*

By Lemma 4.24, we know that

$$\kappa_{23}(M_2(\kappa_{12}(M_1(R_1 \cap M_1^{\text{a}})))) = \kappa_{23}(\Sigma_2^{\text{out}} \cap \gamma_2) = \left\{(\rho_3, \theta_3, y_3, \varepsilon_3) \in \Sigma_3^{\text{in}} : \; y_3 = E^2 h_{y_2}\left(\frac{1}{E}\right)\right\}.$$

In order to determine the exact value of $h_{y_2}\left(\frac{1}{E}\right)$, the following lemma relates the solution of the flow of chart K_3 to the special surface γ_2 of chart K_2.

Lemma 4.28. *For the function h_{y_2} defined in Proposition 4.14, it holds*

$$h_{y_2}\left(\frac{1}{E}\right) = -\Omega_0 + E.$$

Proof. Suppose $(0, \theta_3^*, y_3^*, E) \in \kappa_{23}(\Sigma_2^{\text{out}} \cap \gamma_2)$ with $\theta_3^* \in \mathbb{R}/(s\mathbb{Z})$ and $y_3^* = E^2 h_{y_2}\left(\frac{1}{E}\right)$. Consider the y_3- and ε_3-component of the desingularized system (4.10) in chart K_3, namely

$$\begin{aligned} y_3' &= -2y_3 - \frac{\varepsilon_3^3}{1 - y_3}, \\ \varepsilon_3' &= -\varepsilon_3, \end{aligned}$$

on the time scale $\tilde{t}_3$. We can also obtain this system from the Riccati equation

$$\begin{aligned} r_2' &= r_2^2 - y_2, \\ y_2' &= -1, \end{aligned}$$

in chart K_2 by applying the coordinate transformation κ_{23} of Lemma 3.9

$$\begin{aligned} -\frac{\varepsilon_3'}{\varepsilon_3^2} = r_2' = r_2^2 - y_2 = \frac{1}{\varepsilon_3^2} - \frac{y_3}{\varepsilon_3^2} \quad &\Rightarrow \quad \varepsilon_3' = -1 + y_3, \\ \frac{y_3'}{\varepsilon_3^2} - 2y_3\frac{\varepsilon_3'}{\varepsilon_3^3} = y_2' = -1 \quad &\Rightarrow \quad y_3' = 2y_3\frac{y_3 - 1}{\varepsilon_3} - \varepsilon_3^2, \end{aligned}$$

and desingularizing afterwards by multiplying the right hand side by $\frac{\varepsilon_3}{1-y_3}$. We introduce now the variable $\tilde{\varepsilon}_3 := \varepsilon_3^3$ and obtain the system

$$\begin{aligned} y_3' &= -2y_3 - \frac{\tilde{\varepsilon}_3}{1 - y_3}, \\ \tilde{\varepsilon}_3' &= -3\tilde{\varepsilon}_3. \end{aligned}$$

As no resonance occurs in the two-dimensional system above, a C^1 coordinate transformation $y_3 \mapsto y_{3,l}$ between the system above and its linearization near the fixed point $(y_3, \tilde{\varepsilon}_3) = (0, 0)$ exists by Belitskii's Theorem A.10. The linearized ODE is given by

$$\begin{aligned} y_{3,l}' &= -2y_{3,l} - \tilde{\varepsilon}_3, \\ \tilde{\varepsilon}_3' &= -3\tilde{\varepsilon}_3. \end{aligned}$$

The coordinate $\tilde{\varepsilon}_3$ is not changed, as the ODE in $\tilde{\varepsilon}_3$ is already linear. It holds

$$y_3 = y_{3,l} + \mathcal{O}\left(\tilde{\varepsilon}_3 y_3, \tilde{\varepsilon}_3^2\right) = y_{3,l} + \mathcal{O}\left(\varepsilon_3^3 y_3, \varepsilon_3^6\right),$$

as before the linearization it holds

$$y_3' = -2y_3 - \frac{\tilde{\varepsilon}_3}{1 - y_3} = -2y_3 - \tilde{\varepsilon}_3 + \mathcal{O}\left(\tilde{\varepsilon}_3 y_3\right)$$

and after the linearization

$$y_3' = y_{3,l}' + \mathcal{O}\left(\tilde{\varepsilon}_3 y_3', \tilde{\varepsilon}_3' y_3, \tilde{\varepsilon}_3 \tilde{\varepsilon}_3'\right) = -2y_{3,l} - \tilde{\varepsilon}_3 + \mathcal{O}\left(\tilde{\varepsilon}_3 y_{3,l}, \tilde{\varepsilon}_3^2\right).$$

For an initial condition $\tilde{\varepsilon}_3(0) \neq 0$, we can parameterize the solution of the linearized system in terms of $\tilde{\varepsilon}_3$. If the variable ε_3 has the initial condition $\varepsilon_3(0) = E$, then the variable $\tilde{\varepsilon}_3$ has the initial condition $\tilde{\varepsilon}_3(0) = E^3$. The solution in $\tilde{\varepsilon}_3$ respectively ε_3 is given by

$$\tilde{\varepsilon}_3(\tilde{t}_3) = E^3 e^{-3\tilde{t}_3} \qquad \Leftrightarrow \qquad \varepsilon_3(\tilde{t}_3) = E e^{-\tilde{t}_3}.$$

In $y_{3,l}$, the solution with initial condition $y_{3,l}(0) = y_3^*$ is given by

$$\begin{aligned} & y_{3,l}(\tilde{t}_3) = \left(y_3^* - E^3\right) e^{-2\tilde{t}_3} + E^3 e^{-3\tilde{t}_3}, \\ \Rightarrow \quad & y_{3,l}(\tilde{\varepsilon}_3) = \left(y_3^* - E^3\right) E^{-2} \tilde{\varepsilon}_3^{\frac{2}{3}} + \tilde{\varepsilon}_3, \\ \Rightarrow \quad & y_{3,l}(\varepsilon_3) = \left(y_3^* - E^3\right) E^{-2} \varepsilon_3^2 + \varepsilon_3^3. \end{aligned}$$

Rearranging and taking the limit $\varepsilon_3 \to 0$ leads to

$$\begin{aligned} \left(y_3^* - E^3\right) E^{-2} &= \lim_{\varepsilon_3 \to 0} \left(y_3^* - E^3\right) E^{-2} \\ &= \lim_{\varepsilon_3 \to 0} \left(y_{3,l}(\varepsilon_3) - \varepsilon_3^3\right) \varepsilon_3^{-2} \\ &= \lim_{\varepsilon_3 \to 0} \left(y_3(\varepsilon_3) + \mathcal{O}\left(\varepsilon_3^3 y_3, \varepsilon_3^6\right) - \varepsilon_3^3\right) \varepsilon_3^{-2} \\ &= \lim_{\varepsilon_3 \to 0} y_3(\varepsilon_3) \varepsilon_3^{-2} \end{aligned}$$

Applying the coordinate transformation κ_{23} of Lemma 3.9 results in

$$y_3(\varepsilon_3)\varepsilon_3^{-2} = \frac{y_2(r_2)}{r_2^2} r_2^2 = y_2(r_2)$$

Using now the expansion of the Riccati equation of Proposition 4.14 (c) yields

$$\left(y_3^* - E^3\right) E^{-2} = \lim_{\varepsilon_3 \to 0} y_3(\varepsilon_3)\varepsilon_3^{-2} = \lim_{r_2 \to \infty} y_2(r_2) = \lim_{r_2 \to \infty} \left[-\Omega_0 + \frac{1}{r_2} + \mathcal{O}\left(\frac{1}{r_2^3}\right)\right] = -\Omega_0.$$

Inserting $y_3^* = E^2 h_{y_2}\left(\frac{1}{E}\right)$ leads to the result

$$\left(y_3^* - E^3\right) E^{-2} = h_{y_2}\left(\frac{1}{E}\right) - E = -\Omega_0. \qquad \square$$

Finally, we can combine the last lemma with Proposition 4.26 (a) to obtain a description of the image $\Psi_3(\kappa_{23}(\Psi_2(\kappa_{12}(\Psi_1(R_1 \cap M_1^{\mathrm{a}})))))) \subset \Sigma_3^{\mathrm{out}}$.

Proposition 4.29. *The image $\Psi_3(\kappa_{23}(\Psi_2(\kappa_{12}(\Psi_1(R_1 \cap M_1^{a})))))) \subset \Sigma_3^{out}$ is a smooth surface transverse to the hyperplane $\{\varepsilon_3 = 0\}$ of the form*

$$\left\{(\rho_3, \theta_3, y_3, \varepsilon_3) \in \Sigma_3^{out} : \; y_3 = -\Omega_0 \varepsilon_3^2 + \mathcal{O}\left(\varepsilon_3^3 \ln(\varepsilon_3)\right)\right\}.$$

Proof. By Lemma 4.24 we know, that $\kappa_{23}(\Psi_2(\kappa_{12}(\Psi_1(R_1 \cap M_1^{\mathrm{a}})))) \subset \Sigma_3^{\mathrm{in}}$ is a smooth surface transverse to the hyperplane $\{\rho_3 = 0\}$ of the form

$$\begin{aligned} \kappa_{23}(\Psi_2(\kappa_{12}(\Psi_1(R_1 \cap M_1^{\mathrm{a}})))) &= \left\{(\rho_3, \theta_3, y_3, \varepsilon_3) \in \Sigma_3^{\mathrm{in}} : \; y_3 = E^2 h_{y_2}\left(\frac{1}{E}\right)\right\} \\ &= \left\{(\rho_3, \theta_3, y_3, \varepsilon_3) \in \Sigma_3^{\mathrm{in}} : \; y_3 = -\Omega_0 E^2 + E^3\right\}, \end{aligned}$$

where Lemma 4.28 is used in the second line. Applying now the transition map Ψ_3 of Proposition 4.26 (a) leads to

$$\begin{aligned} & \Psi_3(\kappa_{23}(\Psi_2(\kappa_{12}(\Psi_1(R_1 \cap M_1^{\mathrm{a}})))))) \\ = & \left\{(\rho_3, \theta_3, y_3, \varepsilon_3) \in \Sigma_3^{\mathrm{out}} : \; y_3 = -\Omega_0 \frac{(\rho_3^*)^2}{R^2} E^2 + \mathcal{O}\left((\rho_3^*)^3 \ln\left(\frac{1}{\rho_3^*}\right)\right), \; \varepsilon_3 = \frac{\rho_3^*}{R} E\right\}, \end{aligned}$$

where ρ_3^* is the initial ρ_3-coordinate in $\overline{\Sigma}_3^{\mathrm{in}}$ with $0 \le \rho_3^* \le R$. In $\Psi_3(\kappa_{23}(\Psi_2(\kappa_{12}(\Psi_1(R_1 \cap M_1^{\mathrm{a}})))))$, θ_3 attains all values in $\mathbb{R}/(s\mathbb{Z})$, as the map Ψ_3 increases each initial condition θ_3^* by some additive

constant term for each initial condition ρ_3^*. In $\mathcal{K}_3(\kappa_{23}(\mathcal{K}_2(\kappa_{12}(\mathcal{K}_1(R_1 \cap M_1^a)))))$ it holds $\varepsilon_3 = \frac{\rho_3^*}{R} E$. Hence $0 \leq \varepsilon_3 \leq E$, such that

$$\begin{aligned}&\mathcal{K}_3(\kappa_{23}(\mathcal{K}_2(\kappa_{12}(\mathcal{K}_1(R_1 \cap M_1^a)))))\\ &= \left\{(\rho_3, \theta_3, y_3, \varepsilon_3) \in \Sigma_3^{\text{out}} : \; y_3 = -\Omega_0 \varepsilon_3^2 + \mathcal{O}\left(\varepsilon_3^3 \ln\left(\frac{1}{\varepsilon_3}\right)\right)\right\},\end{aligned}$$

which is a smooth surface transverse to the hyperplane $\{\varepsilon_3 = 0\}$. The result follows now with the observation, that $\ln\left(x^{-1}\right) = -\ln(x)$ for $x \in \mathbb{R}_{>0}$. □

4.4. Proof of Main Theorem 1

In this section, we combine the results obtained in the charts K_1, K_2 and K_3 to prove Main Theorem 1. In Section 3.2, the existence of an attracting slow manifold S_ε^a was shown by Fenichel's Theorems. To keep track of S_ε^a, we defined for small constants E, R, and β the entry section

$$\Delta^{\text{in}} := \left\{(r, \theta, y) \in \mathcal{D} : \; r \in I^{\text{in}}, \; y = R^2\right\}$$

with the interval

$$I^{\text{in}} = \left\{r \in \mathbb{R}_{\geq -v} : \; \left|-1 + \frac{r}{R}\right| \leq \beta\right\}$$

and the exit section

$$\Delta^{\text{out}} := \{(r, \theta, y) \in \mathcal{D} : \; r = R\}.$$

The transition map for the flow of all trajectories close to the attracting slow manifold S_ε^a is denoted by $\pi : \Delta^{\text{in}} \to \Delta^{\text{out}}$. In the three charts we studied the extended system

$$\begin{aligned}r' &= r^2 - y,\\ \theta' &= \varepsilon,\\ y' &= -\varepsilon^3,\\ \varepsilon' &= 0.\end{aligned} \tag{4.12}$$

The attracting slow manifold S_ε^a is obtained as a section $\varepsilon = const.$ of the attracting center-manifold M^a of system (4.12). The existence of this attracting center manifold M^a was shown in Section 3.2. By Lemma 4.6, the entry set of the extended system

$$\Delta_\varepsilon^{\text{in}} := \left\{(r, \theta, y, \varepsilon) \in \mathcal{D}_0 : \; r \in I^{\text{in}}, \; y = R^2, \; \varepsilon \leq ER\right\}$$

with the interval

$$I^{\text{in}} = \left\{r \in \mathbb{R}_{\geq -v} : \; \left|-1 + \frac{r}{R}\right| \leq \beta\right\}$$

transfers in chart K_1 to the rectangle

$$R_1 := \{(r_1, \theta_1, \rho_1 \varepsilon_1) \in \Sigma_1^{\text{in}} : \; |-1 + r_1| \leq \beta\}.$$

By Lemma 4.25, the exit set of the extended system

$$\Delta_\varepsilon^{\text{out}} := \{(r, \theta, y, \varepsilon) \in \mathcal{D}_0 : \; r = R, \; \varepsilon \leq ER\}$$

transferred to chart K_3 is a superset of the exit set Σ_3^{out}. We denote by X the vector field corresponding to the extended system (4.12) with the transition map $\pi_\varepsilon : \Delta_\varepsilon^{\text{in}} \to \Delta_\varepsilon^{\text{out}}$. As system (4.12) is the normal form of the fast-slow LC fold (3.10) extended by the equation $\varepsilon' = 0$, the vector field as well as the transition maps $\pi : \Delta^{\text{in}} \to \Delta^{\text{out}}$ and $\pi_\varepsilon : \Delta_\varepsilon^{\text{in}} \to \Delta_\varepsilon^{\text{out}}$ of both systems are the same in the first three components. As the vector field X vanishes at the fold limit cycle $(0, \theta^*, 0, 0)$, $\theta^* \in \mathbb{R}/(s\mathbb{Z})$, a desingularized vector field $\bar{X}$ induced by the blowup

transformation exists. This is analyzed in different charts by the transition map $\bar{\Pi} : \Sigma_1^{\text{in}} \to \Sigma_3^{\text{out}}$, which is defined as

$$\bar{\Pi} := \bar{\Pi}_3 \circ \kappa_{23} \circ \bar{\Pi}_2 \circ \kappa_{12} \circ \bar{\Pi}_1 .$$

The geometry of the blown-up vector field $\bar{X}$ is shown in Figure 4.7. To analyze the attracting center manifold M^{a}, we will study $\bar{\Pi}(R_1 \cap M_1^{\text{a}})$ and then use appropriate blow-down transformations to obtain results about $\pi_\varepsilon(\Delta_\varepsilon^{\text{in}} \cap M_1^{\text{a}})$. Going back to the normal form of the fast-slow LC fold (3.10), this allows us to prove Main Theorem 1 about the image $\pi(\Delta^{\text{in}} \cap S_\varepsilon^{\text{a}})$. We show the existence of a constant $\varepsilon_0 = E R > 0$, such that Main Theorem 1 holds for all $\varepsilon \leq \varepsilon_0$. Hence, we can assume in the following, that the constants E, R and β are sufficiently small for all statements made in the charts K_1, K_2 and K_3.

To prove part (a), we consider the set $R_1 \cap M_1^{\text{a}}$ in chart K_1. By Proposition 4.29 (a) it follows, that $\bar{\Pi}(R_1 \cap M_1^{\text{a}}) = \bar{\Pi}_3(\kappa_{23}(\bar{\Pi}_2(\kappa_{12}(\bar{\Pi}_1(R_1 \cap M_1^{a})))))$ is a smooth surface transverse to the hyperplane $\{\varepsilon_3 = 0\}$ of the form

$$\left\{(\rho_3, \theta_3, y_3, \varepsilon_3) \in \Sigma_3^{\text{out}} : \; y_3 = -\Omega_0 \varepsilon_3^2 + \mathcal{O}\left(\varepsilon_3^3 \ln(\varepsilon_3)\right)\right\}.$$

We apply now the blow-down transformation of Lemma 3.8, given by $\varepsilon = \varepsilon_3 \rho_3 = \varepsilon_3 R$ and $y = \rho_2^2 y_2 = R^2 y$ in Σ_3^{out} and obtain

$$h_y(\varepsilon) = -\Omega_0 \varepsilon^2 + \mathcal{O}\left(\varepsilon^3 \ln(\varepsilon)\right)$$

for the y-component of $\pi_\varepsilon(\Delta_\varepsilon^{\text{in}} \cap M_1^{\text{a}})$ in the exit set $\Delta_\varepsilon^{\text{out}}$. As $\bar{\Pi}(R_1 \cap M_1^{\text{a}})$ is transverse to the hyperplane $\{\varepsilon_3 = 0\}$, $\pi_\varepsilon(\Delta_\varepsilon^{\text{in}} \cap M_1^{\text{a}})$ is transverse to the hyperplane $\{\varepsilon = 0\}$, such that we can restrict the result to a section $\varepsilon = const.$ to obtain the assertion for the image $\pi(\Delta^{\text{in}} \cap S_\varepsilon^{\text{a}})$ in Main Theorem 1. The constant Ω_0 is specified by Proposition 4.14 (b).

As the θ-coordinate decouples in system (4.12), we can track the evolution in θ separately. The ODE $\theta' = \varepsilon$ with initial condition $\theta(0) = \theta^* \in \mathbb{R}/(s\mathbb{Z})$ has the solution

$$\theta(t) \equiv \theta^* + \varepsilon t \mod s.$$

If we consider θ as a variable with values in $\mathbb{R}$, we can determine the transition time of the map $\pi : \Delta^{\text{in}} \to \Delta^{\text{out}}$ with help of the evolution in the θ-coordinate.

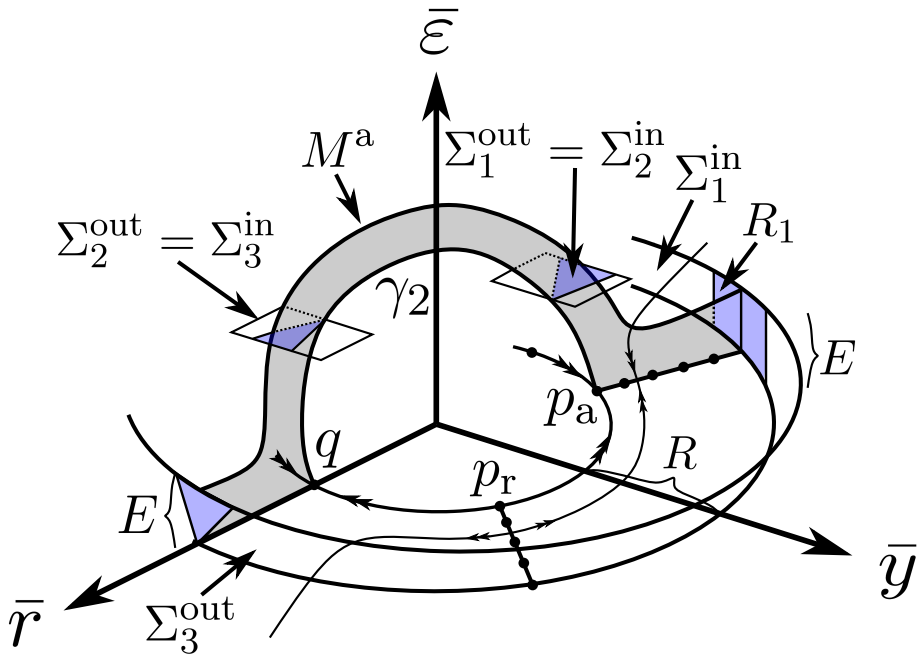


Figure 4.7.: Geometry of the dynamics of the blown-up vector field $\bar{X}$.

In chart K_1, the initial condition $\theta(0) = \theta^* \in \mathbb{R}/(s\mathbb{Z})$ transfers to the initial condition $\theta_1(0) = \theta^* \in \mathbb{R}/(s\mathbb{Z})$. By Proposition 4.11, the evolution of the θ_1-coordinate is given by

$$V_{1,\theta_1}(\theta_1^*, \varepsilon_1^*) \equiv \theta_1^* + \frac{1}{(\varepsilon_1^*)^2} - \frac{1}{E^2} \mod s,$$

where ε_1^* is the initial condition in ε_1 in Σ_1^{in}. By Lemma 3.8, it holds $\varepsilon = \varepsilon_1^* R$, as $\rho_1^* = R$ in Σ_1^{in}, such that we obtain for $\theta_1^{\text{out}} \in \Sigma_1^{\text{out}}$:

$$\theta_1^{\text{out}} \equiv \theta^* + \frac{R^2}{\varepsilon^2} - \frac{1}{E^2} \mod s.$$

Transferred to chart K_2, it holds $\theta_2^{\text{in}} := \kappa_{12}(\theta_1^{\text{out}}) = \theta_1^{\text{out}}$. As we track points on the center manifold M_1^{a}, which lie in chart K_2 on the special surface γ_2, it holds by Proposition 4.20

$$\theta_2^{\text{out}} \equiv \theta_2^{\text{in}} + \frac{1}{E^2} - h_{y_2}\left(\frac{1}{E}\right) \equiv \theta^* + \frac{R^2}{\varepsilon^2} - h_{y_2}\left(\frac{1}{E}\right) \mod s,$$

which is by Lemma 4.28 equivalent to

$$\theta_2^{\text{out}} \equiv \theta^* + \frac{R^2}{\varepsilon^2} + \Omega_0 - E \mod s.$$

Transferred to chart K_3, it holds $\theta_3^{\text{in}} := \kappa_{23}(\theta_2^{\text{out}}) = \theta_2^{\text{out}}$. Applying now the transition map V_3 in chart K_3 leads by Proposition 4.26 (a) to

$$\begin{aligned}\theta_3^{\text{out}} &\equiv \theta_3^{\text{in}} + E - E\frac{\rho_3^*}{R} + \mathcal{O}\left((\rho_3^*)^3 \ln\left(\frac{1}{\rho_3^*}\right)\right) \\ &\equiv \theta^* + \frac{R^2}{\varepsilon^2} + \Omega_0 - E\frac{\rho_3^*}{R} + \mathcal{O}\left((\rho_3^*)^3 \ln\left(\frac{1}{\rho_3^*}\right)\right) \mod s.\end{aligned}$$

By Proposition 4.26 (a), it holds $\varepsilon_3 = E\frac{\rho_3^*}{R}$ in Σ_3^{out}, such that

$$\theta_3^{\text{out}} \equiv \theta^* + \frac{R^2}{\varepsilon^2} + \Omega_0 - \varepsilon_3 + \mathcal{O}\left(\varepsilon_3^3 \ln(\varepsilon_3)\right) \mod s,$$

because $\ln\left(x^{-1}\right) = -\ln(x)$ for $x \in \mathbb{R}_{>0}$. With the blow-down transformation $\varepsilon = \varepsilon_3\rho_3 = \varepsilon_3 R$ in Σ_3^{out}, it follows

$$h_{\theta_3}(\varepsilon) \equiv \theta^* + \frac{R^2}{\varepsilon^2} + \Omega_0 - \frac{\varepsilon}{R} + \mathcal{O}\left(\varepsilon^3 \ln(\varepsilon)\right) \mod s.$$

As we did not simplify the occurring terms for θ modulo s, the transition time for the map π is given by

$$T(\varepsilon) = \frac{h_{\theta_3}(\varepsilon) - \theta^*}{\varepsilon} = \frac{R^2}{\varepsilon^3} + \frac{\Omega_0}{\varepsilon} - \frac{1}{R} + \mathcal{O}\left(\varepsilon^2 \ln(\varepsilon)\right)$$

and part (a) of Main Theorem 1 follows.

To prove assertion (b), we use Proposition 4.11 and infer that $V_1(R_1)$ is a wedge-like region around $V_1(R_1 \cap M_1^{\text{a}})$ of width $\mathcal{O}\left(\exp\left(\frac{2c}{3(\varepsilon_1^*)^3}\right)\right)$ for some negative constant $c > -2$. As the coordinate transformations κ_{12} and κ_{23} as well as the transition map V_2 are diffeomorphisms restricted to the sections Σ_1^{out}, Σ_2^{in} and Σ_2^{out} respectively, it follows that

$$\kappa_{23}(V_2(\kappa_{12}(V_1(R_1))))$$

is again a wedge-like region of width $\mathcal{O}\left(\exp\left(\frac{2c}{3(\varepsilon_1^*)^3}\right)\right)$ for some negative constant $c > -2$ around

$$\kappa_{23}(V_2(\kappa_{12}(V_1(R_1 \cap M_1^{\text{a}})))).$$

The exponential contraction in the r_1-coordinate in chart K_1 transfers to an exponential contraction in the r_2-coordinate in Σ_2^{in}. The map V_2 transfers the exponential contraction to the y_2-coordinate in Σ_2^{out}, which results in an exponential contraction in the y_3-coordinate in Σ_3^{in}, and consequently also in an exponential contraction in the y_3-coordinate in Σ_3^{out}. Hence, $V_i(R_i)$ is a wedge-like region around $V_i(R_i \cap M_i^{\text{a}})$ of width $\mathcal{O}\left(\exp\left(\frac{2c}{3(\varepsilon_i^*)^3}\right)\right)$ for some negative constant $c > -2$. Applying now the blow-down transformation $\varepsilon = \rho_i \varepsilon_i = R_i \varepsilon_i$ for points starting on Σ_i^{in} results in the exponential contraction property for the y-component of the map π. Consequently, the expansion of the function $h_y(\varepsilon)$ is valid for the y-coordinate of all points in $\pi(\Delta^{\text{in}})$. $\square$

Chapter 5

Analysis of the Discrete Fast-Slow Fold

In this chapter, we analyze the Poincaré return map of the fast-slow fold of limit cycles with normal form (3.10). These results can then be transferred to the discrete fast-slow fold singularity with the normal form (3.11). The embedding of the discrete system in the higher dimensional ODE system is defined in Section 3.1. We replicate the structure of the analysis of the continuous case and use many of the results obtained in Chapter 4.

Section 5.1 starts with the analysis of the dynamics in the entry chart. In Section 5.2, exponential contraction in the r-coordinate is observed in the rescaling chart. In contrast to that, the exponential contraction in the continuous case was observed in the y-coordinate. This difference relies on the discrete time scale of the Poincaré return map. In Section 5.3, Main Theorem 2, a local theorem for the normal form of the discrete fast-slow fold singularity (3.11) is proven. It characterizes the dynamics visible in chart K_1 and K_2 and maps the flow from the entry section $\Delta_{\mathcal{P}}^{\text{in}}$ to an ε-dependent exit set $\Delta_{\mathcal{P}}^{\text{out}}$.

In the exit chart, we characterize the loss of well-definedness of the Poincaré return map, which was already indicated by Lemma 3.2. These results allow us to prove Main Theorem 3, which transfers the findings to the blown-down vector field.

5.1. Dynamics in the Entry Chart

The blown-up vector field in chart K_1 is by Lemma 4.1 given by

$$\begin{aligned} r_1' &= \rho_1(1 - r_1^2) + \frac{1}{2}\rho_1\varepsilon_1^3 r_1, \\ \theta_1' &= \rho_1\varepsilon_1, \\ \rho_1' &= -\frac{1}{2}\rho_1^2\varepsilon_1^3, \\ \varepsilon_1' &= \frac{1}{2}\rho_1\varepsilon_1^4, \end{aligned} \tag{5.1}$$

on the time scale t.

To analyze the normal form of the discrete fast-slow fold singularity (3.11) in the entry chart, we explicitly calculate the Poincaré return map. The Poincaré section in chart K_1 is defined as

$$P_1 = \{(r_1, \theta_1, \rho_1, \varepsilon_1) \in \mathcal{D}_{1,\mathcal{P}} : \theta_1 = 0\},$$

where

$$\mathcal{D}_{1,\mathcal{P}} := \left\{(r_1, \theta_1, \rho_1, \varepsilon_1) \in \mathbb{R} \times \mathbb{R}/(s\mathbb{Z}) \times \mathbb{R} \times \mathbb{R} :\ 0 \le \rho_1 \le R,\ 0 \le \varepsilon_1 \le E(1 - sE^2)^{-\frac{1}{2}}\right\},$$

as $\theta = \theta_1$ by the coordinate transformation of Lemma 3.9. Applying the coordinate transformation does not change the dynamics in the θ_1-coordinate, such that the Poincaré section P_1 is hit by the flow of system (5.1), if $\theta_1(t) \equiv 0 \mod s$. Considering θ_1 as a coordinate with values in $\mathbb{R}$, P_1 is hit for the n-th time if $\theta_1(t) = ns$ with $n \in \mathbb{N}_{\ge 1}$.

In Section 4.1, we simplified system (5.1) and analyzed the desingularized system

$$\begin{aligned} r_1' &= r_1^2 - 1 + \frac{1}{2}\varepsilon_1^3 r_1, \\ \theta_1' &= \varepsilon_1, \\ \rho_1' &= -\frac{1}{2}\rho_1 \varepsilon_1^3, \\ \varepsilon_1' &= \frac{1}{2}\varepsilon_1^4, \end{aligned} \tag{5.2}$$

on the time scale t_1 defined by

$$\rho_1 \, \mathrm{d}t = \mathrm{d}t_1 .$$

We consider initial conditions on the Poincaré section, which are part of the entry set

$$\Sigma_{1,\mathcal{P}}^{\mathrm{in}} \coloneqq \{(r_1, \theta_1, \rho_1, \varepsilon_1) \in \mathcal{D}_{1,\mathcal{P}} : \ \theta_1 = 0, \ \rho_1 = R, \ \varepsilon_1 \leq E\} = \Sigma_1^{\mathrm{in}} \cap \{\theta_1 = 0\}.$$

To study the attracting slow manifold M_1^{a}, we introduce the rectangle

$$R_{1,\mathcal{P}} \coloneqq \left\{(r_1, \theta_1, \rho_1, \varepsilon_1) \in \Sigma_{1,\mathcal{P}}^{\mathrm{in}} : |-1 + r_1| \leq \beta\right\} = R_1 \cap \{\theta_1 = 0\}$$

with the constant β, which defines the interval I^{in} of the entry set $\Delta_{\varepsilon,\mathcal{P}}^{\mathrm{in}}$ in the original coordinates. We choose the constants E, R and β in such a way, that $\Sigma_{1,\mathcal{P}}^{\mathrm{in}} \cap M_1^{\mathrm{a}} \subset R_{1,\mathcal{P}}$.

Lemma 5.1. *The rectangle $R_{1,\mathcal{P}}$ in chart K_1 corresponds to the entry set $\Delta_{\varepsilon,\mathcal{P}}^{in}$ in the original coordinates.*

Proof. We recall, that the entry set $\Delta_{\varepsilon,\mathcal{P}}^{\mathrm{in}}$ is defined by

$$\Delta_{\varepsilon,\mathcal{P}}^{\mathrm{in}} \coloneqq \left\{(r, \theta, y, \varepsilon) \in \mathcal{D}_0 : \ r \in I^{\mathrm{in}}, \ \theta = 0 \ y = R^2, \ \varepsilon \leq ER\right\}$$

with

$$I^{\mathrm{in}} = \left\{r \in \mathbb{R}_{\geq -v} : \left|-1 + \frac{r}{R}\right| \leq \beta\right\},$$

which corresponds to the entry set $\Delta_{\varepsilon}^{\mathrm{in}}$ with the additional constraint $\theta = 0$.

By Lemma 4.6, the rectangle R_1 in chart K_1 corresponds to the entry set $\Delta_{\varepsilon}^{\mathrm{in}}$ in the original coordinates. Consequently, the rectangle $R_{1,\mathcal{P}} = R_1 \cap \{\theta_1 = 0\}$ in chart K_1 corresponds to the entry set $\Delta_{\varepsilon,\mathcal{P}}^{\mathrm{in}} = \Delta_{\varepsilon}^{\mathrm{in}} \cap \{\theta = 0\}$ in the original coordinates. □

The following Lemma 5.3 transfers the condition $\theta_1(t) = ns$ with $n \in \mathbb{N}_{\geq 1}$ for the n-th hit of the Poincaré section P_1 from the time scale t to the time scale t_1, such that we can calculate the number of returns to P_1 as well as the corresponding transition times in the desingularized system (5.2).

For that purpose, a special notation of rounding down brackets is introduced.

Definition 5.2. *The brackets $\lfloor \cdot \rfloor_*$ are defined as*

$$\lfloor x \rfloor_* = \begin{cases} x - 1 & \text{if } x \in \mathbb{Z}, \\ \lfloor x \rfloor & \text{if } x \in \mathbb{R} \backslash \mathbb{Z}, \end{cases}$$

such that it holds $\lfloor x \rfloor_* \in \mathbb{Z}$ and $\lfloor x \rfloor_* < x$ for all $x \in \mathbb{R}$.

Lemma 5.3. *For $E < s^{-\frac{1}{2}}$, the flow of the system (5.2) with initial condition $(r_1^*, 0, R, \varepsilon_1^*) \in \Sigma_{1,\mathcal{P}}^{in}$ hits the Poincaré section P_1*

$$N_1(\varepsilon_1^*) = \left\lfloor \frac{1}{s(\varepsilon_1^*)^2} \right\rfloor_* \geq 1$$

times. The n-th return time $T_{P_1}(n)$ with $n \in \mathbb{N}$, $1 \leq n \leq N_1(\varepsilon_1^*)$ to the Poincaré section P_1, is given by

$$T_{P_1}(n) = \frac{2}{3(\varepsilon_1^*)^3}\left(1 - \left(1 - ns(\varepsilon_1^*)^2\right)^{\frac{3}{2}}\right).$$

Proof. We desingularized the flow in the entry chart by applying a non-linear, positive transformation of time by dividing the right hand side of system (5.1) by ρ_1. The desingularized system (5.2) has the same solution curves, passed through on the new time scale t_1. Theorem A.8 provides a formula for the solution curves of system (5.1) on the time scale t, if the solution curves in the desingularized system (5.2) on the time scale t_1 are known.

Using the notion of Theorem A.8, the function $B : J \to \mathbb{R}$ is defined by

$$B(t_1) := \int_0^{t_1} \frac{1}{\rho_1(\bar{t})} \, \mathrm{d}\bar{t},$$

where $\rho_1(t_1)$ is the solution of the ρ_1-component of the desingularized flow (5.2) and $J \subset \mathbb{R}$ is the interval of definition with $0 \in J$. With the explicit solution for $\rho_1(t_1)$ given by Lemma 4.3, we obtain

$$B(t_1) = \int_0^{t_1} \frac{1}{R\varepsilon_1^*} \left(\frac{1}{(\varepsilon_1^*)^3} - \frac{3}{2}\bar{t} \right)^{-\frac{1}{3}} \mathrm{d}\bar{t} = \frac{1}{R(\varepsilon_1^*)^3} \left(1 - \left(1 - \frac{3}{2}(\varepsilon_1^*)^3 t_1 \right)^{\frac{2}{3}} \right)$$

for $t_1 \in J := \left[0, \frac{2}{3(\varepsilon_1^*)^3} \right)$. Even though $B(t_1)$ is well-defined for $t_1 = \frac{2}{3(\varepsilon_1^*)^3}$, we exclude this point from the interval J to have well-defined solutions in all coordinates of system (5.2), see Lemma 4.3. Furthermore, by Theorem A.8, B is invertible on its range $K := B(J) = \left[0, \frac{1}{R(\varepsilon_1^*)^3} \right)$. Its inverse $B^{-1} : K \to J$ is given by

$$B^{-1}(t) := \frac{2}{3(\varepsilon_1^*)^3} \left(1 - \left(1 - R(\varepsilon_1^*)^3 t \right)^{\frac{3}{2}} \right).$$

If $\gamma(t_1)$ solves the desingularized system (5.2), then $\tilde{\gamma}(t) := \gamma(B^{-1}(t))$ solves the singular system (5.1). Hence, it holds $t_1 = B^{-1}(t)$.

When considering θ_1 as a variable in $\mathbb{R}$, the Poincaré section P_1 is hit for the n-th time if $\theta_1(t) = ns$ with $n \in \mathbb{N}_{\geq 1}$ for the time scale t. Thus, we need to solve the evolution in the θ_1-coordinate in the singular system (5.1). By Lemma 3.8 it holds $\varepsilon = \rho_1 \varepsilon_1$ and $\varepsilon' = 0$ in system (3.5), such that the product $\rho_1 \varepsilon_1$ is constant in chart K_1. Consequently, it holds in system (5.1)

$$\theta_1' = \rho_1 \varepsilon_1 = R\varepsilon_1^*$$

due to the initial condition $\rho_1(0)\varepsilon_1(0) = R\varepsilon_1^*$. Integrating leads to

$$\theta_1(t) \equiv R\varepsilon_1^* t \mod s$$

for $t \in K$. Combining this result with the condition $\theta_1(t) = ns$ with $n \in \mathbb{N}_{\geq 1}$ leads to

$$t_{P_1}(n) = \frac{ns}{R\varepsilon_1^*}$$

for the n-th return time to the Poincaré section P_1 on the time scale t. From this relation we can determine the maximal number of returns $N_1(\varepsilon_1^*)$ to P_1:

$$t \in K = \left[0, \frac{1}{R(\varepsilon_1^*)^3} \right) \quad \Rightarrow \quad n = \frac{R\varepsilon_1^*}{s} t_{P_1}(n) < \frac{R\varepsilon_1^*}{s} \frac{1}{R(\varepsilon_1^*)^3} = \frac{1}{s(\varepsilon_1^*)^2} \quad \Rightarrow \quad N_1(\varepsilon_1^*) = \left\lfloor \frac{1}{s(\varepsilon_1^*)^2} \right\rfloor_*.$$

For $E < s^{-\frac{1}{2}}$ and each $\varepsilon_1^* \in (0, E]$, the flow returns at least once to the Poincaré section P_1, as

$$N_1(\varepsilon_1^*) = \left\lfloor \frac{1}{s(\varepsilon_1^*)^2} \right\rfloor_* \geq \left\lfloor \frac{1}{sE^2} \right\rfloor_* \geq 1.$$

By changing the time scale from t to $t_1 = B^{-1}(t)$, we obtain for the n-th return time $T_{P_1}(n)$ to P_1 in system (5.2)

$$T_{P_1}(n) = B^{-1}\left(t_{P_1}(n)\right) = B^{-1}\left(\frac{ns}{R\varepsilon_1^*} \right) = \frac{2}{3(\varepsilon_1^*)^3} \left(1 - \left(1 - ns(\varepsilon_1^*)^2 \right)^{\frac{3}{2}} \right). \qquad \square$$

Remark 5.4. *By assuming E to be small enough, it holds for a fixed constant s that $E < s^{-\frac{1}{2}}$, such that returns to the Poincaré section P_1 are observed in the entry chart.*

Given the return time $\mathcal{T}_{P_1}(n)$ of Lemma 5.3, we can determine for each initial condition in $R_{1,\mathcal{P}} \subset \Sigma^{\text{in}}_{1,\mathcal{P}}$ the concrete form of the n-th Poincaré return map of system (5.2).

Lemma 5.5. *The n-th Poincaré return map $\mathcal{P}_1^n : \Sigma^{in}_{1,\mathcal{P}} \to \mathbb{R} \times \mathbb{R}/(s\mathbb{Z}) \times \mathbb{R} \times \mathbb{R}$ of system (5.2) has the following properties:*

(a) For fixed $c > -2$ and constants E, R and β sufficiently small, the image of a point $(r_1^*, 0, R, \varepsilon_1^*) \in R_{1,\mathcal{P}}$ under the map $\mathcal{P}_1^n$ is the point

$$\mathcal{P}_1^n(r_1^*, 0, R, \varepsilon_1^*) = \left(\mathcal{P}^n_{1,r_1}(r_1^*, \varepsilon_1^*), 0, R(1 - ns(\varepsilon_1^*)^2)^{\frac{1}{2}}, \varepsilon_1^*(1 - ns(\varepsilon_1^*)^2)^{-\frac{1}{2}}\right),$$

with

$$\mathcal{P}^n_{1,r_1}(r_1^*, \varepsilon_1^*) = h_{r_1}\left(\varepsilon_1^*(1 - ns(\varepsilon_1^*)^2)^{-\frac{1}{2}}\right) + \mathcal{O}\left(\exp\left(\frac{cns}{\varepsilon_1^*}\right)\right),$$

where the function h_{r_1} is defined in Proposition 4.4. It holds

$$h_{r_1}\left(\varepsilon_1^*(1 - ns(\varepsilon_1^*)^2)^{-\frac{1}{2}}\right) = -1 - \frac{1}{4}(\varepsilon_1^*)^3 + \mathcal{O}\left(n(\varepsilon_1^*)^5\right).$$

(b) $\mathcal{P}_1^n$ is an exponential contraction in the r_1-coordinate with respect to the initial condition r_1^*, i.e.

$$\frac{\partial \mathcal{P}^n_{1,r_1}}{\partial r_1^*} = \mathcal{O}\left(\exp\left(\frac{cns}{\varepsilon_1^*}\right)\right)$$

for some negative constant $c > -2$.

Proof. By Lemma 5.3, the n-th return time to the Poincaré section P_1 is

$$\mathcal{T}_{P_1}(n) = \frac{2}{3(\varepsilon_1^*)^3}\left(1 - \left(1 - ns(\varepsilon_1^*)^2\right)^{\frac{3}{2}}\right).$$

Inserting $\mathcal{T}_{P_1}(n)$ into the solutions for the flow in the ε_1- and the ρ_1-coordinate given in Lemma 4.3 leads to

$$\varepsilon_1(\mathcal{T}_{P_1}(n)) = \left(\frac{1}{(\varepsilon_1^*)^3} - \frac{3}{2}\frac{2}{3(\varepsilon_1^*)^3}\left(1 - \left(1 - ns(\varepsilon_1^*)^2\right)^{\frac{3}{2}}\right)\right)^{-\frac{1}{3}} = \varepsilon_1^*(1 - ns(\varepsilon_1^*)^2)^{-\frac{1}{2}},$$

$$\rho_1(\mathcal{T}_{P_1}(n)) = R\varepsilon_1^*\left(\frac{1}{(\varepsilon_1^*)^3} - \frac{3}{2}\frac{2}{3(\varepsilon_1^*)^3}\left(1 - \left(1 - ns(\varepsilon_1^*)^2\right)^{\frac{3}{2}}\right)\right)^{\frac{1}{3}} = R\left(1 - ns(\varepsilon_1^*)^2\right)^{\frac{1}{2}}.$$

As $\mathcal{P}_1^n(r_1^*, 0, R, \varepsilon_1^*)$ is a point on the Poincaré section P_1, its θ_1-coordinate is zero. For the r_1-coordinate we infer from Proposition 4.11, that

$$\mathcal{P}^n_{1,r_1}(r_1^*, \varepsilon_1^*) = h_{r_1}\left(\varepsilon_1\left(\mathcal{T}_{P_1}(n)\right)\right) + \mathcal{O}\left(\exp\left(c\mathcal{T}_{P_1}(n)\right)\right),$$

where the function h_{r_1} is defined in Proposition 4.4 and $c > -2$ is some constant. The point $h_{r_1}\left(\varepsilon_1\left(\mathcal{T}_{P_1}(n)\right)\right)$ on the center manifold M_1^a only depends on the ε_1-coordinate $\varepsilon_1\left(\mathcal{T}_{P_1}(n)\right)$, whereas the remainder term $R(r_1^*, \varepsilon_1^*) = \mathcal{O}\left(\exp\left(c\mathcal{T}_{P_1}(n)\right)\right)$ can depend on the initial condition r_1^*. Inserting the transition time $\mathcal{T}_{P_1}(n)$ leads to

$$\begin{aligned}
\mathcal{P}^n_{1,r_1}(r_1^*, \varepsilon_1^*) &= h_{r_1}\left(\varepsilon_1^*(1 - ns(\varepsilon_1^*)^2)^{-\frac{1}{2}}\right) + \mathcal{O}\left(\exp\left(\frac{2c}{3(\varepsilon_1^*)^3}\left(1 - (1 - ns(\varepsilon_1^*)^2)^{\frac{3}{2}}\right)\right)\right) \\
&= -1 - \frac{1}{4}\left(\varepsilon_1^*(1 - ns(\varepsilon_1^*)^2)^{-\frac{1}{2}}\right)^3 + \mathcal{O}\left(\left(\varepsilon_1^*(1 - ns(\varepsilon_1^*)^2)^{-\frac{1}{2}}\right)^6\right) \\
&\quad + \mathcal{O}\left(\exp\left(\frac{2c}{3(\varepsilon_1^*)^3}\left(1 - \left(1 - \frac{3}{2}ns(\varepsilon_1^*)^2 + \mathcal{O}\left(n^2(\varepsilon_1^*)^4\right)\right)\right)\right)\right)
\end{aligned}$$

$$= -1 - \frac{1}{4}(\varepsilon_1^*)^3\left(1 + \mathcal{O}\left(n(\varepsilon_1^*)^2\right)\right) + \mathcal{O}\left((\varepsilon_1^*)^6\left(1 + \mathcal{O}\left(n(\varepsilon_1^*)^2\right)\right)\right)$$
$$+ \mathcal{O}\left(\exp\left(\frac{cns}{\varepsilon_1^*} + \mathcal{O}\left(n^2\varepsilon_1^*\right)\right)\right)$$
$$= -1 - \frac{1}{4}(\varepsilon_1^*)^3 + \mathcal{O}\left(n(\varepsilon_1^*)^5\right) + \mathcal{O}\left(\exp\left(\frac{cns}{\varepsilon_1^*}\right)\right).$$

As only the remainder term $R(r_1^*, \varepsilon_1^*) = \mathcal{O}\left(\exp\left(c\mathcal{T}_{P_1}(n)\right)\right) = \mathcal{O}\left(\exp\left(\frac{cns}{\varepsilon_1^*}\right)\right)$ depends on r_1^*, it holds

$$\frac{\partial \mathcal{P}_{1,r_1}^n}{\partial r_1^*} = \mathcal{O}\left(\exp\left(\frac{cns}{\varepsilon_1^*}\right)\right),$$

such that there is exponential contraction in the r_1-component of the map $\mathcal{P}_1^n$ with respect to the initial condition r_1^* for a negative constant $c > -2$. □

In Figure 5.1, the image of the rectangle $R_{1,\mathcal{P}}$ under the first Poincaré return map $\mathcal{P}_1^i$ is shown. The ε_1-component of $\mathcal{P}_1^i$ is monotonically increasing in the initial condition $\varepsilon_1^* \in (0, E]$, such that the ε_1-coordinate of $\mathcal{P}_1^i(R_{1,\mathcal{P}})$ is bounded by $E(1 - sE^2)^{-\frac{i}{2}}$ from above. From below, the ε_1-coordinate of $\mathcal{P}_1^i(R_{1,\mathcal{P}})$ is bounded by zero. By Lemma 3.9, it holds $y_2 = \varepsilon_1^{-2}$ for the coordinate transformation κ_{12}. For $\varepsilon_1 \to 0^+$ it holds $y_2 \to \infty$. To define a suitable exit box in chart K_1, we need to bound the ε_1-coordinate of the rectangle $R_{1,\mathcal{P}}$ under the transition map in the entry chart from below by a positive constant. This is achieved by defining the number n of iterates of the Poincaré return map dependent on the initial condition $\varepsilon_1^* \in (0, E]$. In the following we show, that a number of iterates $n_1(\varepsilon_1^*)$ exists, such that $\mathcal{P}_1^{n_1(\varepsilon_1^*)}(\Sigma_{1,\mathcal{P}}^{\text{in}})$ is a subset of the exit set

$$\Sigma_{1,\mathcal{P}}^{\text{out}} := \left\{(r_1, \theta_1, \rho_1, \varepsilon_1) \in \mathcal{D}_{1,\mathcal{P}} : \ \theta_1 = 0, \ E \le \varepsilon_1 \le E(1 - sE^2)^{-\frac{i}{2}}\right\}.$$

Given the number $n_1(\varepsilon_1^*)$ of iterates of the Poincaré return map, we define the transition map $K_1^{\mathcal{P}} : \Sigma_{1,\mathcal{P}}^{\text{in}} \to \Sigma_{1,\mathcal{P}}^{\text{out}}$ in the entry chart to be $K_1^{\mathcal{P}} = \mathcal{P}_1^{n_1(\varepsilon_1^*)}$.

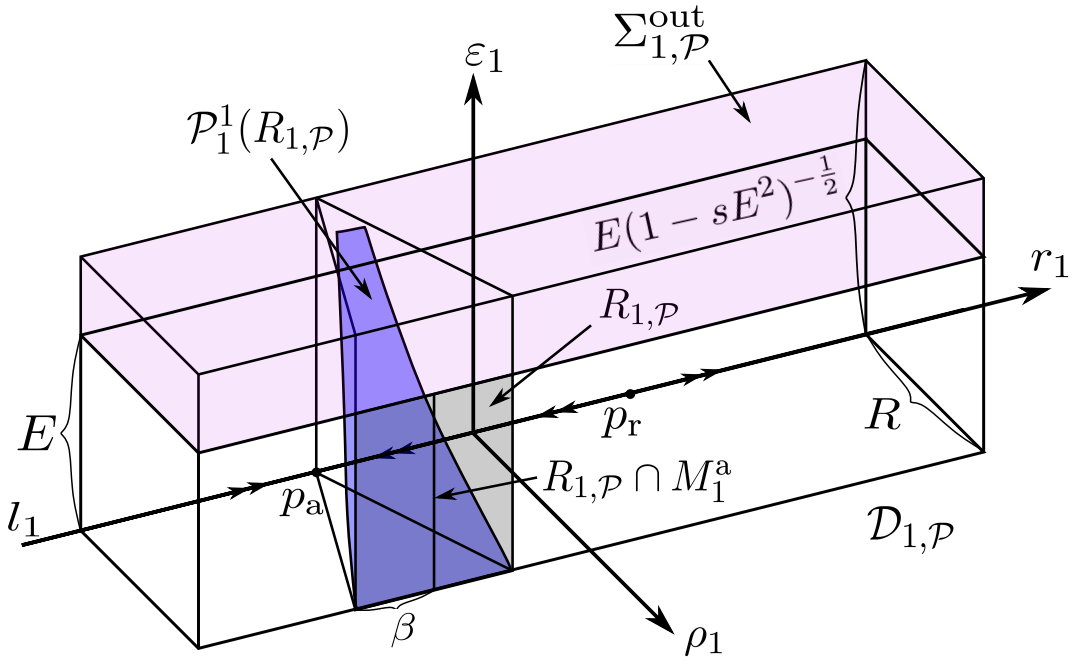


Figure 5.1.: Image of the rectangle R_i under the first Poincaré return map $\mathcal{P}_i^i$ in the coordinates ρ_i, r_i and ε_i for $\theta_i = 0$.

Lemma 5.6. *Let the number $n_1(\varepsilon_1^*)$ of returns of a point $(r_1^*, 0, R, \varepsilon_1^*) \in \Sigma_{1,\mathcal{P}}^{in}$ to the Poincaré section P_1 be defined as*

$$n_1(\varepsilon_1^*) = \left\lfloor \frac{1}{s(\varepsilon_1^*)^2} - \frac{1}{sE^2} \right\rfloor + 1.$$

Then $n_1(\varepsilon_1^*) \in \mathbb{N}_{\geq 1}$ is the unique number such that

$$E < \varepsilon_1(T_{P_1}(n_1(\varepsilon_1^*))) \leq E(1 - sE^2)^{-\frac{1}{2}}.$$

Hence $\Psi_1^{\mathcal{P}}\left(\Sigma_{1,\mathcal{P}}^{in}\right) \subset \Sigma_{1,\mathcal{P}}^{out}$ and the map $\Psi_1^{\mathcal{P}} = \mathcal{P}_1^{n_1(\varepsilon_1^*)}$ is well-defined.

Proof. Recall, that in Remark 5.4 we assumed $\frac{1}{sE^2} > 1$. The number $n_1(\varepsilon_1^*)$ is well-defined, i.e. it is less or equal to the maximal number of returns $N_1(\varepsilon_1^*) = \left\lfloor \frac{1}{s(\varepsilon_1^*)^2} \right\rfloor_*$:

$$\text{if } \frac{1}{s(\varepsilon_1^*)^2} \in \mathbb{Z}: \quad n_1(\varepsilon_1^*) = \left\lfloor \frac{1}{s(\varepsilon_1^*)^2} - \frac{1}{sE^2} \right\rfloor + 1 \leq \frac{1}{s(\varepsilon_1^*)^2} - 2 + 1 = \frac{1}{s(\varepsilon_1^*)^2} - 1 = N_1(\varepsilon_1^*),$$
$$\text{if } \frac{1}{s(\varepsilon_1^*)^2} \notin \mathbb{Z}: \quad n_1(\varepsilon_1^*) = \left\lfloor \frac{1}{s(\varepsilon_1^*)^2} - \frac{1}{sE^2} \right\rfloor + 1 \leq \left\lfloor \frac{1}{s(\varepsilon_1^*)^2} - 1 \right\rfloor + 1 = \left\lfloor \frac{1}{s(\varepsilon_1^*)^2} \right\rfloor = N_1(\varepsilon_1^*).$$

Inserting the definition of $n_1(\varepsilon_1^*)$ in the ε_1-component of the Poincaré return map $\mathcal{P}_1^{n_1(\varepsilon_1^*)}$ given in Lemma 5.5 yields

$$\varepsilon_1(T_{P_1}(n_1(\varepsilon_1^*))) = \varepsilon_1^* \left(1 - \left(\left\lfloor \frac{1}{s(\varepsilon_1^*)^2} - \frac{1}{sE^2} \right\rfloor + 1\right) s(\varepsilon_1^*)^2\right)^{-\frac{1}{2}}.$$

As $(1-x)^{-\frac{1}{2}}$ is strictly increasing for $x \in [0, 1)$, it holds

$$\varepsilon_1(T_{P_1}(n_1(\varepsilon_1^*))) \leq \varepsilon_1^* \left(1 - \left(\frac{1}{s(\varepsilon_1^*)^2} - \frac{1}{sE^2} + 1\right) s(\varepsilon_1^*)^2\right)^{-\frac{1}{2}} = E\left(1 - sE^2\right)^{-\frac{1}{2}},$$

as well as

$$\varepsilon_1(T_{P_1}(n_1(\varepsilon_1^*))) > \varepsilon_1^* \left(1 - \left(\frac{1}{s(\varepsilon_1^*)^2} - \frac{1}{sE^2}\right) s(\varepsilon_1^*)^2\right)^{-\frac{1}{2}} = E,$$

such that $E < \varepsilon_1(T_{P_1}(n_1(\varepsilon_1^*))) \leq E(1 - sE^2)^{-\frac{1}{2}}$. $n_1(\varepsilon_1^*)$ is the only natural number with this property, as $\varepsilon_1(T_{P_1}(n_1(\varepsilon_1^*)))$ is strictly increasing in $n_1(\varepsilon_1^*)$ and

$$\varepsilon_1(T_{P_1}(n_1(\varepsilon_1^*) + 1)) > \varepsilon_1^* \left(1 - \left(\frac{1}{s(\varepsilon_1^*)^2} - \frac{1}{sE^2} + 1\right) s(\varepsilon_1^*)^2\right) = E\left(1 - sE^2\right)^{-\frac{1}{2}},$$

as well as

$$\varepsilon_1(T_{P_1}(n_1(\varepsilon_1^*) - 1)) \leq \varepsilon_1^* \left(1 - \left(\frac{1}{s(\varepsilon_1^*)^2} - \frac{1}{sE^2}\right) s(\varepsilon_1^*)^2\right)^{-\frac{1}{2}} = E.$$

To show $\Psi_1^{\mathcal{P}}\left(\Sigma_{1,\mathcal{P}}^{\text{in}}\right) \subset \Sigma_{1,\mathcal{P}}^{\text{out}}$, it remains to verify the restrictions of the θ_1- and the ρ_1-coordinate. Clearly it holds $\theta_1 = 0$ in $\Psi_1^{\mathcal{P}}\left(\Sigma_{1,\mathcal{P}}^{\text{in}}\right)$, as $\Psi_1^{\mathcal{P}}$ is a Poincaré return map. The ρ_1-component of $\Psi_1^{\mathcal{P}}\left(\Sigma_{1,\mathcal{P}}^{\text{in}}\right)$ is by Lemma 5.5 given by

$$0 \leq R(1 - n_1(\varepsilon_1^*)s(\varepsilon_1^*)^2)^{\frac{1}{2}} \leq R,$$

as $0 \leq n_1(\varepsilon_1^*) \leq N_1(\varepsilon_1^*) \leq \frac{1}{s(\varepsilon_1^*)^2}$. Hence, $\Psi_1^{\mathcal{P}}\left(\Sigma_{1,\mathcal{P}}^{\text{in}}\right) \subset \Sigma_{1,\mathcal{P}}^{\text{out}}$ and the transition map $\Psi_1^{\mathcal{P}}$ is well-defined. □

In Figure 5.2, the map $\Pi_1^{\mathcal{P}}$ is visualized in the ε_1-ρ_1 plane. Dependent on the initial ε_1-coordinate ε_1^* in $\Sigma_{1,\mathcal{P}}^{\text{in}}$, a different number of iterates $n_1(\varepsilon_1^*)$ is carried out to obtain an image point with ε_1-coordinate in the interval $\left[E, E(1-sE^2)^{-\frac{1}{2}}\right]$. The initial conditions in $\Sigma_{1,\mathcal{P}}^{\text{in}}$ with the same number of iterates $n_1(\varepsilon_1^*)$ are visualized in the same color. They divide the entry set $\Sigma_{1,\mathcal{P}}^{\text{in}}$ in the ε_1-ρ_1 plane in half-open intervals, in which the same number of iterates of the Poincaré return map are applied to the initial conditions. Their respective images in $\Sigma_{1,\mathcal{P}}^{\text{out}}$ are represented by the same color.

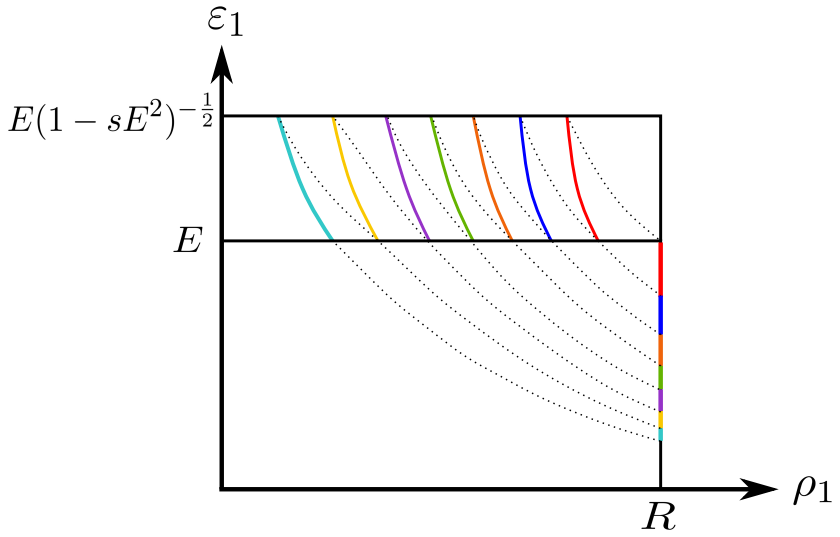


Figure 5.2.: The transition map $\Pi_1^{\mathcal{P}}$ in the ε_1-ρ_1 plane for $\theta_1 = 0$. The image of interval is shown in the same color as the interval itself.

The three-dimensional exit set $\Sigma_{1,\mathcal{P}}^{\text{out}}$ is visualized in Figure 5.3 in the coordinates r_1, ρ_1 and ε_1 for $\theta_1 = 0$. Compared to the three-dimensional exit set Σ_1^{out} of the analysis in Section 4.1, the ε_1-coordinate is not restricted to the value E, but θ_1 is restricted to the value zero. Hence, $\Sigma_1^{\text{out}} \cap \{\theta_1 = 0\}$ is a face of $\Sigma_{1,\mathcal{P}}^{\text{out}}$.

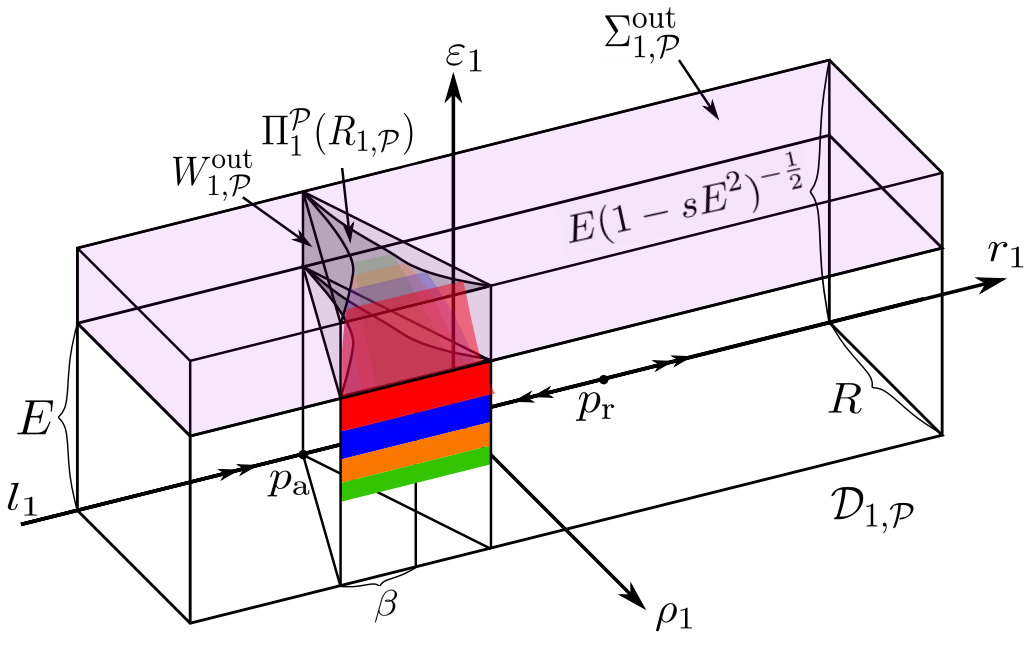


Figure 5.3.: The transition map $\Pi_1^{\mathcal{P}}$ in the coordinates ρ_1, r_1 and ε_1 for $\theta_1 = 0$.

In the following proposition we collect all important properties of the transition map $\mathcal{M}_1^{\mathcal{P}}$ in the entry chart.

Proposition 5.7. *The transition map $\mathcal{M}_1^{\mathcal{P}} : \Sigma_{1,\mathcal{P}}^{in} \to \Sigma_{1,\mathcal{P}}^{out}$ of system (5.2) has the following properties:*

(a) For fixed $c > -2$ and constants E, R and β sufficiently small, the image of a point $p = (r_1^*, 0, R, \varepsilon_1^*) \in R_{1,\mathcal{P}}$ under the map $\mathcal{M}_1^{\mathcal{P}}$ is the point

$$\mathcal{M}_1^{\mathcal{P}}(r_1^*, 0, R, \varepsilon_1^*) = \left(\mathcal{M}_{1,r_1}^{\mathcal{P}}(r_1^*, \varepsilon_1^*), 0, \frac{R}{E}\varepsilon_1^*(1 - (1 - \delta_1(\varepsilon_1^*))sE^2)^{\frac{1}{2}}, E(1 - (1 - \delta_1(\varepsilon_1^*))sE^2)^{-\frac{1}{2}} \right),$$

with

$$\delta_1(\varepsilon_1^*) := \frac{1}{s(\varepsilon_1^*)^2} - \frac{1}{sE^2} \mod 1.$$

It holds that

$$\mathcal{M}_{1,r_1}^{\mathcal{P}}(r_1^*, \varepsilon_1^*) = h_{r_1}\left(E(1 - \delta_1(\varepsilon_1^*)sE^2)^{-\frac{1}{2}}\right) + \mathcal{O}\left(\exp\left(\frac{2c}{3(\varepsilon_1^*)^3}\right)\right)$$

is a smooth function with respect to the initial condition r_1^*, where the function h_{r_1} is defined in Proposition 4.4.

(b) $\mathcal{M}_1^{\mathcal{P}}$ is an exponential contraction in the r_1-coordinate with respect to r_1^*, i.e.

$$\frac{\partial \mathcal{M}_{1,r_1}^{\mathcal{P}}}{\partial r_1^*} = \mathcal{O}\left(\exp\left(\frac{2c}{3(\varepsilon_1^*)^3}\right)\right)$$

for some negative constant $c > -2$.

(c) The image $\mathcal{M}_1^{\mathcal{P}}(R_{1,\mathcal{P}} \cap \mathcal{M}_1^a)$ is a union of smooth curves contained in the two-dimensional set

$$\Sigma_{1,\mathcal{P}}^{out} \cap \mathcal{M}_1^a = \left\{(r_1, \theta_1, \rho_1, \varepsilon_1) \in \Sigma_{1,\mathcal{P}}^{out} : r_1 = h_{r_1}(\varepsilon_1)\right\}.$$

Furthermore, the image $\mathcal{M}_1^{\mathcal{P}}(R_{1,\mathcal{P}})$ is a union of smooth surfaces contained in the three-dimensional set

$$W_{1,\mathcal{P}}^{out} := \left\{(r_1, \theta_1, \rho_1, \varepsilon_1) \in \Sigma_{1,\mathcal{P}}^{out} : h_{r_1}(\varepsilon_1) - \frac{\rho_1}{R}\beta \le r_1 \le h_{r_1}(\varepsilon_1) + \frac{\rho_1}{R}\beta\right\}.$$

Proof. The θ_1-component of $\mathcal{M}_1^{\mathcal{P}}(p)$ is zero, as $\mathcal{M}_1^{\mathcal{P}}$ is a Poincaré return map. To determine the ρ_1- and the ε_1-component of $\mathcal{M}_1^{\mathcal{P}}(p)$, we define

$$\delta_1(\varepsilon_1^*) := \frac{1}{s(\varepsilon_1^*)^2} - \frac{1}{sE^2} \mod 1.$$

Inserting now the number of iterates

$$n_1(\varepsilon_1^*) = \left\lfloor \frac{1}{s(\varepsilon_1^*)^2} - \frac{1}{sE^2} \right\rfloor + 1$$

of the map $\mathcal{M}_1^{\mathcal{P}} = \mathcal{P}_1^{n_1(\varepsilon_1^*)}$ in the formula for $\mathcal{P}_1^n(p)$ given in Lemma 5.5, we obtain

$$\begin{aligned}
\mathcal{M}_{1,\rho_1}^{\mathcal{P}}(\varepsilon_1^*) &= R\left(1 - \left(\left\lfloor \frac{1}{s(\varepsilon_1^*)^2} - \frac{1}{sE^2} \right\rfloor + 1\right) s(\varepsilon_1^*)^2\right)^{\frac{1}{2}} \\
&= R\left(1 - \left(\frac{1}{s(\varepsilon_1^*)^2} - \frac{1}{sE^2} + 1 - \delta_1(\varepsilon_1^*)\right) s(\varepsilon_1^*)^2\right)^{\frac{1}{2}} \\
&= R\left(\frac{(\varepsilon_1^*)^2}{E^2} - (1 - \delta_1(\varepsilon_1^*))s(\varepsilon_1^*)^2\right)^{\frac{1}{2}} = \frac{R}{E}\varepsilon_1^*(1 - (1 - \delta_1(\varepsilon_1^*))sE^2)^{\frac{1}{2}}
\end{aligned}$$

and

$$\begin{aligned}
\mathcal{V}_{1,\varepsilon_1}^{\mathcal{P}}(\varepsilon_1^*) &= \varepsilon_1^* \left(1 - \left(\left\lfloor \frac{1}{s(\varepsilon_1^*)^2} - \frac{1}{sE^2} \right\rfloor + 1\right) s(\varepsilon_1^*)^2\right)^{-\frac{1}{2}} \\
&= \varepsilon_1^* \left(1 - \left(\frac{1}{s(\varepsilon_1^*)^2} - \frac{1}{sE^2} + 1 - \delta_1(\varepsilon_1^*)\right) s(\varepsilon_1^*)^2\right)^{-\frac{1}{2}} \\
&= \varepsilon_1^* \left(\frac{(\varepsilon_1^*)^2}{E^2} - (1 - \delta_1(\varepsilon_1^*)) s(\varepsilon_1^*)^2\right)^{-\frac{1}{2}} = E(1 - (1 - \delta_1(\varepsilon_1^*))sE^2)^{-\frac{1}{2}}.
\end{aligned}$$

For the r_1-coordinate we infer from Proposition 4.11, that

$$\mathcal{V}_{1,r_1}^{\mathcal{P}}(r_1^*, \varepsilon_1^*) = \mathcal{P}_1^{n_1(\varepsilon_1^*)}(r_1^*, \varepsilon_1^*) = h_{r_1}\left(\varepsilon_1\left(\mathcal{T}_{P_1}(n_1(\varepsilon_1^*))\right)\right) + \mathcal{O}\left(\exp\left(c\mathcal{T}_{P_1}(n_1(\varepsilon_1^*))\right)\right),$$

where the function h_{r_1} is defined in Proposition 4.4 and $c > -2$ is some negative constant. The point $h_{r_1}(\varepsilon_1(\mathcal{T}_{P_1}(n_1(\varepsilon_1^*))))$ on the center manifold $\mathcal{M}_1^{\mathrm{a}}$ only depends on the ε_1-coordinate given by $\varepsilon_1(\mathcal{T}_{P_1}(n_1(\varepsilon_1^*)))$, whereas the remainder term $\mathcal{R}(r_1^*, \varepsilon_1^*) = \mathcal{O}\left(\exp\left(c\mathcal{T}_{P_1}(n_1(\varepsilon_1^*))\right)\right)$ can depend on r_1^*. The function $\mathcal{V}_{1,r_1}^{\mathcal{P}}(r_1^*, \varepsilon_1^*)$ is a smooth function with respect to r_1^*, as the transition time does not depend on the initial r_1-coordinate. From the calculation of $\mathcal{V}_{1,\varepsilon_1}^{\mathcal{P}}(\varepsilon_1^*)$, we deduce that

$$\varepsilon_1(\mathcal{T}_{P_1}(n_1(\varepsilon_1^*))) = E(1 - (1 - \delta_1(\varepsilon_1^*))sE^2)^{-\frac{1}{2}}.$$

This yields with the transition time $\mathcal{T}_{P_1}(n_1(\varepsilon_1^*))$ of Lemma 5.3

$$\begin{aligned}
\mathcal{V}_{1,r_1}^{\mathcal{P}}(r_1^*, \varepsilon_1^*) &= h_{r_1}\left(E(1 - (1 - \delta_1(\varepsilon_1^*))sE^2)^{-\frac{1}{2}}\right) + \mathcal{O}\left(\exp\left(\frac{2c}{3(\varepsilon_1^*)^3}\left(1 - (1 - n_1(\varepsilon_1^*)s(\varepsilon_1^*)^2)^{\frac{3}{2}}\right)\right)\right) \\
&= h_{r_1}\left(E(1 - (1 - \delta_1(\varepsilon_1^*))sE^2)^{-\frac{1}{2}}\right) \\
&\quad + \mathcal{O}\left(\exp\left(\frac{2c}{3(\varepsilon_1^*)^3}\left(1 - \left(1 - \left(\frac{1}{s(\varepsilon_1^*)^2} - \frac{1}{sE^2} + 1 - \delta_1(\varepsilon_1^*)\right) s(\varepsilon_1^*)^2\right)^{\frac{3}{2}}\right)\right)\right) \\
&= h_{r_1}\left(E(1 - (1 - \delta_1(\varepsilon_1^*))sE^2)^{-\frac{1}{2}}\right) \\
&\quad + \mathcal{O}\left(\exp\left(\frac{2c}{3(\varepsilon_1^*)^3} - \frac{2c}{3}\left(\frac{1}{E^2} - (1 - \delta_1(\varepsilon_1^*))s\right)^{\frac{3}{2}}\right)\right) \\
&= h_{r_1}\left(E(1 - (1 - \delta_1(\varepsilon_1^*))sE^2)^{-\frac{1}{2}}\right) + \mathcal{O}\left(\exp\left(\frac{2c}{3(\varepsilon_1^*)^3}\right)\right).
\end{aligned}$$

As only the remainder term $\mathcal{R}(r_1^*, \varepsilon_1^*) = \mathcal{O}\left(\exp\left(c\mathcal{T}_{P_1}(n_1(\varepsilon_1^*))\right)\right) = \mathcal{O}\left(\exp\left(\frac{2c}{3(\varepsilon_1^*)^3}\right)\right)$ depends on r_1^* and the function $\mathcal{V}_{1,r_1}^{\mathcal{P}}(r_1^*, \varepsilon_1^*)$ is smooth with respect to r_1^*, it holds

$$\frac{\partial \mathcal{V}_{1,r_1}^{\mathcal{P}}}{\partial r_1^*} = \mathcal{O}\left(\exp\left(\frac{2c}{3(\varepsilon_1^*)^3}\right)\right),$$

such that there is exponential contraction in the r_1-component of the map $\mathcal{V}_1^{\mathcal{P}}$ with respect to the initial condition r_1^* for a negative constant $c > -2$.

As the center manifold $\mathcal{M}_1^{\mathrm{a}}$ is invariant, $\mathcal{V}_1^{\mathcal{P}}(\mathcal{R}_{1,\mathcal{P}} \cap \mathcal{M}_1^{\mathrm{a}})$ has the r_1-coordinate $h_{r_1}(\varepsilon_1)$ with $E \leq \varepsilon_1 \leq E(1 - sE^2)^{-\frac{1}{2}}$, because $E \leq \varepsilon_1 \leq E(1 - sE^2)^{-\frac{1}{2}}$ in the exit set $\Sigma_{1,\mathcal{P}}^{\mathrm{out}}$. $\mathcal{R}_{1,\mathcal{P}} \cap \mathcal{M}_1^{\mathrm{a}}$ is a one-dimensional object, hence $\mathcal{V}_1^{\mathcal{P}}(\mathcal{R}_{1,\mathcal{P}} \cap \mathcal{M}_1^{\mathrm{a}})$ is a one-dimensional subset of the two-dimensional set

$$\Sigma_{1,\mathcal{P}}^{\mathrm{out}} \cap \mathcal{M}_1^{\mathrm{a}} = \left\{(r_1, \theta_1, \rho_1, \varepsilon_1) \in \Sigma_{1,\mathcal{P}}^{\mathrm{out}} : r_1 = h_{r_1}(\varepsilon_1)\right\}.$$

Due to the ε_1^*-dependent number of iterates, the image $\mathcal{V}_1^{\mathcal{P}}(\mathcal{R}_{1,\mathcal{P}} \cap \mathcal{M}_1^{\mathrm{a}})$ is disconnected. This can be observed in the transition map in statement (a) by the piece-wise continuous function $\delta_1(\varepsilon_1^*)$.

As the center manifold M_1^a and the flow of system (5.2) are smooth, the image $\Pi_1^{\mathcal{P}}(R_{1,\mathcal{P}} \cap M_1^a) \subset \Sigma_{1,\mathcal{P}}^{\text{out}}$ is a piece-wise smooth curve.

For the last statement, we consider the image of the rectangle $R_{1,\mathcal{P}}$ under the map $\Pi_1^{\mathcal{P}}$. As the evolution in the θ_1-, ρ_1- and ε_1-coordinate do not depend on the initial condition r_1^*, the additional expansion in the r_1-coordinate of $R_{1,\mathcal{P}}$ only influences the r_1-coordinate of the image $\Pi_1^{\mathcal{P}}(R_{1,\mathcal{P}})$. Due to the exponential contraction in the r_1-coordinate, which is stronger than a linear contraction, $\Pi_1^{\mathcal{P}}(R_{1,\mathcal{P}})$ is a two-dimensional, non-connected, piece-wise smooth subset of the set

$$W_{1,\mathcal{P}}^{\text{out}} := \left\{(r_1, \theta_1, \rho_1, \varepsilon_1) \in \Sigma_{1,\mathcal{P}}^{\text{out}} : h_{r_1}(\varepsilon_1) - \frac{\rho_1}{R}\beta \leq r_1 \leq h_{r_1}(\varepsilon_1) + \frac{\rho_1}{R}\beta\right\}. \qquad \square$$

Remark 5.8. *The formula for the transition map Π_1 given in Proposition 4.11 and for the transition map $\Pi_1^{\mathcal{P}}$ given in Proposition 5.7 only differ by the additional term $(1-\delta_1(\varepsilon_1^*)) \in (0,1]$. This leads to an expansion in the ε_1-coordinate in the discrete case, but the θ_1-coordinate is restricted to zero. The exponential contraction property in the r_1-coordinate is the same in the continuous and the discrete case.*

5.2. Dynamics in the Rescaling Chart

The blown-up vector field in chart K_2 is by Lemma 4.12 given by

$$\begin{aligned} r_2' &= \rho_2(r_2^2 - y_2), \\ \theta_2' &= \rho_2, \\ y_2' &= -\rho_2, \\ \rho_2' &= 0, \end{aligned} \tag{5.3}$$

on the time scale t.

To analyze the normal form of the discrete fast-slow fold singularity in the rescaling chart, we explicitly calculate the Poincaré return map. The Poincaré section in chart K_2 is defined as

$$P_2 = \{(r_2, \theta_2, y_2, \rho_2) \in \mathcal{D}_{2,\mathcal{P}} : \theta_2 = 0\},$$

where

$$\mathcal{D}_{2,\mathcal{P}} := \{(r_2, \theta_2, y_2, \rho_2) \in \mathbb{R} \times \mathbb{R}/(s\mathbb{Z}) \times \mathbb{R} \times \mathbb{R} :\ 0 \leq \rho_2 \leq ER\},$$

as $\theta = \theta_2$ by the coordinate transformation of Lemma 3.9. Applying the coordinate transformation does not change the dynamics in the θ_2-coordinate, such that the Poincaré section P_2 is hit by the flow of system (5.3), if $\theta_2(t) \equiv 0 \mod s$. Considering θ_2 as a coordinate with values in $\mathbb{R}$, P_2 is hit for the n-th time if $\theta_2(t) = ns$ with $n \in \mathbb{N}_{\geq 1}$.

In Section 4.2, we simplified system (5.3) and analyzed the desingularized system

$$\begin{aligned} r_2' &= r_2^2 - y_2, \\ \theta_2' &= 1, \\ y_2' &= -1, \\ \rho_2' &= 0, \end{aligned} \tag{5.4}$$

on the time scale t_2 defined by

$$\rho_2 \, \mathrm{d}t = \mathrm{d}t_2.$$

As ρ_2 is constant in chart K_2, it additionally holds $t_2 = \rho_2 t$. In the rescaling chart, we consider initial conditions in the exit set $W_{1,\mathcal{P}}^{\text{out}} \subset \Sigma_{1,\mathcal{P}}^{\text{out}}$ transferred to chart K_2.

Lemma 5.9. *The exit set $\Sigma_{1,\mathcal{P}}^{out}$ of chart K_1 maps under the coordinate transformation κ_{12} given in Lemma 3.9 to the entry set*

$$\Sigma_{2,\mathcal{P}}^{in} := \left\{(r_2, \theta_2, y_2, \rho_2) \in \mathcal{D}_{2,\mathcal{P}} :\ \theta_2 = 0,\ \frac{1}{E^2} - s \leq y_2 \leq \frac{1}{E^2}\right\}$$

in chart K_2. Furthermore, the image $\kappa_{12}\left(W_1^{\mathcal{P}}(R_{1,\mathcal{P}} \cap M_1^a)\right)$ is a union of smooth curves contained in the two-dimensional set

$$\Sigma_{2,\mathcal{P}}^{in} \cap \gamma_2 = \left\{(r_2, \theta_2, y_2, \rho_2) \in \Sigma_{2,\mathcal{P}}^{in} : \ r_2 = h_{r_2}(y_2)\right\}.$$

The exit set $W_{1,\mathcal{P}}^{out}$, which is a superset of the image $W_1^{\mathcal{P}}(R_{1,\mathcal{P}})$ maps to the entry set

$$W_{2,\mathcal{P}}^{in} := \left\{(r_2, \theta_2, y_2, \rho_2) \in \Sigma_{2,\mathcal{P}}^{in} : \ h_{r_2}(y_2) - \frac{\rho_2}{E^2 R}\beta \le r_2 \le h_{r_2}(y_2) + \frac{\rho_2}{E^2 R}\beta\right\},$$

where the function $h_{r_2}(y_2)$ is defined in Lemma 4.16.

Proof. The exit set $\Sigma_{1,\mathcal{P}}^{\text{out}}$ in chart K_1 is given by

$$\begin{aligned}\Sigma_{1,\mathcal{P}}^{\text{out}} &:= \left\{(r_1, \theta_1, \rho_1, \varepsilon_1) \in \mathcal{D}_{1,\mathcal{P}} : \ \theta_1 = 0, \ E \le \varepsilon_1 \le E(1 - sE^2)^{-\frac{1}{2}}\right\} \\ &= \left\{(r_1, \theta_1, \rho_1, \varepsilon_1) \in \mathbb{R} \times \mathbb{R}/(s\mathbb{Z}) \times \mathbb{R} \times \mathbb{R} : \ \theta_1 = 0, \ 0 \le \rho_1 \le R, \ E \le \varepsilon_1 \le E(1 - sE^2)^{-\frac{1}{2}}\right\}.\end{aligned}$$

Therefore we obtain under the coordinate transformation κ_{12} of Lemma 3.9:

$$\begin{aligned} r_2 = r_1 \varepsilon_1^{-1} \quad &\Rightarrow \quad r_2 \in \mathbb{R}, \\ \theta_2 = \theta_1 \quad &\Rightarrow \quad \theta_2 = 0, \\ y_2 = \varepsilon_1^{-2} \quad &\Rightarrow \quad \frac{1}{E^2} - s \le y_2 \le \frac{1}{E^2}, \\ \rho_2 = \rho_1 \varepsilon_1 \quad &\Rightarrow \quad 0 \le \rho_2 \le ER. \end{aligned}$$

It holds $y_2 > 0$ as we assume $E < s^{-\frac{1}{2}}$ by Remark 5.4. The image $W_1^{\mathcal{P}}(R_{1,\mathcal{P}} \cap M_1^{\text{a}})$ is contained in a set with the additional constraint

$$r_1 = h_{r_1}(\varepsilon_1),$$

and the exit set $W_{1,\mathcal{P}}^{\text{out}}$ has the additional constraint

$$h_{r_1}(\varepsilon_1) - \frac{\rho_1}{R}\beta \le r_1 \le h_{r_1}(\varepsilon_1) + \frac{\rho_1}{R}\beta.$$

By Proposition 4.17, the unique branch of the center manifold M_1^{a} in $\{\varepsilon_1 > 0\}$ corresponds to a part of the special surface γ_2 in chart K_2. Hence, the constraint $r_1 = h_{r_1}(\varepsilon_1)$ transfers in chart K_2 to

$$r_2 = h_{r_2}(y_2),$$

where $h_{r_2}(y_2)$ is the r_2-coordinate of a point on the special surface γ_2 dependent on its y_2-coordinate. Due to the relationships $\rho_1 = \rho_2 y_2^{\frac{1}{2}}$ and $r_2 = r_1 \varepsilon_1^{-1} = r_1 y^{\frac{1}{2}}$, the additional constraint in the r_1-coordinate of $W_{1,\mathcal{P}}^{\text{out}}$ becomes in chart K_2

$$h_{r_2}(y_2) - \frac{\rho_2 y_2}{R}\beta \le r_2 \le h_{r_2}(y_2) + \frac{\rho_2 y_2}{R}\beta.$$

With $y_2 \le \frac{1}{E^2}$, we obtain

$$h_{r_2}(y_2) - \frac{\rho_2}{E^2 R}\beta \le r_2 \le h_{r_2}(y_2) + \frac{\rho_2}{E^2 R}\beta$$

and the result follows. □

In Figure 5.4, the entry sets $\Sigma_{2,\mathcal{P}}^{\text{in}}$ and $W_{2,\mathcal{P}}^{\text{in}}$ are visualized in the r_2-, y_2- and ρ_2-coordinates for $\theta_2 = 0$.

The following lemma transfers the condition $\theta_2(t) = ns$ with $n \in \mathbb{N}_{\ge 1}$ for the n-th hit of the Poincaré section P_2 from the time scale t to the time scale t_2. Then we can calculate the number of returns to P_2 as well as the corresponding transition times in the desingularized system (5.4) for points in $\Sigma_{2,\mathcal{P}}^{\text{in}}$, which lie on the special surface γ_2.

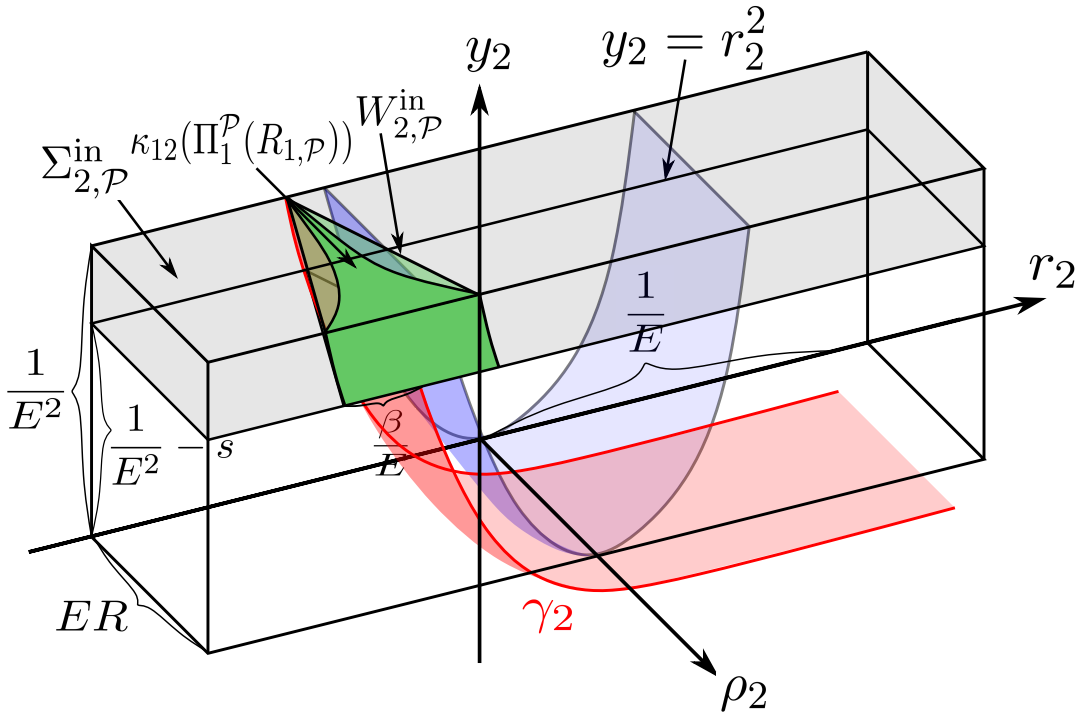


Figure 5.4.: Geometry of the dynamics in chart K_2 in the coordinates r_2, ρ_2 and y_2 for $\theta_2 = 0$.

Lemma 5.10. *For $E^2(2s - \Omega_0) < 1$, the flow of the system (5.4) with specified initial condition $(r_2^*, 0, y_2^*, \rho_2^*) \in \Sigma^{in}_{2,\mathcal{P}} \cap \gamma_2$ hits the Poincaré section P_2*

$$\mathcal{N}_2(y_2^*) = \left\lfloor \frac{y_2^* + \Omega_0}{s} \right\rfloor_* \geq 1$$

times. The n-th return time $\mathcal{T}_{P_2}(n)$ with $n \in \mathbb{N}$, $1 \leq n \leq \mathcal{N}_2(y_2^*)$ to the Poincaré section P_2, is given by

$$\mathcal{T}_{P_2}(n) = ns.$$

Proof. We desingularized the flow in the rescaling chart by applying the linear time rescaling $t_2 = \rho_2 t$ with constant ρ_2 by dividing the right hand side of system (5.3) by ρ_2. The desingularized system (5.4) has the same solution curves, passed through on the new time scale t_2.

When considering θ_2 as a variable in $\mathbb{R}$, the Poincaré section P_2 is hit for the n-th time, if $\theta_2(t) = ns$ with $n \in \mathbb{N}_{\geq 1}$ on the time scale t. Thus, we need to solve the evolution in the θ_2-coordinate in the singular system (5.3). In system (5.3) it holds $\theta_2' = \rho_2$ with initial condition $\theta_2(0) = 0$. Integration leads to

$$\theta_2(t) \equiv \rho_2 t \mod s$$

for $t \in \mathbb{R}_{\geq 0}$, as ρ_2 is constant. Combining this result with the condition $\theta_2(t) = ns$ with $n \in \mathbb{N}_{\geq 1}$ leads to

$$t_{P_2}(n) = \frac{ns}{\rho_2}$$

for the n-th return time to the Poincaré section P_2 on the time scale t.

By changing the time scale from t to $t_2 = \rho_2 t$, we obtain for the n-th return time $\mathcal{T}_{P_2}(n)$ to P_2 in system (5.4)

$$\mathcal{T}_{P_2}(n) = \rho_2 \frac{ns}{\rho_2} = ns.$$

To determine the number of returns to the Poincaré section P_2, we solve the dynamics in the y_2-component in the desingularized system (5.4):

$$y_2' = -1 \qquad \Rightarrow \qquad y_2(t_2) = y_2^* - t_2.$$

By Proposition 4.14, the orbit γ_2 approaches backwards asymptotically the horizontal asymptote $y_2 = -\Omega_0$ from above as $r_2 \to \infty$. Consequently $y_2(t_2) > -\Omega_0$ and

$$t_2 = y_2^* - y_2(t) < y_2^* + \Omega_0.$$

For the maximal number of returns to the Poincaré section P_2 we therefore obtain

$$T_{P_2}(n) = ns < y_2^* + \Omega_0 \qquad \Rightarrow \qquad n < \frac{y_2^* + \Omega_0}{s} \qquad \Rightarrow \qquad N_2(y_2^*) = \left\lfloor \frac{y_2^* + \Omega_0}{s} \right\rfloor_*.$$

Due to the restriction $y_2^* \geq \frac{1}{E^2} - s$ in $\Sigma_{2,\mathcal{P}}^{\text{in}}$ and the assumption $E^2(2s - \Omega_0) < 1$, it holds

$$N_2(y_2^*) = \left\lfloor \frac{y_2^* + \Omega_0}{s} \right\rfloor_* \geq \left\lfloor \frac{1}{sE^2} - 1 + \frac{\Omega_0}{s} \right\rfloor_* \geq 1. \qquad \square$$

Remark 5.11. *By assuming E to be small enough, it holds for a fixed constant s, that $E^2(2s - \Omega_0) < 1$, such that for each initial condition in $\Sigma_{2,\mathcal{P}}^{in} \cap \gamma_2$, returns to the Poincaré section P_2 are observed in the rescaling chart. The condition is also fulfilled for $s < \frac{\Omega_0}{2}$, which is implied by an upcoming condition on s in Lemma 5.13.*

Given the return time $T_{P_2}(n)$ of Lemma 5.10, we can determine the concrete form of the n-th Poincaré return map of system (5.4).

Lemma 5.12. *Let*

$$\tilde{q} := (r_{\tilde{q}}, 0, y_{\tilde{q}}, \rho_2^*) \in \Sigma_{2,\mathcal{P}}^{in} \cap \gamma_2$$

with $y_{\tilde{q}} \in \left[\frac{1}{E^2} - s, \frac{1}{E^2}\right]$ and $r_{\tilde{q}} < 0$ uniquely defined by the property, that $\tilde{q} \in \Sigma_{2,\mathcal{P}}^{in} \cap \gamma_2$. It holds $r_{\tilde{q}} = r_2(y_{\tilde{q}})$, where the function $h_{r_2}(y_2)$ is defined in Lemma 4.16. Then the n-th Poincaré return map $\mathcal{P}_2^n : \Sigma_{2,\mathcal{P}}^{in} \to \mathbb{R} \times \mathbb{R}/(s\mathbb{Z}) \times \mathbb{R} \times \mathbb{R}$ of system (5.4) has for $n \leq N_2(y_{\tilde{q}})$ and E sufficiently small the following properties:

(a) It holds

$$\mathcal{P}_2^n(\tilde{q}) = (h_{r_2}(y_{\tilde{q}} - ns), 0, y_{\tilde{q}} - ns, \rho_2^*),$$

where the function h_{r_2} is defined in Lemma 4.16.

(b) Each neighborhood of $\tilde{q}$ is mapped diffeomorphically onto a neighborhood of $\mathcal{P}_2^n(\tilde{q})$. This means, that the transition map $\mathcal{P}_2^n : \Sigma_{2,\mathcal{P}}^{in} \to \mathbb{R} \times \mathbb{R}/(s\mathbb{Z}) \times \mathbb{R} \times \mathbb{R}$ has for a point $(r_2^*, 0, y_{\tilde{q}}, \rho_2^*) \in \Sigma_{2,\mathcal{P}}^{in}$ with $\Delta_{r_2} := r_2^* - r_{\tilde{q}}$ the form

$$\mathcal{P}_2^n(r_2^*, 0, y_{\tilde{q}}, \rho_2^*) = (h_{r_2}(y_{\tilde{q}} - ns) + \mathcal{O}(\Delta_{r_2}), 0, y_{\tilde{q}} - ns, \rho_2^*),$$

as $\Delta_{r_2} \to 0$.

(c) For the entry set $W_{2,\mathcal{P}}^{in}$ it holds for $n \leq N_2\left(\frac{1}{E^2} - s\right)$ and β sufficiently small:

$$\mathcal{P}_2^n\left(W_{2,\mathcal{P}}^{in}\right) \subset \left\{(r_2, \theta_2, y_2, \rho_2) \in \mathcal{P}_2^n\left(\Sigma_{2,\mathcal{P}}^{in}\right) : \; h_{r_2}(y_2) - K\frac{\rho_2\beta}{E^2 R} \leq r_2 \leq h_{r_2}(y_2) + K\frac{\rho_2\beta}{E^2 R}\right\},$$

for some constant $K > 0$.

Proof. By Lemma 5.10, the n-th return time to the Poincaré section P_2 is $T_{P_2}(n) = ns$. Inserting this time into the solution for the y_2-flow given by Lemma 4.13 leads to

$$y_2(T_{P_2}(n)) = y_{\tilde{q}} - ns.$$

As the image under the map $\Psi_2^{\mathcal{P}}$ is part of the Poincaré section P_2, the θ_2-component is zero. In chart K_2, the dynamics in the ρ_2-component is determined by $\rho_2' = 0$, therefore $\rho_2(T_{P_2}(n)) = \rho_2^*$. By Proposition 4.14, the special surface γ_2 is invariant and therefore the r_2-component of $\mathcal{P}_2^n(\tilde{q})$

is given by $h_{r_2}(y_{\tilde{q}} - ns)$, where the function $h_{r_2}(y_2)$ is the inverse of the function $h_{y_2}(r_2)$, whose expansions are given by Proposition 4.14 (c).

For statement (b) we observe, that the θ_2- and the ρ_2-coordinate decouple from the dynamics in the r_2- and y_2-component. Hence, the θ_2-component of $\mathcal{P}_2^n(r_2^*, 0, y_{\tilde{q}}, \rho_2^*)$ is again zero and the ρ_2-component is ρ_2^*. The flow in the y_2-coordinate only depends on the initial condition and the transition time, such that it holds again, that the y_2-component is $y_{\tilde{q}} - ns$. By Theorem A.1, the flow map $\varphi_2^{\mathcal{P}}$ is a diffeomorphism, such that each neighborhood of $\tilde{\varsigma}$ is mapped diffeomorphically on a neighborhood of $\varphi_2^{\mathcal{P}}(\tilde{\varsigma})$. For Δ_{r_2} small enough, the n-th Poincaré return map $\varphi_2^{\mathcal{P}}$ with $n \leq \mathcal{N}_2(y_{\tilde{q}})$ is also well-defined for the initial condition $(r_2^*, 0, y_{\tilde{q}}, \rho_2^*)$, as the dynamics in the Riccati equation only depends on r_2 and y_2. Due to the diffeomorphic structure it then holds

$$\mathcal{P}_{2,r_2}^n(r_2^*, 0, y_{\tilde{q}}, \rho_2^*) = h_{r_2}(y_{\tilde{q}} - ns) + \mathcal{O}(\Delta_{r_2}),$$

where $h_{r_2}(y_{\tilde{q}} - ns)$ is the r_2-coordinate of the point on the surface γ_2 with the y_2-coordinate $y_{\tilde{q}}$.

For statement (c) we apply the map of statement (b) to all points of the entry set $\mathcal{W}_{2,\mathcal{P}}^{\text{in}}$, which restricts the r_2-coordinate to have at most the distance $\frac{\beta}{E}$ to the special surface γ_2 in r_2-direction. For β sufficiently small, the n-th iterate of the Poincaré return map exists for all points in $\mathcal{W}_{2,\mathcal{P}}^{\text{in}}$, such that $\mathcal{P}_2^n(\mathcal{W}_{2,\mathcal{P}}^{\text{in}})$ is well-defined. Due to the diffeomorphic structure of statement (b), a constant $\mathcal{K} > 0$ exists, such that it holds for the r_2-coordinate of $\mathcal{P}_2^n\left(\mathcal{W}_{2,\mathcal{P}}^{\text{in}}\right)$

$$h_{r_2}(y_2) - \mathcal{K}\frac{\rho_2}{E^2\mathcal{R}}\beta \leq r_2 \leq h_{r_2}(y_2) + \mathcal{K}\frac{\rho_2}{E^2\mathcal{R}}\beta$$

for all y_2-values in $\mathcal{P}_2^n\left(\mathcal{W}_{2,\mathcal{P}}^{\text{in}}\right)$. □

In Figure 5.5, the entry set $\mathcal{W}_{2,\mathcal{P}}^{\text{in}}$ as well as its first few Poincaré return maps are shown in the $y_2 - r_2$ plane for $\rho_2 = E\mathcal{R}$. For $\rho_2 = E\mathcal{R}$, the set $\mathcal{W}_{2,\mathcal{P}}^{\text{in}}$ has in the r_2-direction its maximal expansion.

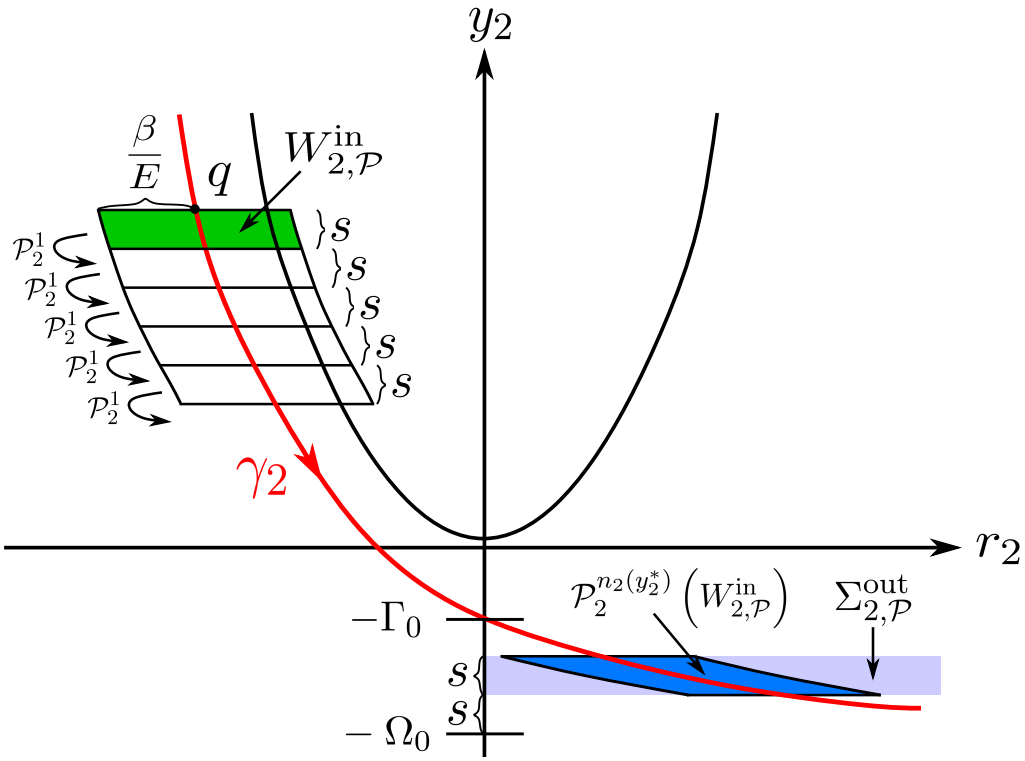


Figure 5.5.: Visualization of the Poincaré return maps $\mathcal{P}_2^i$ in chart $\mathcal{K}_2$ in the coordinates r_2 and y_2 for $\rho_2 = ER$ and $\theta_2 = 0$.

To define a suitable exit set in Chart K_2, we aim to map all points of the entry set $W^{\text{in}}_{2,\mathcal{P}}$ into the half-space $\{r_2 > 0\}$. The following Lemma 5.13 guarantees the existence of a number $n_2(y_2^*) \in \mathbb{N}_{\geq 1}$ of iterates of the Poincaré return map, such that the r_2-coordinates of all points in $\mathcal{P}_2^{n_2(y_2^*)}\left(W^{\text{in}}_{2,\mathcal{P}}\right)$ is positive. We show, that for s sufficiently small, $\mathcal{P}_2^{n_2(y_2^*)}\left(W^{\text{in}}_{2,\mathcal{P}}\right)$ is a subset of the exit set defined by

$$\Sigma^{\text{out}}_{2,\mathcal{P}} := \{(r_2, \theta_2, y_2, \rho_2) \in \mathcal{D}_{2,\mathcal{P}} : \ r_2 > 0, \ \theta_2 = 0, \ -\Omega_0 + s \leq y_2 \leq -\Omega_0 + 2s\}\,.$$

Given the number $n_2(y_2^*)$ of iterates of the Poincaré return map in chart K_2, we define the transition map $T^{\mathcal{P}}_2 : W^{\text{in}}_{2,\mathcal{P}} \to \Sigma^{\text{out}}_{2,\mathcal{P}}$ in the rescaling chart to be $T^{\mathcal{P}}_2 = \mathcal{P}_2^{n_2(y_2^*)}$.

For the following Lemma 5.13 we need to further restrict the constant s. To that end, we introduce the constant $Y_0 > 0$, which is defined to be the negative of the y_2-axis intercept of the special orbit γ_2 of the Riccati equation. By Proposition 4.14 it holds

$$-\Omega_0 < -Y_0 := h_{y_2}(0) < 0,$$

where Ω_0 is the y_2-value of the horizontal asymptote of the special orbit γ_2. The constant Y_0 and the exit set $\Sigma^{\text{out}}_{2,\mathcal{P}}$ are visualized in Figure 5.5.

Lemma 5.13. *Let the number $n_2(y_2^*)$ of returns of a point $(r_2^*, 0, y_2^*, \rho_2^*) \in W^{in}_{2,\mathcal{P}}$ to the Poincaré section P_2 be defined as*

$$n_2(y_2^*) = \left\lfloor \frac{y_2^* - s + \Omega_0}{s} \right\rfloor \geq 1$$

for E sufficiently small. Then for $s < \frac{\Omega_0 - Y_0}{2}$ and β sufficiently small, it holds $T^{\mathcal{P}}_2\left(W^{in}_{2,\mathcal{P}}\right) \subset \Sigma^{out}_{2,\mathcal{P}}$, hence the transition map $T^{\mathcal{P}}_2 = \mathcal{P}_2^{n_2(y_2^*)} : W^{in}_{2,\mathcal{P}} \to \Sigma^{out}_{2,\mathcal{P}}$ is well-defined.

Proof. The number of returns $n_2(y_2^*)$ to the Poincaré section P_2 is by Lemma 5.10 well-defined for all initial conditions $(r_2^*, 0, y_2^*, \rho_2^*) \in W^{\text{in}}_{2,\mathcal{P}} \cap \gamma_2$, as

$$n_2(y_2^*) = \left\lfloor \frac{y_2^* - s + \Omega_0}{s} \right\rfloor = \left\lfloor \frac{y_2^* + \Omega_0}{s} \right\rfloor - 1 \leq \left\lfloor \frac{y_2^* + \Omega_0}{s} \right\rfloor_* = N_2(y_2^*)$$

and

$$n_2(y_2^*) = \left\lfloor \frac{y_2^* - s + \Omega_0}{s} \right\rfloor \geq \left\lfloor \frac{\frac{1}{E^2} - 2s + \Omega_0}{s} \right\rfloor \geq 1$$

for E sufficiently small. The distance in r_2-direction to the special surface γ_2 is for points in $W^{\text{in}}_{2,\mathcal{P}}$ smaller or equal than

$$\frac{\rho_2}{E^2 R}\beta \leq \frac{\beta}{E}.$$

Hence, by choosing β small enough, the $n_2(y_2^*)$-th return to the Poincaré section P_2 is well-defined for all points in $W^{\text{in}}_{2,\mathcal{P}}$.

We aim to show $T^{\mathcal{P}}_2\left(W^{\text{in}}_{2,\mathcal{P}}\right) \subset \Sigma^{\text{out}}_{2,\mathcal{P}}$. By Lemma 5.13, the θ_2-coordinate of points under the map $T^{\mathcal{P}}_2$ is zero and the ρ_2-coordinate stays constant. Hence, the θ_2- and ρ_2-restrictions are the same in $T^{\mathcal{P}}_2\left(W^{\text{in}}_{2,\mathcal{P}}\right)$ and $\Sigma^{\text{out}}_{2,\mathcal{P}}$. It remains to show $-\Omega_0 + s \leq y_2 \leq -\Omega_0 + 2s$ and $r_2 \geq 0$ in $T^{\mathcal{P}}_2\left(W^{\text{in}}_{2,\mathcal{P}}\right)$. To show these estimates we introduce

$$\delta_2(y_2^*) := \frac{y_2^* - s + \Omega_0}{s} \mod 1.$$

For the first condition we now estimate

$$\begin{aligned} K^{\mathcal{P}}_{2,y_2}(r_2^*, 0, y_2^*, \rho_2^*) &= y_2^* - \left\lfloor \frac{y_2^* - s + \Omega_0}{s} \right\rfloor s \\ &= y_2^* - \left(\frac{y_2^* - s + \Omega_0}{s} - \delta_2(y_2^*) \right) s \\ &= -\Omega_0 + (1 + \delta_2(y_2^*))s. \end{aligned}$$

As $\delta_2(y_2^*) \in [0, 1)$, it holds $-\Omega_0 + s \leq y_2 \leq -\Omega_0 + 2s$ for all initial conditions in $K^{\mathcal{P}}_2\left(W^{\text{in}}_{2,\mathcal{P}}\right)$. By the restriction $s < \frac{\Omega_0 - \nu_0}{2}$, it follows that

$$y_2 \leq -\Omega_0 + 2s < -\nu_0.$$

We deduce from Proposition 4.14, that the r_2-coordinate of $K^{\mathcal{P}}_2(r_2^*, 0, y_2^*, \rho_2^*)$ is positive, as the y_2-coordinate of the considered point on the special surface γ_2 is smaller than $-\nu_0$, which is the y_2-axis intercept of the special orbit γ_2 in the Riccati equation.

By Lemma 5.12, the distance in r_2-direction to the special surface γ_2 for the image of a point $(r_2^*, 0, y_2^*, \rho_2^*) \in W^{\text{in}}_{2,\mathcal{P}}$ under the map $K^{\mathcal{P}}_2$ is at most

$$K \frac{\rho_2}{E^2 R} \beta \leq K \frac{\beta}{E}.$$

Hence, by choosing β sufficiently small, the distance in r_2-direction is small enough, such that all points in $K^{\mathcal{P}}_2\left(W^{\text{in}}_{2,\mathcal{P}}\right)$ have a positive r_2-coordinate. □

Remark 5.14. *To be able to map points under the transition map $K^{\mathcal{P}}_2$, we need to assume $s < \frac{\Omega_0 - \nu_0}{2}$, which is a condition independent of the constant E. Hence, in the analysis of the normal form of the discrete fast-slow fold singularity we need to assume that E is sufficiently small and that $s < \frac{\Omega_0 - \nu_0}{2}$.*

In the following proposition we collect all important properties of the transition map $K^{\mathcal{P}}_2$ in the rescaling chart.

Proposition 5.15. *Let*

$$\tilde{q} := (r_{\tilde{q}}, 0, y_{\tilde{q}}, \rho_2^*) \in W^{in}_{2,\mathcal{P}} \cap \gamma_2$$

with $y_{\tilde{q}} \in \left[\frac{1}{E^2} - s, \frac{1}{E^2}\right]$ and $r_{\tilde{q}} < 0$ uniquely defined by the property, that $\tilde{q} \in W^{in}_{2,\mathcal{P}} \cap \gamma_2$. It holds $r_{\tilde{q}} = r_2(y_{\tilde{q}})$, where the function $h_{r_2}(y_2)$ is defined in Lemma 4.16. Then the transition map $K^{\mathcal{P}}_2 : W^{in}_{2,\mathcal{P}} \to \Sigma^{out}_{2,\mathcal{P}}$ of system (5.4) has for $s < \frac{\Omega_0 - \nu_0}{2}$, and constants E and β sufficiently small the following properties:

(a) It holds

$$K^{\mathcal{P}}_2(\tilde{q}) = \left(\tilde{h}_{r_2}\left((1 + \delta_2(y_{\tilde{q}}))s\right), 0, -\Omega_0 + (1 + \delta_2(y_{\tilde{q}}))s, \rho_2^* \right),$$

with

$$\delta_2(y_2^*) := \frac{y_2^* - s + \Omega_0}{s} \mod 1$$

and

$$\tilde{h}_{r_2}(y_2) = \frac{1}{y_2 + \mathcal{O}\left(y_2^3\right)} \qquad \text{as } y_2 \to 0^+.$$

(b) Each neighborhood of $\tilde{q}$ is mapped diffeomorphically onto a neighborhood of $K^{\mathcal{P}}_2(\tilde{q})$. This means, that the transition map $K^{\mathcal{P}}_2 : W^{in}_{2,\mathcal{P}} \to \Sigma^{out}_{2,\mathcal{P}}$ has for a point $(r_2^*, 0, y_{\tilde{q}}, \rho_2^*) \in W^{in}_{2,\mathcal{P}}$ with $\Delta_{r_2} := r_2^* - r_{\tilde{q}}$ the form

$$K^{\mathcal{P}}_2(r_2^*, 0, y_{\tilde{q}}, \rho_2^*) = \left(\tilde{h}_{r_2}\left((1 + \delta_2(y_{\tilde{q}}))s\right) + \mathcal{O}(\Delta_{r_2}), 0, -\Omega_0 + (1 + \delta_2(y_{\tilde{q}}))s, \rho_2^* \right)$$

as $\Delta_{r_2} \to 0$.

(c) *The image* $\Psi_2^{\mathcal{P}}\left(\kappa_{12}\left(\Psi_1^{\mathcal{P}}(R_{1,\mathcal{P}} \cap M_1^a)\right)\right)$ *is a union of smooth curves contained in the two-dimensional set*

$$\Sigma_{2,\mathcal{P}}^{out} \cap \gamma_2 = \left\{(r_2, \theta_2, y_2, \rho_2) \in \Sigma_{2,\mathcal{P}}^{out} : \; r_2 = h_{r_2}(y_2)\right\}.$$

Furthermore, the image $\Psi_2^{\mathcal{P}}\left(\kappa_{12}\left(\Psi_1^{\mathcal{P}}(R_{1,\mathcal{P}})\right)\right)$ *is a union of smooth surfaces contained the three-dimensional set*

$$W_{2,\mathcal{P}}^{out} := \left\{(r_2, \theta_2, y_2, \rho_2) \in \Sigma_{2,\mathcal{P}}^{out} : \; h_{r_2}(y_2) - K\frac{\rho_2\beta}{E^2 R} \le r_2 \le h_{r_2}(y_2) + K\frac{\rho_2\beta}{E^2 R}\right\}$$

for some constant $K > 0$.

Proof. Statement (a) and statement (b) follow from Lemma 5.12 with the number of iterates $n_2(y_2^*)$ defined in Lemma 5.13 as

$$n_2(y_2^*) = \left\lfloor \frac{y_2^* - s + \Omega_0}{s} \right\rfloor_* \ge 1$$

for E sufficiently small. The θ_2- and ρ_2-coordinate do not depend on $n_2(y_2^*)$, hence we only need to explicitly calculate the r_2- and y_2-component of the transition map $\Psi_2^{\mathcal{P}}$. For that purpose we use the constant

$$\delta_2(y_2^*) := \frac{y_2^* - s + \Omega_0}{s} \mod 1.$$

Inserting now the number of iterates $n_2(y_2^*)$ into the formula for the n-th Poincaré return map $\mathcal{P}_2^n$, we obtain

$$\begin{aligned}
\Psi_{2,y_2}^{\mathcal{P}}(y_{\tilde{q}}) &= y_{\tilde{q}} - \left\lfloor \frac{y_{\tilde{q}} - s + \Omega_0}{s} \right\rfloor_* s \\
&= y_{\tilde{q}} - \left(\frac{y_{\tilde{q}} - s + \Omega_0}{s} - \delta_2(y_{\tilde{q}})\right) s \\
&= -\Omega_0 + (1 + \delta_2(y_{\tilde{q}}))s
\end{aligned}$$

and

$$\begin{aligned}
\Psi_{2,r_2}^{\mathcal{P}}(y_{\tilde{q}}) &= h_{r_2}\left(y_{\tilde{q}} - \left\lfloor \frac{y_{\tilde{q}} - s + \Omega_0}{s} \right\rfloor_* s\right) \\
&= h_{r_2}\left(-\Omega_0 + (1 + \delta_2(y_{\tilde{q}}))s\right) \\
&= \tilde{h}_{r_2}\left((1 + \delta_2(y_{\tilde{q}}))s\right),
\end{aligned}$$

where

$$\tilde{h}_{r_2}(y_2) = \frac{1}{y_2 + \mathcal{O}\left(y_2^3\right)} \qquad \text{as } y_2 \to 0^+,$$

by Lemma 4.16.

For statement (c) we use, that by Proposition 5.7, $\Psi_1^{\mathcal{P}}(R_{1,\mathcal{P}} \cap M_1^a)$ is a union of smooth curves contained in $\Sigma_{1,\mathcal{P}}^{\text{out}} \cap M_1^a$. Consequently, $\kappa_{12}\left(\Psi_1^{\mathcal{P}}(R_{1,\mathcal{P}} \cap M_1^a)\right)$ is by Proposition 4.17 a union of smooth curves contained in $\Sigma_{2,\mathcal{P}}^{\text{in}} \cap \gamma_2$. As $\Psi_2^{\mathcal{P}}$ is a diffeomorphism, the image $\Psi_2^{\mathcal{P}}\left(\kappa_{12}\left(\Psi_1^{\mathcal{P}}(R_{1,\mathcal{P}} \cap M_1^a)\right)\right)$ is a union of smooth curves contained in $\Sigma_{2,\mathcal{P}}^{\text{out}} \cap \gamma_2$.

Analogously we obtain for the image $\Psi_2^{\mathcal{P}}\left(\kappa_{12}\left(\Psi_1^{\mathcal{P}}(R_{1,\mathcal{P}})\right)\right)$, that by Proposition 5.7, $\Psi_1^{\mathcal{P}}(R_{1,\mathcal{P}})$ is a union of smooth surfaces contained in the three-dimensional set $W_{1,\mathcal{P}}^{\text{out}}$. By Lemma 5.9 it holds that $\kappa_{12}\left(\Psi_1^{\mathcal{P}}(R_{1,\mathcal{P}})\right)$ is a union of smooth surfaces contained in $W_{2,\mathcal{P}}^{\text{in}}$. By statement (b), the image $\Psi_2^{\mathcal{P}}\left(\kappa_{12}\left(\Psi_1^{\mathcal{P}}(R_{1,\mathcal{P}})\right)\right)$ is contained in $\Sigma_{2,\mathcal{P}}^{\text{out}}$ and its r_2-coordinate can be bounded by

$$h_{r_2}(y_2) - K\frac{\rho_2\beta}{E^2 R} \le r_2 \le h_{r_2}(y_2) + K\frac{\rho_2\beta}{E^2 R}$$

for some constant $K > 0$. Hence, $W_2^{\mathcal{P}}\left(\kappa_{12}\left(W_1^{\mathcal{P}}(R_{1,\mathcal{P}})\right)\right)$ is a union of smooth surfaces contained the three-dimensional set

$$W_{2,\mathcal{P}}^{\text{out}} := \left\{(r_2, \theta_2, y_2, \rho_2) \in \Sigma_{2,\mathcal{P}}^{\text{out}} : \; h_{r_2}(y_2) - K\frac{\rho_2\beta}{E^2 R} \leq r_2 \leq h_{r_2}(y_2) + K\frac{\rho_2\beta}{E^2 R}\right\}$$

for some constant $K > 0$. □

Remark 5.16. *By Proposition 5.15 (b), the initial expansion in the r_2-coordinate in the entry set $W_{2,\mathcal{P}}^{in}$ leads to an expansion in the r_2-coordinate in the exit set $W_{2,\mathcal{P}}^{out}$, as for each return of the Poincaré return map, the y_2-component decreases by the same amount. In contrast to that, for the normal form of the continuous fast-slow fold singularity Proposition 4.20 (b) implies, that the initial expansion in the r_2-coordinate in the entry set W_2^{in} transfers to an expansion in the y_2-coordinate in the exit set Σ_2^{out}. Due to different, not discretized transition times, it is possible to define in the continuous case an exit set Σ_2^{out} with constant r_2-coordinate.*

5.3. Proof of Main Theorem 2

In this section, we combine the results obtained in the charts K_1 and K_2 to prove Main Theorem 2. In Section 3.2, the existence of an attracting slow manifold S_ε^{a} was shown by Fenichel's Theorems. In the entry and rescaling chart we studied the extended system

$$\begin{aligned} r' &= r^2 - y, \\ \theta' &= \varepsilon, \\ y' &= -\varepsilon^3, \\ \varepsilon' &= 0. \end{aligned} \tag{5.5}$$

The attracting slow manifold S_ε^{a} is obtained as a section $\varepsilon = const.$ of the attracting center-manifold M^{a} of system (5.5). The existence of this attracting center manifold M^{a} was shown in Section 3.2. By Lemma 5.1, the entry set of the extended system

$$\Delta_{\varepsilon,\mathcal{P}}^{\text{in}} := \left\{(r, \theta, y, \varepsilon) \in \mathcal{D}_0 : \; r \in I^{\text{in}}, \; \theta = 0, \; y = R^2, \; \varepsilon \leq ER\right\}$$

with the interval

$$I^{\text{in}} = \left\{r \in \mathbb{R}_{\geq -v} : \; \left|-1 + \frac{r}{R}\right| \leq \beta\right\}$$

transfers in chart K_1 to the rectangle

$$R_{1,\mathcal{P}} := \{(r_1, \theta_1, \rho_1\varepsilon_1) \in \Sigma_{1,\mathcal{P}}^{\text{in}} : |-1 + r_1| \leq \beta\}.$$

We denote by X the vector field corresponding to the extended system (5.5) with the transition map $\pi_\varepsilon^{\text{loc}} : \Delta_{\varepsilon,\mathcal{P}}^{\text{in}} \to \Delta_{\varepsilon,\mathcal{P}}^{\text{out}}$. As system (5.5) is the normal form of the fast-slow LC fold (3.10) extended by the equation $\varepsilon' = 0$, the vector field as well as the transition maps $\pi^{\text{loc}} : \Delta_{\mathcal{P}}^{\text{in}} \to \Delta_{\mathcal{P}}^{\text{out}}$ and $\pi_\varepsilon^{\text{loc}} : \Delta_{\varepsilon,\mathcal{P}}^{\text{in}} \to \Delta_{\varepsilon,\mathcal{P}}^{\text{out}}$ of both systems are the same in the first three components. As the vector field X vanishes at $(0, \theta^*, 0, 0)$, $\theta^* \in \mathbb{R}/(s\mathbb{Z})$, a desingularized vector field $\bar{X}$ induced by the blowup transformation exists. This is analyzed in different charts by the transition map $W^{\text{loc}} : \Sigma_{1,\mathcal{P}}^{\text{in}} \to \Sigma_{2,\mathcal{P}}^{\text{out}}$, which is defined as

$$W^{\text{loc}} := W_2^{\mathcal{P}} \circ \kappa_{12} \circ W_1^{\mathcal{P}}.$$

To analyze the attracting center manifold M^{a} under the Poincaré return map, we will study $W^{\text{loc}}(R_{1,\mathcal{P}} \cap M_1^{\text{a}})$ and then use appropriate blow-down transformations to obtain results about $\pi_\varepsilon^{\text{loc}}(\Delta_{\varepsilon,\mathcal{P}}^{\text{in}} \cap M^{\text{a}})$. Restricting the results to the first three coordinates, this allows us to prove Main Theorem 2 about the transition map $\pi^{\text{loc}}(\Delta_{\mathcal{P}}^{\text{in}} \cap S_\varepsilon^{\text{a}})$.

To prove part (a), we consider the set $P_1^{\mathcal{P}}(R_{1,\mathcal{P}} \cap M_1^{\mathrm{a}})$. By Proposition 5.7, we have that $P_1^{\mathcal{P}}(R_{1,\mathcal{P}} \cap M_1^{\mathrm{a}}) \subset \Sigma_{1,\mathcal{P}}^{\mathrm{out}}$ is a union of smooth curves contained in the two-dimensional set

$$\Sigma_{1,\mathcal{P}}^{\mathrm{out}} \cap M_1^{\mathrm{a}} = \left\{(r_1, \theta_1, \rho_1, \varepsilon_1) \in \Sigma_{1,\mathcal{P}}^{\mathrm{out}} : r_1 = h_{r_1}(\varepsilon_1)\right\}$$

with

$$\Sigma_{1,\mathcal{P}}^{\mathrm{out}} := \left\{(r_1, \theta_1, \rho_1, \varepsilon_1) \in \mathcal{D}_{1,\mathcal{P}} :\ \theta_1 = 0,\ \ E \le \varepsilon_1 \le E(1 - sE^2)^{-\frac{1}{2}}\right\}.$$

Dependent on the initial condition ε_1^*, the transition map $P_1^{\mathcal{P}}$ for a point $(r_1^*, 0, R, \varepsilon_1^*) \in R_{1,\mathcal{P}} \cap M_1^{\mathrm{a}}$ is by Proposition 5.7 given by

$$P_1^{\mathcal{P}}(r_1^*, 0, R, \varepsilon_1^*) = \left(P_{1,r_1}^{\mathcal{P}}(r_1^*, \varepsilon_1^*), 0, \frac{R}{E}\varepsilon_1^*(1 - (1 - \delta_1(\varepsilon_1^*))sE^2)^{\frac{1}{2}}, E(1 - (1 - \delta_1(\varepsilon_1^*))sE^2)^{-\frac{1}{2}}\right),$$

with

$$\delta_1(\varepsilon_1^*) := \frac{1}{s(\varepsilon_1^*)^2} - \frac{1}{sE^2} \mod 1$$

and

$$P_{1,r_1}^{\mathcal{P}}(r_1^*, \varepsilon_1^*) = h_{r_1}\left(E(1 - \delta_1(\varepsilon_1^*)sE^2)^{-\frac{1}{2}}\right) + \mathcal{O}\left(\exp\left(\frac{2c}{3(\varepsilon_1^*)^3}\right)\right).$$

With the coordinate change κ_{12} given in Lemma 3.9, we obtain by Lemma 5.9, that the image $\kappa_{12}\left(P_1^{\mathcal{P}}(R_{1,\mathcal{P}} \cap M_1^{\mathrm{a}})\right)$ is a union of smooth curves contained in the two-dimensional set

$$\Sigma_{2,\mathcal{P}}^{\mathrm{in}} \cap \gamma_2 = \left\{(r_2, \theta_2, y_2, \rho_2) \in \Sigma_{2,\mathcal{P}}^{\mathrm{in}} :\ r_2 = h_{r_2}(y_2)\right\}$$

with

$$\Sigma_{2,\mathcal{P}}^{\mathrm{in}} := \left\{(r_2, \theta_2, y_2, \rho_2) \in \mathcal{D}_{2,\mathcal{P}} :\ \theta_2 = 0,\ \frac{1}{E^2} - s \le y_2 \le \frac{1}{E^2}\right\}.$$

To characterize the union of smooth curves, we apply the same coordinate transformation to the map $P_1^{\mathcal{P}}(r_1^*, 0, R, \varepsilon_1^*)$ resulting in

$$\kappa_{12}\left(P_1^{\mathcal{P}}(r_1^*, 0, R, \varepsilon_1^*)\right) = \left(h_{r_2}\left(\frac{1}{E^2} - (1 - \delta_1(\varepsilon_1^*))s\right), 0, \frac{1}{E^2} - (1 - \delta_1(\varepsilon_1^*))s, R\varepsilon_1^*\right).$$

Applying now the transition map $P_2^{\mathcal{P}}$, the image $P_2^{\mathcal{P}}\left(\kappa_{12}\left(P_1^{\mathcal{P}}(R_{1,\mathcal{P}} \cap M_1^{\mathrm{a}})\right)\right)$ is by Proposition 5.15 a union of smooth curves contained in the two-dimensional set

$$\Sigma_{2,\mathcal{P}}^{\mathrm{out}} \cap \gamma_2 = \left\{(r_2, \theta_2, y_2, \rho_2) \in \Sigma_{2,\mathcal{P}}^{\mathrm{out}} :\ r_2 = h_{r_2}(y_2)\right\}$$

with

$$\Sigma_{2,\mathcal{P}}^{\mathrm{out}} = \left\{(r_2, \theta_2, y_2, \rho_2) \in \mathcal{D}_{2,\mathcal{P}} :\ r_2 > 0,\ \theta_2 = 0,\ -\Omega_0 + s \le y_2 \le -\Omega_0 + 2s\right\},$$

where the constant Ω_0 is specified in Proposition 4.14 (b).

By Lemma 3.8, it holds $r = \varepsilon r_2$, $y = \varepsilon^2 y_2$ and $\rho_2 = \varepsilon$. As the y_2-component is bounded in $\Sigma_{2,\mathcal{P}}^{\mathrm{out}}$ and h_{r_2} is a continuous function decreasing in r_2, the r_2-coordinate has the upper bound

$$r_2 \le R := h_{r_2}(-\Omega_0 + s) = \tilde{h}_{r_2}(s)$$

in $\Sigma_{2,\mathcal{P}}^{\mathrm{out}} \cap \gamma_2$ by Lemma 4.16. It follows, that $\Sigma_{2,\mathcal{P}}^{\mathrm{out}} \cap \gamma_2$ is a subset of the exit set $\Delta_{\varepsilon,\mathcal{P}}^{\mathrm{out}}$ in the original coordinates with the constant $R = \tilde{h}_{r_2}(s)$.

For a point $(r_{\tilde{q}}, 0, y_{\tilde{q}}, \rho_2^*) \in \kappa_{12}\left(P_1^{\mathcal{P}}(r_1^*, 0, R, \varepsilon_1^*)\right)$, the transition map $P_2^{\mathcal{P}}$ has by Proposition 5.15 the form

$$P_2^{\mathcal{P}}(r_{\tilde{q}}, 0, y_{\tilde{q}}, \rho_2^*) = \left(\tilde{h}_{r_2}\left((1 + \delta_2(y_{\tilde{q}}))s\right), 0, -\Omega_0 + (1 + \delta_2(y_{\tilde{q}}))s, \rho_2^*\right),$$

with

$$\delta_2(y_2^*) := \frac{y_2^* - s + \Omega_0}{s} \mod 1$$

and

$$\tilde{h}_{r_2}(y_2) = \frac{1}{y_2 + \mathcal{O}\left(y_2^3\right)} \qquad \text{as } y_2 \to 0^+.$$

Consequently it holds

$$\begin{aligned}
&\Psi_2^{\mathcal{P}}(\kappa_{12}(\Psi_1^{\mathcal{P}}(r_1^*, 0, R, \varepsilon_1^*))) \\
&= \left(\tilde{h}_{r_2}\left(1 + \delta_2\left(\frac{1}{E^2} - (1 - \delta_1(\varepsilon_1^*))s\right)s\right), 0, -\Omega_0 + \left(1 + \delta_2\left(\frac{1}{E^2} - (1 - \delta_1(\varepsilon_1^*))s\right)s\right), R\varepsilon_1^*\right).
\end{aligned}$$

We can simplify this expression using

$$\begin{aligned}
\delta^{\mathrm{loc}}(\varepsilon_1^*) := \delta_2\left(\frac{1}{E^2} - (1 - \delta_1(\varepsilon_1^*))s\right) &\equiv \frac{\frac{1}{E^2} - (1 - \delta_1(\varepsilon_1^*))s - s + \Omega_0}{s} \\
&\equiv \frac{\frac{1}{E^2} - \left(1 - \frac{1}{s(\varepsilon_1^*)^2} + \frac{1}{sE^2}\right)s - s + \Omega_0}{s} \\
&\equiv \frac{1}{s(\varepsilon_1^*)^2} - 2 + \frac{\Omega_0}{s} \\
&\equiv \frac{1}{s}\left(\frac{1}{(\varepsilon_1^*)^2} + \Omega_0\right) \mod 1
\end{aligned}$$

and obtain

$$\Psi_2^{\mathcal{P}}(\kappa_{12}(\Psi_1^{\mathcal{P}}(r_1^*, 0, R, \varepsilon_1^*))) = \left(\tilde{h}_{r_2}\left((1 + \delta^{\mathrm{loc}})s\right), 0, -\Omega_0 + \left(1 + \delta^{\mathrm{loc}}\right)s, R\varepsilon_1^*\right).$$

The number of iterates in the entry and rescaling chart are given by Lemma 5.6 and Lemma 5.13 and yield together

$$n(\varepsilon_1^*) := n_1(\varepsilon_1^*) + n_2(y_2^*) = \left\lfloor \frac{1}{s(\varepsilon_1^*)^2} - \frac{1}{sE^2} \right\rfloor + 1 + \left\lfloor \frac{y_2^* - s + \Omega_0}{s} \right\rfloor \geq 2,$$

where $y_2^* = \frac{1}{E^2} - (1 - \delta_1(\varepsilon_1^*))s$ in $\kappa_{12}(\Psi_1^{\mathcal{P}}(r_1^*, 0, R, \varepsilon_1^*))$. It follows

$$\begin{aligned}
n(\varepsilon_1^*) &= \left\lfloor \frac{1}{s(\varepsilon_1^*)^2} - \frac{1}{sE^2} \right\rfloor + 1 + \left\lfloor \frac{y_2^* - s + \Omega_0}{s} \right\rfloor \\
&= \frac{1}{s(\varepsilon_1^*)^2} - \frac{1}{sE^2} - \delta_1(\varepsilon_1^*) + 1 + \frac{\frac{1}{E^2} - (1 - \delta_1(\varepsilon_1^*))s - s + \Omega_0}{s} - \delta_2\left(\frac{1}{E^2} - (1 - \delta_1(\varepsilon_1^*))s\right) \\
&= \frac{1}{s}\left(\frac{1}{(\varepsilon_1^*)^2} + \Omega_0\right) - 1 - \delta^{\mathrm{loc}} \geq 2.
\end{aligned}$$

Using the relationships $\varepsilon = R\varepsilon_1^*$, $r = \varepsilon r_2$ and $y = \varepsilon^2 y_2$ given in Lemma 3.8, assertion (a) of Main Theorem 2 follows.

To proof statement (b), we use that by Proposition 5.7, the map $\Psi_1^{\mathcal{P}}$ is an exponential contraction in the r_1-coordinate with respect to the initial condition r_1^*, i.e.

$$\frac{\partial \Psi_{1,r_1}^{\mathcal{P}}}{\partial r_1^*} = \mathcal{O}\left(\exp\left(\frac{2c}{3(\varepsilon_1^*)^3}\right)\right)$$

for some negative constant $c > -2$. The coordinate transformation κ_{12} and the transition map $\Psi_2^{\mathcal{P}}$ are diffeomorphisms restricted to the sets $\Sigma_{1,\mathcal{P}}^{\mathrm{out}}$, $\Sigma_{2,\mathcal{P}}^{\mathrm{in}}$ and $\Sigma_{2,\mathcal{P}}^{\mathrm{out}}$ respectively, which keep the exponential contraction in the r_1- respectively r_2-coordinate. Hence, the map

$$\Psi^{\mathrm{loc}} = \Psi_2^{\mathcal{P}}(\kappa_{12}(\Psi_1^{\mathcal{P}}(R_{1,\mathcal{P}})))$$

is an exponential contraction in the r_2-coordinate with respect to the initial condition r_1^*. Applying now the blow-down transformation $\varepsilon = R\varepsilon_1^*$ for points starting on $\Sigma^{\text{in}}_{1,\mathcal{P}}$ yields the result.

In assertion (c), we specify the necessary condition for the constant s, that $s < \frac{\Omega_0 - V_0}{2}$ for the analysis in chart K_2. The constant V_0 depends like the constant Ω_0 on the solution of the Riccati equation, whose properties are stated in Proposition 4.14. □

5.4. Dynamics in the Exit Chart

The blown-up vector field in chart K_3 is by Lemma 4.21 given by

$$\begin{aligned} \rho_3' &= \rho_3^2(1 - y_3), \\ \theta_3' &= \rho_3\varepsilon_3, \\ y_3' &= -2\rho_3 y_3(1 - y_3) - \rho_3\varepsilon_3^3, \\ \varepsilon_3' &= -\rho_3\varepsilon_3(1 - y_3), \end{aligned} \tag{5.6}$$

on the time scale t.

To analyze the normal form of the discrete fast-slow fold singularity in the exit chart, we explicitly calculate the Poincaré return map. The Poincaré section in chart K_3 is defined as

$$P_3 = \{(\rho_3, \theta_3, y_3, \varepsilon_3) \in \mathcal{D}_{3,\mathcal{P}} : \theta_3 = 0\},$$

where

$$\mathcal{D}_{3,\mathcal{P}} := \{(\rho_3, \theta_3, y_3, \varepsilon_3) \in \mathbb{R} \times \mathbb{R}/(s\mathbb{Z}) \times \mathbb{R} \times \mathbb{R} :\ \rho_3 \geq 0,\ y_3 < 0,\ \varepsilon_3 > 0\},$$

as $\theta = \theta_3$ by the coordinate transformation of Lemma 3.9. Applying the coordinate transformation does not change the dynamics in the θ_3-coordinate, such that the Poincaré section P_3 is hit by the flow of system (5.6), if $\theta_3(t) \equiv 0 \mod s$. Considering θ_3 as a coordinate with values in $\mathbb{R}$, P_3 is hit for the n-th time if $\theta_3(t) = ns$ with $n \in \mathbb{N}_{\geq 1}$.

In Section 4.3 we simplified system (5.6) and analyzed the desingularized system

$$\begin{aligned} \rho_3' &= \rho_3, \\ \theta_3' &= \frac{\varepsilon_3}{1 - y_3}, \\ y_3' &= -2y_3 - \frac{\varepsilon_3^3}{1 - y_3}, \\ \varepsilon_3' &= -\varepsilon_3, \end{aligned} \tag{5.7}$$

on the time scale $\tilde{t}_3$ defined by

$$\rho_3(1 - y_3)\,\mathrm{d}t = \mathrm{d}\tilde{t}_3.$$

In chart K_3, we consider initial conditions in $W^{\text{out}}_{2,\mathcal{P}} \subset \Sigma^{\text{out}}_{2,\mathcal{P}}$ transferred to the exit chart.

Lemma 5.17. *The exit set $\Sigma^{out}_{2,\mathcal{P}}$ of chart K_2 maps under the coordinate transformation κ_{23} given in Lemma 3.9 to the entry set*

$$\Sigma^{in}_{3,\mathcal{P}} := \{(\rho_3, \theta_3, y_3, \varepsilon_3) \in \mathcal{D}_{3,\mathcal{P}} : \theta_3 = 0\}$$

in chart K_2. Furthermore, the image $\kappa_{23}(W_2^{\mathcal{P}}(\kappa_{12}(W_1^{\mathcal{P}}(R_{1,\mathcal{P}} \cap M_1^a))))$ is for E sufficiently small a union of smooth curves contained in the three-dimensional set

$$\overline{W}^{in}_{3,\mathcal{P}} = \left\{ (\rho_3, \theta_3, y_3, \varepsilon_3) \in \Sigma^{in}_{3,\mathcal{P}} :\ \rho_3 \leq R,\ \frac{-\Omega_0 + s}{(h_{r_2}(-\Omega_0 + 2s))^2} \leq y_3 \leq E^2(-\Omega_0 + 2s), \right.$$
$$\left. E \leq \varepsilon_3 \leq \frac{1}{h_{r_2}(-\Omega_0 + 2s)} \right\}.$$

The exit set $W_{2,\mathcal{P}}^{out}$, which is a superset of the image $T_2^{\mathcal{P}}(\kappa_{12}(T_1^{\mathcal{P}}(R_{1,\mathcal{P}})))$, maps for E and β sufficiently small to the entry set

$$W_{3,\mathcal{P}}^{in} := \Bigg\{ (\rho_3, \theta_3, y_3, \varepsilon_3) \in \Sigma_{3,\mathcal{P}}^{in} : \ \rho_3 \leq R + K R\beta, \\ \frac{-\Omega_0 + s}{(h_{r_2}(-\Omega_0 + 2s) - K R\beta)^2} \leq y_3 \leq \frac{-\Omega_0 + 2s}{\left(\frac{1}{E} + K R\beta\right)^2}, \\ \frac{1}{\frac{1}{E} + K R\beta} \leq \varepsilon_3 \leq \frac{1}{h_{r_2}(-\Omega_0 + 2s) - K R\beta} \Bigg\},$$

where the function $h_{r_2}(y_2)$ is defined in Lemma 4.16.

Proof. The exit set $\Sigma_{2,\mathcal{P}}^{\text{out}}$ in chart K_2 is given by

$$\Sigma_{2,\mathcal{P}}^{\text{out}} := \{(r_2, \theta_2, y_2, \rho_2) \in \mathcal{D}_{2,\mathcal{P}} : \ r_2 > 0, \ \theta_2 = 0, \ -\Omega_0 + s \leq y_2 \leq -\Omega_0 + 2s\},$$

where $y_2 \leq -\Omega_0 + 2s < 0$ and $\rho_2 \leq ER$. Under the coordinate transformation κ_{12} of Lemma 3.9 we obtain:

$$\begin{aligned} \rho_3 &= \rho_2 r_2 && \Rightarrow \quad \rho_3 \geq 0, \\ \theta_3 &= \theta_2 && \Rightarrow \quad \theta_3 = 0, \\ y_3 &= y_2 r_2^{-2} && \Rightarrow \quad y_3 < 0, \\ \varepsilon_3 &= r_2^{-1} && \Rightarrow \quad \varepsilon_3 > 0. \end{aligned}$$

The image $T_2^{\mathcal{P}}(\kappa_{12}(T_1^{\mathcal{P}}(R_{1,\mathcal{P}} \cap M_1^{\text{a}})))$ is by Proposition 5.15 (c) contained in $\Sigma_{2,\mathcal{P}}^{\text{out}} \cap \gamma_2$, which has with respect to $\Sigma_{2,\mathcal{P}}^{\text{out}}$ the additional constraint

$$r_2 = h_{r_2}(y_2) > 0.$$

As the function h_{r_2} is monotonically decreasing in y_2, the constraints for the superset $\Sigma_{2,\mathcal{P}}^{\text{out}} \cap \gamma_2$ of $T_2^{\mathcal{P}}(\kappa_{12}(T_1^{\mathcal{P}}(R_{1,\mathcal{P}} \cap M_1^{\text{a}})))$ become in chart K_3:

$$\begin{aligned} \rho_3 &= \rho_2 r_2 && \Rightarrow \quad 0 \leq \rho_3 \leq ER h_{r_2}(-\Omega_0 + s), \\ \theta_3 &= \theta_2 && \Rightarrow \quad \theta_3 = 0, \\ y_3 &= y_2 r_2^{-2} && \Rightarrow \quad \frac{-\Omega_0 + s}{(h_{r_2}(-\Omega_0 + 2s))^2} \leq y_3 \leq \frac{-\Omega_0 + 2s}{(h_{r_2}(-\Omega_0 + s))^2}, \\ \varepsilon_3 &= r_2^{-1} && \Rightarrow \quad \frac{1}{h_{r_2}(-\Omega_0 + s)} \leq \varepsilon_3 \leq \frac{1}{h_{r_2}(-\Omega_0 + 2s)}, \end{aligned}$$

where we denote the resulting set by $\overline{W}_{3,\mathcal{P}}^{\text{in}}$.

As $y_2 < 0$, it also holds $y_3 < 0$. The exit set $W_{2,\mathcal{P}}^{\text{out}}$ has the additional constraint

$$h_{r_2}(y_2) - K \frac{\rho_2}{E^2 R} \beta \leq r_2 \leq h_{r_2}(y_2) + K \frac{\rho_2}{E^2 R} \beta,$$

for some constant $K > 0$, which simplifies with $\rho_2 \leq ER$ to

$$h_{r_2}(y_2) - K \frac{\beta}{E} \leq r_2 \leq h_{r_2}(y_2) + K \frac{\beta}{E}.$$

For β sufficiently small, the r_2-coordinate is positive. Consequently, the constraints of the exit set $W_{2,\mathcal{P}}^{\text{out}}$ become in chart K_3:

$$\begin{aligned} \rho_3 &= \rho_2 r_2 && \Rightarrow \quad 0 \leq \rho_3 \leq ER h_{r_2}(-\Omega_0 + s) + K R\beta, \\ \theta_3 &= \theta_2 && \Rightarrow \quad \theta_3 \in \mathbb{R}/(s\mathbb{Z}), \\ y_3 &= y_2 r_2^{-2} && \Rightarrow \quad \frac{-\Omega_0 + s}{(h_{r_2}(-\Omega_0 + 2s) - K R\beta)^2} \leq y_3 \leq \frac{-\Omega_0 + 2s}{(h_{r_2}(-\Omega_0 + s) + K R\beta)^2}, \\ \varepsilon_3 &= r_2^{-1} && \Rightarrow \quad \frac{1}{h_{r_2}(-\Omega_0 + s) + K R\beta} \leq \varepsilon_3 \leq \frac{1}{h_{r_2}(-\Omega_0 + 2s) - K R\beta}. \end{aligned}$$

For β sufficiently small, the y_3-coordinate of $\kappa_{23}(W^{\text{out}}_{2,\mathcal{P}})$ is negative and the ε_3-coordinate is positive, hence $\kappa_{23}(W^{\text{out}}_{2,\mathcal{P}})$ is contained in $\mathcal{D}_3$.

By Proposition 4.14, the special orbit γ_2 of the Riccati equation lies to the left of the parabola $y_2 = r_2^2$, such that $r_2' > 0$ for points on γ_2. Consequently, the solution of the r_2-component $h_{r_2}(y_2)$ is strictly decreasing in y_2. For E sufficiently small it holds $E < s$, such that

$$h_{r_2}(-\Omega_0 + 2s) < h_{r_2}(-\Omega_0 + s) < h_{r_2}(-\Omega_0 + E) = \frac{1}{E},$$

where the last equality follows from Lemma 4.28. With these inequalities, the expressions for $\overline{W}^{\text{in}}_{3,\mathcal{P}}$ and $W^{\text{in}}_{3,\mathcal{P}}$ simplify and the result is obtained. □

In Figure 5.6, the entry sets $\overline{W}^{\text{in}}_{3,\mathcal{P}}$ and $W^{\text{in}}_{3,\mathcal{P}}$ are visualized in the ρ_3-, y_3- and ε_3-coordinate for $\theta_3 = 0$.

The following lemma transfers the condition $\theta_3(t) = ns$ with $n \in \mathbb{N}_{\geq 1}$ for the n-th hit of the Poincaré section P_3 from the time scale t to the time scale $\tilde{t}_3$. Then we can estimate the number of returns to P_3 as well as the corresponding transition times in the desingularized system (5.7) for points in $\Sigma^{\text{in}}_{3,\mathcal{P}}$.

Lemma 5.18. *For E sufficiently small, the flow of the system (5.7) with initial condition $(\rho_3^*, 0, y_3^*, \varepsilon_3^*) \in W^{in}_{3,\mathcal{P}}$ hits the Poincaré section P_3 at most $N_3(\varepsilon_3^*)$ times, where*

$$\left\lfloor \frac{C_{y_3}\varepsilon_3^*}{s} \right\rfloor \leq N_3(\varepsilon_3^*) < \left\lfloor \frac{\varepsilon_3^*}{s} \right\rfloor_* < \infty$$

with some constant $0 < C_{y_3} < 1$. The n-th return time $T_{P_3}(n)$ with $n \in \mathbb{N}$, $n \leq N_3(\varepsilon_1^*)$ to the Poincaré section P_3 can be estimated by

$$\ln\left(\frac{\varepsilon_3^*}{\varepsilon_3^* - ns}\right) \leq T_{P_3}(n) \leq \ln\left(\frac{\varepsilon_3^*}{\varepsilon_3^* - \frac{ns}{C_{y_3}}}\right).$$

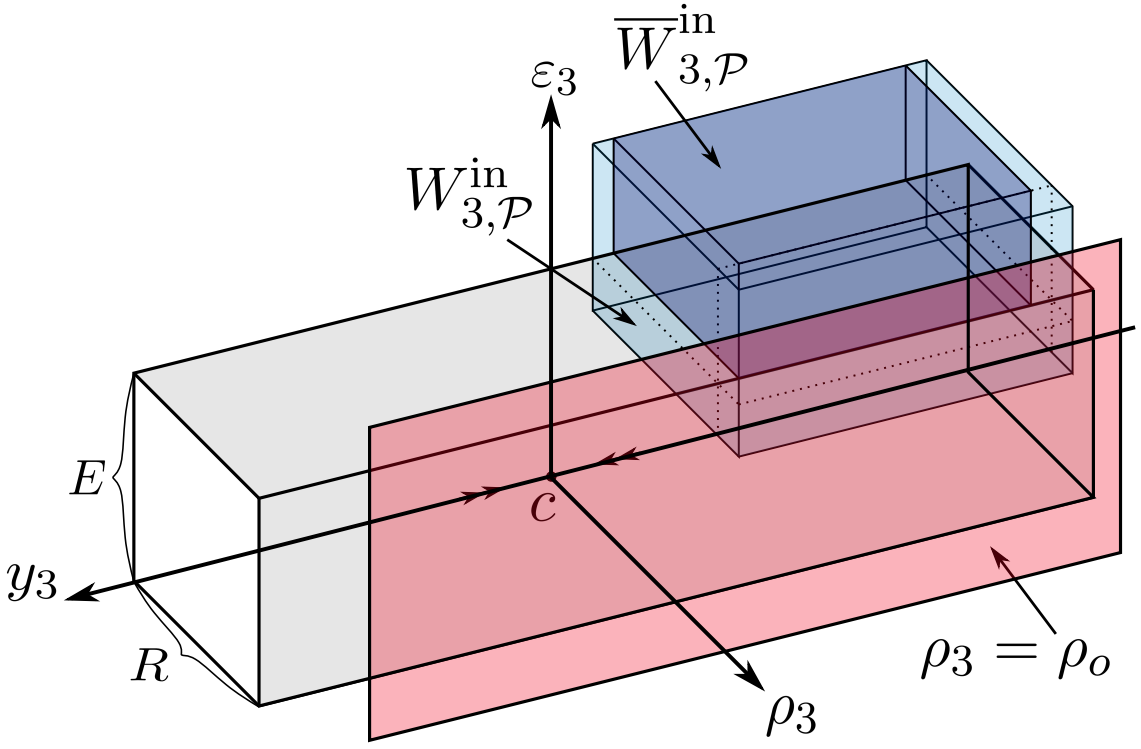


Figure 5.6.: Geometry of the dynamics in chart K_3 in the coordinates ρ_3, y_3 and ε_3 for $\theta_3 = 0$.

Proof. We desingularized the flow in the exit chart by applying a non-linear, positive transformation of time by dividing the right hand side of system (5.6) by $\rho_3(1 - y_3)$. The desingularized system (5.7) has the same solution curves, passed through on the new time scale $\tilde{t}_3$. Theorem A.8 provides a formula for the solution curves of system (5.6) on the time scale t, if the solution curves in the desingularized system (5.7) on the time scale $\tilde{t}_3$ are known.

Using the notion of Theorem A.8, the function $B : J \to \mathbb{R}$ is defined by

$$B(\tilde{t}_3) := \int_0^{\tilde{t}_3} \frac{1}{\rho_3(\bar{t})(1 - y_3(\bar{t}))} \, \mathrm{d}\bar{t},$$

where $\rho_3(\tilde{t}_3)$ is the solution of the ρ_3-component and $y_3(\tilde{t}_3)$ is the solution of the y_3-component of the desingularized flow (5.7) and $J \subset \mathbb{R}$ is an interval with $0 \in J$.

For an initial condition in $W^{\mathrm{in}}_{3,\mathcal{P}}$, it holds by Lemma 5.17, that the initial condition y_3^* can be bounded by

$$-c_{y_3} < y_3^* < 0$$

with a positive constants c_{y_3}. By Proposition 4.26 (b), it holds for the dynamics in the ε_3-coordinate

$$\varepsilon_3 = \varepsilon_3^* e^{-\tilde{t}_3} \leq \varepsilon_3^*$$

for $\tilde{t}_3 \geq 0$. The initial condition ε_3^* is bounded from above by some constant by Lemma 5.17. Hence, we can choose c_{y_3} large enough, such that

$$y_3'|_{y_3 = -c_{y_3}} = 2c_{y_3} - \frac{\varepsilon_3^3}{1 + c_{y_3}} \geq 2c_{y_3} - \frac{(\varepsilon_3^*)^3}{1 + c_{y_3}} > 0.$$

As additionally $y_3'|_{y_3=0} < 0$, the interval $(-c_{y_3}, 0)$ is invariant under the flow of y_3. It follows, that a positive constant $C_{y_3} := \frac{1}{1+c_{y_3}} < 1$ exists, such that

$$C_{y_3} < \frac{1}{1 - y_3(\tilde{t}_3)} < 1.$$

With the explicit solution for $\rho_3(\tilde{t}_3)$ given by Proposition 4.26 (b), we can estimate

$$B(\tilde{t}_3) \leq B^{\mathrm{u}}(\tilde{t}_3) := \int_0^{\tilde{t}_3} \frac{1}{\rho_3^* e^{\bar{t}}} \, \mathrm{d}\bar{t} = \frac{1}{\rho_3^*} \left(1 - e^{-\tilde{t}_3}\right)$$

and

$$B(\tilde{t}_3) \geq B^{\mathrm{l}}(\tilde{t}_3) := C_{y_3} \int_0^{\tilde{t}_3} \frac{1}{\rho_3^* e^{\bar{t}}} \, \mathrm{d}\bar{t} = \frac{C_{y_3}}{\rho_3^*} \left(1 - e^{-\tilde{t}_3}\right)$$

for $\tilde{t}_3 \in [0, \infty)$. As the function $B(\tilde{t}_3)$ is continuous and for $\tilde{t}_3 \geq 0$ bounded from below by the continuous function $B^{\mathrm{l}}(\tilde{t}_3)$ and from above by the continuous function $B^{\mathrm{u}}(\tilde{t}_3)$, which exist both for all $\tilde{t}_3 \in [0, \infty)$, also $B(\tilde{t}_3)$ has to exist for all $\tilde{t}_3 \in [0, \infty)$. Consequently $J = [0, \infty)$ is the interval of definition for $B(\tilde{t}_3)$, $B^{\mathrm{u}}(\tilde{t}_3)$ and $B^{\mathrm{l}}(\tilde{t}_3)$. By Theorem A.8, B is invertible on its range $K := B(J)$. It holds

$$\left[0, \frac{C_{y_3}}{\rho_3^*}\right) = B^{\mathrm{l}}(J) \subset K \subset B^{\mathrm{u}}(J) = \left[0, \frac{1}{\rho_3^*}\right).$$

The inverse of $B^{\mathrm{u}}(\tilde{t}_3)$ is given by $(B^{\mathrm{u}})^{-1} : \left[0, \frac{1}{\rho_3^*}\right) \to J$,

$$(B^{\mathrm{u}})^{-1}(t) := \ln\left(\frac{1}{1 - \rho_3^* t}\right)$$

and the inverse of $B^{\mathrm{l}}(\tilde{t}_3)$ is given by $(B^{\mathrm{l}})^{-1} : \left[0, \frac{C_{y_3}}{\rho_3^*}\right) \to J$,

$$(B^{\mathrm{l}})^{-1}(t) := \ln\left(\frac{1}{1 - \frac{\rho_3^*}{C_{y_3}} t}\right).$$

As $B^{\mathrm{l}}(\tilde{t}_3) \leq B(\tilde{t}_3) \leq B^{\mathrm{u}}(\tilde{t}_3)$ for all $\tilde{t}_3 \in J$, it holds

$$(B^{\mathrm{l}})^{-1}(t) \geq B^{-1}(t) \geq (B^{\mathrm{u}})^{-1}(t) \qquad \text{for all } t \in K.$$

If $\gamma(\tilde{t}_3)$ solves the desingularized system (5.7), then $\tilde{\gamma}(t) \coloneqq \gamma(B^{-1}(t))$ solves the singular system (5.6). Hence, it holds $\tilde{t}_3 = B^{-1}(t)$.

When considering θ_3 as a variable in $\mathbb{R}$, the Poincaré section P_3 is hit for the n-th time if $\theta_3(t) = ns$ with $n \in \mathbb{N}_{\geq 1}$ for the time scale t. Thus, we need to solve the evolution in the θ_3-coordinate in the singular system (5.6). By Lemma 3.8, it holds $\varepsilon = \rho_3\varepsilon_3$ and $\varepsilon' = 0$ in the normal form of the fast-slow LC fold (3.5), such that the product $\rho_3\varepsilon_3$ is constant in chart K_3. Thus, it holds in system (5.6)

$$\theta_3' = \rho_3\varepsilon_3 = \rho_3^*\varepsilon_3^*$$

due to the initial condition $\rho_3(0)\varepsilon_3(0) = \rho_3^*\varepsilon_3^*$. Integrating leads to

$$\theta_3(t) \equiv \rho_3^*\varepsilon_3^* t \mod s$$

for $t \in K$. Combining this result with the condition $\theta_3(t) = ns$ with $n \in \mathbb{N}_{\geq 1}$ leads to

$$t_{P_3}(n) = \frac{ns}{\rho_3^*\varepsilon_3^*}$$

for the n-th return time to the Poincaré section P_3 on the time scale t. From this relation we can determine an upper bound for the maximal number of returns $N_3(\rho_3^*, \varepsilon_3^*)$ to P_3

$$t \in K \subset \left[0, \frac{1}{\rho_3^*}\right) \quad \Rightarrow \quad n = \frac{\rho_3^*\varepsilon_3^*}{s} t_{P_3}(n) < \frac{\rho_3^*\varepsilon_3^*}{s}\frac{1}{\rho_3^*} = \frac{\varepsilon_3^*}{s} \quad \Rightarrow \quad N_3(\rho_3^*, \varepsilon_3^*) < \left\lfloor \frac{\varepsilon_3^*}{s} \right\rfloor_*,$$

which is finite, as s is constant and the ε_3^* is bounded for initial conditions in $V_{3,\mathcal{P}}^{\mathrm{in}}$. Furthermore, we can determine a lower bound for the maximal number of returns $N_3(\rho_3^*, \varepsilon_3^*)$ to P_3:

$$t \in K \supset \left[0, \frac{C_{y_3}}{\rho_3^*}\right) \quad \Rightarrow \quad N_3(\rho_3^*, \varepsilon_3^*) \geq \frac{\rho_3^*\varepsilon_3^*}{s}\frac{C_{y_3}}{\rho_3^*} = \frac{C_{y_3}\varepsilon_3^*}{s} \geq \left\lfloor \frac{C_{y_3}\varepsilon_3^*}{s} \right\rfloor.$$

By changing the time scale from t to $\tilde{t}_3 = B^{-1}(t)$, we obtain a lower bound for the n-th return time $T_{P_3}(n)$ to P_3 in system (5.7)

$$T_{P_3}(n) = B^{-1}\left(t_{P_3}(n)\right) = B^{-1}\left(\frac{ns}{\rho_3^*\varepsilon_3^*}\right) \geq (B^{\mathrm{u}})^{-1}\left(\frac{ns}{\rho_3^*\varepsilon_3^*}\right) = \ln\left(\frac{1}{1 - \frac{ns}{\varepsilon_3^*}}\right) = \ln\left(\frac{\varepsilon_3^*}{\varepsilon_3^* - ns}\right)$$

as well as an upper bound for the n-th return time $T_{P_3}(n)$ to the Poincaré section P_3:

$$T_{P_3}(n) \leq (B^{\mathrm{l}})^{-1}\left(\frac{ns}{\rho_3^*\varepsilon_3^*}\right) = \ln\left(\frac{1}{1 - \frac{ns}{C_{y_3}\varepsilon_3^*}}\right) = \ln\left(\frac{\varepsilon_3^*}{\varepsilon_3^* - \frac{ns}{C_{y_3}}}\right). \qquad \square$$

Using the result from the last Lemma, that there exist for each initial condition in $V_{3,\mathcal{P}}^{\mathrm{in}}$ only finitely many returns to the Poincaré section P_3, we show in the following, that the embedding of the normal form of the discrete fast-slow fold singularity (3.11) in the continuous system (3.10) loses its well-definedness in chart K_3.

Proposition 5.19. *No constant $\rho_o > 0$ exists, such that it is possible to map all points of $V_2^{\mathcal{P}}(\kappa_{12}(V_1^{\mathcal{P}}(R_{1,\mathcal{P}} \cap M_1^a))) \cap \{\rho_3 > 0\}$ under Poincaré return maps into the half-space $\{\rho_3 \geq \rho_o\}$.*

Proof. By Lemma 5.18, the number of returns to the Poincaré section P_3 is for each fixed $s > 0$ finite in chart K_3. As the ρ_3-coordinate decouples in system (5.7), the number of returns to the Poincaré section P_3 is independent of the initial ρ_3-coordinate ρ_3^*. Hence, the transition time

$T_3^*(y_3^*, \varepsilon_3^*) > 0$ needed to hit the last time the Poincaré section P_3 only depends on y_3^* and ε_3^*. In the time interval $(T_3^*(y_3^*, \varepsilon_3^*), \infty)$ no returns to P_3 are observed.

In $V_2^{\mathcal{P}}(\kappa_{12}(V_1^{\mathcal{P}}(R_{1,\mathcal{P}} \cap M_1^{\mathrm{a}}))) \cap \{\rho_3 > 0\}$, it holds $0 < \rho_3^* \leq R$ for E sufficiently small. The condition, $\rho_3^* > 0$ is tight, as in chart K_1 the initial condition ε_1^* is defined to attain values arbitrary close to zero. By Proposition 5.7, it holds in chart K_1, that $\rho_1^{\mathrm{out}} = \frac{R}{E}\varepsilon_1^*(1 - (1 - \delta_1(\varepsilon_1^*))sE^2)^{-\frac{1}{2}}$, such that ρ_1^{out} attains values arbitrary close to zero. This transfers in chart K_2 to the condition, that $\rho_2^{\mathrm{in}} = \rho_1^{\mathrm{out}}\varepsilon_1^{\mathrm{out}}$ attains values arbitrary close to zero, as $\varepsilon_1^{\mathrm{out}} = E(1 - (1 - \delta_1(\varepsilon_1^*))sE^2)^{-\frac{1}{2}}$ is finite by Proposition 5.7. In chart K_2 it holds $\rho_2' = 0$, hence $\rho_2^{\mathrm{out}} = \rho_2^{\mathrm{in}}$. In chart K_3, this transfers to the condition, that $\rho_3^{\mathrm{in}} = \rho_2^{\mathrm{out}} r_2^{\mathrm{out}}$ attains values arbitrary close to zero, as r_2^{out} is by Proposition 5.7 bounded for points in $V_2^{\mathcal{P}}(\kappa_{12}(V_1^{\mathcal{P}}(R_{1,\mathcal{P}}))$. Hence, the lower boundary zero for the ρ_3-coordinate in $V_2^{\mathcal{P}}(\kappa_{12}(V_1^{\mathcal{P}}(R_{1,\mathcal{P}} \cap M_1^{\mathrm{a}}))) \cap \{\rho_3 > 0\}$ is tight and we can choose arbitrary small initial conditions ρ_3^* in chart K_3.

Choosing for fixed y_3^* and ε_3^* an initial condition $0 < \rho_3^* < \rho_o e^{-T_3^*(y_3^*, \varepsilon_3^*)}$ yields

$$\rho_3(T_3^*(y_3^*, \varepsilon_3^*)) = \rho_3^* e^{T_3^*(y_3^*, \varepsilon_3^*)} < \rho_o e^{-T_3^*(y_3^*, \varepsilon_3^*)} e^{T_3^*(y_3^*, \varepsilon_3^*)} = \rho_o,$$

where the solution in the ρ_3-coordinate is given by Proposition 4.26 (b). Hence, points in $V_2^{\mathcal{P}}(\kappa_{12}(V_1^{\mathcal{P}}(R_{1,\mathcal{P}} \cap M_1^{\mathrm{a}}))) \cap \{\rho_3 > 0\}$ exist, which are never mapped by Poincaré return maps into the half-space $\{\rho_3 \geq \rho_o\}$. □

Remark 5.20. *Proposition 5.19 shows, that the embedding of the normal form of the discrete fast-slow fold singularity defined in Section 3.1 loses its well-definedness in chart K_3. This is to be expected, as the solution of system 3.5 blows up in finite time and the evolution of the θ_3-coordinate is directly proportional to the transition time, see Lemma 3.2.*

5.5. Proof of Main Theorem 3

In this section, we use the results obtained in chart K_3 to prove Main Theorem 3. In Section 3.2, the existence of an attracting slow manifold $S_\varepsilon^{\mathrm{a}}$ was shown by Fenichel's Theorems. In the charts K_1, K_2 and K_3, we studied the extended system

$$\begin{aligned} r' &= r^2 - y, \\ \theta' &= \varepsilon, \\ y' &= -\varepsilon^3, \\ \varepsilon' &= 0. \end{aligned} \tag{5.8}$$

The attracting slow manifold $S_\varepsilon^{\mathrm{a}}$ is obtained as a section $\varepsilon = const.$ of the attracting center-manifold M^{a} of system (5.8). The existence of this attracting center manifold M^{a} was shown in Section 3.2. By Lemma 5.1, the entry set of the extended system

$$\Delta_{\varepsilon,\mathcal{P}}^{\mathrm{in}} := \left\{(r, \theta, y, \varepsilon) \in \mathcal{D}_0 : \; r \in I^{\mathrm{in}}, \; \theta = 0, \; y = R^2, \; \varepsilon \leq ER\right\}$$

with the interval

$$I^{\mathrm{in}} = \left\{r \in \mathbb{R}_{\geq -v} : \; \left|-1 + \frac{r}{R}\right| \leq \beta\right\}$$

transfers in chart K_1 to the rectangle

$$R_{1,\mathcal{P}} := \{(r_1, \theta_1, \rho_1\varepsilon_1) \in \Sigma_{1,\mathcal{P}}^{\mathrm{in}} : |-1 + r_1| \leq \beta\}.$$

We denote by X the vector field corresponding to the extended system (5.8). As system (5.8) is the normal form of the fast-slow LC fold (3.10) extended by the equation $\varepsilon' = 0$, the vector fields of both systems are the same in the first three components. As the vector field X vanishes at $(0, \theta^*, 0, 0)$, $\theta^* \in \mathbb{R}/(s\mathbb{Z})$, a desingularized vector field $\bar{X}$ induced by the blowup transformation

exists. This is analyzed in different charts by the transition map $\overline{\mathcal{T}} : \Sigma^{\text{in}}_{1,\mathcal{P}} \to \Sigma^{\text{in}}_{3,\mathcal{P}}$, which is defined by

$$\overline{\mathcal{T}} := \kappa_{23} \circ \mathcal{T}^{\mathcal{P}}_2 \circ \kappa_{12} \circ \mathcal{T}^{\mathcal{P}}_1 .$$

To analyze the attracting center manifold $\mathcal{M}^{\text{a}}$ under the Poincaré return map, we will study $\overline{\mathcal{T}}(\mathcal{R}_{1,\mathcal{P}} \cap \mathcal{M}^{\text{a}}_1)$. By Lemma 5.17, the image $\overline{\mathcal{T}}(\mathcal{R}_{1,\mathcal{P}} \cap \mathcal{M}^{\text{a}}_1) = \kappa_{23}(\mathcal{T}^{\mathcal{P}}_2(\kappa_{12}(\mathcal{T}^{\mathcal{P}}_1(\mathcal{R}_{1,\mathcal{P}} \cap \mathcal{M}^{\text{a}}_1))))$ is for E sufficiently small a union of smooth curves contained in the three-dimensional set

$$\left\{ (\rho_3, \theta_3, y_3, \varepsilon_3) \in \Sigma^{\text{in}}_{3,\mathcal{P}} : \ \rho_3 \leq R, \ \frac{-\Omega_0 + s}{(h_{r_2}(-\Omega_0 + 2s))^2} \leq y_3 \leq E^2(-\Omega_0 + 2s), \right.$$
$$\left. E \leq \varepsilon_3 \leq \frac{1}{h_{r_2}(-\Omega_0 + 2s)} \right\}.$$

Our goal is to prove a statement for all values $\varepsilon \in (0, \varepsilon_0]$ for some constant $\varepsilon_0 > 0$. In chart K_1, this implies, that the initial condition ε^*_1 attains values arbitrary close to zero, as $\varepsilon = R\varepsilon^*_1$. In the proof of Proposition 5.19, this transfers to the condition, that the initial condition ρ^*_3 attains values arbitrary close to zero. With this information, we showed in Lemma 5.19, that no constant $\rho_o > 0$ exists, such that it is possible to map all points of $\mathcal{T}^{\mathcal{P}}_2(\kappa_{12}(\mathcal{T}^{\mathcal{P}}_1(\mathcal{R}_{1,\mathcal{P}} \cap \mathcal{M}^{\text{a}}_1))) \cap \{\rho_3 > 0\}$ under Poincaré return maps into the half-space $\{\rho_3 \geq \rho_o\}$.

Using the blow-down transformation of Lemma 3.8, we obtain, that no constants $R_0 > 0$, $S > 0$ and $\varepsilon_0 > 0$ exist, such that the point $x := S^{\text{a}}_\varepsilon \cap \Delta^{\text{in}}_{\mathcal{P}}$ can for each $\varepsilon \in (0, \varepsilon_0]$ be mapped under Poincaré return maps into the half-space

$$\{(r, \theta, y) \in \mathbb{R} \times \mathbb{R}/(s\mathbb{Z}) \times \mathbb{R} : \ r \geq R_0, \ y \in \mathbb{R}\} .$$

This characterizes the break down of the fold embedding proposed in Section 3.1. □

Chapter 6

Outlook, Extensions and Limitations

In this chapter, we briefly describe in Section 6.1 the motivation for this thesis, what we have achieved and what is left open for future work. Afterwards, in Section 6.2, we discuss how different choices of the rotation velocity in the normal form of the fast-slow fold of limit cycles (3.2) effect the utility of our methods. This includes the choice of a fast and a non-constant rotation velocity. In Section 6.3, the idea of the dual limit $\varepsilon, s \to 0$ is introduced, which adapts the embedding with the goal to observe more iterates in the exit chart. Section 6.4 explains, how the method of this master's thesis can be transferred to the fast-slow flip singularity. Finally, in Section 6.5, an alternate approach to apply the blowup method to fast-slow maps is presented.

6.1. Outlook

The original motivation for this thesis has been, to try to apply the blowup method to singularities of fast-slow maps. Despite the fact that fast-slow maps are often used in applications, they are less studied in the literature. One possible reason could be, that by a direct application of the blowup method to maps, the usual desingularization step via time resclaing introduced in Section 2.4 is not possible.

In this master's thesis we studied a normal form of the discrete fast-slow fold singularity, which is obtained by adding a slow parameter drift to the one-dimensional discrete fold bifurcation. To evade the problems which arise by applying the blowup methods directly to maps, we proposed a local embedding of the normal form of the discrete fold singularity (3.1) in Section 3.1 into a higher dimensional three time scale ODE system (3.2) with one additional rotational coordinate. System (3.2) defines a normal form of the fast-slow fold of limit cycles with parameter drift $-\delta$ and rotation velocity ε. In Section 3.3 we determined a particular, constant rotation velocity, for which it is possible to desingularize the ODE system. The choice $\delta = \varepsilon^3$ obtained for system (3.10) is only possible in a three timescale setting.

To study the normal form of the fast-slow LC fold (3.10), we built upon previous work by Krupa and Szmolyan for the continuous fast-slow fold singularity with the blowup method [17]. In Chapter 4, we carried out the analysis in three charts, resulting in Main Theorem 1, which is stated in Section 3.4 and proven in Section 4.4. We tracked the trajectories in a neighborhood of the singular limit cycle, analyzed how Fenichel's attracting slow manifold extends in the non-hyperbolic regime and showed an exponential contraction property of the transition map towards the slow manifold. Furthermore, the evolution of the rotational coordinate is determined and the transition time is calculated. Main Theorem 1 extends the results obtained by Krupa and Szmolyan by examining the dynamics of the fast-slow fold of limit cycles.

In Chapter 5, the Poincaré return map of the normal form of the fast-slow LC fold (3.10) is calculated to track iterates of the normal form of the discrete fast-slow fold singularity (3.11). In the entry and rescaling chart, the embedding is well-defined and a local theorem for a ε-dependent neighborhood of the singularity is obtained. Main Theorem 2 for the Poincaré return map is stated in Section 3.4 and proven in Section 5.3. A direct consequence is Main Corollary 2 for the discrete fast-slow fold singularity (3.11), which is presented in Section 5.3. Main Corollary 2 determines a number of iterates dependent on ε mapping an initial condition on the attracting Fenichel slow manifold into a ε-dependent neighborhood of the fold point. Due to the finite time blowup of the solution curves of the normal form of the continuous fast-slow fold singularity

(3.2), our proposed embedding loses its well-definedness in the exit chart. In Section 5.5, Main Theorem 3 is proven, which characterized the break down of the fold embedding with a constant rotation velocity.

This work not only answered, but also raised a lot of questions. In the following, we briefly discuss some possible future research directions. The ideas presented in Sections 6.2 and 6.3 adjust the embedding of the normal form of the discrete fast-slow fold singularity with the goal to track all iterates of the discrete system. In Section 6.4, we propose how to apply the approach of this master's thesis to the fast-slow flip singularity, which is again a two-dimensional fast-slow system with a generic bifurcation in the one-dimensional fast limiting map for $\varepsilon = 0$. Finally in Section 6.5 we discuss, how to apply the blowup method directly to maps.

6.2. Different Rotation Velocities

In order to find a globally well-defined embedding for the discrete fast-slow fold singularity, it could be worth to keep the normal form of the fast-slow LC fold (3.2), but to adapt the rotation velocity. It is natural to consider a faster rotation velocity, such that the 'last return' of the Poincaré map is outside a neighborhood of the fold point. In this master's thesis we proposed to choose the rotation velocity ε for a slow parameter drift $-\varepsilon^3$. It turns out, that in our setting it is not possible with the methods used to resolve the fold singularity for a fast rotation velocity on the $\mathcal{O}(1)$ timescale of the dynamics in r. Furthermore, the particular ratio between the rotation velocity and the parameter drift is necessary to desingularize the normal form of the fast-slow LC fold (3.2) after applying the quasi-homogeneous blowup transformation.

It's also possible that the finite time blow-up of the map could be controlled globally by suitable higher order terms, corresponding to a variable (non-constant) rotation velocity. An open question is to find a non-constant rotation velocity, which defines a globally well-defined embedding and for which it is possible to desingularize the fold singularity.

Appendix B further discusses the choice of the rotation velocity.

6.3. The Dual Limit $\varepsilon, s \to 0$

Besides the choice of the rotation velocity, we also have freedom to choose the constant s defining the embedding in Section 3.1. In the new coordinate system, the rotational coordinate θ can assume values in $\mathbb{R}/(s\mathbb{Z})$. During our analysis we assumed the parameter s to be fixed and positive.

An idea to overcome the issue of the finite time blowup of the solution curves is to adapt the parameter s. A decrease of the parameter s is an alternative of an increase of the rotation velocity. Our goal is to observe more iterates in the exit chart by choosing s dependent on ε. In Appendix C, the effects of the choice

$$s := \varepsilon^n \tilde{s}$$

with $n \in \mathbb{N}_{\geq 1}$ and a constant $\tilde{s} \in \mathbb{R}_{>0}$ are sketched.

6.4. Extension to the Fast-Slow Flip Singularity

Our initial motivation to apply the blowup method to maps was to study the fast-slow flip singularity, which is based on the one-dimensional flip bifurcation. Besides the discrete fold bifurcation, the flip bifurcation is one of the simplest possible bifurcation occurring in one-dimensional maps. The flip bifurcation leads to period two orbits and has no direct continuous analogue as it is the case for the discrete and the continuous fold bifurcation. Hence, there is no pre-existing analysis of a continuous time system similar to that of Krupa and Szmolyan for the fold singularity, upon which an analysis can be directly extended.

In Appendix D, the normal form of the flip bifurcation and its fast-slow variant is introduced. In principle it should be possible to analyze the normal form of the fast-slow flip singularity with the same methods used for the discrete fast-slow fold singularity. We propose an embedding of the normal form of the fast-slow flip singularity in a three timescale system of ordinary differential equations. Due to the period two orbits of the flip bifurcation, two additional rotational coordinates are needed for the embedding. It is possible to choose particular rotation velocities to obtain a quasi-homogeneous vector field, such that we expect a resolution of the fast-slow flip singularity via the blowup method.

6.5. Alternate Approaches for Fast-Slow Maps

In this master's thesis we did not apply the blowup method directly to fast-slow maps. Due to the discrete time scale, no desingularization step via time rescaling analogous to the continuous case is possible. It is still an open question how to adapt the blowup method to be applicable to fast-slow maps.

In Appendix E, the blowup transformation in spherical coordinates is applied to the normal forms of the fast-slow fold and the fast-slow flip singularity. A desingularization step not based on a time rescaling is presented. In the two considered cases this coordinate transformation results in non-trivial dynamics on the sphere. Nevertheless, all obtained fixed points on the sphere are still non-hyperbolic.

Appendix A

Background of Ordinary Differential Equations

In this chapter, some mathematical background about ordinary differential equations is provided, which is used in the main part of this master's thesis. First, in Section A.1, three elementary theorems of differential calculus are stated. In Section A.2, the definitions of conjugacy and equivalence of maps and flows follow, categorizing similar behavior of different systems. Section A.3 covers two manipulations of ODE systems, namely coordinate transformations and time rescaling, which lead to conjugated or equivalent systems. Then we introduce in Section A.4 the Hartmann-Grobmann and the Belitskii Theorem, characterizing the relationship between an ODE system and its linearization. Finally, in Section A.5, the Center Manifold Theorem is stated and fibers and foliations are introduced.

A.1. Elementary Theorems of Differential Calculus

First, a foundational theorem from the theory of ordinary differential equations is presented, which guarantees the existence and uniqueness of solutions, as well as smooth dependence on initial conditions.

Theorem A.1 [4]. *Let $F : \mathbb{R}^d \to \mathbb{R}^d$ be a C^k vector field in an open region $\mathcal{O} \subset \mathbb{R}^d$. Consider the ODE*

$$x' = F(x), \quad x = x(t) \in \mathbb{R}^d, \quad x(0) = x_0 \tag{A.1}$$

for an initial conditions $x_0 \in \mathbb{R}^d$. Then a unique C^k-map

$$(t, x_0) \mapsto \varphi_t(x_0)$$

exists, which satisfies for each $x_0 \in \mathcal{O}$ the initial condition $\varphi_0(x_0) = x_0$, and a maximal interval $\mathcal{J} = (-t_1, t_2)$ with $t_{1,2} = t_{1,2}(x_0) > 0$ exists, such that for all $t \in \mathcal{J}$ it holds $x(t) = \varphi_t(x_0)$ and the ODE (A.1) *is fulfilled.*

The flow map φ_t fulfills $\varphi_s \circ \varphi_t = \varphi_{s+t}$ for all $s, t \in \mathcal{J}$, such that the inverse of φ_t is φ_{-t}. Thus, for fixed $t \in \mathbb{R}$, φ_t is a local diffeomorphism from its input onto its image.

The following Implicit Function Theorem gives a criterion, when an implicit function, for example a system of equations, can be locally be described as a graph of another function.

Theorem A.2 (Implicit Function Theorem) [10]. *Let $\mathcal{O}_1 \subset \mathbb{R}^k$, $\mathcal{O}_2 \subset \mathbb{R}^m$ be open and consider the continuously differentiable mapping*

$$F : \mathcal{O}_1 \times \mathcal{O}_2 \to \mathbb{R}^m, \quad (x, y) \to F(x, y).$$

Let $(a, b) \in \mathcal{O}_1 \times \mathcal{O}_2$ with $F(a, b) = 0$ and suppose that the $m \times m$-matrix

$$\frac{\partial F}{\partial y} := \begin{pmatrix} \frac{\partial F_1}{\partial y_1} & \cdots & \frac{\partial F_1}{\partial y_m} \\ \vdots & & \vdots \\ \frac{\partial F_m}{\partial y_1} & \cdots & \frac{\partial F_m}{\partial y_m} \end{pmatrix}$$

is invertible at the point (a, b).

Then there exists an open neighborhood $V_1 \subset \mathcal{O}_1$ of a, a neighborhood $V_2 \subset \mathcal{O}_2$ of b and a continuously differentiable mapping $g : V_1 \to V_2 \subset \mathbb{R}^m$ with $g(a) = b$, such that

$$F(x, g(x)) = 0 \quad \text{for all } x \in V_1.$$

If $(x, y) \in V_1 \times V_2$ is a point with $F(x, y) = 0$, then it follows $y = g(x)$.

The Inverse Function Theorem is a direct consequence of the Implicit Function Theorem and characterizes under which conditions a function locally has an inverse.

Theorem A.3 (Inverse Function Theorem) [10]. *Let $\mathcal{O} \subset \mathbb{R}^n$ be open, $f : \mathcal{O} \to \mathbb{R}^n$ a continuously differentiable function, $a \in \mathcal{O}$ and $b := f(a)$. Suppose that the Jacobian Matrix $Df(a)$ is invertible. Then there exists an open neighborhood $\mathcal{O}_0 \subset \mathcal{O}$ of a and an open neighborhood V_0 of b, such that the function $f : \mathcal{O}_0 \to V_0$ is bijective and its inverse*

$$g = f^{-1} : V_0 \to \mathcal{O}_0$$

is continuously differentiable. Furthermore it holds

$$Dg(b) = (Df(a))^{-1}.$$

A.2. Conjugacy and Equivalence

By analyzing maps and flows, it is often helpful to consider easier systems, which locally behave similarly as the original system. Mathematically, this is expressed by the term *conjugacy*, which we first define for maps.

Definition A.4 [12]. *Two C^r-maps*

$$f : \mathbb{R}^d \to \mathbb{R}^d, \qquad g : \mathbb{R}^d \to \mathbb{R}^d$$

are called (locally) topologically C^k conjugate for $k \leq r$ if (locally) a C^k diffeomorphism $h : \mathbb{R}^d \to \mathbb{R}^d$ exists, such that

$$h \circ f = g \circ h.$$

Now we consider an ODE system

$$x' = F(x)$$

for $x \in \mathbb{R}^d$ with a vector field $F : \mathbb{R}^d \to \mathbb{R}^d$. The solution curve $x(t)$ of this ODE system with initial condition $x(0) = x_0 \in \mathbb{R}^d$ is given by the flow map $\varphi_t^F(x_0)$. With help of the flow map, conjugacy is also defined for flows. As we have in the continuous setting an additional time parameter in the flow map, we also define the term *equivalence* of vector fields for the case, that the time parametrization of the ODE systems is not preserved.

Definition A.5 [12]. *Two C^r vector fields*

$$F : \mathbb{R}^d \to \mathbb{R}^d, \qquad G : \mathbb{R}^d \to \mathbb{R}^d$$

are called (locally) topologically C^k-equivalent for $k \leq r$, if (locally) a C^k diffeomorphism $h : \mathbb{R}^d \to \mathbb{R}^d$ exists, which maps the orbits $\varphi_t^F(x_0)$ of F to the orbits $\varphi_t^G(x_0)$ of G and the direction of time is preserved. If additionally the time parametrization is preserved, the vector fields are called (locally) topologically C^k conjugate.

This definition implies that for (locally) topologically C^k equivalent C^r vector fields F and G, a strongly monotonically increasing function $\beta : \mathbb{R}_{\geq 0} \to \mathbb{R}_{\geq 0}$ with $\beta(0) = 0$ exists, such that for any $x_0 \in \mathbb{R}^d$ it holds

$$h(\varphi_t^F(x_0)) = \varphi_{\beta(t)}^G(h(x_0)). \tag{A.2}$$

F and G are (locally) topologically C^k conjugate, if $\beta(t) = t$ for all $t \geq 0$. It follows, that two C^r vector field are (locally) topologically C^k conjugate if and only if their flow maps $\varphi_t^F(x_0)$ and $\varphi_t^G(x_0)$ are (locally) topologically C^k conjugate.

A.3. Coordinate Transformations and Time Rescaling

In this section, we discuss structural properties of ODE systems under coordinate transformations and time rescaling. These two methods are common ways to manipulate an ordinary differential equation to obtain a system, where we expect similar qualitative behavior. In the case of a coordinate transformations, we obtain a topologically conjugated system and in the case of time rescaling a topologically equivalent system, especially an orbitally equivalent system.

First, we consider an ODE system for $x \in \mathbb{R}^d$ and apply a coordinate transformation

$$y = h(x),$$

where $h : \mathbb{R}^d \to \mathbb{R}^d$ is a diffeomorphism. The following proposition shows, that the flow map of a given ODE system is topologically conjugate to the flow map of this ODE system under a coordinate transformation.

Proposition A.6 [19]. *Consider two C^r vector fields*

$$F : \mathbb{R}^d \to \mathbb{R}^d, \qquad G : \mathbb{R}^d \to \mathbb{R}^d$$

and the flow maps φ_t^F and φ_t^G generated by the ODE systems

$$x' = F(x), \quad x \in \mathbb{R}^d, \qquad \text{and} \qquad y' = G(y), \quad y \in \mathbb{R}^d.$$

Suppose that the ODE system in y is (locally) obtained from the ODE system in x by a (local) coordinate transformation $y = h(x)$ for some C^k diffeomorphism $h : \mathbb{R}^d \to \mathbb{R}^d$. Then the flow maps φ_t^F and φ_t^G are (locally) topologically C^k conjugate, which implies that the vector fields F and G are (locally) topologically C^k conjugate. Furthermore it holds

$$F(x) = (\mathrm{D}h)^{-1}(x)G(h(x)). \tag{A.3}$$

Proof. Differentiating the definition of the coordinate transformation, we obtain

$$y = h(x) \qquad \Rightarrow \qquad y' = \mathrm{D}h(x)x'.$$

Inserting this relationship into the ODE system yields

$$\mathrm{D}h(x)F(x) = \mathrm{D}h(x)x' = y' = G(y) = G(h(x))$$

and equation (A.3) follows. The flow maps φ_t^F and φ_t^G are (locally) topologically C^k conjugate as for arbitrary initial conditions $x(0) = x_0 \in \mathbb{R}^d$ and $y(0) = y_0 \in \mathbb{R}^d$ it holds

$$h(\varphi_t^F(x_0)) = h(x(t)) = y(t) = \varphi_t^G(y_0) = \varphi_t^G(h(x_0)). \qquad \square$$

Now we consider an ODE system

$$\frac{\mathrm{d}x}{\mathrm{d}t} = F(x)$$

under time rescaling, that means we introduce a new time

$$\tau = \frac{1}{\mu(x)}t \qquad \Rightarrow \qquad \frac{\mathrm{d}x}{\mathrm{d}\tau} = \mu(x)F(x)$$

with a smooth positive scalar function $\mu : \mathbb{R}^d \to (0, \infty)$. In general, the time parametrization is not preserved, thus we cannot achieve topological conjugacy, but we obtain a special case of topological equivalence. As the orbits do not change under a time rescaling, but are only passed in a different speed, the systems are equivalent: equation (A.2) is fulfilled with the identity function $h(x) = x$.

Definition A.7 [19]. *Two ODE systems*

$$x' = F(x) \qquad \text{and} \qquad x' = \mu(x)F(x)$$

for $x \in \mathbb{R}^d$ with a vector field $F : \mathbb{R}^d \to \mathbb{R}^d$ and a smooth positive scalar function $\mu : \mathbb{R}^d \to (0, \infty)$ are called orbitally equivalent.

For orbitally equivalent systems, equation (A.2) simplifies with the diffeomorphism h chosen as the identity function to

$$\varphi_t^F(x_0) = \varphi_{\beta(t)}^G(x_0).$$

The following theorem shows, how an ODE system behaves under time rescaling and gives the relationship between the function μ and β. If we know the solution of the original ODE system, we have a formula to calculate the solution of the rescaled system and vice versa.

Theorem A.8 [4]. *Let $F : \mathbb{R}^d \to \mathbb{R}^d$ be a smooth vector field, $\mu : \mathbb{R}^d \to (0, \infty)$ a smooth positive scalar function and $x \in \mathbb{R}^d$. Then the orbits of the solution curves of the ODE systems*

$$x' = F(x) \tag{A.4}$$

and

$$x' = \mu(x)F(x) \tag{A.5}$$

are the same. The multiplication of the right hand side of the ODE system (A.4) *with a smooth, positive function μ corresponds to a (possibly non-linear) rescaling of time.*

Let $J \subset \mathbb{R}$ be an interval with $0 \in J$ and suppose $\gamma(t)$ solves the ODE system (A.4). *Then the function $B : J \to \mathbb{R}$ defined by*

$$B(t) := \int_0^t \frac{1}{\mu(\gamma(s))}\,\mathrm{d}s$$

is invertible on its range $K \subset \mathbb{R}$ with inverse $B^{-1} : K \to J$ and the rescaled solution

$$\tilde{\gamma}(t) := \gamma(B^{-1}(t))$$

solves the ODE system (A.5) *for $t \in K$. Hence, we can introduce the time scale $\beta(t) = B^{-1}(t)$ for system* (A.5).

Proof. As the function

$$B'(t) = \frac{1}{\mu(\gamma(t))}$$

is continuous and positive on J, B is strongly monotonically increasing and therefore invertible on its range. Thus

$$B(B^{-1}(t)) = t \qquad \Rightarrow \qquad (B^{-1})'(t) = \frac{1}{B'(B^{-1}(t))} = \mu(\gamma(B^{-1}(t)))$$

for $t \in K$. The rescaled solution $\tilde{\gamma}(t) := \gamma(B^{-1}(t))$ solves for $t \in K$ the ODE system (A.5) as

$$\begin{aligned}\tilde{\gamma}'(t) &= (B^{-1})'(t)\gamma'(B^{-1}(t)) \\ &= \mu(\gamma(B^{-1}(t)))F(\gamma(B^{-1}(t))) \\ &= \mu(\tilde{\gamma}(t))F(\tilde{\gamma}(t)).\end{aligned}$$

Hence, the time scale of the rescaled system is $\beta(t) = B^{-1}(t)$. □

A.4. Hartman-Grobman and Belitski Theorem

Systems near hyperbolic equilibria can locally be analyzed by considering the linearization. The following Hartman-Grobman Theorem characterizes this phenomenon for general diffeomorphisms, which can be maps or flow maps induced by flows.

Theorem A.9 (Hartman-Grobman Theorem) [12]. *Let $F : \mathbb{R}^n \to \mathbb{R}^n$ be a C^1 diffeomorphism with a hyperbolic fixed point x^*. Then a homeomorphism h defined in some neighborhood $\mathcal{O}$ of x^* exists, such that $h(F(x)) = DF(x^*)h(x)$ for all $x \in \mathcal{O}$, such that the diffeomorphism is locally topologically conjugate to its linearization at x^*.*

The homeomorphism h in the Hartman-Grobman Theorem does not need to be differentiable. Sometimes it is desired to have a C^1 coordinate transformation to make asymptotic statements in an ODE system. The existence of such a coordinate transformation is guaranteed, if certain conditions on the eigenvalues hold:

Theorem A.10 (Belitskii Theorem) [3, 14]. *Let $F : \mathbb{R}^n \to \mathbb{R}^n$ be a C^2 vector field with a hyperbolic equilibrium point x^*. Denote the eigenvalues of $DF(x^*)$ by λ_j, $j = 1, ..., n$ repeated with multiplicity and order them by increasing real part, such that*

$$Re\ \lambda_1 \leq Re\ \lambda_2 \leq \cdots \leq Re\ \lambda_k < 0 < Re\ \lambda_{k+1} \leq \cdots \leq Re\ \lambda_{n-1} \leq Re\ \lambda_n.$$

If it holds

$$Re\ \lambda_i \neq Re\ \lambda_{j_1} + Re\ \lambda_{j_2}$$

for each $i \in 1, ..., n$ and all $1 \leq j_1 \leq k \leq j_2 \leq n$, then a local C^1 coordinate transformation exists that transforms locally near x^* the ODE into its linearization.

In case it holds

$$\text{Re}\ \lambda_i = \text{Re}\ \lambda_{j_1} + \text{Re}\ \lambda_{j_2}$$

for some $i \in 1, ..., n$ and $1 \leq j_1 \leq k \leq j_2 \leq n$, then we say a *resonance* occurs.

A.5. Invariant Manifold Theory

In multi-scale dynamics, center manifolds frequently play an important role, as the fast dynamics is often attracted to some center manifold, on which the slow dynamics evolves. The following theorem guarantees the existence of such a center manifold near a partially hyperbolic equilibrium. In the directions of the hyperbolic eigenvalues, stable and unstable manifolds exist.

Theorem A.11 (Center Manifold Theorem) [12]. *Let $F : \mathbb{R}^n \to \mathbb{R}^n$ be a C^r vector field vanishing at the origin, i.e. $F(0) = 0$, and denote its linearization at the origin by $J = Df(0)$. Then the spectrum of J subdivides in three parts σ_s, σ_c and σ_u with*

$$Re\ \lambda \begin{cases} < 0 & \text{if } \lambda \in \sigma_s, \\ = 0 & \text{if } \lambda \in \sigma_c, \\ > 0 & \text{if } \lambda \in \sigma_u. \end{cases}$$

Denote the (generalized) eigenspaces of σ_s, σ_c and σ_u by E^s, E^c and E^u, respectively. Then C^r stable and unstable invariant manifolds W^s and W^u tangent to E^s and E^u at the origin and a C^{r-1} center manifold W^c tangent to E^c at the origin exist. The manifolds W^s, W^u and W^c are all invariant for the flow of the vector field F. The stable and the unstable manifold are unique, but the center manifold does not need to be unique.

The following theorem introduces the concept of fibers and foliations. These are often used to characterize the dynamics near partially hyperbolic equilibria.

Theorem A.12 [18]. *Let $\mathcal{X}$ be a C^r vector field on $\mathbb{R}^d$ and consider the ODE $x' = \mathcal{X}(x)$, $x \in \mathbb{R}^d$. Furthermore, let $\mathcal{M}$ be a normally hyperbolic attracting invariant manifold under the flow ϕ_t induced by the vector field $\mathcal{X}$. Then for each $p \in \mathcal{M}$ a manifold $\mathcal{F}^s(p)$ exists, called the stable fiber, such that*

(a) $\mathcal{F}^s := \bigcup_{p \in \mathcal{M}} \mathcal{F}^s(p) = \mathcal{W}^s_{loc}(\mathcal{M})$, where $\mathcal{W}^s_{loc}(\mathcal{M})$ is the stable manifold of $\mathcal{M}$.

(b) $\mathcal{F}^s(p)$ is positively invariant, i.e. $\phi_t(\mathcal{F}^s(p)) \subset \mathcal{F}^s(\phi_t(p))$ for all $t \geq 0$ and $p \in \mathcal{M}$.

(c) $\mathcal{F}^s(p)$ is tangent to $\mathcal{N}^s_p$ at p, where $\mathcal{N}^s_p$ denotes the stable part of the normal bundle at p.

(d) There exists constants $C_s, c_s > 0$, such that if $q \in \mathcal{F}^s(p)$, then

$$\|\phi_t(p) - \phi_t(q)\| < C_s e^{-c_s t} \qquad \text{for all } t \geq 0.$$

(e) For $q \in \mathcal{F}^s(p)$ and $q' \in \mathcal{F}^s(p')$ it holds

$$\frac{\|\phi_t(p) - \phi_t(q)\|}{\|\phi_t(p) - \phi_t(q')\|} < C_s e^{-c_s t} \qquad \text{for all } t \geq 0 \text{ unless } p = p'.$$

(f) $\mathcal{F}^s(p) \cap \mathcal{F}^s(p') = \emptyset$ unless $p = p'$.

(g) $\mathcal{F}^s(p)$ is C^r with respect to the base point p.

In case of a normally hyperbolic repelling invariant manifold $\mathcal{M}$, for each $p \in \mathcal{M}$ a manifold $\mathcal{F}^u$, called the unstable fiber, exists, such that the same conclusions $(a) - (g)$ hold by replacing the stable objects by the corresponding unstable objects and reversing the direction of time. This means, that the unstable fiber is negatively invariant, i.e. $\phi_{-t}(\mathcal{F}^s(p)) \subset \mathcal{F}^s(\phi_{-t}(p))$ for all $t \geq 0$ and $p \in \mathcal{M}$.

The sets $\{(p, \mathcal{F}^s) : p \in \mathcal{M}\}$ or $\{(p, \mathcal{F}^u) : p \in \mathcal{M}\}$ are called fiber bundles over $\mathcal{M}$. The union of the fibers $\mathcal{F}^s$ or $\mathcal{F}^u$ are called asymptotic rate foliations, as they foliate the stable manifold $\mathcal{W}^s_{loc}(\mathcal{M})$ or the unstable manifold $\mathcal{W}^u_{loc}(\mathcal{M})$.

Appendix B

Discussion about the Rotation Velocity

The general system we considered for the embedding of the discrete fast-slow fold singularity is given by

$$\begin{aligned} r' &= r^2 - y, \\ \theta' &= \varepsilon, \\ y' &= -\delta, \end{aligned}$$

with two parameters $0 < \delta \ll \varepsilon \ll 1$.

As already mentioned in Remark 3.4, the assumption $0 < \delta \ll \varepsilon$ is necessary to observe in the (partial) singular limit $\delta = 0$, $\varepsilon \neq 0$ a fold bifurcation of limit cycles, which has a slow parameter drift in the full system. For $0 < \varepsilon \leq \delta \ll 1$, the system above has in the (partial) singular limit $\varepsilon = 0$, $\delta \neq 0$ on the slow time scale δt a constant parameter drift in y without rotation. It is not useful to consider super slow rotation, as the problem then basically reduces to the planar continuous-time fold dynamics. On the other hand, it is possible to define the embedding with a fast rotation in $\mathcal{O}(1)$. However, in Section B.1 we explain, why it is not possible to achieve a desingularization of the fold point in that way.

In Section 3.3, we decided to work with the parameter drift $\delta = \varepsilon^3$ to have a quasi-homogeneous vector field. In Section B.2, we sketch the effects of another ratio between the rotation velocity and the parameter drift.

Furthermore, it is not necessary to chose a constant rotation velocity. In Section B.3, we impose conditions on the rotation velocity and the parameter drift of the normal form of the fast-slow LC fold, such that the resulting parameter drift of the Poincaré return map is constant. We need this condition to re-obtain the normal form of the discrete fast-slow fold bifurcation.

B.1. Fast Rotation Velocity

By introducing a rotational coordinate, it is natural to consider a fast rotation velocity in $\mathcal{O}(1)$. Then it is easy to interpret the system and define a Poincaré return map. The normal form of the fast-slow LC fold takes in this case up to a rescaling of variables the form

$$\begin{aligned} r' &= r^2 - y, \\ \theta' &= 1, \\ y' &= -\varepsilon, \end{aligned}$$

with one parameter $0 < \varepsilon \ll 1$. Consequently, r and θ are fast variables and y is the only slow variable. As no equilibrium in θ exists, there is no two-dimensional critical manifold. As the rotational coordinate decouples, we can introduce the manifold

$$S_0 := \{(r, \theta, y) \in \mathbb{R}_{\geq -v} \times \mathbb{R}/(s\mathbb{Z}) \times \mathbb{R} : \ y = r^2\},$$

which is invariant in the singular limit $\varepsilon = 0$. Fenichel theory is also not directly applicable, but we can infer the existence of a slow manifold from the existence of the slow manifold in system

$$\begin{aligned} r' &= r^2 - y, \\ y' &= -\varepsilon, \end{aligned}$$

complemented by the decoupled variable $\theta \in \mathbb{R}/(s\mathbb{Z})$.

The problem of the fast rotation velocity is, that it is not possible to analyze the map obtained via an embedding in a continuous-time system by the blowup method. The blowup transformation introduced in Section 2.4 requires the underlying system to have an equilibrium at the considered point, which is not possible for $\theta \in \mathcal{O}(1)$. When applying the blowup transformation, no factor ρ appears in the ODE for θ such as for example in Lemma 4.1, such that a desingularization via time resclaing is not possible.

B.2. Relationship between δ and ε

In Section 3.3, we showed that the vector field of the normal form of the fast-slow LC fold is only quasi-homogeneous for the choice $\delta = \varepsilon^3$. For $\delta \propto \varepsilon^\alpha$, $\alpha \in \mathbb{R} \setminus \{3\}$, we show in the rescaling chart, why a desingularization of the fold point is not possible. To have a quasi-homogeneous vector field in the r-component and to not blow up the θ-coordinate, we keep like in Proposition 3.6 the coefficients $a_1 = 1$, $a_2 = 0$ and $a_3 = 2$. As we change the velocity of the parameter drift, we keep the coefficient $a_4 \in \mathbb{R}_{>0}$ flexible. With the blowup transformation

$$(r, \theta, y, \varepsilon) = (\rho_2 r_2, \theta_2, \rho_2^2 y_2, \rho_2^{a_4}),$$

we obtain in the rescaling chart:

$$\begin{aligned}
&\varepsilon' = 0 && \Rightarrow && (\rho_2^{a_4})' = 0 && \Rightarrow && \rho_2' = 0,\\
&r' = r^2 - y && \Rightarrow && (\rho_2 r_2)' = \rho_2^2(r_2^2 - y_2) && \Rightarrow && r_2' = \rho_2(r_2^2 - y_2),\\
&\theta' = \varepsilon && \Rightarrow && \theta_2' = \rho_2^{a_4} && \Rightarrow && \theta_2' = \rho_2^{a_4},\\
&y' = -\varepsilon^\alpha && \Rightarrow && (\rho_2^2 y_2)' = -\rho_2^{\alpha a_4} && \Rightarrow && y_2' = -\rho_2^{\alpha a_4 - 2}.
\end{aligned}$$

To desingularize the vector field, we aim to observe dynamics on the blown-up surface $S^1 \times S^2$ in all coordinates. In chart K_2, the blown-up surface corresponds to the invariant hyperplane $\{\rho_2 = 0\}$. To observe the Riccati dynamics in the r_2- and y_2-coordinate, we divide the right hand side of the ODE system by ρ_2 and demand

$$\alpha a_4 - 2 = 1 \qquad \Leftrightarrow \qquad a_4 = \frac{3}{\alpha}.$$

Hence, for $\alpha \in (0, 3)$ it holds $a_4 > 1$, such that after the desingularization step we obtain on the time scale $t_2 = \rho_2 t$ the equation $\theta' = \rho_2^{a_4 - 1}$. Consequently $\theta' = 0$ in the hyperplane $\{\rho_2 = 0\}$, such that the rotation velocity is too small to observe returns to the Poincaré section P_2.

On the other hand for $\alpha > 3$ it holds $a_4 < 1$, such the transformation to the time scale $t_2 = \rho_2 t$ is not possible, as it would result in the hyperplane $\{\rho_2 = 0\}$ to an infinite rotation velocity. Introducing the time scale $\tilde{t}_2 = \rho_2^{a_4} t$, leads independent of the choice of α to a trivial dynamics in r_2 in the hyperplane $\{\rho_2 = 0\}$. Hence, the rotation velocity is in this case too fast, such that the Poincaré return map does not capture the important dynamics.

B.3. Non-Constant Rotation Velocity

Our goal is to embed the normal form of the discrete fast-slow fold singularity with a constant parameter drift in an ODE system with an additional rotational coordinate. In general, however, we could consider a non-constant flow in either or both y and θ. We consider the system

$$\begin{aligned}
r' &= r^2 - y,\\
\theta' &= j_\theta(r, y, \varepsilon),\\
y' &= -j_y(r, y, \varepsilon),
\end{aligned}$$

with two functions $j_\theta : \mathbb{R}_{\geq -v} \times \mathbb{R}/(s\mathbb{Z}) \times \mathbb{R} \to \mathbb{R}$ and $j_y : \mathbb{R}\mathbb{R}_{\geq -v} \times \mathbb{R}/(s\mathbb{Z}) \times \mathbb{R} \to \mathbb{R}$. When considering θ as a variable in $\mathbb{R}$, the Poincaré section P is hit for the n-th time at the time $T(n)$, if

$$\int_0^{T(n)} j_\theta(r, y, \varepsilon)\,\mathrm{d}t = ns.$$

This is equivalent to the condition, that

$$\int_{T(n)}^{T(n+1)} j_\theta(r, y, \varepsilon)\,\mathrm{d}t = s$$

for all $n \in \mathbb{N}_{>0}$. To model a constant parameter drift, the decrease in y has to be the same in each time interval, such that the following condition is equivalent to a constant parameter drift in y

$$\int_{T(n)}^{T(n+1)} -j_y(r, y, \varepsilon)\,\mathrm{d}t = k \cdot s = \int_{T(n)}^{T(n+1)} k \cdot j_\theta(r, y, \varepsilon)\,\mathrm{d}t$$

for some constant $\mathbb{R}_{>0}$. The easiest possibility to fulfill this integral condition is to choose

$$-j_y(r, y, \varepsilon) = k \cdot j_\theta(r, y, \varepsilon) \qquad \text{for all } t \geq 0.$$

To imitate the finite time blowup in the r-coordinate, and hence observe infinitely many returns to the Poincaré section, we could choose

$$j_\theta(r, y, \varepsilon) = \varepsilon(r^2 + 1),$$

which is always positive. The problem is, that in this case we cannot find coefficients of the blowup transformation, for which the resulting vector field is quasi-homogeneous. It is still an open question to find an adequate rotation velocity for the blowup method, being always positive, easy enough to carry out the analysis and with a solution for θ blowing up in finite time.

Appendix C

The Dual Limit $\varepsilon, s \to 0$

For the embedding and the analysis of the normal form of the discrete fast-slow fold singularity, we assumed the constant s introduced in Section 3.1 to be fixed and positive. In this section, we sketch what happens if we choose s to be ε-dependent. We define

$$s := \varepsilon^n \tilde{s}$$

for some $n \in \mathbb{N}_{\geq 1}$ and a small constant $\tilde{s} \in \mathbb{R}_{>0}$. In the following, we discuss in Section C.1 different steps in the analysis from the embedding up to the rescaling chart. We assume, that the embedding is well-defined in the limit $\varepsilon, s \to 0$. A proof or disproof of the validity of this is left for future work. Under the assumption made, we adapt the analysis in the entry and rescaling chart to obtain a comparable result to Main Theorem 2. In Section C.2, we show that for a suitable choice of n, the number of returns to the Poincaré section increases in the exit chart, but better estimates are needed to show weather it is possible to define a transition map in chart K_3.

C.1. Validity of the Local Results

In the following, the local results until the analysis in chart K_2 are adapted to the choice $s = \varepsilon^n \tilde{s}$ under the assumption, that the dual limit $\varepsilon, s \to 0$ is well-defined. This includes the embedding, the analysis of the normal form of the continuous fast-slow LC fold (3.10) and the analysis in the entry and rescaling chart of the normal form of the discrete fast-slow fold singularity (3.11).

Section 3.1: Embedding as a Poincaré Return Map

As s depends on ε, also the parametrization of the space $\mathbb{R}^3$ by

$$(r, \theta, y) \in \mathcal{D} := \mathbb{R}_{\geq -v} \times \mathbb{R}/(\varepsilon^n \tilde{s}\mathbb{Z}) \times \mathbb{R} \cong \mathbb{R}^3, \tag{C.1}$$

depends on ε. Hence, (C.1) defines an ε-family of parametrizations of $\mathbb{R}^3$.

The interpretation of the coordinate system only makes sense, if ε is fixed and positive. The main theorems make assertions, which hold for each value of ε smaller than ε_0 separately, such that it may be no restriction to choose for each value of ε a different parametrization of the space $\mathbb{R}^3$. However, the analysis in the charts strongly depends on regular perturbation of results obtained in the singular limit $\varepsilon = 0$. Hence, it has to be checked, whether the limiting space, i.e. the parametrization (C.1) for $\varepsilon = s = 0$, is in some sense 'nicely connected' to the ε-family of parametrizations of $\mathbb{R}^3$ for $\varepsilon > 0$. In the following we assume, that the embedding is well defined in the limit $\varepsilon, s \to 0$ and sketch the consequences of the assumption afterwards.

Assumption C.1. *The ε-family* (C.1) *of parametrizations of $\mathbb{R}^3$ is well defined in the limit $\varepsilon, s \to 0$ and compatible with the analysis made in Chapter 4 and in Chapter 5.*

In the following we sketch how to adapt the analysis for the choice $s = \varepsilon^n \tilde{s}$ under Assumption C.1. We recall, that we consider the ODE system

$$\begin{aligned} r' &= r^2 - y, \\ \theta' &= \varepsilon, \\ y' &= -\delta, \end{aligned}$$

with $0 < \delta \ll \varepsilon \ll 1$. Due to the constant rotation velocity $\theta' = \varepsilon$, the n-th return time to the Poincaré section P is now given by

$$\tilde{T}_{\mathcal{P}}(n) = \frac{ns}{\varepsilon} = n\varepsilon^{n-1}\tilde{s}.$$

and the resulting parameter drift in y for the discrete system is

$$\Delta y = -\delta \cdot \tilde{T}_{\mathcal{P}}(1) = -\delta\varepsilon^{n-1}\tilde{s},$$

which is still constant and slow due to the assumption $\delta \ll \varepsilon \ll 1$ and $n \geq 1$. The proof of Lemma 3.2 is not influenced by the new choice of s, such that again only finitely many iterates of the Poincaré map $\mathcal{P}$ are observed for the normal form of the fast-slow LC fold. The goal of the choice $s = \varepsilon^n\tilde{s}$ is, that the last return is observed later, as the distance between Poincaré returns decreases with ε, such that a transition map can be well-defined in the exit chart.

The subsequent Sections 3.2 and 3.3 do not use any properties of the constant s. Thus, again the slow parameter drift $\delta = \varepsilon^3$ is used and the system analyzed is extended by the equation $\varepsilon' = 0$.

Chapter 4: Analysis of the Fast-Slow LC Fold

In Chapter 4, the constant s is only used to define the evolution in θ. All results obtained also hold for $s = \varepsilon^n\tilde{s}$ under Assumption C.1. To state the Lemmata and Propositions in the different charts, we can transfer the constant s to the coordinate charts in chart K_1, K_2 and K_3. By Lemma 3.8 we obtain

$$\begin{aligned}
&\text{for } K_1: \quad s = \rho_1^n\varepsilon_1^n\tilde{s},\\
&\text{for } K_2: \quad s = \rho_2^n\tilde{s},\\
&\text{for } K_3: \quad s = \rho_3^n\varepsilon_3^n\tilde{s}.
\end{aligned}$$

All these terms are due to the constraint $\varepsilon' = 0$ constant in their corresponding charts, such that the Euclidean division $\bmod s$ is well-defined.

Section 5.1: Dynamics in the Entry Chart

In the analysis of the normal form of the discrete fast-slow fold singularity, the first occurrence of the constant s in chart K_1 is in the definition of the set $\mathcal{D}_{1,\mathcal{P}}$. As we aim to cover all dynamics of chart K_1 in a box $\tilde{\mathcal{D}}_{1,\mathcal{P}}$, we define

$$\tilde{\mathcal{D}}_{1,\mathcal{P}} := \left\{(r_1,\theta_1,\rho_1,\varepsilon_1) \in \mathbb{R}\times\mathbb{R}/(s\mathbb{Z})\times\mathbb{R}\times\mathbb{R} :\ 0 \leq \rho_1 \leq R,\ 0 \leq \varepsilon_1 \leq E(1 - E^{2+n}R^n\tilde{s})^{-\frac{1}{2}}\right\},$$

as in the entry set $\Delta^{\text{in}}_{\varepsilon,\mathcal{P}}$ in the original coordinates it holds $\varepsilon \leq ER$, hence $s \leq E^nR^n\tilde{s}$. In Remark 5.4 we explained, that the condition $E < s^{-1/2}$ necessary for Lemma 5.3 is fulfilled for E sufficiently small. This is also the case for $s = \varepsilon^n\tilde{s}$, as

$$Es^{\frac{1}{2}} = E^{1+n/2}R^{n/2}\tilde{s}^{\frac{1}{2}} < 1$$

for E sufficiently small. As all points in the entry set $\Sigma^{\text{in}}_{1,\mathcal{P}}$ have initial ρ_1-coordinate R, the constant ε transfers in the entry chart to $\varepsilon = R\varepsilon_1^*$, where $\varepsilon_1^* \in [0,E]$. Hence, Lemma 5.4 for the number of returns to the Poincaré section P_1 and the corresponding return time hold by replacing s by $R^n(\varepsilon_1^*)^n\tilde{s}$. Analogously, also Lemma 5.5 holds by inserting the new definition for s. The exit set $\Sigma^{\text{out}}_{1,\mathcal{P}}$ has in the ε_1-coordinate a constraint depending on s. To have a rectangular exit set, we enlarge the set by replacing s by its upper bound $E^nR^n\tilde{s}$ and define

$$\tilde{\Sigma}^{\text{out}}_{1,\mathcal{P}} := \left\{(r_1,\theta_1,\rho_1,\varepsilon_1) \in \mathcal{D}_{1,\mathcal{P}} :\ \theta_1 = 0,\ E \leq \varepsilon_1 \leq E(1 - E^{2+n}R^n\tilde{s})^{-\frac{1}{2}}\right\}.$$

In that way, the transition map $\mathcal{T}_1^{\mathcal{P}} : \Sigma_{1,\mathcal{P}}^{\text{in}} \to \tilde{\Sigma}_{1,\mathcal{P}}^{\text{out}}$ of Lemma 5.6 is well-defined by replacing s by $R^n(\varepsilon_1^*)^n\tilde{s}$, but $n_1(\varepsilon_1^*)$ is then not necessarily the unique number mapping an initial condition with ε_1-coordinate ε_1^* into the exit set $\tilde{\Sigma}_{1,\mathcal{P}}^{\text{out}}$. This property is not needed in the further analysis. All important properties about the transition map $\mathcal{T}_1^{\mathcal{P}}$ collected in Proposition 5.7 also hold by replacing s by $R^n(\varepsilon_1^*)^n\tilde{s}$ and $\Sigma_{1,\mathcal{P}}^{\text{out}}$ by $\tilde{\Sigma}_{1,\mathcal{P}}^{\text{out}}$ under Assumption C.1.

Section 5.2: Dynamics in the Rescaling Chart

In chart K_2, the constant ρ_2 is constant and by the coordinate transformation of Lemma 3.9 it holds $\rho_2^* = R\varepsilon_1^*$. The entry set of the rescaling chart depends on s. To have a rectangular entry set, we define

$$\tilde{\Sigma}_{2,\mathcal{P}}^{\text{in}} := \kappa_{12}\left(\tilde{\Sigma}_{1,\mathcal{P}}^{\text{out}}\right) = \left\{(r_2, \theta_2, y_2, \rho_2) \in \mathcal{D}_{2,\mathcal{P}} :\ \theta_2 = 0,\ \frac{1}{E^2} - E^n R^n\tilde{s} \le y_2 \le \frac{1}{E^2}\right\},$$

which follows by Lemma 5.9 by replacing s by its upper bound $E^n R^n\tilde{s}$. In Remark 5.11 we explained, that the condition $E^2(2s - \Omega_0) < 1$, which is necessary for Lemma 5.10, is fulfilled for E sufficiently small. This is also the case for $s = \varepsilon^n\tilde{s}$, as

$$E^2(2s - \Omega_0) \le E^2(2E^n R^n\tilde{s} - \Omega_0) < 1$$

for E sufficiently small. Hence, Lemma 5.10 for the number of returns to the Poincaré section P_2 and the corresponding return time hold by replacing s by $(\rho_2^*)^n\tilde{s} = R^n(\varepsilon_1^*)^n\tilde{s}$. Analogously, also Lemma 5.12 for the n-th return in the rescaling chart holds for the new choice of s. The exit set $\Sigma_{2,\mathcal{P}}^{\text{out}}$ has in the y_2-coordinate a constraint depending on s. To have the same exit set for all values of ε, we define

$$\tilde{\Sigma}_{2,\mathcal{P}}^{\text{out}} := \{(r_2, \theta_2, y_2, \rho_2) \in \mathcal{D}_{2,\mathcal{P}} :\ r_2 > 0,\ \theta_2 = 0,\ -\Omega_0 + \tilde{s} \le y_2 \le -\Omega_0 + 2\tilde{s}\}.$$

In Lemma 5.13, we replace the number $n_2(y_2^*)$ of returns of a point $(r_2^*, 0, y_2^*, \rho_2^*) \in W_{2,\mathcal{P}}^{\text{in}} \subset \tilde{\Sigma}_{2,\mathcal{P}}^{\text{in}}$ to the Poincaré section P_2 by

$$\tilde{n}_2(y_2^*, \rho_2^*) := \left\lfloor \frac{y_2^* - \tilde{s} + \Omega_0}{(\rho_2^*)^n\tilde{s}} \right\rfloor \ge 1$$

and define

$$\tilde{\delta}_2(y_2^*, \rho_2^*) := \left\lfloor \frac{y_2^* - \tilde{s} + \Omega_0}{(\rho_2^*)^n\tilde{s}} \right\rfloor \mod 1,$$

such that

$$\mathcal{T}_{2,y_2}^{\mathcal{P}}(r_2^*, 0, y_2^*, \rho_2^*) = y_2^* - \left\lfloor \frac{y_2^* - \tilde{s} + \Omega_0}{(\rho_2^*)^n\tilde{s}} \right\rfloor (\rho_2^*)^n\tilde{s} = -\Omega_0 + \tilde{s} + \tilde{\delta}_2(y_2^*, \rho_2^*)(\rho_2^*)^n\tilde{s}$$

and the transition map $\mathcal{T}_2^{\mathcal{P}}$ maps into the exit set $\tilde{\Sigma}_{2,\mathcal{P}}^{\text{out}}$. In this case, we have the condition $\tilde{s} < \frac{\Omega_0 - \rho_0}{2}$. All important properties about the transition map $\mathcal{T}_2^{\mathcal{P}}$ collected in Proposition 5.15 also hold by replacing s by $(\rho_2^*)^n\tilde{s}$, $\Sigma_{2,\mathcal{P}}^{\text{in}}$ by $\tilde{\Sigma}_{2,\mathcal{P}}^{\text{in}}$, $\Sigma_{2,\mathcal{P}}^{\text{out}}$ by $\tilde{\Sigma}_{2,\mathcal{P}}^{\text{out}}$ and $\delta_2(y_2^*)$ by $\tilde{\delta}_2(y_2^*, \rho_2^*)$.

To state a theorem analogously to Main Theorem 2, we need to calculate $\tilde{\delta}^{\text{loc}}$, which is analogously to the proof of Main Theorem 2 given by

$$\tilde{\delta}^{\text{loc}} := \tilde{\delta}_2\left(\frac{1}{E^2} - (1 - \tilde{\delta}_1(\varepsilon_1^*))R^n(\varepsilon_1^*)^n\tilde{s}, \rho_2^*\right) \equiv \frac{1}{R^n(\varepsilon_1^*)^{2+n}\tilde{s}} + \frac{\Omega_0}{R^n(\varepsilon_1^*)^n\tilde{s}} - \frac{1}{R^n(\varepsilon_1^*)^n} \mod 1$$

and the number of returns is given by

$$\begin{aligned}\tilde{n}(\varepsilon_1^*) =& \left\lfloor \frac{1}{R^n(\varepsilon_1^*)^{2+n}\tilde{s}} - \frac{1}{R^n(\varepsilon_1^*)^n E^2\tilde{s}} \right\rfloor + 1 + \left\lfloor \frac{y_2^* - \tilde{s} + \Omega_0}{(\rho_2^*)^n s} \right\rfloor \\ =& \frac{1}{R^n(\varepsilon_1^*)^{2+n}\tilde{s}} - \frac{\Omega_0}{R^n(\varepsilon_1^*)^n\tilde{s}} - \frac{1}{R^n(\varepsilon_1^*)^n} - \tilde{\delta}^{\text{loc}} \ge 2.\end{aligned}$$

Transferred to the original coordinates, we obtain under Assumption C.1 the following theorem, which is similar to Main Theorem 2. The exit set is defined by

$$\tilde{\Delta}_{\mathcal{P}}^{\text{out}} := \left\{(r,\theta,y) \in \mathbb{R}\times\mathbb{R}/(s\mathbb{Z})\times\mathbb{R} :\ 0 \le r \le \varepsilon\tilde{R},\ \theta = 0,\ \varepsilon^2(-\Omega_0+\tilde{s}) \le y \le \varepsilon^2(-\Omega_0+2\tilde{s})\right\},$$

where $\tilde{R} = h_r(\tilde{s})$. The function h_r and the constant Ω_0 are specified in the following theorem.

Theorem C.2. *Under Assumption C.1 and the assumptions made in Section 3.2 and $\tilde{s}$ sufficiently small and fixed, $s = \varepsilon^n\tilde{s}$ with $n \in \mathbb{N}_{\ge 1}$, a constant $\varepsilon_0 > 0$ exists, such that for the transition map $\tilde{\pi}^{loc} : \Delta_{\mathcal{P}}^{in} \to \tilde{\Delta}_{\mathcal{P}}^{out}$ the following holds for all $\varepsilon \in (0,\varepsilon_0]$:*

(a) Let $\tilde{\delta}^{loc}$ be defined as

$$\tilde{\delta}^{loc} := \frac{1}{s}\left(\frac{R^2}{\varepsilon^2} + \Omega_0 + \tilde{s}\right) \mod 1.$$

Then the point $x := S_\varepsilon^a \cap \Delta_{\mathcal{P}}^{in}$ on the attracting slow manifold maps under the transition map $\tilde{\pi}^{loc}$, which is defined to be the $\tilde{n}$-th Poincaré return map $\mathcal{P}^{\tilde{n}}$ with

$$\tilde{n} := \left\lfloor \frac{1}{s}\left(\frac{R^2}{\varepsilon^2} + \Omega_0 + \tilde{s}\right)\right\rfloor = \frac{1}{s}\left(\frac{R^2}{\varepsilon^2} + \Omega_0 + \tilde{s}\right) - \delta^{loc} \ge 2,$$

to the point

$$\tilde{\pi}^{loc}(x) = \mathcal{P}^{\tilde{n}}(x) = \left(\varepsilon h_r(\tilde{s}+\delta^{loc}s), 0, -\Omega_0\varepsilon^2 + (\tilde{s}+\delta^{loc}s)\varepsilon^2\right) \in \tilde{\Delta}_{\mathcal{P}}^{out},$$

as $\varepsilon \to 0$, where

$$h_r(\alpha) = \frac{1}{\alpha + \mathcal{O}(\alpha^3)} \qquad \text{as } \alpha \to 0^+.$$

The constant Ω_0 is the smallest positive zero of

$$J_{-\frac{1}{3}}\left(\frac{2z^{\frac{3}{2}}}{3}\right) + J_{\frac{1}{3}}\left(\frac{2z^{\frac{3}{2}}}{3}\right),$$

where $J_{-\frac{1}{3}}$ and $J_{\frac{1}{3}}$ are Bessel functions of the first kind.

(b) The r-component π_r^{loc} of the transition map π^{loc} is a strong contraction with respect to the coordinate r, i.e.

$$\frac{\partial\tilde{\pi}_r^{loc}(r,\varepsilon)}{\partial r} = \mathcal{O}\left(\exp\left(\frac{2cR^2}{3\varepsilon^3}\right)\right)$$

for some negative constant $c > -2$ as $\varepsilon \to 0$.

(c) The constant $\tilde{s}$ is sufficiently small for this theorem, if it holds $\tilde{s} < \frac{\Omega_0 - V_0}{2}$. The constant $V_0 < \Omega_0$ is defined as $V_0 := -h_y(0) > 0$, where h_y describes the y-component of the special solution of the Riccati equation

$$\begin{aligned} r' &= r^2 - y, \\ y' &= -1, \end{aligned}$$

which is further specified in Proposition 4.14 and [20].

We observe, that the number of iterates $\tilde{n}$ and the coordinates of $\tilde{\pi}^{\text{loc}}$ slightly change. This is due to the fact, that we cannot use the exit set

$$\Delta_{\mathcal{P}}^{\text{out}} = \left\{(r,\theta,y) \in \mathbb{R}\times\mathbb{R}/(s\mathbb{Z})\times\mathbb{R} :\ 0 \le r \le \varepsilon R,\ \theta = 0,\ \varepsilon^2(-\Omega_0+s) \le y \le \varepsilon^2(-\Omega_0+2s)\right\},$$

with $R = h_r(s)$, as in the limit $\varepsilon \to 0$ it now also holds $s \to 0$, such that $R = h_r(s) \to \infty$ for $s \to 0$. To apply the coordinate change κ_{23} to the exit chart, we aim to have a bounded exit set in the rescaling chart.

C.2. Extension to the Exit Chart

In this section, we observe how under Assumption C.1 the number of returns to the Poincaré section changes in the exit chart. To prove or disprove if it is possible to define a transition map in the rescaling chart, better estimates for the occurring integrals are needed.

In chart K_3 it holds by the coordinate transformation of Lemma 3.9 $\rho_3^*\varepsilon_3^* = \rho_2^* = R\varepsilon_1^*$. Similar to Lemma 5.17, the exit set $\tilde{\Sigma}_{2,\mathcal{P}}^{\text{out}}$ of the rescaling chart maps under the coordinate transformation of Lemma 3.9 to the entry set

$$\tilde{\Sigma}_{3,\mathcal{P}}^{\text{in}} \coloneqq \{(\rho_3, \theta_3, y_3, \varepsilon_3) \in \mathcal{D}_{3,\mathcal{P}} : \theta_3 = 0\}$$

and the exit set $\tilde{W}_{2,\mathcal{P}}^{\text{out}}$, which is a superset of the image $T_2^{\mathcal{P}}(\kappa_{12}(T_1^{\mathcal{P}}(R_{1,\mathcal{P}})))$ maps for E and β sufficiently small to an entry set $\tilde{W}_{3,\mathcal{P}}^{\text{in}}$. As in Lemma 5.18, the flow in the exit chart with initial condition $(\rho_3^*, \theta_3^*, y_3^*, \varepsilon_3^*) \in \tilde{W}_{3,\mathcal{P}}^{\text{in}}$ hits the Poincaré section P_3 for E sufficiently small at most $\tilde{N}_3(\varepsilon_3^*, \rho_3^*)$ times, where

$$\left\lfloor \frac{C_{y_3}\varepsilon_3^*}{s} \right\rfloor = \left\lfloor \frac{C_{y_3}}{(\rho_3^*)^n(\varepsilon_3^*)^{n-1}\tilde{s}} \right\rfloor \leq \tilde{N}_3(\varepsilon_3^*, \rho_3^*) < \left\lfloor \frac{\varepsilon_3^*}{s} \right\rfloor_* = \left\lfloor \frac{1}{(\rho_3^*)^n(\varepsilon_3^*)^{n-1}\tilde{s}} \right\rfloor_*$$

with some constant $0 < C_{y_3} < 1$. It follows, that for $n \in \mathbb{N}_{\geq 1}$, the maximal number of returns to the Poincaré section P_3 is not independent of the initial condition ρ_3^*. In the analysis in Section 5.4, it was not possible to define a transition map in chart K_3 for initial conditions ρ_3^*, which are too small. As now the number of returns $\tilde{N}_3(\varepsilon_3^*, \rho_3^*)$ converges to infinity for $\rho_3^* \to 0$, the argument of Proposition 5.19 is not applicable anymore. To find out, if a number of returns in $\mathcal{O}\left((\rho_3^*)^{-n}(\varepsilon_3^*)^{-n+1}\right)$ suffices to define a transition map in chart K_3, better estimates for the n-th return time than the ones given in Lemma 5.18 are needed.

Appendix D

Geometric Analysis of the Fast-Slow Flip Singularity

In this chapter, we introduce the one-dimensional flip bifurcation and its induced fast-slow map. Unlike the discrete fold bifurcation, no direct analogue of the flip bifurcation exists in the continuous case. In Section D.1, the normal form of the generic flip bifurcation is presented and the normal form of the fast-slow flip singularity is defined. In Section D.2 an embedding of the normal form of the fast-slow flip singularity in a higher dimensional ODE system is proposed, which undergoes in the singular limit a flip bifurcation of limit cycles.

D.1. Flip Bifurcation

The flip bifurcation can occur in one-dimensional maps with one parameter. The following proposition gives non-degeneracy conditions for a flip bifurcation and determines the two possible normal forms.

Proposition D.1 [19]. *Suppose, that the one-dimensional map*

$$x \mapsto f(x, y)$$

with a smooth function $f : \mathbb{R}^2 \to \mathbb{R}$ has for the parameter $y = 0$ a non-hyperbolic fixed point at $x_0 = 0$ with multiplier $\mu = f_x(0,0) = -1$. Assume that the following two non-degeneracy conditions hold:

$$\frac{1}{2}(f_{xx}(0,0))^2 + \frac{1}{3}f_{xxx}(0,0) \neq 0, \qquad f_{xy}(0,0) \neq 0.$$

Then the one-dimensional map is locally near $(x, y) = (0, 0)$ topologically equivalent to the map

$$x \mapsto -(1+y)x \pm x^3 + \mathcal{O}(x^4).$$

The higher order terms do locally not influence the dynamics, such that the considered system is locally near the origin topologically equivalent to the map

$$x \mapsto -(1+y)x \pm x^3.$$

Analogously to the proof of Proposition 2.5, the normal form is obtained through Taylor expansions, coordinate shifts and the Implicit Function Theorem A.2. The + sign in front of y is arbitrary, through the coordinate shift $y \mapsto -y$, the sign can be changed. In contrast to that, the coordinate shift $x \mapsto -x$ does not change the structure of the normal form. The sign in front of the cubic term changes the fundamental behavior of the map. The map

$$x \mapsto -(1+y)x + x^3 = f_1(x, y) \tag{D.1}$$

is called 'supercritical' or 'soft' flip bifurcation, whereas the map

$$x \mapsto -(1+y)x - x^3 = f_2(x, y) \tag{D.2}$$

is called 'subcritical' or 'sharp' flip bifurcation.

For the flip bifurcation, the linearization around a fixed point x^* is given by

$$\partial_x f(x^*, y^*) = -(1 + y^*) \pm 3(x^*)^2.$$

Independent of the value of y, the fixed point $x^* = 0$ with multiplier $\partial_x f(0,0) = -(1 + y^*)$ exists, which is locally near the origin stable for $y^* < 0$, non-hyperbolic for $y^* = 0$, and unstable for $y^* > 0$. In Figure D.1, the supercritical flip bifurcation and in Figure D.2, the subcritical flip bifurcation is visualized by cobwebbing for different values of the parameter y. We observe, that for y^*, the non-hyperbolic fixed point $x^* = 0$ is non-linearly stable for the supercritical flip bifurcation and non-linearly unstable for the subcritical flip bifurcation. Locally near $x^* = 0$ no other fixed points arise by varying the parameter y.

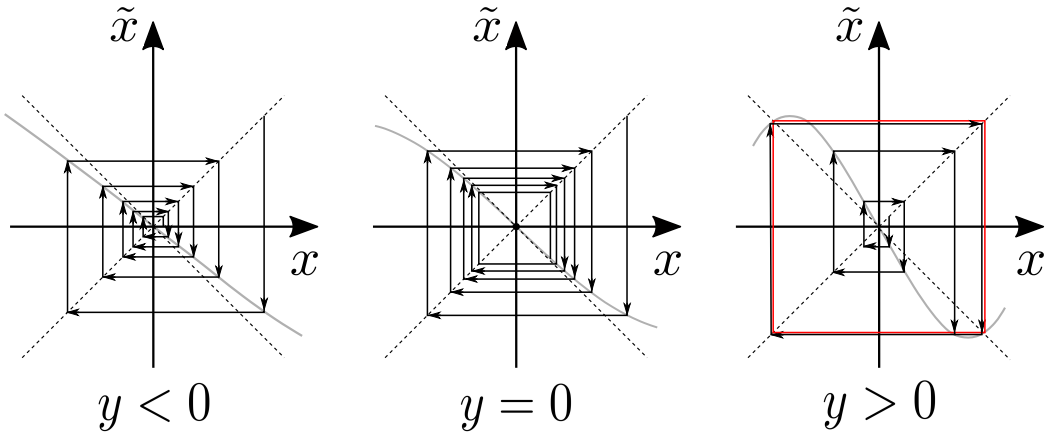


Figure D.1.: One-dimensional supercritical flip bifurcation visualized by cobwebbing. The stable period two orbit is shown in red.

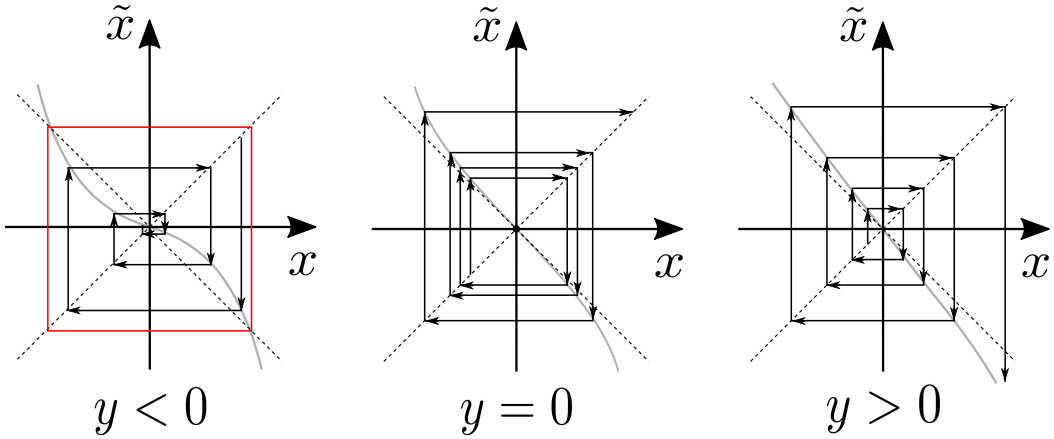


Figure D.2.: One-dimensional subcritical flip bifurcation visualized by cobwebbing. The unstable period two orbit is shown in red.

For the supercritical flip bifurcation a period two orbit arises for $y > 0$ between the points $x_1 = \sqrt{y}$ and $x_2 = -\sqrt{y}$ as

$$f_1(\sqrt{y}, y) = -\sqrt{y}, \qquad f_1(-\sqrt{y}, y) = \sqrt{y}.$$

The period two orbit is stable, as

$$|\partial_x f(\pm\sqrt{y^*}, y^*)| = |-(1 + y^*) + 3y^*| = |-1 + 2y^*| < 1$$

for $y^* > 0$ sufficiently small.

For the subcritical flip bifurcation a period two orbit arises for $y < 0$ between the points $x_1 = \sqrt{-y}$ and $x_2 = -\sqrt{-y}$ as

$$f_2(\sqrt{y}, y) = -\sqrt{-y}, \qquad f_2(-\sqrt{y}, y) = \sqrt{-y}.$$

The period two orbit is unstable, as

$$|\partial_x f(\pm\sqrt{-y^*}, y^*)| = |-(1 + y^*) - 3(-y^*)| = |-1 + 2y^*| > 1$$

for $y^* < 0$ sufficiently large. The period two orbits are visualized in Figures D.1 and D.2.

As periodic orbits cannot exist in one-dimensional ordinary differential equations, no direct one-dimensional continuous analogue for the flip bifurcation exists. It is interesting to consider the dynamics version, the fast-slow flip singularity, which has for $0 < \varepsilon \ll 1$ one of the following normal forms:

$$\begin{aligned} x &\mapsto -(1 + y)x \pm x^3 \\ y &\mapsto y \pm \varepsilon. \end{aligned} \tag{D.3}$$

To the one-dimensional flip bifurcation a slow parameter drift is added. In [2], the fast-slow flip singularity is analyzed analytically. The qualitatively different behavior of a positive or negative parameter drift is characterized by asymptotic calculations. However, up to now there is no treatment via geometric singular perturbation theory and blowup method.

D.2. Embedding as a Poincaré Return Map

To analyze the normal form of the fast-slow flip singularity geometrically, we aim to use the blowup method. The goal is to find a higher dimensional ODE system exhibiting in the singular limit $\varepsilon = 0$ a flip bifurcation of limit cycles, such that the normal form of the fast-slow flip bifurcation can be re-obtained as a Poincaré return map.

The embedding of the normal form of the discrete fast-slow fold bifurcation in Section 3.1 was achieved by introducing an additional coordinate θ. For a fixed value of the parameter y, a fixed point of the map was transferred to a limit cycle in the x-θ plane (or r-θ plane in the new coordinates). To embed the period two orbit of flip bifurcation, it is not sufficient to add one rotational coordinate in the same way as in Section 3.1: as visualized in Figure D.3 for a radial component r and an angular component θ, the constantly in the same direction rotating flow hitting the section $\{\theta = 0\}$ first at $r = r_1^*$ and then at $r = r_2^* \neq r_1^*$ cannot come back to $r = r_1^*$ without crossing the invariant solution curves. Hence, no period two orbits can exit in

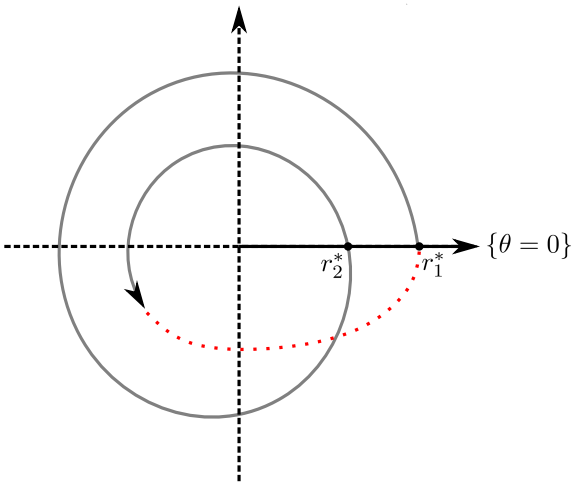


Figure D.3.: For an embedding of the fast-slow flip singularity, at least two rotational coordinates are needed.

the plane parameterized by r and θ. The embedding introduced in the following was first used by Crawford and Omohundro to study the global flow of period-doubling flows [5]. The space $\mathbb{R}^4$ is parameterized by

$$(r, \theta, \phi, y) \in \mathbb{R}_{\geq -v} \times \mathbb{R}/(s\mathbb{Z}) \times \mathbb{R}/(s\mathbb{Z}) \times \mathbb{R}$$

with fixed parameters $s, v \in \mathbb{R}_{>0}$. The coordinates $z = v + r$ and θ can be interpreted as the usual polar coordinates parameterizing the space $\mathbb{R}^2$. A point $x \in \mathbb{R}^4$ in Euclidean coordinates is given by

$$x = \left(\left(v + r\cos\left(\frac{2\pi}{s}\phi\right)\right)\cos\left(\frac{2\pi}{s}\theta\right), \left(v + r\cos\left(\frac{2\pi}{s}\phi\right)\right)\cos\left(\frac{2\pi}{s}\theta\right), \sin\left(\frac{2\pi}{s}\theta\right), y\right).$$

The coordinate system is visualized in Figure D.4. If r and ϕ are constant and θ is a variable in $[0, s)$, a limit cycle with radius $v + r\cos\left(\frac{2\pi}{s}\phi\right)$ occurs. The parameter shift $z = r + v$ is defined in the radial component to have the flip point located at $r = 0$ to simplify the calculations. In this coordinate system, we consider the ODE system

$$\begin{aligned} r' &= -yr \pm r^3, \\ \theta' &= \varepsilon, \\ \phi' &= \frac{1}{2}\varepsilon, \\ y' &= \pm\delta, \end{aligned} \tag{D.4}$$

with $0 < \delta \ll \varepsilon \ll 1$. In the (partial) singular limit $\delta = 0$, $\varepsilon \neq 0$, a flip bifurcation of limit cycles occurs: for $r = 0$, an equilibrium occurs in the radial component, which is stable for $y > 0$, non-hyperbolic for $y = 0$ and unstable for $y > 0$. In the supercritical case, where the cubic term has a $+$ sign in system (D.4), for $y > 0$, the radial component has additionally the stable fixed points $r = \pm\sqrt{y}$. However in the subcritical case, where the cubic term has a $-$ sign in system (D.4), for $y < 0$, the radial component has additionally the unstable fixed points $r = \pm\sqrt{y}$. As the rotation velocity for θ is twice the rotation velocity for ϕ, in both cases a limit cycle of

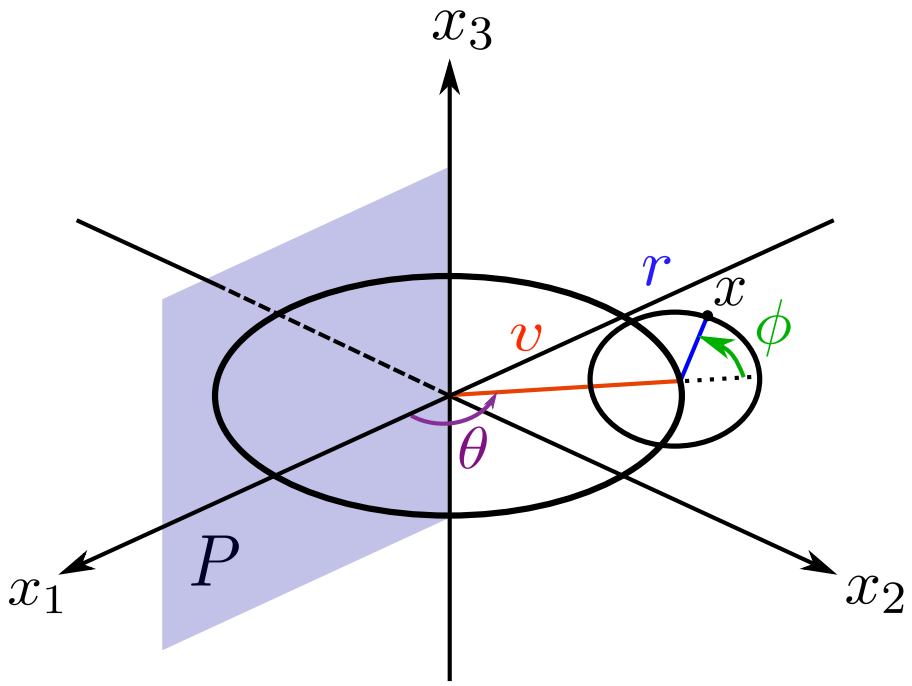


Figure D.4.: Coordinate System for the embedding of the fast-slow flip singularity in the first three coordinates, the coordinate $x_4 = y$ is not shown.

period two arises. We call system (D.4) the fast-slow flip singularity of limit cycles. Defining the Poincaré section as

$$P \coloneqq \{(r, \theta, \phi, y) \in \mathbb{R}_{\geq -v} \times \mathbb{R}/(s\mathbb{Z}) \times \mathbb{R}/(s\mathbb{Z}) \times \mathbb{R} : \ \theta = 0\},$$

up to rescaling of the variables, the normal form of the fast-slow flip singularity (D.3) is obtained as the Poincaré return map.

System (D.4) extended by the equation $\varepsilon' = 0$ can now be analyzed with the quasi-homogeneous blowup transformation introduced in Section 2.4. Due to the same arguments as for the discrete fast-slow fold singularity, we propose to apply the blowup transformation only to the coordinates r, y and ε. To apply the quasi-homogeneous blowup transformation of Definition 2.19, we aim that the right hand side of system (D.4) is a quasi-homogeneous vector field. We assume that δ can be expressed in terms of ε as

$$\delta = \varepsilon^{\alpha}$$

for some $\alpha > 1$. The following proposition determines the value of α, which results in a quasi-homogeneous vector field.

Proposition D.2. *To be able to apply the quasi-homogeneous blowup transformation of Definition 2.19, we need $\alpha = 2$ in system* (D.4) *leading to the extended ODE system*

$$\begin{aligned} r' &= -yr \pm r^3, \\ \theta' &= \varepsilon, \\ \phi' &= \frac{1}{2}\varepsilon, \\ y' &= \pm\varepsilon^2, \\ \varepsilon' &= 0, \end{aligned} \tag{D.5}$$

which is quasi-homogeneous of degree 3 with coefficients $a_1 = 1$, $a_2 = 0$, $a_3 = 0$, $a_4 = 2$ and $a_5 = 2$.

Proof. To apply the quasi-homogeneous blowup transformation, we need system (D.4) extended by the equation $\varepsilon' = 0$ to be a quasi-homogeneous vector field of type $(a_1, a_2, a_3, a_4, a_5)$ with $a_2 = 0$, $a_3 = 0$ and degree $k + 1$. Inserting Definition 2.18 of quasi-homogeneity into system (D.4) leads to

$$\begin{aligned} -\rho^{a_1+a_4} yr \pm \rho^{3a_1} r^3 &\stackrel{!}{=} \rho^{a_1+k}(-yr \pm r^3), \\ \rho^{a_5}\varepsilon &\stackrel{!}{=} \rho^{a_2+k}\varepsilon, \\ \frac{1}{2}\rho^{a_5}\varepsilon &\stackrel{!}{=} \frac{1}{2}\rho^{a_3+k}\varepsilon, \\ \pm\rho^{a_5\alpha}\varepsilon^{\alpha} &\stackrel{!}{=} \pm\rho^{a_4+k}\varepsilon^{\alpha}, \\ 0 &\stackrel{!}{=} \rho^{a_5+k} \cdot 0. \end{aligned}$$

This yields the following system of algebraic equations:

$$a_1 + a_4 = a_1 + k, \quad 3a_1 = a_1 + k, \quad a_5 = k, \quad a_5\alpha = a_4 + k.$$

We have some choices as the last constraint does not give any algebraic relation. Using these equations we obtain the following value for α:

$$\alpha = \frac{a_4 + k}{a_5} = \frac{2k}{k} = 2.$$

As all coefficients a_i, $i \in \{1, ..., 5\}$ should be natural numbers, we deduce from the relation $3a_1 = a_1 + k$, that $k = 2a_1$ is an even number. To keep the system as easy as possible, we choose $k = 2$ and obtain system (D.5) with the coefficients

$$a_1 = 1, \quad a_2 = 0, \quad a_3 = 2, \quad a_4 = 2, \quad a_5 = 2. \qquad \square$$

To apply the quasi-homogeneous blowup transformation of Definition 2.19, we choose the interval $I = [0, P]$ with $P > 0$ and introduce the two manifolds

$$B = S^2 \times \mathbb{R} \times \mathbb{R}/(s\mathbb{Z}) \times \mathbb{R}/(s\mathbb{Z}) \quad \text{and} \quad B_0 = S^2 \times [0, P] \times \mathbb{R}/(s\mathbb{Z}) \times \mathbb{R}/(s\mathbb{Z}).$$

Based on Proposition D.2, we define the blowup transformation

$$\varphi : B_0 \to \mathcal{D}_0, \quad (\bar{r}, \bar{y}, \bar{\varepsilon}, \rho, \theta, \phi) \mapsto (r, \theta, \phi, y, \varepsilon) = (\rho\bar{r}, \theta, \phi, \rho^2\bar{y}, \rho^2\bar{\varepsilon}), \tag{D.6}$$

with $(\bar{r}, \bar{y}, \bar{\varepsilon}) \in S^2$ and $\mathcal{D}_0 = \mathbb{R}_{\geq -v} \times \mathbb{R}/(s\mathbb{Z}) \times \mathbb{R}/(s\mathbb{Z}) \times \mathbb{R} \times \mathbb{R}_{\geq 0}$. The remaining task is now to analyze system (D.5) in the different charts. This is left for future work.

Appendix E

Blowup of Discrete Fast-Slow Singularities

In this chapter we introduce an alternate approach to apply the blowup method to maps. In Section E.1, the polar blowup in spherical coordinates is introduced and a desingularization step, which does not rely on a time rescaling, is proposed. In Sections E.2 and E.3, the results received with this method for the normal forms of the fast-slow fold and the fast-slow flip singularity are stated. In both cases, non-trivial dynamics is obtained on the sphere, but all fixed points are non-hyperbolic.

E.1. Blowup of Maps in Spherical Coordinates

When applying the quasi-homogeneous blowup transformation introduced in Section 2.4 directly to fast-slow maps, we cannot use the same desingularization step via time rescaling as for fast-slow ordinary differential equations. This problem is based on the fact that the time scale is discrete. An additional problem in our setting is, that the extended normal form of the discrete fast-slow fold singularity

$$\begin{aligned} x &\mapsto x + x^2 - y, \\ y &\mapsto y - \varepsilon, \\ \varepsilon &\mapsto \varepsilon, \end{aligned}$$

with $x, y \in \mathbb{R}$, is not a quasi-homogeneous map, as in the 'fast' map the terms x and x^2 occur.

Another idea is to use the blowup transformation in spherical coordinates. To that purpose, the space $\mathbb{R}^3$ is parameterized by

$$(x_1, x_2, x_3) = (r \sin\theta \cos\phi, r \sin\theta \sin\phi, r \cos\theta)$$

with the radial component $r \in \mathbb{R}_{\geq 0}$, an angle $\phi \in [-\pi, \pi)$ describing the angular position in the x_1-x_2 plane and an angle $\theta \in [0, \pi]$ parameterizing the x_3-coordinate. For fast-slow maps with a positive parameter ε, the upper half of the sphere obtained for $\theta \in \left[0, \frac{\pi}{2}\right]$ is of major interest. The spherical coordinates are visualized in Figure E.1. The corresponding coordinate transformation φ and its inverse φ^{-1} are given by

$$\begin{aligned} \varphi &: S^2 \times [0, \infty) \to \mathbb{R}^3, & \varphi(\theta, \phi, r) &= (r \sin\theta \cos\phi, r \sin\theta \sin\phi, r \cos\theta), \\ \varphi^{-1} &: \mathbb{R}^3 \to S^2 \times [0, \infty), & \varphi^{-1}(x, y, \epsilon) &= \left(\arccos\frac{\epsilon}{r}, \operatorname{atan2}(y, x), r\right), \end{aligned}$$

with the function

$$\operatorname{atan2}(y, x) = \begin{cases} \arctan\frac{y}{x} & \text{if } x > 0, \\ \operatorname{sgn}(y)\frac{\pi}{2} & \text{if } x = 0, \\ \arctan\frac{y}{x} + \pi & \text{if } x < 0 \text{ and } y \geq 0, \\ \arctan\frac{y}{x} - \pi & \text{if } x < 0 \text{ and } y < 0. \end{cases}$$

For $r = 0$, the spherical coordinate transformation φ is not one-to-one, such that the origin is blown-up to a sphere by the inverse φ^{-1}. The following theorem proposes a transformation for three-dimensional polynomial blown-up maps resulting in non-trivial dynamics on the sphere.

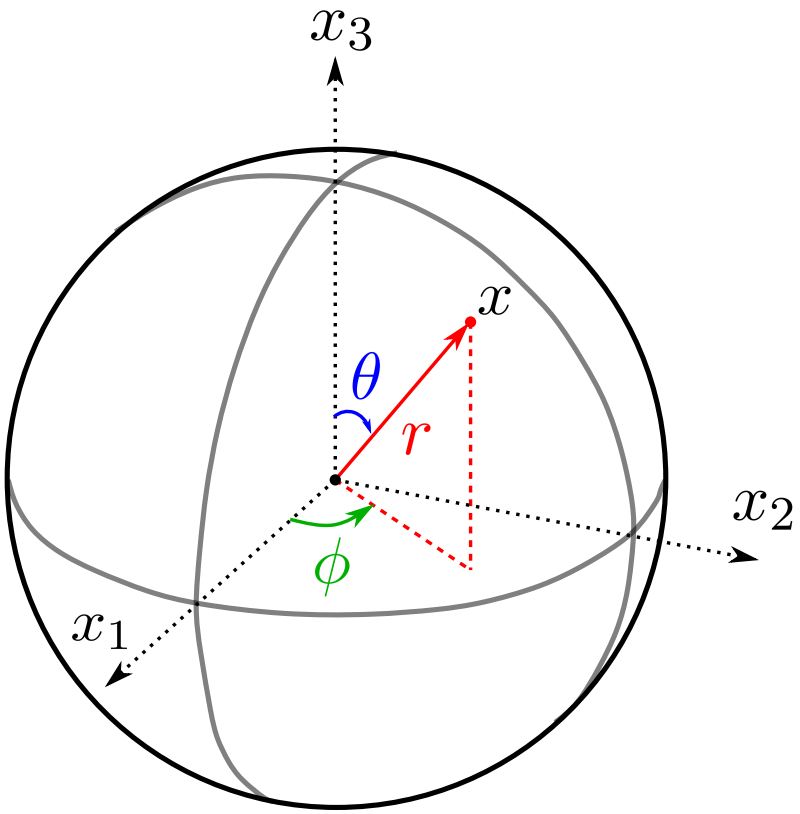


Figure E.1.: Spherical coordinates parameterizing the space $\mathbb{R}^3$.

Theorem E.1. *Let $G : \mathbb{R}^3 \to \mathbb{R}^3$ be a polynomial map in x, y and ϵ with $G(0) = 0$. The spherical blowup is defined as*

$$\bar{G}(\theta, \phi, r) = \varphi^{-1} \circ G \circ \varphi(\theta, \phi, r) = (\bar{\theta}, \bar{\phi}, \bar{r}), \tag{E.1}$$

for $r \neq 0$ and for $r = 0$ by continuous extension of (E.1)*, where φ is the transformation in spherical coordinates. Consider for $r \neq 0$ the transformed map*

$$\mathcal{G}(\theta, \phi, r) = \begin{pmatrix} [\varphi^{-1} \circ \frac{1}{r} G \circ \varphi(\theta, \phi, r)]_\theta \\ [\varphi^{-1} \circ \frac{1}{r} G \circ \varphi(\theta, \phi, r)]_\phi \\ [\varphi^{-1} \circ \quad G \circ \varphi(\theta, \phi, r)]_r \end{pmatrix} \tag{E.2}$$

and its continuous extension to $r = 0$. The subscripts θ, ϕ and r denote the corresponding components of the map. Then for $r > 0$, the maps $\bar{G}$ and $\mathcal{G}$ coincide.

Proof. By definition, the r-coordinates of $\bar{G}$ and $\mathcal{G}$ coincide.

As G is a polynomial map with $G(0) = 0$, each component of the map $G \circ \varphi(\theta, \phi, r) : S^2 \times [0, \infty) \to \mathbb{R}^3$ has the factor r, hence we can write the map G as

$$G \circ \varphi(\theta, \phi, r) = r \cdot \tilde{H}(\theta, \phi, r),$$

where $\tilde{H}(\theta, \phi, r)$ is a polynomial map in $\cos\theta$, $\sin\theta$, $\cos\phi$, $\sin\phi$ and r. Consequently, the map

$$\frac{1}{r} G \circ \varphi(\theta, \phi, r) = \tilde{H}(\theta, \phi, r)$$

evaluated at $r = 0$ is finite and well-defined.

For $r > 0$, the θ-coordinate of the maps $\bar{G}(\theta, \phi, r)$ and $\mathcal{G}(\theta, \phi, r)$ coincides, as

$$\begin{aligned}
\bar{G}(\theta,\phi,r)_\theta &= \arccos\left(\frac{[G\circ\varphi(\theta,\phi,r)]_\epsilon}{\sqrt{[G\circ\varphi(\theta,\phi,r)]_x^2+[G\circ\varphi(\theta,\phi,r)]_y^2+[G\circ\varphi(\theta,\phi,r)]_\epsilon^2}}\right)\\
&= \arccos\left(\frac{[r\cdot R(\theta,\phi,r)]_\epsilon}{\sqrt{[r\cdot R(\theta,\phi,r)]_x^2+[r\cdot R(\theta,\phi,r)]_y^2+[r\cdot R(\theta,\phi,r)]_\epsilon^2}}\right)\\
&= \arccos\left(\frac{[R(\theta,\phi,r)]_\epsilon}{\sqrt{[R(\theta,\phi,r)]_x^2+[R(\theta,\phi,r)]_y^2+[R(\theta,\phi,r)]_\epsilon^2}}\right)\\
&= \arccos\left(\frac{[\frac{1}{r}G\circ\varphi(\theta,\phi,r)]_\epsilon}{\sqrt{[\frac{1}{r}G\circ\varphi(\theta,\phi,r)]_x^2+[\frac{1}{r}G\circ\varphi(\theta,\phi,r)]_y^2+[\frac{1}{r}G\circ\varphi(\theta,\phi,r)]_\epsilon^2}}\right)\\
&= \mathcal{G}(\theta,\phi,r)_\theta
\end{aligned}$$

Analogously, also the θ-coordinate of the maps $\bar{G}(\theta, \phi, r)$ and $\mathcal{G}(\theta, \phi, r)$ coincides for $r > 0$, because

$$\begin{aligned}
\bar{G}(\theta,\phi,r)_\phi &= \operatorname{atan2}([G\circ\varphi(\theta,\phi,r)]_y,[G\circ\varphi(\theta,\phi,r)]_x)\\
\mathcal{G}(\theta,\phi,r)_\phi &= \operatorname{atan2}([\frac{1}{r}G\circ\varphi(\theta,\phi,r)]_y,[\frac{1}{r}G\circ\varphi(\theta,\phi,r)]_x)\\
&= \operatorname{atan2}([R(\theta,\phi,r)]_y,[R(\theta,\phi,r)]_x).
\end{aligned}$$

As we consider only the case $r > 0$, the map $G \circ \varphi(\theta, \phi, r)$ has for all input values in each component the same sign as the corresponding component of $R(\theta, \phi, r)$. So the case distinction of the atan2-function in the inverse of the spherical coordinate transformation is the same for the maps $\bar{G}$ and $\mathcal{G}$. Furthermore, it holds

$$\arctan\left(\frac{[G\circ\varphi(\theta,\phi,r)]_y}{[G\circ\varphi(\theta,\phi,r)]_x}\right) = \arctan\left(\frac{r\cdot[R(\theta,\phi,r)]_y}{r\cdot[R(\theta,\phi,r)]_x}\right) = \arctan\left(\frac{[R(\theta,\phi,r)]_y}{[R(\theta,\phi,r)]_x}\right)$$

and

$$\operatorname{sgn}([G\circ\varphi(\theta,\phi,r)]_y) = \operatorname{sgn}(r\cdot R(\theta,\phi,r)_y) = \operatorname{sgn}(R(\theta,\phi,r)_y).$$

It follows, that $\bar{G}(\theta, \phi, r) = \mathcal{G}(\theta, \phi, r)$ for $r > 0$, such that the two maps coincide. □

The disadvantage of the transformation of Theorem E.1 is, that on the blown-up sphere $S^2 \times \{r = 0\}$ only dynamics of the linear terms of the map is observed due to the fact, that the non-linear terms depend non-linearly on r in the spherical coordinate transformation. Considering the surface $S^2 \times \{r = 0\}$, these terms become zero, whereas the linear terms are non-zero due to the factor $\frac{1}{r}$ in the coordinate transformation (E.2). By weighting terms as in the quasi-homogeneous blowup transformation, it could be possible to find coordinate transformations which result for quasi-homogeneous maps in topologically equivalent maps, which keep the non-linear terms on the sphere. However, the discrete fast-slow fold and the fast-slow flip singularity are no quasi-homogeneous systems, hence other manipulations than introducing weights are required. This is left for future work.

Nevertheless, the dynamics on the sphere $S^2 \times \{r = 0\}$ is already nontrivial for the transformation of Theorem E.1. Due to the parametrization in spherical coordinates, it is also nonlinear. In the following two Sections E.2 and E.3, the dynamics on $S^2 \times \{r = 0\}$ is sketched for the normal forms of the discrete fast-slow fold and the discrete fast-slow flip singularity.

E.2. Results for the Discrete Fast-Slow Fold

The normal form of the fast-slow fold singularity is given by

$$\begin{aligned} x &\mapsto x + x^2 - y, \\ y &\mapsto y \pm \varepsilon, \\ \varepsilon &\mapsto \varepsilon, \end{aligned} \tag{E.3}$$

where the direction of the parameter drift is not specified.

Applying the coordinate transformation of Theorem E.1 results in the map

$$\mathcal{G}(\theta, \phi, r = 0) = \varphi^{-1} \circ \begin{pmatrix} \sin\theta\cos\phi - \sin\theta\sin\phi \\ \sin\theta\sin\phi \pm \cos\theta \\ \cos\theta \end{pmatrix}$$

on the sphere $S^2 \times \{r = 0\}$. By construction of the map $\mathcal{G}(\theta, \phi, r = 0)$, the blown-up sphere $S^2 \times \{r = 0\}$ is invariant. In Figure E.2, the fixed points of the map $\mathcal{G}$ in θ and ϕ are shown. The two fixed points

$$\left(\theta = \frac{\pi}{2}, \phi = -\pi\right), \qquad \left(\theta = \frac{\pi}{2}, \phi = 0\right),$$

are both non-hyperbolic in all three coordinates. The qualitative behavior of the discrete fast-slow fold singularity (E.3) with negative parameter drift is sketched in Figure E.2. The Figure for positive parameter drift is obtained by reflecting the Figure at the line $\{\theta = \frac{\pi}{2}\}$.

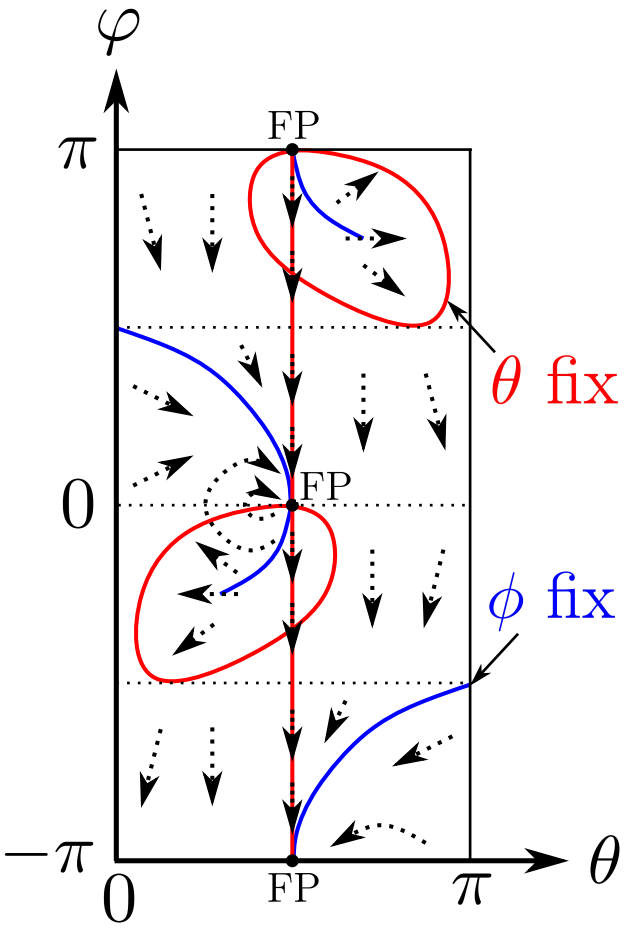


Figure E.2.: Qualitative behavior of the discrete fast-slow fold singularity (E.3) with negative parameter drift on the blown-up sphere $S^2 \times \{r = 0\}$. The fixed points are abbreviated by 'FP'.

E.3. Results for the Fast-Slow Flip

The normal form of the discrete fast-slow flip singularity is given by

$$\begin{aligned} x &\mapsto -(1+y)x \pm x^3, \\ y &\mapsto y \pm \varepsilon, \\ \varepsilon &\mapsto \varepsilon, \end{aligned} \tag{E.4}$$

where the direction of the parameter drift is not specified.

Applying the coordinate transformation of Theorem E.1 results in the map

$$\mathcal{G}(\theta, \phi, r=0) = \varphi^{-1} \circ \begin{pmatrix} -\sin\theta\cos\phi \\ \sin\theta\sin\phi \pm \cos\theta \\ \cos\theta \end{pmatrix}$$

on the sphere $S^2 \times \{r=0\}$. By construction of the map $\mathcal{G}(\theta, \phi, r=0)$, the blown-up sphere $S^2 \times \{r=0\}$ is invariant. In Figure E.3, the fixed points of the map $\mathcal{G}$ in θ and ϕ are shown. The two fixed points

$$\left(\theta = \frac{\pi}{2}, \phi = -\frac{\pi}{2}\right), \qquad \left(\theta = \frac{\pi}{2}, \phi = \frac{\pi}{2}\right),$$

are both non-hyperbolic in all three coordinates. For the fast-slow flip singularity, we consider

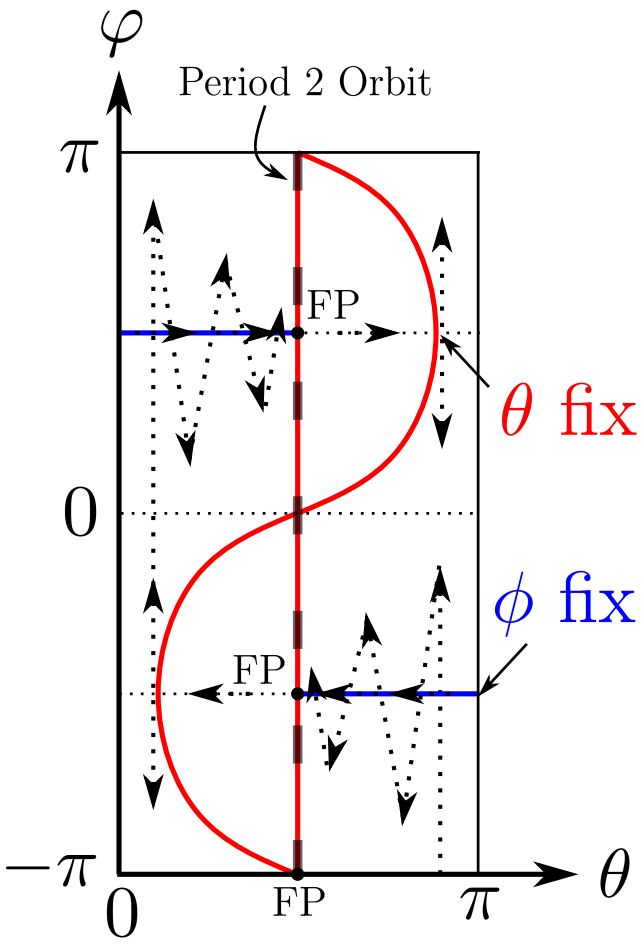


Figure E.3.: Qualitative behavior of the fast-slow flip singularity (E.4) with negative parameter drift on the blown-up sphere $S^2 \times \{r=0\}$. The fixed points are abbreviated by 'FP'.

additionally the blown-up map of the second iterate, which is given by

$$\mathcal{G}^2(\theta, \phi, r = 0) = \varphi^{-1} \circ \begin{pmatrix} \sin\theta \cos\phi \\ \sin\theta \sin\phi \pm 2\cos\theta \\ \cos\theta \end{pmatrix}.$$

The map $\mathcal{G}^2(\theta, \phi, r = 0)$ has the circle of fixed points $\{\theta = \frac{\pi}{2}\}$, which are period two orbits in the map $\mathcal{G}(\theta, \phi, r = 0)$. The qualitative behavior of the fast-slow flip singularity (E.3) with negative parameter drift is sketched in Figure E.3. The Figure for positive parameter drift is obtained by reflecting the Figure at the line $\{\theta = \frac{\pi}{2}\}$.

Bibliography

[1] L. Arcidiacono, M. Engel, and C. Kuehn. Discretized fast-slow systems near pitchfork singularities. *Journal of Difference Equations and Applications*, 25:1024–1051, 2019.

[2] C. Baesens. Slow sweep through a period-doubling cascade: Delayed bifurcations and renormalization. *Physica D*, 53:319–375, 1991.

[3] G. R. Belitskii. Functional equations and conjugacy of local diffeomorphisms of a finite smoothness class. *Functional analysis and its applications*, 7(4):268–277, 1973.

[4] C. Chicone. *Ordinary Differential Equations with Applications*, volume 34 of *Texts in Applied Mathematics*. Springer, second edition, 2006.

[5] J. Crawford and S. Omohundro. On the global structure of period doubling flow. *Physica D*, 1983.

[6] F. Dumortier. Techniques in the theory of local bifurcations: blow-up, normal forms, nilpotent bifurcations, singular perturbations. In *Bifurcations and periodic orbits of vector fields*, volume 408 of *Advanced Science Institute Series C, Mathematical and Physical Sciences*, pages 19–73. 1933.

[7] F. Dumortier. *Singularities of vector fields*, volume 32 of *Monografías de Matemática*. Instituto de Matemática Pura e Aplicada, Rio de Janeiro, 1978.

[8] F. Dumortier and R. Roussarie. *Canard Cycles and Center Manifolds*, volume 121 of *Memoirs of the American Mathematical Society*. American Mathematical Society, 1996.

[9] M. Engel and C. Kuehn. Discretized fast-slow systems near transcritical singularities. *Nonlinearity*, 32(7):2365–2391, 2019.

[10] O. Forster. *Analysis 2, Differentialrechnung im $\mathbb{R}^n$, gewöhnliche Differentialgleichungen*. Grundkurs Mathematik. Springer Spektrum, 11 edition, 2017.

[11] J. Grasman. *Aymptotic Methods for Relaxation Oscillations and Applications*, volume 63 of *Applied Mathematical Sciences*. Springer Science + Business Media, LLC, first edition, 1987.

[12] J. Guckenheimer and P. Holmes. *Nonlinear Oscillations, Dynamical Systems, and Bifurcations of Vector Fields*, volume 42 of *Applied Mathematical Sciences*. Springer, first edition, 1983.

[13] M. W. Hirsch, C. C. Pugh, and M. Shub. Invariant manifolds. *Bulletin of the American Mathematical Society*, 76:1015–1019, 1970.

[14] A. J. Homburg and B. Sandstede. Homoclinic and heteroclinic bifurcations in vector fields. 2010.

[15] S. Jelbart and C. Kuehn. Discrete geometric singular perturbation theory. *arXiv:2201.06996v2 [math.DS] 19 Jan 2022*.

[16] M. Krupa and P. Szmolyan. Extending slow manifolds near transcritical and pitchfork singularities. *Nonlinearity*, 14(6):1473–1491, 2001.

[17] M. Krupa and P. Szmolyan. Geometric analysis of the singularly perturbed planar fold. In C. K. Jones and A. I. Khibnik, editors, *Multiple-Time-Scale Dynamical Systems*, volume 122 of *The IMA Volumes in Mathematics and its Applications*, pages 89–116. Springer, 2001.

[18] C. Kuehn. *Multiple Time Scale Dynamics*, volume 191 of *Applied Mathematical Sciences*. Springer, first edition, 2015.

[19] Y. A. Kuznetsov. *Elements of Applied Bifurcation Theory*, volume 112 of *Applied Mathematical Sciences*. Springer, third edition, 2004.

[20] E. Mishchenko and N. K. Rozov. *Differential Equations with Small Parameters and Relaxation Oscillations*, volume 13 of *Mathematical Concepts and Methods in Science and Engineering*. Plenum Press, first edition, 1980.

[21] K. Nipp and D. Stoffer. Attractive invariant manifolds for maps: existence, smoothness and continuous dependence on the map. *Research Report / Eidgenössische Technische Hichschule Zürich, Seminar für Angewandte Mathematik, ETH Zürich*, 92(11), 1992.

[22] K. Nipp and D. Stoffer. *Invariant manifolds in discrete and continuous dynamical systems*, volume 21 of *EMS Tracts in Mathematis*. European Mathemaical Society (EMS) Zürich, first edition, 2013.

[23] C. Poetzsche. Slow and fast variables in non-autonomous difference equations. *Journal of Difference Equations and Applications*, 9:473–487, 2003.

[24] F. Takens. Singularities of vector fields. *Publications mathématiques de l'I.H.É.S.*, 43:47–100, 1974.